miR-181c Modulates T Cell Function By Regulating the Expression of BRK1

Lim, Shok Ping

Awarding institution:
King's College London

miR-181c Modulates T Cell Function By Regulating the Expression of BRK1

Shok Ping Lim

Thesis submitted for the degree of
Doctor of Philosophy

Department of Haemato-Oncology
Division of Cancer Studies
Faculty of Life Sciences & Medicine
King's College London
London
United Kingdom

2017

Declaration

I hereby confirm that the work presented in this thesis is my own, except where otherwise stated.

Shok Ping Lim

March 2017

Acknowledgements

First and foremost, I would like to express my sincere gratitude to my first supervisor Dr Joop Gäken for his encouragement and support throughout my PhD. I am very grateful for his patience, motivation and the freedom he has given me to pursue my own independent work. I would also like to express my deepest thanks to my second supervisor Professor Ghulam J Mufti for his critical feedback and insightful comment on my work. This thesis would not have been possible without their guidance throughout my research and writing of the thesis.

I am grateful to all my colleagues in the Department of Haemato-Oncology for their support and advice during my PhD. I would like to thank members in our group, Heba Alkhatabi, Terry Gaymes, Richard Beswick, Jie Jiang, Azim Mohamedali, Shreyans Ghandi, Austin Kulasekararaj, Syed Mian, Alexander Smith and Andreas for sharing their reagents in the time of need, and their valuable advice and encouraging words. Special thanks to my friends, Nazia Matto and Sneha Chitre, for sharing thoughts, stimulating discussions, working together in the laboratory, listening to and supporting me in everything over the past three years. Thank you to all my friends in the department, Kholood, Samia, Monera, Dickson, Glenda, Aytug, Najeem, Tom, Benedetta, Sun, Jackie, Jamal, Chiara, Giuliana and Lauren for their invaluable support. A special thank to Lu for his valuable advice on this project as well as proof reading of my thesis.

A great thank you goes to Dr Alan Ramsay, Dr Nikolaos Ioannou and Dr David Darling for their help with parts of the experiments. I am especially thankful to Rajani Chelliah for providing invaluable patient samples and to Dr Donal McLornan for providing clinical data needed for this project. Thank you Dr Stephen Orr and Dr

Nermina Lamadema for willing to teach me with some of the laboratory techniques. Many thanks to Dr Alan Ramsay, PhD co-ordinator, for being a wonderful mentor as well, providing guidance, prompt help and kind words.

I would also like to thank all my friends in the UK who have been true companions, especially Chi Ching, Xin Yi, Tiong Kit, Andy and Benjamin for sharing stress and joy as well as their encouragement and support for the past few years.

Last but not least, a very big thank you to my parents and siblings for their unconditional love, support and encouragement. Without them, this dream would not have come true.

Finally, I would also like to take this opportunity to acknowledge the Malaysian Government (Public Service Department) for sponsoring my PhD study at the King's College London.

Abstract

MicroRNAs are short endogenous non-coding RNAs that play pivotal roles in a diverse range of cellular processes. The *miR-181* family is important in T cell development, proliferation and activation. In this study, we identified BRK1 as a novel target of *miR-181c* using a dual selection functional assay. Given the importance of *miR-181* in T cell functions and the potential role of BRK1 in the WAVE2 complex as well as actin polymerisation in T cells, we therefore investigated the influence of the *miR-181c*-BRK1 axis in T cell functions. Stimulation of PBMC derived $CD3^+$ T cells resulted in reduced expression of *miR-181c* and upregulation of BRK1 protein expression, suggesting that the *miR-181c*-BRK1 axis might be important in T cell activation. To further assess the role of *miR-181c*-BRK1 axis in T cell activation, we overexpressed *miR-181c* in Jurkat T cells and suppressed *BRK1* in Jurkat and primary T cells. We showed that overexpression of *miR-181c* or suppression of *BRK1* resulted in reduction in T cell activation and actin polymerisation coupled with impairment in lamellipodia generation and immunological synapse formation. Additionally, we found that *BRK1* silencing led to reduced expressions of other proteins in the WAVE2 complex including WAVE2, ABI1 and SRA1, suggesting that impairment of actin polymerisation-dependent T cell functions were a result of the instability of the WAVE2 complex following *BRK1* depletion. We also demonstrated a reciprocal relationship of *miR-181c* and BRK1 in BM derived $CD3^+$ T cells from MDS patients associated with T-LGL leukaemia, suggesting the regulation of BRK1 protein expression by *miR-181c* in this group of MDS patients. Collectively, we demonstrated that BRK1 is a novel downstream target of *miR-181c* and highlighted the important role of *miR-181c*-BRK1 axis in T cell activation and actin polymerisation-mediated T cell functions.

Table of Contents

List of Figures

List of Tables

List of Abbreviations

AA	Aplastic anaemia
ABI1	Abelson interactor 1
AGO	Argonaute
ALL	Acute lymphocytic leukaemia
AML	Acute myeloid leukaemia
APC	Antigen presenting cell
APC	Allophycocyanin
ARP2	Actin-related protein 2
ARP3	Actin-related protein 3
ARP2/3	Actin-related proteins 2/3
β-ACTIN	Beta-actin
BRK1	BRICK1, SCAR/WAVE actin-nucleating complex subunit
BM	Bone marrow
bp	Base pair
BSA	Bovine serum albumin
C-terminal	Carboxyl-terminal
Ca^{2+}	Calcium
CD	Cluster of differentiation
CDC42	Cell division control protein 42 homolog
cDNA	Complementary deoxyribonucleic acid
CFU	Colony forming unit
CLL	Chronic lymphocytic leukaemia
CML	Chronic myeloid leukaemia
CO_2	Carbon dioxide
CRAC	Calcium release-activated channel
Ct	Cycle threshold
CYFIP1	Cytoplasmic FMR1 interacting protein 1
CYFIP2	Cytoplasmic FMR1 interacting protein 2
DAG	Diacylglycerol
DAPI	4’,6-diamidino-2-phenylindole
DHTKD1	Dehydrogenase E1 and transketolase domain containing 1
DMEM	Dulbecco’s Modified Eagle medium

DMSO	Dimethyl sulphoxide
DNA	Deoxyribonucleic acid
DTT	Dithiothreitol
E. coli	*Escherichia coli*
ECL	Enhanced chemiluminescence
EDTA	Ethylene diamine tetra-acetic acid
FACS	Fluorescence-activated cell sorting
FBS	Foetal bovine serum
g	Acceleration of gravity
GAPDH	Glyceraldehyde-3-phosphate dehydrogenase
GCV	Ganciclovir
GDP	Guanosine diphosphate
GTP	Guanosine-5'-triphosphate
HEM1	Haematopoietic protein 1
HEM2	Haematopoietic protein 2
h	Hour
HRP	Horseradish peroxidase
HS1	Haematopoietic cell-specific protein 1
HSPC	Haematopoietic stem/progenitor cell
IFU	Infectious unit
IL-2	Interleukin-2
IP_3	Inositol triphosphate
ITAM	Immunoreceptor tyrosine-based activation motif
ITK	Interleukin-2-inducible T cell kinase
kb	kilobase pair
kDa	kilodalton
LAT	Linker for the activation of T cell
LB	Luria-Bertani broth
LGL	Large granular lymphocyte
M	Molar
MDS	Myelodysplastic syndrome
mfe	Minimum free energy
MFI	Mean fluorescence intensity
MHC	Major histocompatibility complex
min	Minute

miRISC	microRNA-induced silencing complex
miRNA	microRNA
mRNA	Messenger ribonucleic acid
MOI	Multiplicity of infection
MSC	Mesenchymal stem cell
mg	milligram
ml	millilitre
mm	millimetre
mM	millimolar
µg	microgram
µl	microlitre
µm	micrometre
μm^2	square micrometre
µM	micromolar
N-terminal	Amino-terminal
NaN_3	Sodium azide
NCBI	National Centre for Biotechnology Information
NCK1	NCK adaptor protein 1
NAP1/NAP125/NCKAP1	NCK associated protein 1
NK	Natural killer
NPF	Actin nucleation-promoting factor
NSCLC	Non-small cell lung carcinoma
ng	nanogram
nm	nanometre
nM	nanomolar
PAGE	Polyacrylamide gel electrophoresis
PB	Peripheral blood
PBMC	Peripheral blood mononuclear cell
PBS	Phosphate buffered saline
PCR	Polymerase chain reaction
PE	Phycoerythrin
PI	Propidium iodide
PIR121	P53-inducible protein 121
PLCγ1	Phospholipase Cγ1
PMA	Phorbol 12-myristate 13-acetate

PMSF	Phenylmethylsulfonyl fluoride
Pre-miRNA	Precursor microRNA
Pri-miRNA	Primary microRNA
qPCR	Quantitative real time polymerase chain reaction
RAC1	Ras-related C3 botulinum toxin substrate 1
RCMD	Refractory anaemia with multilineage dysplasia
RIPA	Radio-Immunoprecipitation sssay
Rn	Reporter normalised
RNA	Ribonucleic acid
rpm	Revolutions per minute
RPMI 1640	Roswell Park Memorial Institute 1640 medium
RT	Reverse transcription
RT-PCR	Reverse transcription polymerase chain reaction
RT-qPCR	Quantitative reverse transcription polymerase chain reaction
sAg	Superantigen
SEA	Superantigen A
SEB	Superantigen B
SD	Standard deviation
SDS	Sodium dodecyl sulphate
sec	Second
SEM	Standard error of the mean
SH3	SRC homology 3
shRNA	Short hairpin ribonucleic acid
siRNA	Small interfering ribonucleic acid
SLP76	SRC homology 2 (SH2) domain-containing leukocyte protein of 76kDa
SRA1	Steroid receptor RNA activator 1
T-LGL	T cell large granular lymphocyte
TAE	Tris acetate-EDTA
TBS	Tris buffered saline
TCR	T cell receptor
TKzeo	Thymidine kinase-zeocin
U	Unit
UTR	Untranslated region

UV	Ultraviolet
V	Volt
VAV1	Vav guanine nucleotide exchange factor 1
WASH	WAVE homolog
WASP	Wiskott-Aldrich Syndrome protein
WAVE	Wiskott-Aldrich Syndrome protein (WASP) family verprolin-homologous protein
WHO	World Health Organisation
X-Gal	5-bromo-4-chloro-3-indolyl-β-D-Galactopyranoside

1 Chapter 1 – Introduction

1.1 MicroRNA

1.1.1 Background of MicroRNA

microRNAs (miRNAs) are short endogenous non-coding RNAs of 18-25 nucleotides in length which play an important role as negative regulators of gene expression either through mRNA degradation or translational repression (Ambros, 2001; Bartel, 2004). The first miRNA, which is *Lin-4,* was discovered in 1993 and it was shown to be involved in the development of nematodes (Lee et al., 1993; Wightman et al., 1993). In 2000, *Let-7* was reported as a second miRNA discovered and similarly, it took part in the temporal development of *C. elegans* (Reinhart et al., 2000). A year later, more miRNAs were found and it is believed that miRNAs participate in regulatory functions in both vertebrates and invertebrates (Lagos-Quintana et al., 2001). Sequences of miRNA are highly conserved among species and they have been shown to play critical roles in controlling a variety of biological processes, including cell differentiation, proliferation and apoptosis of haematopoietic progenitors (Almeida et al., 2011; Chen et al., 2004b; Cheng et al., 2005; Karp and Ambros, 2005). According to miRBase Sequence Database (Release 21, June 2014), there are 1881 identified human hairpin precursor miRNAs and 2603 identified human mature miRNAs, although the functional importance of many of these miRNA annotations remains to be determined.

1.1.2 MicroRNA Biogenesis

The canonical biogenesis pathway of mammalian miRNAs is a two-step (nuclear and cytoplasmic) enzymatic processing of their precursors, which are encoded in the genome [reviewed in (Ha and Kim, 2014; Lin and Gregory, 2015; Milunović et al., 2016; Stroynowska-Czerwinska et al., 2014)]. miRNAs are evolutionarily conserved and most of the human miRNAs are encoded within protein coding genes or in the intergenic regions (Rodriguez et al., 2004). The miRNA genes are typically transcribed by RNA polymerase II (Lee et al., 2004), or less frequently by RNA polymerase III (Borchert et al., 2006) into long, capped and poly-adenylated immature primary miRNA (pri-miRNA) containing a stem-loop structure. Pri-miRNAs are co-transcriptionally recognised by a large protein complex, called the Microprocessor, the main components of which are the RNase III DROSHA and DiGeorge syndrome critical region 8 (DGCR8) (Denli et al., 2004; Gregory et al., 2004; Han et al., 2004; Lee et al., 2003; Morlando et al., 2008). DROSHA is responsible for processing the pri-miRNAs into hairpin precursor molecules (pre-miRNAs) of 70-100 nucleotides in length in the nucleus (Kim and Kim, 2007; Lee et al., 2003). Pre-miRNAs are then actively transported from the nucleus into the cytoplasm by Exportin 5 (Lund et al., 2004). In the cytoplasm, another RNase III, DICER, functioning with its protein partners, Argonaute (AGO), TRBP and/or PACT (Chendrimada et al., 2005; Koscianska et al., 2011; Lee et al., 2006) recognises the pre-miRNAs and cleaves them into miRNA/miRNA* duplexes of approximately 22 nucleotides in length (Koscianska et al., 2011; MacRae et al., 2007). Subsequently, miRNA/miRNA* duplexes are loaded onto AGO protein to form an effector complex called miRNA-induced silencing complex (miRISC). The duplex is then unwound in which the N-terminal domain of AGO actively wedges

between miRNA strands and the PAZ domain unwinds the miRNA duplex. The AGO protein consists of four domains: PAZ (binds the 3' end of the miRNA strand), middle (MID, binds the 5' phosphate group of the miRNA), C-terminal PIWI (may possess endonucleolytic activity) and N-terminal domain (facilitates duplex unwinding). The passenger strand (miRNA*) is removed from miRISC and undergoes rapid degradation. miRNA within the mature miRISC is then bound to potential mRNA targets and regulates RNA levels either through mRNA degradation or translational repression [reviewed in (Ha and Kim, 2014; Lin and Gregory, 2015; Milunović et al., 2016; Stroynowska-Czerwinska et al., 2014)].

Apart from the canonical pathway of miRNA biogenesis described above, various alternative mechanisms can generate miRNA that are independent of DROSHA (wherein miRNAs are generated from pre-miRNA-like introns, called mirtrons) or DICER activity (Cheloufi et al., 2010; Ha and Kim, 2014; Ruby et al., 2007). The biogenesis of miRNA in human is depicted in Figure 1.1.

(a)

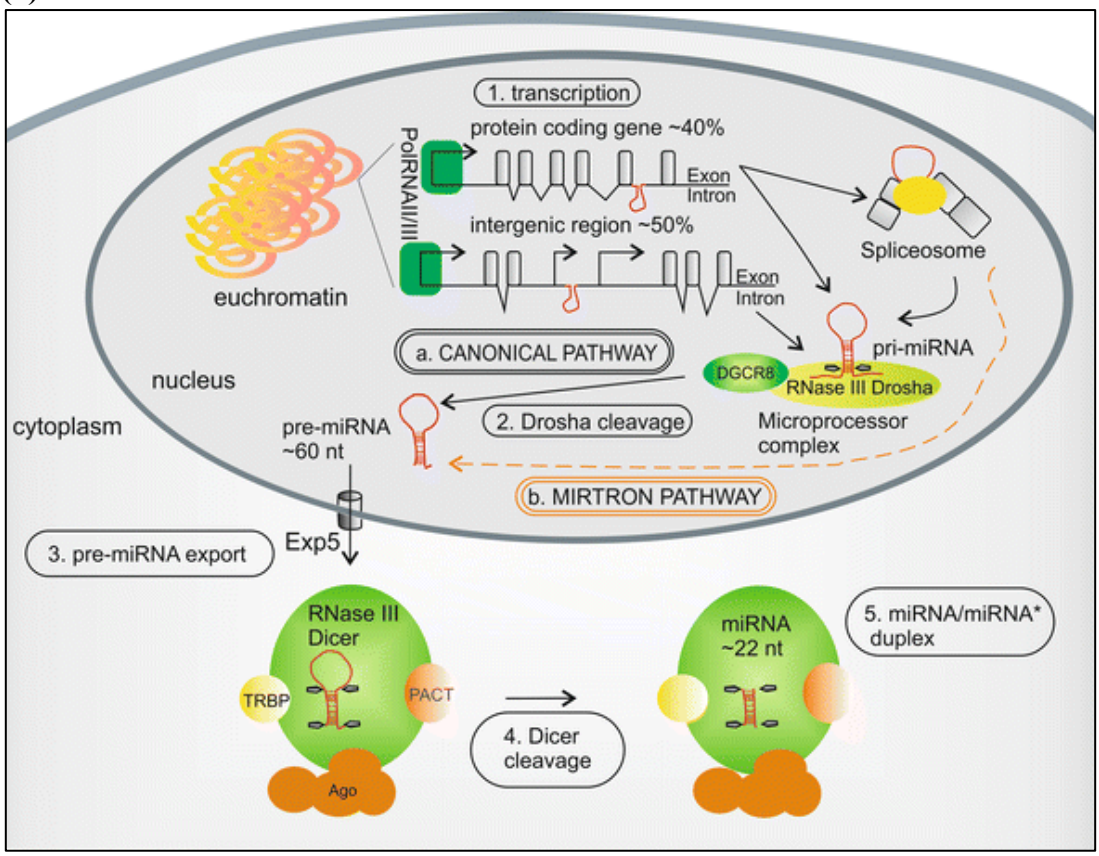

(b)

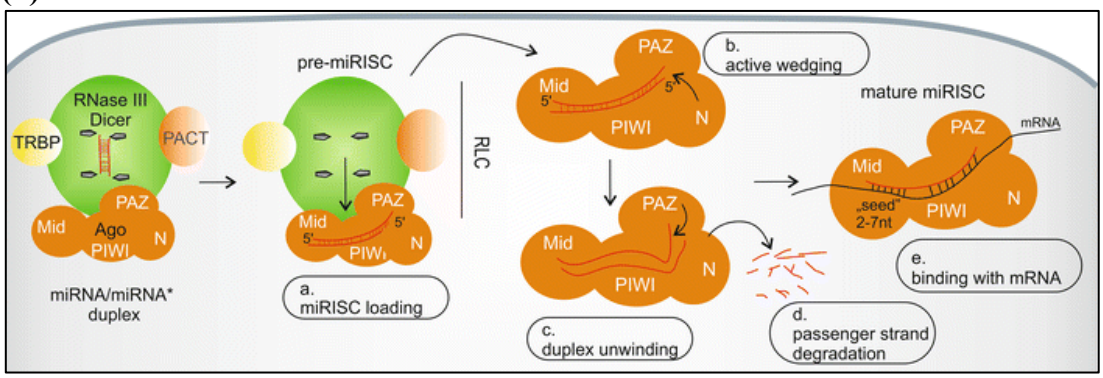

Figure 1.1: Biogenesis of miRNA in human. (a) miRNA genes are first transcribed as primary miRNA (pri-miRNA) by polymerase II. The pri-mRNA is then processed by DROSHA into hairpin precursor miRNA (pre-miRNA). The pre-miRNA is exported from nucleus into cytoplasm by Exportin 5 (Exp5) and then further processed by DICER to form a miRNA/miRNA* duplex. The alternative DROSHA-independent biogenesis pathway (mirtron pathway) is indicated by the orange dashed line. (b) miRNA/miRNA* duplex is then incorporated into miRISC loading complex (RLC). The duplex is unwound and the passenger strand (miRNA*) is degraded. Mature miRNA strand within the miRISC binds to its mRNA target for gene regulation [Taken from (Stroynowska-Czerwinska et al., 2014)].

1.1.3 MicroRNA Regulation

According to computational predictions and genome-wide identification of miRNA targets, each miRNA is estimated to regulate hundreds of different mRNAs, suggesting that more than half of the protein coding genes is modulated by miRNA in human (Friedman et al., 2009). The first mechanism by which miRNA regulates gene expression is through translational repression (Figure 1.2a). Translation repression can occur during the initiation or post-initiation step of translation. miRISC inhibits the initiation of translation by interfering with the recognition of the 5' terminal cap of mRNA by eukaryotic initiation factor 4F (eIF4F) complex and the recruitment of 40S small ribosomal subunit. miRISC can also block the translational initiation by preventing 60S subunit from joining the translational complex and inhibiting 80S ribosomal complex formation. In addition, the miRISC might also repress the translation at post-initiation steps by inhibiting protein elongation. Multiple proteins in the miRISC complex, such as AGO, GW182 and poly(A)-binding protein (PABP), might be involved in the process of translational inhibition, but the exact mechanism of how this complex initiates translation block is currently unknown. The second mechanism of miRNA-mediated gene silencing is through mRNA decay via deadenylation (Figure 1.2b). The deadenylation process is characterised by two phases, which are rapid deadenylation mediated by PAN2-PAN3 and poly(A) tail shortening mediated by CCR4-NOT complex. Following deadenylation, the 5' terminal cap is removed by the decapping complex, DCP1-DCP2 and the mRNA is degraded by cytoplasmic nuclease 5'-3' exoribonuclease 1 (XRN1). Alternatively, targeted mRNA can be directly degraded by 3'-5' cytoplasmic exonuclease without undergoing the decapping process [reviewed in

(Fabian and Sonenberg, 2012; Jonas and Izaurralde, 2015; Milunović et al., 2016; Stroynowska-Czerwinska et al., 2014)].

In humans, partial pairing between miRNA and mRNA target sites is sufficient for gene regulation. It is believed that the most effective mRNA targeting is through seed-match pairing, which is the perfect pairing of the miRNA seed sequence (nucleotide 2 to 7 at the 5' end of miRNA) to the target sites in 3' untranslated region (3'UTR) of mRNA. In some cases, base pairing between the seed sequence in miRNA plus the miRNA nucleotide 8 and the 3'UTR of mRNA has also been observed. Seed-match pairing was believed to be both necessary and sufficient to confer mRNA recognition by miRNA and thus leads to the suppression of gene expression (Bartel, 2009; Voinnet, 2009). Nevertheless, there are a number of studies reporting that miRNA could regulate gene expression without pairing between miRNA seed sequence and 3'UTR of mRNA. For instance, Lytle *et al.* suggested that miRNA could bind to any part of their target mRNA such as the 5'UTR of target mRNA, resulting in repression of gene expression (Lytle et al., 2007). In addition, Grimson *et al.* have demonstrated that mRNA binding sites are present in the 3' end of miRNA (Grimson et al., 2007) and Shin *et al.* have reported the binding sites at the central region of miRNA (Shin et al., 2010). Furthermore, *miR-24* was shown to regulate several genes (*E2F2*, *MYC*, *AURKB*, *CCNA2*, *CDC2*, *CDK4* and *FEN1*) by binding to seedless 3'UTR miRNA recognition elements (Lal et al., 2009) and *miR-146a* regulates murine *Stat1* in the absence of canonical target seed sequences (Lu et al., 2010).

(a)

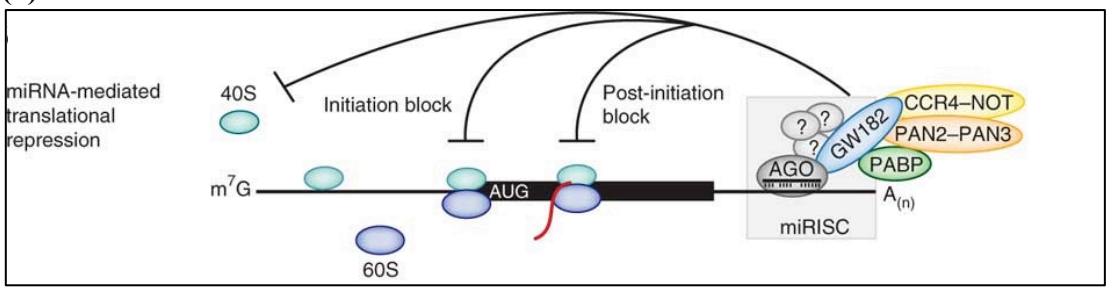

(b)

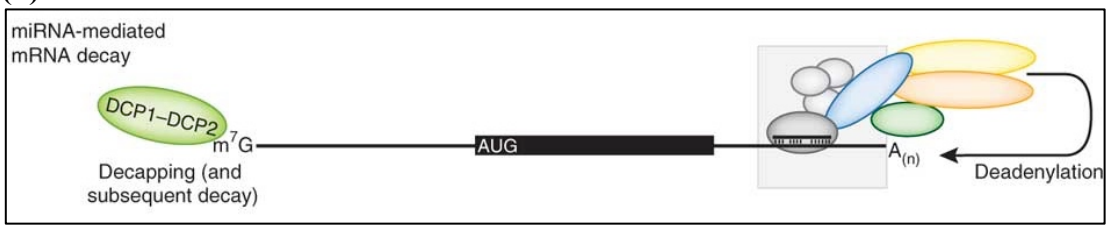

Figure 1.2: The mechanisms of miRNA-mediated gene silencing in human. (a) miRNA-mediated translational repression: the miRISC inhibits translation initiation by interfering with eIF4F-cap recognition and 40S small ribosomal subunit recruitment. Alternatively, miRISC can also inhibit translation at the initiation step by antagonising 60S subunit joining and preventing 80S ribosomal complex formation. The miRISC might also inhibit translation at post-initiation steps by inhibiting ribosome elongation. (b) miRNA-mediated mRNA decay: the miRISC interacts with the CCR4-NOT and PAN2-PAN3 deadenylase complexes to facilitate deadenylation of the poly(A) tail (indicated by $A_{(n)}$). Following deadenylation, the 5' terminal cap (indicated by m^7G) is removed by the DCP1-DCP2 decapping complex, and mRNA decay by the 5'-3' exonuclease, XRN1 [Taken from (Fabian and Sonenberg, 2012)].

1.2 miR-181

1.2.1 Background of *miR-181*

The *miR-181* family is composed of four members, *miR-181a*, *miR-181b*, *miR-181c* and *miR-181d*, which are encoded by three independent paralog precursor transcripts on three separate chromosomes. *miR-181a* and *miR-181b* are located on chromosome 1q32.1 (*miR-181a-1* and *miR-181b-1*) and chromosome 9q33.3 (*miR-181a-2* and *miR-181b-2*), while *miR-181c* and *miR-181d* are located on chromosome 19p13.12 (Figure 1.3). In terms of sequence homology, the mature forms of *miR-181a-1* and *miR-181a-2*, as well as *miR-181b-1* and *miR-181b-2*, are identical. All four members of the *miR-181* family have the same sequence at the 5' seed region (nucleotide 2 to 8), suggesting a significant degree of functional redundancy, but they differ either in the centre or 3' end by no more than four nucleotides (Figure 1.4) (Ji et al., 2009).

Although sequence variations are evident among the four mature *miR-181*s, each *miR-181* is highly conserved among species and each transcript contains two *miR-181* paralogs in most species. In addition, it has been shown that *miR-181a* and *miR-181c* are closely linked, while *miR-181b* and *miR-181d* are closely related (Figure 1.3) (Ji et al., 2009). Albeit the seed region of the four members of *miR-181* family are the same and most of their predicted target genes are overlapping, they might have different functions in different types of cancer (Lin et al., 2013). As reported by Liu *et al.*, the different biological activities of *miR-181a-1* and *miR-181c* are not determined by their mature sequences but largely rely on their unique loop nucleotides (Liu et al., 2008).

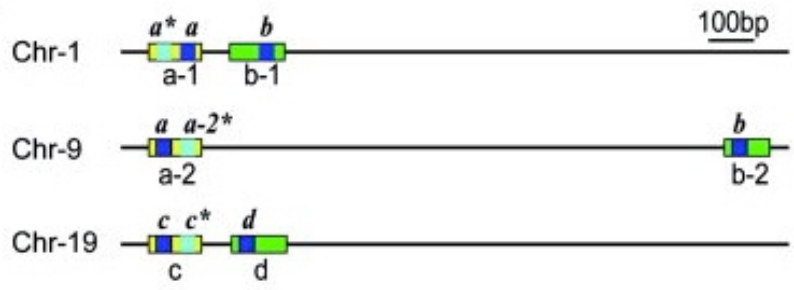

Figure 1.3: Location of *miR-181* family on chromosome. *miR-181a* and *b* are located on chromosome 1 and chromosome 9 while *miR-181c* and *d* are located on chromosome 19. There are two paralog groups of precursor *miR-181*, which are *miR-181a-1*/*a-2*/*c* (yellow) and *miR-181b-1*/*b-2*/*d* (green), suggesting that *miR-181a* is closely linked to *miR-181c* while *miR-181b* is closely related to *miR-181d*. The mature *miR-181*s are indicated by blue boxes [Taken from (Ji et al., 2009)].

miR-181a	5' AACAUUCAACGCUGUCGGUGAGU 3'
miR-181b	5' AACAUUCAUUGCUGUCGGUGGGU 3'
miR-181c	5' AACAUUCAAC - CUGUCGGUGAGU 3'
miR-181d	5' AACAUUCAUUGUUGUCGGUGGGU 3'

Figure 1.4: Mature *miR-181* sequences. The underlined nucleotides show the conserved bases among the four members of *miR-181* family. The red letters indicate the seed sequence.

1.2.2 Role of *miR-181* in Haematopoiesis

There is accumulating data providing evidence for the critical roles of *miR-181* as regulators of the haematopoiesis. Firstly, *miR-181* was suggested to be a positive regulator of B cell differentiation as *miR-181* was found to be preferentially expressed in B lymphoid cells in mouse bone marrow (BM) and its overexpression in haematopoietic stem/progenitor cells (HSPC) resulted in an elevated fraction of B lineage cells both *in vitro* and *in vivo* (Chen et al., 2004a). Besides that, both Lu *et al.* and Choong *et al.* reported that *miR-181a* and *miR-181b* were overexpressed during erythroid differentiation in human umbilical cord blood-derived $CD34^+$ cells (Choong et al., 2007; Lu et al., 2005). Furthermore, Li *et al.* demonstrated that in both K562 cells and human umbilical cord blood-derived $CD34^+$ progenitor cells, *miR-181* overexpression promoted megakaryocytic differentiation by repressing *Lin28* expression, disrupting the *Lin28-Let-7* reciprocal regulatory loop and in turn upregulating *Let-7* (Li et al., 2012a). However, this finding contradicts Garzon *et al.* study where they reported that *miR-181b* and *miR-181c* were downregulated during *in vitro* megakaryocytic differentiation in $CD34^+$ BM progenitors (Garzon et al., 2006). Moreover, *miR-181* family has also been shown to inhibit granulocytic and macrophage-like differentiation in HL-60 cells and $CD34^+$ HSPC (Su et al., 2015). Additionally, *miR-181a* was suggested to regulate molecules that are critical to very early steps in haematopoiesis, blocking the differentiation of all haematopoietic lineages. Using computational analysis, this study predicted that *miR-181a* regulates various genes that are important in erythroid (*MYB*, *CREBBP* and *AGTR2*), myeloid (*ERI-1*, *ETS*, *MEIS-1* and *HOXA5*) and lymphoid (*PU.1*, *MEF*, *SPI-B* and *MYB*) differentiation in $CD34^+$ HSPC. Also, *CXCR4* was found to be modulated by *miR-181a* using a reporter assay (Georgantas et al., 2007). Moreover, *miR-181a* has been

shown to be involved in T cell related immune responses by regulating the T cell receptor (TCR) signalling strength and the sensitivity of T cells to antigens. *miR-181a* was shown to repress the expression of multiple negative regulators in TCR signalling pathway (phosphatases *PTPN22*, *SHP-2*, *DUSP5* and *DUSP6*) and increase the basal level of LCK and ERK activation. This enhances the TCR signalling strength and sensitivity of T cells to antigens, thereby augmenting the TCR-mediated T cell activation (Li et al., 2007). In addition, Cichocki *et al.* demonstrated that *miR-181a* and *miR-181b* promoted the development of natural killer (NK) cells from umbilical cord blood-derived $CD34^+$ haematopoietic progenitor cells and enhanced the NK cell function as shown by increased IFN-γ production in primary $CD56^+$ NK cells. Also, *miR-181a* and *miR-181b* were found to modulate the expression of nemo-like kinase (NLK), an inhibitor of NOTCH signalling, suggesting that *miR-181a* and *miR-181b* promote NK cell development through the regulation of NOTCH signalling pathway (Cichocki et al., 2011). The role of *miR-181* in NK cell development was confirmed later in another study where they showed that *miR-181a/b*-deficient mice exhibited a complete absence of mature NKT cells in thymus and periphery. *miR-181a/b* was subsequently found to modulate the expression of the phosphatase *PTEN*, a regulator of phosphoinositide 3-kinase (PI3K) signalling pathway. *miR-181a/b*-deficient mice were also shown to exhibit other haematological defects including defects in T cell proliferation and development as well as early B cell development, associated with impaired PI3K signalling (Henao-Mejia et al., 2013). Besides that, *miR-181c* has been reported to modulate both T cell activation and proliferation by regulating the expression of *IL-2*. Exogenous overexpression of *miR-181c* reduced the *IL-2* expression, and decreased both the T cell activation and proliferation (Xue et al., 2011).

1.2.3 Differential Expression of *miR-181* in Haematological Malignancies

Due to the crucial roles of *miR-181* in haematopoiesis, it is not surprising that increasing evidence supports the notion of the involvement of *miR-181* in haematological malignancies. There are multiple studies reporting the differential expression of *miR-181* in different types of leukaemia and their potential role in the diagnosis and prognosis of leukaemia and the development of novel therapeutic approaches.

In acute myeloid leukaemia (AML), Debernardi *et al*. found that the expression of *miR-181a* was elevated in M1 and M2 subtypes as compared to the M4 and M5 subtypes in a miRNA expression study of 30 AML samples with normal karyotype (Debernardi et al., 2007). This was then confirmed by Isken *et al.* who observed the same differential expression in 14 normal karyotype AML samples and found *miR-181b* to be overexpressed in AML M1 and M2 subtypes (Isken et al., 2008). These findings were further supported by another more recent study performed by Su *et al.* reporting that *miR-181* family was upregulated in M1, M2 and M3 subtypes of adult AML patients (Su et al., 2015). Moreover, higher *miR-181a* expression has been reported in cytogenetically normal AML (CN-AML) patients with the presence of *CEBPA* mutations, associated with favourable clinical outcomes (Marcucci et al., 2008a). Hickey *et al.* have also shown that in xenograft mouse models, either forced expression of *miR-181a* or lenalidomide treatment significantly inhibited the tumour growth in AML (Hickey et al., 2013). In addition, Butrym *et al.* showed that *miR-181* expression was increased in AML patients as compared to healthy controls. The elevated expression of *miR-181* at diagnosis was positively correlated with better prognosis but negatively correlated with the higher risk of disease relapse (Butrym et al., 2016). In cytogenetically abnormal AML (CA-AML), Li *et al.* showed the

elevated expression of *miR-181* family in CA-AML patients with favourable cytogenetic abnormalities such as t(8;12), inv(16) and t(15;17). On the contrary, downregulation of *miR-181a* and *miR-181b* was observed in CA-AML patients with unfavourable cytogenetic abnormalities such as MLL-rearrangements and this was associated with upregulation of a *HOXA-PBX3* homeobox-gene signature (Li et al., 2012b). Furthermore, reduced expression of *miR-181a* and *miR-181b* has also been found in a molecular subset of high risk CN-AML patients (*FLT3-ITD* positive and/or *NPM1* wild-type) (Marcucci et al., 2008b; Schwind et al., 2010). It was believed that decreased expression of *miR-181* family contributed to the aggressive leukaemia phenotype in high risk CN-AML and the downregulation was inversely correlated with the expression level of proteins involved in the toll-like receptor (TLR) and IL-1β innate immune response pathways (Marcucci et al., 2008b). In another study, Lu *et al.* showed that *miR-181b* was downregulated in human multidrug-resistant leukaemia cells and relapsed/refractory AML patient samples. Ectopic expression of *miR-181b* sensitised these leukaemia cells to cytotoxic chemotherapeutic drugs and promoted drug-induced apoptosis by targeting *HMGB1* (Lu et al., 2014). This finding is consistent with Nanbakhsh *et al.* study where they found that downregulation of *miR-181a* was associated with the acquisition of resistance to daunorubicin and cross-resistance of NK cell-mediated cytotoxicity in AML cell lines (U937 and KG1) through regulation of the tyrosine kinases, MAP3K10 and MAP2K1, and the BCL2 (BCL2 and MCL1) family. Reduced expression of *miR-181a* was also observed in refractory primary AML blasts and overexpression of *miR-181a* in AML blasts attenuated their resistance to daunorubicin and to NK cell-mediated killing (Nanbakhsh et al., 2015). In a more recent study, downregulation of *miR-181* was seen in older AML patients treated

with the hypomethylating drug azacitidine and the lower *miR-181* expression was shown as an independent predictor for good response to treatment and prolonged survival in this patient group (Butrym et al., 2016).

Furthermore, *miR-181* has also been implicated in chronic myeloid leukaemia (CML). Mosakhani *et al*. reported the decreased expression of *miR-181c* in CML patients who are resistant to imatinib as compared to imatinib-responders, suggesting that reduced *miR-181c* expression is associated with imatinib resistance in CML (Mosakhani et al., 2013). A more recent study showed that the expression level of *miR-181a* was significantly reduced in K562 cells and in patients with CML as compared to healthy controls. Overexpression of *miR-181a* in K562 cells inhibited cell growth and induced cell apoptosis and differentiation, in turn enhancing the sensitivity of these cells to imatinib (Wang et al., 2015). This finding is in line with Fei *et al.* who showed that in K562 cells, *miR-181a* overexpression suppressed cell growth, induced G2 arrest and promoted apoptosis by targeting *RALA*, suggesting that *miR-181a* is a tumour suppressor in CML (Fei et al., 2012).

Moreover, differential expression of *miR-181* has also been revealed in acute lymphocytic leukaemia (ALL). *miR-181b* has been found to be upregulated in patients with ALL in a miRNA expression profiling study performed by Zanette and colleagues (Zanette et al., 2007). Besides that, a more recent study reported that *miR-181a* acts as an oncogene in ALL by reducing the expression of tumour suppressor gene, *EGR1*. In this study, they performed miRNA/mRNA expression profiling in 20 ALL patients and observed a negative correlation between *miR-181a* and *EGR1*. Also, overexpression of *miR-181a* in Jurkat T-ALL cells reduced the expression of *EGR1* and enhanced cell proliferation (Verduci et al., 2015).

In addition, dysregulation of *miR-181* has also been demonstrated in chronic lymphocytic leukaemia (CLL). Pekarsky *et al.* showed the downregulation of *miR-181b* in aggressive B cell CLL patients carrying 11q deletion, correlated with increased expression of *TCL1* (Pekarsky et al., 2006). Moreover, reduced expression of *miR-181* family was seen in CLL 17p-aggressive groups (patients carrying 17p deletion received a treatment over time periods ranging from 0 to 24 months) as compared to CLL 17p-indolent groups (patients carrying 17p deletion treated or not in a time longer than 24 months), suggesting that the downregulation of *miR-181* is associated with disease progression in CLL bearing 17p deletion. In contrast, in CLL patients harbouring trisomy 12, increased expression of *miR-181a* was observed and the upregulation was associated with a shorter time interval before treatment, suggesting that the upregulation of *miR-181a* is correlated with more aggressive disease in this group of CLL patients (Visone et al., 2009). Zhu *et al.* reported the downregulation of *miR-181a* and *miR-181b* in CLL patients as compared to healthy controls. The expression levels of *miR-181a* and *miR-181b* were shown to be significantly lower in poor prognosis subgroups of CLL (unmutated *IGHV* gene and *p53* aberrations). The downregulation of *miR-181a* and *miR-181b* was also associated with shorter overall survival and treatment-free survival in CLL patients. Enforced expression of *miR-181a* and *miR-181b* in primary CLL cells from p53 wild-type patients sensitised these cells to fludarabin-induced apoptosis but *miR-181a* and *miR-181b* overexpression in CLL cells from p53-mutant patients did not promote apoptosis, suggesting that apoptosis-inducing effects of *miR-181a* and *miR-181b* may require *p53* activation. *miR-181a* and *b* were also found to regulate anti-apoptosis genes, *BCL-2*, *MCL-1* and *XIAP*, which are characteristically associated with leukaemic cell resistance to chemotherapeutic agents (Zhu et al., 2012).

1.3 WAVE Protein

WAVE protein [Wiskott-Aldrich Syndrome Protein (WASP) Family Verprolin-Homologous Protein] is a member of the WASP family, which are well known as regulators of actin cytoskeletal dynamics (Campellone and Welch, 2010; Padrick and Rosen, 2010; Pollitt and Insall, 2009b). The WASP family consists of eight members, namely WASP, neural-WASP (N-WASP), WAVE1, WAVE2, WAVE3, WASP and WAVE homolog (WASH), junction mediating regulating protein (JMY), and WASP homolog associated with actin, membrane and microtubules (WHAMM) (Campellone and Welch, 2010; Kurisu and Takenawa, 2009). In mammals, there are three isoforms of WAVE, which are WAVE1, WAVE2 and WAVE3 (Suetsugu et al., 1999). WAVE1 and WAVE3 are predominantly expressed in neuronal cells while WAVE2 is ubiquitously distributed (Kurisu and Takenawa, 2009; Oda and Eto, 2013). WAVE proteins are essential in actin polymerisation, which is necessary to carry out diverse roles in physiological and pathological processes, ranging from embryogenesis, tissue morphogenesis and plasticity, pathogen infection, immune cell activation and chemotaxis, to cancer invasion and metastasis (Pollitt and Insall, 2009b; Takenawa and Suetsugu, 2007).

Structurally, the WAVE protein consists of a WAVE/SCAR homology domain (WHD/SHD) at their N-terminal, followed by a basic (B) domain, a proline-rich region (PRR) and a C-terminal VCA (V for verprolin-homology; C for cofilin-homology; A for acidic) domain. At the N-terminal, WAVE protein is constitutively incorporated into a conserved, heteropentameric complex of around 400kDa, named WAVE regulatory complex. The WAVE regulatory complex consists of WAVE1/SCAR (or the orthologs WAVE2 and WAVE3), SRA1/CYFIP1 (or the ortholog PIR121/CYFIP2), NAP1/HEM2/Kette/NAP125/NCKAP1 (or the ortholog

HEM1), ABI1 (or the orthologs ABI2 and ABI3) and BRK1/HSPC300 (Chen et al., 2010; Gautreau et al., 2004). Different WAVE regulatory complex isoforms can be assembled from combinations of different orthologs of each component (Takenawa and Suetsugu, 2007). The WAVE regulatory complex can be viewed as two sub-complexes, a dimer formed by pseudosymmetric association of the two large homologous proteins SRA1 and HEM1, and a trimer formed by the N-terminal of WAVE, ABI and BRK1 forming a four-helix bundle (Chen et al., 2010). It has been shown that the WAVE protein exists in a basal inactive state, where its activity towards the actin-related proteins 2/3 (ARP2/3) complex is inhibited by intracomplex sequestration of the C-terminal VCA domain, in which the VCA region is bound to SRA1 and therefore it is inaccessible for the ARP2/3 complex (Chen et al., 2010; Derivery et al., 2009; Eden et al., 2002; Ismail et al., 2009). In response to upstream signals, the WAVE regulatory complex is recruited to the membrane where it is triggered to release the inhibition, leading to the activation of WAVE protein. The Rho family GTPase, RAC1 was believed to play a crucial role in activation of WAVE proteins by two cooperative mechanisms. Firstly, interaction of the GTP-loaded form of RAC1 with WAVE regulatory complex via SRA1 activates the WAVE protein by allosterically releasing the bound VCA domain (Chen et al., 2010). Second, the proline-rich region of WAVE protein interacts with the SH3 domain of the membrane-associated insulin receptor substrate p53 (IRSp53) and simultaneously, activated RAC1 binds to the RCB (RAC binding)/IMD (IRSp53-MIM homology domain) domain of IRSp53, contributing to the localisation and activation of WAVE proteins (Miki et al., 2000; Suetsugu et al., 2006). Through its basic domain, WAVE proteins bind to acidic phospholipids (phosphatidylinositol (3,4,5)-triphosphate, PIP_3), which enhances its association with membranes (Oikawa et al., 2004). In

addition, the phosphorylation of the WAVE proteins by kinases, such as ABL, CDK5 and ERK2 leads to its activation by destabilising VCA sequestration and its regulation of the association of proteins in the WAVE regulatory complex (Takenawa and Suetsugu, 2007). Hence, the activation of WAVE proteins is a highly cooperative process which requires the simultaneous interaction of WAVE with activated RAC1 and acidic phospholipids, as well as a specific state of phosphorylation of the WAVE proteins achieved by kinases (Chen et al., 2010; Lebensohn and Kirschner, 2009). Following activation, the bound VCA region is released from SRA1 and is now able to carry out actin polymerisation. During actin filament nucleation, the V region at the C-terminal recruits actin monomer (G-actin) to the nascent filaments, while the C and A regions bind ARP2/3 complex, inducing conformational changes in the ARP2/3 complex, in turn promoting production of branched networks of filamentous actin (F-actin) (Goley and Welch, 2006; Takenawa and Suetsugu, 2007). The structure of the WAVE protein and the regulation of its activation are illustrated in Figure 1.5.

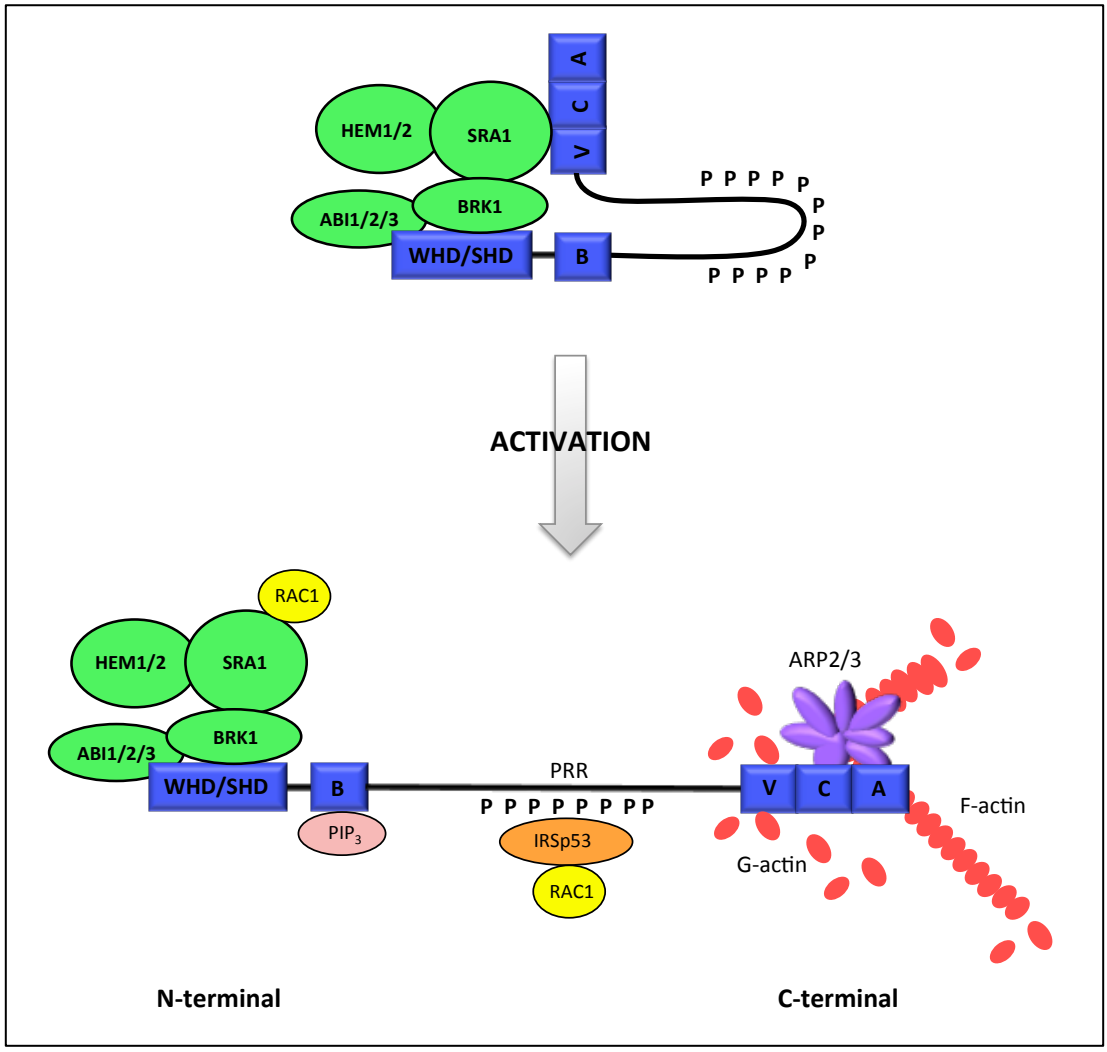

Figure 1.5: The structure of WAVE protein and the regulation of its activation.WAVE protein consists of an N-terminal WAVE/SCAR homology domain (WHD/SHD), followed by a basic (B) domain, a proline-rich region (PRR) and a C-terminal VCA domain. WAVE regulatory complex at its N-terminal consists of WAVE (1, 2 or 3), SRA1, HEM (1 or 2), ABI (1, 2 or 3) and BRK1. The WAVE protein exists in an inactive form where VCA domain is bound to SRA1 protein. The activation of WAVE protein is stimulated by the binding of activated RAC1 to WAVE regulatory complex through SRA1 or to PRR through insulin receptor substrate p53 (IRSp53), the binding of phosphatidylinositol (3,4,5)-triphosphate (PIP_3) to the B domain, and the phosphorylation of WAVE by kinases. Upon activation, VCA domain is released from SRA1 and subsequently, actin monomer (G-actin) is recruited to the V region and ARP2/3 complex is able to bind to the C and A regions. This causes conformational changes in the ARP2/3 complex, thereby promoting actin nucleation to produce filamentous actin (F-actin).

1.3.1 BRK1 – A Component of WAVE Complex

BRK1 (BRICK1, SCAR/WAVE Actin-Nucleating Complex Subunit), a small protein of 9kDa, is located on chromosome 3p25.3 and is a component of the WAVE complex that plays a critical role in actin nucleation (Takenawa and Suetsugu, 2007). BRK1 is the only subunit in WAVE complex for which no paralogous gene has been identified and is also the most conserved subunit in the complex (Derivery et al., 2008). Interestingly, BRK1 is a homotrimer that remains stable as a free sub-complex in the absence of other WAVE regulatory complex subunits (Derivery et al., 2008; Gautreau et al., 2004). This free pool of BRK1 homotrimers dissociate to form monomers before directly binding and stabilising the WAVE and ABI subunits to form a WAVE-ABI-BRK1 heterotrimeric complex. This heterotrimer in turn associates with SRA1-HEM1 dimer, mainly via interaction between BRK1 and conserved surface of SRA1 (Chen et al., 2010; Linkner et al., 2011). Thus, in the assembly of WAVE regulatory complex, BRK1 acts as an adaptor protein to stabilise and coordinate the assembly of the WAVE-ABI-BRK1 heterotrimer and the subsequent binding of WAVE-ABI-BRK1 heterotrimer to SRA1-HEM1 dimer platform (Derivery et al., 2008; Linkner et al., 2011).

Whereas most members of the WAVE complex have been widely studied in recent years, the function of BRK1 is less well understood. The maize *Brk1* orthologue was first shown, by genetic screening, to be responsible for morphologic defects in leaf epithelia due to a recessive mutation (Frank and Smith, 2002). Subsequently, a *Arabidopsis Brk1* mutant was found to cause severe defects in trichome morphogenesis, and the participation of *Brk1* in actin reorganisation in *Arabidopsis* is well documented (Djakovic et al., 2006; Le et al., 2006; Szymanski, 2005). RNA interference studies have suggested similar roles for *Brk1* in *Drosophila* as

knockdown of *Brk1* in cultured *Drosophila* cells resulted in a reduction of cortical F-actin and alterations in cell morphology (Kunda et al., 2003). Additionally, Qurashi *et al.* showed for the first time, in *Drosophila*, that BRK1 is an indispensable component of the WAVE complex and plays an important role in the development of the nervous system. The authors showed that the *Drosophila Brk1* expression profile resembled that of other members in WAVE complex and BRK1 protein was co-immunoprecipated with WAVE and SRA1. Also, in *Drosophila*, *Brk1* mutation as well as mutations in the other WAVE complex subunits led to defects in axonal and neuromuscular junction growth *in vivo* (Qurashi et al., 2007). In *Dictyostelium*, loss of *Brk1* caused reduction in WAVE protein expression and *Wave* mutant-like phenotypes such as slow migration, roundness and lack of large pseudopods were observed (Pollitt and Insall, 2009a).

In humans, it is evident that BRK1 plays a key role in cellular processes that are dependent on actin filaments, such as cell attachment, stretching, endocytosis, cell division and mobility (Li et al., 2014). Depletion of *BRK1* in HeLa cells has been shown to cause defective lamellipodia formation (Derivery et al., 2008; Eden et al., 2002). Furthermore, gene expression profiling of non-small cell lung carcinoma (NSCLC) revealed that *BRK1* is one of the genes upregulated in tumour tissues as compared to adjacent normal tissues (Liu et al., 2007b; Sun et al., 2004). The same group subsequently delineated the exact roles of *BRK1* in the development of NSCLC. They found that suppression of *BRK1* caused actin filament reorganisation, inhibited pseudopodia formation and blocked cell migration in PG NSCLC cell line, suggesting the metastatic role of *BRK1* in the carcinoma (Cai et al., 2009). Moreover, Escobar *et al.* reported that loss of *BRK1* resulted in abnormal actin stress fibre formation and vinculin distribution as well as loss of ARP2/3 and WAVE proteins at

the cellular protrusions. They also showed that downregulation of *BRK1* led to defective directional migration and invasive growth, coupled with reduced proliferation in SN12C and U031 renal cell carcinoma cell lines as well as U2OS osteosarcoma cell line. Interestingly, the authors also revealed that genetic ablation of *Brk1* in mice resulted in dramatic defects in embryo compaction and development, suggesting an essential role for this protein in actin dynamics and cell survival during embryo development (Escobar et al., 2010). In addition, *BRK1* has also been shown to regulate actin dynamics during the processes of neurite outgrowth in human IMR-32 neuroblastoma cell line and primary rat hippocampal neurons as knockdown of *BRK1* increased neurite outgrowth (Wang et al., 2013a).

Strikingly, the clinical relevance of *BRK1* in Von Hippel-Lindau (VHL) syndrome, an autosomal dominant familial cancer syndrome, has been reported by multiple studies. In VHL patients, the *VHL* tumour suppressor gene is partially or completely deleted and thus is predisposed to multiple tumours, primarily of the central nervous system, eyes, adrenals and kidney. The *BRK1* gene is located 30kb downstream of *VHL* on chromosome 3p and large *VHL* gene deletions involving *BRK1* are associated with a significant lower risk of developing tumours. This is due to the compromised proliferation, polarisation and motility in *BRK1*-deficient cells which leads to the inability of the cells to properly support tumour development. On the contrary, retention of the *BRK1* gene is correlated with the development of tumours in VHL patients (Cascón et al., 2007; Franke et al., 2009; Maranchie et al., 2004; McNeill et al., 2009).

1.4 T Cell Activation

T cells play a central role in adoptive immunity, both in cell-mediated cytotoxicity and in the activation of the humoral immune response, and hence it is important to understand how they are activated and regulated. Ligation of TCR to peptide-major histocompatibility complex (peptide-MHC) molecules, either from endogenously encoded self molecules or exogenously encoded pathogen molecules, on antigen presenting cell (APC) is a prerequisite for T cell activation. The mutual recognition of the T cell and APC results in the engagement and clustering of the TCR, and the formation of the T cell-APC interface, known as the immunological synapse. Signalling molecules are recruited to this site, resulting in activation of multiple signalling pathways that lead to calcium flux, gene transcription, actin polymerisation and affinity maturation of integrins, which are all required to initiate and sustain T cell activation (Huang et al., 2013; Manz et al., 2011; O'Donoghue et al., 2013). Interestingly, studies from the past decade suggest that T cell signal transduction is an intricately branching network, rather than a top-down signalling pathway (Brownlie and Zamoyska, 2013).

The TCR consists of a single αβ heterodimer and associates with several immunoreceptor tyrosine-based activation motifs (ITAMs) (γ-chain, δ-chain, ε-chains and ζ-chains) in the CD3 subunits. The recognition of peptide-MHC class I and II by TCR αβ heterodimer is assisted with the co-receptors CD8 and CD4, respectively. The co-receptors bring the SRC family kinase (SFK), LCK which is associated with their cytoplasmic regions, into close proximity to the TCR-associated CD3 and the ζ-chain ITAMs (Artyomov et al., 2010). LCK phosphorylates the tyrosine residues in the ITAMs of TCR-associated γ-chain, δ-chain, ε-chains and ζ-chains, thereby allowing the recruitment and phosphorylation of the SYK family

kinase, ZAP70 (ζ-chain associated protein kinase of 70kDa) (Acuto et al., 2008). The phosphorylation causes conformational changes in ZAP70, which promotes its kinase activity (Deindl et al., 2007), leading to phosphorylation of the transmembrane adapter protein, LAT (linker for the activation of T cell) and the cytosolic adapter protein, SLP76 [SRC homology 2 (SH2) domain-containing leukocyte protein of 76kDa] (Wardenburg et al., 1996; Zhang et al., 1998). The phosphorylated residues of LAT, in turn, recruit multiple downstream adaptors and signalling molecules, allowing assembly of a multiprotein complex called LAT signalosome. The molecules that constitute this complex include SLP76, PLCγ1 (phospholipase Cγ1), GRB2 (growth factor receptor-bound protein 2), GADS (GRB2-related adaptor protein), ADAP (adhesion- and degranulation-promoting adaptor protein), ITK (interleukin-2-inducible T cell kinase), NCK1 (NCK adaptor protein 1) and VAV1 (Vav guanine nucleotide exchange factor 1). This complex plays a pivotal role in propagating the TCR signals into multiple and diverse distal signalling pathways, including the PLCγ1-dependent pathways [diacylglycerol (DAG)- and Ca^{2+}-induced signalling pathways] as well as the cytoskeletal rearrangements and integrin activation pathways (Brownlie and Zamoyska, 2013; Roncagalli et al., 2014).

The major TCR signalling pathways that are PLCγ1-dependent and result from induction of DAG and Ca^{2+} include the NFAT (nuclear factor of activated T cell), the MAPK (mitogen-activated protein kinase) and the NF-κB (nuclear factor kappa-light-chain-enhancer of activated B) signalling. The activation of these three pathways lead to the coordinated mobilisation of transcription factors that are crucial for the expression of genes necessary for T cell growth and differentiation. Following TCR ligation, the phosphorylated LAT and SLP76 form a complex via the

GADS. Phosphorylated SLP76 in turn interacts with PLCγ1, where PLCγ1 is phosphorylated and activated by ITK. Activated PLCγ1 thereby hydrolyses the membrane lipid, Ptdlns(4,5)P_2 (phosphatidylinositol 4,5-bisphosphate) producing second messengers, DAG and IP_3 (Smith-Garvin et al., 2009). The TCR-induced production of DAG results in the activation of two major pathways involving RAS and protein kinase Cθ (PKCθ). RAS, a guanine nucleotide-binding protein, is required for the activation of the serine-threonine kinase RAF-1, a MAPK kinase kinase (MAPKKK), which initiates a MAPK phosphorylation and activation cascade. RAF-1 phosphorylates and activates MAPK kinase (MAPKK), which result in the phosphorylation and activation of ERK1 (extracellular signal-regulated kinase 1) and ERK2. ERK kinase activity leads to the activation of the transcription factor ELK1, which in turn contributes to the activation of AP-1 (activator protein-1) and STAT3 (signal transducer and activator of transcription 3) [reviewed in (Genot and Cantrell, 2000)]. RAS is only active in the GTP-bound state, and it is activated by RAS GEF (RAS guanine nucleotide-exchange factor) and suppressed by GAP (GTPase-activating protein). There are two RAS GEFs present in T cells, which are SOS (son of sevenless) and RASGRP (RAS guanyl nucleotide-releasing protein) (Dower et al., 2000; Ebinu et al., 2000; Egan et al., 1993). RASGRP is inducibly recruited to the membrane through a DAG-binding domain (Ebinu et al., 1998), where it is phosphorylated by PKC (Roose et al., 2005). SOS is constitutively bound to the adapter protein GRB2, and upon TCR stimulation, the GRB2 SH2 domain is recruited to and binds phosphorylated tyrosines on LAT, thereby bringing SOS into the proximal signalling complex, where it can facilitate the localised activation of RAS (Finco et al., 1998). Besides RAS pathway, the second signalling pathway regulated by DAG is mediated by PKCθ, a member of the PKC family that contains

a lipid-binding domain specific for DAG, which is important for recruiting PKCθ to the plasma membrane following T cell activation. One of the critical pathways that PKCθ regulates is NF-κB activation. In resting cells, NF-κB is found in the cytosol associated with inhibitor of NF-κB (IκB) family members that prevent NF-κB translocation into the nucleus. However, following T cell activation, IκB is phosphorylated by the IκB kinase (IKK) complex, ubiquitylated, and degraded, which allows NF-κB to translocate into the nucleus, where it activates genes involved in the T cell function, survival and homeostasis [reviewed in (Schulze-Luehrmann and Ghosh, 2006)]. Apart from DAG, TCR-stimulated PLCγ1 activity also generates IP_3 which stimulates Ca^{2+}-permeable ion channel receptors (IP_3R) on the endoplasmic reticulum (ER) membrane, resulting in the release of ER Ca^{2+} stores into the cytoplasm [reviewed in (Oh-Hora and Rao, 2008)]. TCR signalling induces an increase in the intracellular Ca^{2+} levels, leading to the activation of Ca^{2+} and calmodulin-dependent transcription factors such as MEF2 (myocyte-enhancing factor 2) and DREAM (downstream regulatory element antagonist modulator), as well as signalling proteins, including the phosphatase calcineurin and the CaMK (Ca^{2+}-calmodulin-dependent kinase), that in turn activate a variety of transcription pathways [reviewed in (Savignac et al., 2007)]. Activated calcineurin dephosphorylates members of the NFAT family, which allows them to translocate into the nucleus. In the nucleus, NFAT isoforms form complexes with a variety of transcription factors, thereby integrating signalling pathways, which lead to differential gene expression patterns and functional outcomes, depending on the TCR signal. One of the interaction is between NFAT and AP-1, which integrates Ca^{2+} and RAS signals, resulting in the expression of genes such as *IL-2* that is important for T cell activation (Macián et al., 2002).

In addition to the PLCγ1-dependent pathways, the LAT signalosome also propagates signals that are initiated from TCR ligation, to the integrin activation which promotes cell adhesion, and the actin reorganisation which is essential for T cell activation, proliferation and adhesion. Integrins are αβ heterodimeric receptors that play an important role in mediating cell-cell or cell-matrix adhesion. Integrins that are expressed on T cells include leukocyte function-associated antigen-1 (LFA-1) and very late antigen-4 (VLA-4), which bind to ligands, intercellular adhesion molecule (ICAM) and vascular cell adhesion molecule (VCAM), respectively. They also bind to fibronectin on other immune cells, endothelial cells and fibroblasts, as well as extracellular matrix proteins. Activation of integrins (increasing their affinity and avidity for ligands) is crucial for T cell activation and critically dependent upon the biochemical events initiated by TCR in a process called inside-out signalling (Ménasché et al., 2007). Signalling molecules that are essential for this process include LCK, ZAP70 and SLP76 (Epler et al., 2000), as well as complexes containing RAP1, either RAPL (also known as RASSF5) or RIAM (RAP1-GTP-interacting adaptor molecule, also known as APBB1IP), SKAP55 (SRC kinase-associated phosphoprotein of 55kDa, also known as SKAP1) and ADAP (Hogg et al., 2011; Raab et al., 2010). The phosphorylation of LAT recruits SLP76-VAV1 and ADAP, resulting in the activation of RAP1 and the initiation of signalling to LFA1. The inside-out signals induce a conformational change in LFA-1, increasing its affinity to ICAM1, allowing the formation of stable conjugates, which are required for the prolonged signalling for the full activation of T cell. Besides integrin activation, assembly of LAT signalosome also leads to actin reorganisation in T cells. Following TCR engagement, phosphorylated SLP76 regulates actin polymerisation by bringing the Rho family GTPase exchange factor VAV1, the

adaptor protein NCK1 and actin nucleation-promoting factor (NPF), such as the WASP and WAVE proteins, into close proximity. Rearrangement of the actin cytoskeleton is important in several aspects of T cell activation, including the engagement of TCR (Monks et al., 1998), the formation of immunological synapse (Delon et al., 1998) and its function as a scaffold for the further assembly and stabilisation of signalling complexes (Dustin and Cooper, 2000).

Taken together, the TCR signalling pathways need to be properly coordinated and regulated in order to initiate and sustain T cell activation. An overview of TCR signalling that lead to T cell activation is illustrated in Figure 1.6.

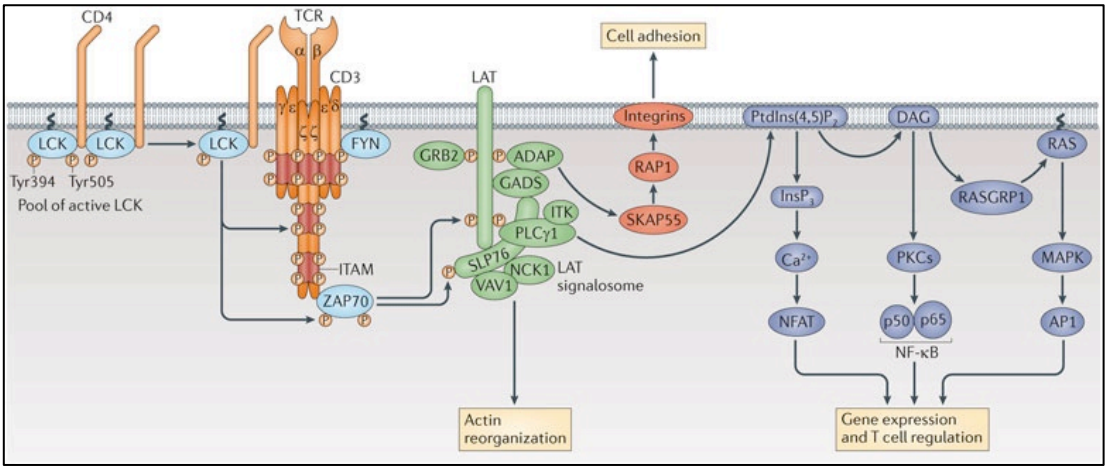

Figure 1.6: Overview of TCR signalling. TCR signal transduction is initiated by the recognition of cognate peptide-MHC molecules. The first molecule to be recruited to the TCR-CD3 complex is the SRC family kinase (SFK) member LCK, which phosphorylates immunoreceptor tyrosine-based activation motifs (ITAMs) of the CD3 γ-chain, δ-chain, ε-chains and ζ-chains. Phosphorylation of the ITAMs enables the recruitment of ZAP70 (ζ-chain associated protein kinase of 70kDa), its phosphorylation by LCK and its activation. Activated ZAP70 phosphorylates four key tyrosine residues on LAT (linker for activation of T cell), which recruits numerous signalling molecules to form a multiprotein complex, termed LAT signalosome. Important molecules that constitute this complex include PLCγ1 (phospholipase Cγ1), GRB2 (growth factor receptor-bound protein 2), GADS (GRB2-related adaptor protein), SLP76 (SH2 domain-containing leukocyte protein of 76kDa), ADAP (adhesion- and degranulation-promoting adaptor protein), ITK (interleukin-2-inducible T cell kinase), NCK1 (NCK adaptor protein 1) and VAV1 (Vav guanine nucleotide exchange factor 1 protein). The LAT signalosome propagates signal branching to three major signalling pathways, NFAT (nuclear factor of activated T cell), MAPK (mitogen-activated protein kinase) and NF-κB (nuclear factor kappa-light-chain-enhancer of activated B), leading to the mobilisation of transcription factors that are critical for gene expression and essential for T cell growth and differentiation. Signals initiated from the TCR through LAT signalosome also result in actin reorganisation and the activation of integrins by inside-out signalling [Taken from (Brownlie and Zamoyska, 2013)].

1.4.1 The Actin Cytoskeleton in T Cell Activation

Reorganisation of the actin cytoskeleton is a requisite event in controlling T cell activation and it is important in multiple aspects of T cell function (Holsinger et al., 1998). To become activated, T cells must first efficiently recognise APC, thereby translating external cues through tightly regulated intracellular signalling pathways, into specific T cell effector responses. Several cellular processes, including cellular polarisation, receptor sequestration and signalling, integrin-mediated adhesion, immunological synapse formation, and releases of cytokines and lytic granules, are required to initiate and sustain T cell activation. All these cellular processes in T cells are dependent upon the lymphocyte cytoskeleton. The actin cytoskeleton controls T cell shape, which changes dramatically depending on whether the cell is circulating in the bloodstream, migrating through tissues, or interacting with APC. At the immunological synapse, actin is likely to provide a scaffold for clustering, translocation and spatial segregation of proteins and signalling molecules, amplifying and sustaining the T cell signalling. Therefore, actin dynamics have been envisaged to participate extensively from the very first step of TCR triggering to the completion of a successful T cell activation, serving as a highly versatile machinery (Billadeau et al., 2007; Burkhardt et al., 2008; Kumari et al., 2014; Yu et al., 2013).

Engagement of the TCR activates multiple actin-regulatory proteins that work together to drive actin polymerisation at the immunological synapse. The primary signalling pathway leading from TCR ligation to actin remodelling involves signalling through LCK and ZAP70, which results in phosphorylation of LAT and SLP76. Phosphorylated LAT and SLP76 in turn serve as a scaffold for other actin-regulatory proteins, PLCγ1, NCK1, ITK and VAV1. These proteins stabilise one another at the sites of TCR engagement, and loss of any of these molecules causes

disruption in actin polymerisation at the immunological synapse (Fuller et al., 2003). PLCγ1 activity leads to calcium mobilisation, which is essential for F-actin remodelling in T cells (Bunnell et al., 2001). VAV1 catalyses the exchange of GDP for GTP on the small Rho GTPases CDC42 and RAC1, thereby activating them (Turner and Billadeau, 2002). GTP-bound CDC42 and RAC1 in turn activate WASP and WAVE respectively, promoting actin polymerisation (Dombroski et al., 2005; Labno et al., 2003).

Accumulation of F-actin at the immunological synapse is the result of TCR-induced activation of multiple actin regulatory and polymerising pathways. The most extensive studied pathway involves the ARP2/3 complex, in which its activation requires interaction with NPF. The ARP2/3 complex, containing two actin-related proteins, ARP2 and ARP3, binds to the side of an existing actin filament, where ARP2 and ARP3 mimic two actin monomers as part of the core nucleus. NPF then binds to the ARP2/3 complex and present an actin monomer, allowing elongation of actin filaments to take place. Suppression of either ARP2 or ARP3 in Jurkat T cells has been shown to impair F-actin polymerisation at the immunological synapse and lamellipodia formation, demonstrating that the ARP2/3 complex and its upstream activators (NPF) are central effectors of actin polymerisation at the immunological synapse (Gomez et al., 2007).

The best-characterised activator of the ARP2/3 complex is WASP, one of the NPF. WASP is recruited to the site of TCR activation through its interaction with the SLP76-associated adapter protein NCK, where it is activated via VAV1-dependent stimulation of the Rho family GTPase CDC42 (Zeng et al., 2003). Several studies showed that T cells from patients with Wiskott-Aldrich syndrome (WAS), an X-linked immunodeficiency disorder resulting from mutations in the *WAS* gene,

exhibits cytoskeletal defects, aberrant morphology and impaired proliferation in response to TCR activation (Calvez et al., 2011; Cianferoni et al., 2005; Molina et al., 1993). Furthermore, it has been shown that T cells from WASP-knockout mice are proliferation deficient in response to antigenic stimulus, have unstable synapses, reduced Ca^{2+} influx and decreased IL-2 production (Cannon and Burkhardt, 2004; Sims et al., 2007; Snapper et al., 1998; Zhang et al., 1999). However, multiple studies have reported that under certain experimental condition, WASP-deficient T cells are still able to polymerise F-actin normally at the immunological synapse, forming conjugates and exhibiting normal TCR-mediated integrin activation (Cannon and Burkhardt, 2004; Krawczyk et al., 2002; Nolz et al., 2006). A possible explanation for these findings is that other proteins, including the close homolog N-WASP, as well as less closely related proteins such as WAVE and haematopoietic cell-specific protein 1 (HS1), might have partially overlapping functions. Interestingly, impairment in T cell development has been observed in mice with both WASP and N-WASP knockout, but T cells develop normally in WASP-knockout mice, suggesting that WASP has a redundant role with N-WASP in T cell development (Cotta-de-Almeida et al., 2007).

The WAVE protein, which similar to WASP, regulates ARP2/3-dependent F-actin remodelling through its VCA region. WAVE protein, activated through VAV1-mediated activation of Rho family GTPase RAC1, has emerged as a central regulator of F-actin polymerisation downstream of the TCR (Burkhardt et al., 2008). WAVE2 has been shown to be required for proper conjugate formation and F-actin accumulation at the immunological synapse (Nolz et al., 2006; Zipfel et al., 2007). WAVE2 has also been implicated in lamellipodia formation and regulation of CRAC-mediated calcium entry (Nolz et al., 2006). In addition, WAVE2 has also

been demonstrated to play a role in IL-2 production (Nolz et al., 2006; Nolz et al., 2008) and the inside-out signalling for activation of integrins in T cells (Nolz et al., 2006; Nolz et al., 2007; Nolz et al., 2008).

WASH, the most recent NPF identified in T cells, localises at the plasma membrane and intracellular vesicles, and regulates endosome-associated ARP2/3 activity (Gomez and Billadeau, 2009). Although T cells derived from WASH-knockout mice showed normal T cell signalling and activation, they showed a reduction in T cell proliferation and impairment in trafficking of TCR. Also, WASH has been shown to regulate T cell endomembrane trafficking via maintenance of actin dynamics at the endosomes (Gomez et al., 2012).

HS1, the haematopoietic lineage-restricted homolog of the actin-binding protein cortactin, functions primarily to stabilise existing branched actin filaments by bridging the ARP2/3 complex with F-actin (Billadeau and Burkhardt, 2006). Studies demonstrated that HS1-deficient T cells show defects in lamellipodia formation and F-actin polymerisation at the immunological synapse as well as impairment in Ca^{2+} influx and T cell proliferation (Gomez et al., 2006; Taniuchi et al., 1995). Although the exact role of HS1 in T cell activation is not clear, existing data indicate that it regulates PLCγ1 dynamics at the immunological synapse. TCR engagement induces ZAP70-dependent tyrosine phosphorylation and ITK-dependent recruitment of HS1 at the immunological synapse. Phosphorylated HS1 in turn interacts with PLCγ1 and regulates its association with F-actin (Carrizosa et al., 2009; Gomez et al., 2006). In addition, phosphorylated tyrosine residues on HS1 also serve as docking sites for VAV1 which stabilises it and leads to actin accumulation at the immunological synapse (Gomez et al., 2006). Moreover, another study reported the interaction

between HS1 and WASP, further supporting the notion of HS1 involvement in actin remodelling in T cells (Dehring et al., 2011).

In addition to pathways that promote actin nucleation in T cells, mechanisms for the negative regulation of F-actin assembly must also concomitantly occur for the cytoskeleton to function dynamically. Accordingly, several studies reported that actin-severing proteins such as cofilin and coronin-1 are important in T cell function. Cofilin has been shown to be crucial in regulating actin dynamics at the immunological synapse. Cell-permeable peptides that block the costimulation-induced cofilin/F-actin interaction in human T lymphocytes blocked T cell proliferation, reduced cytokine (IL-2, IFN-γ, TNF-α, TNF-β, IL-10, IL-4 and IL-13) production, impaired receptor capping and decreased T cell-APC conjugate formation (Eibert et al., 2004). In addition, coronin-1, which binds and inhibits ARP2/3-mediated F-actin polymerisation, has emerged as a regulator of steady-state F-actin formation in T cells. Although T cells from coronin-1-deficient mice showed normal F-actin accumulation at the immunological synapse, these cells exhibited defects in migration and homing in response to chemokines and failed to generate uropod and accumulate talin beneath the membrane on the leading edge. Furthermore, naive T cells from coronin-1-deficient mice also showed increase in apoptosis, coupled with a decreased pool of G-actin which is dependent on the ability of coronin-1 to interact with the ARP2/3 complex (Föger et al., 2006).

Additionally, the large GTPases dynamin-2, recruited by VAV1 to the immunological synapse, has been shown to regulate F-actin reorganisation. Dynamin-2 is able to recruit several actin-regulatory proteins such as the adaptor protein NCK1 and ABI1/2, thereby linking dynamin-2 to WASP- and WAVE-mediated actin dynamics, respectively (Gomez et al., 2005). Moreover, the EZH2

(enhancer of zeste homologue-2) methyltransferase, a VAV1-interacting protein, has also emerged as a regulator of TCR-induced F-actin assembly. A study by Su *et al*. indicated that some of the F-actin regulators might require methylation by EZH2 for their activation (Su et al., 2005). It has also been suggested that the actin-binding adaptor protein HIP55 (haematopoietic progenitor kinase-1-interacting protein of 55kDa) has a role in the regulation of TCR internalisation at the immunological synapse by connecting the TCR to actin and therefore the endocytic machinery (Han et al., 2005; Le Bras et al., 2004).

Collectively, the regulation of F-actin polymerisation and depolymerisation at the immunological synapse is a complex and integrated process. Therefore, the activity of actin dynamics in T cells needs to be tightly controlled for proper T cell activation. The regulation of F-actin polymerisation during T cell-APC interaction is illustrated in Figure 1.7.

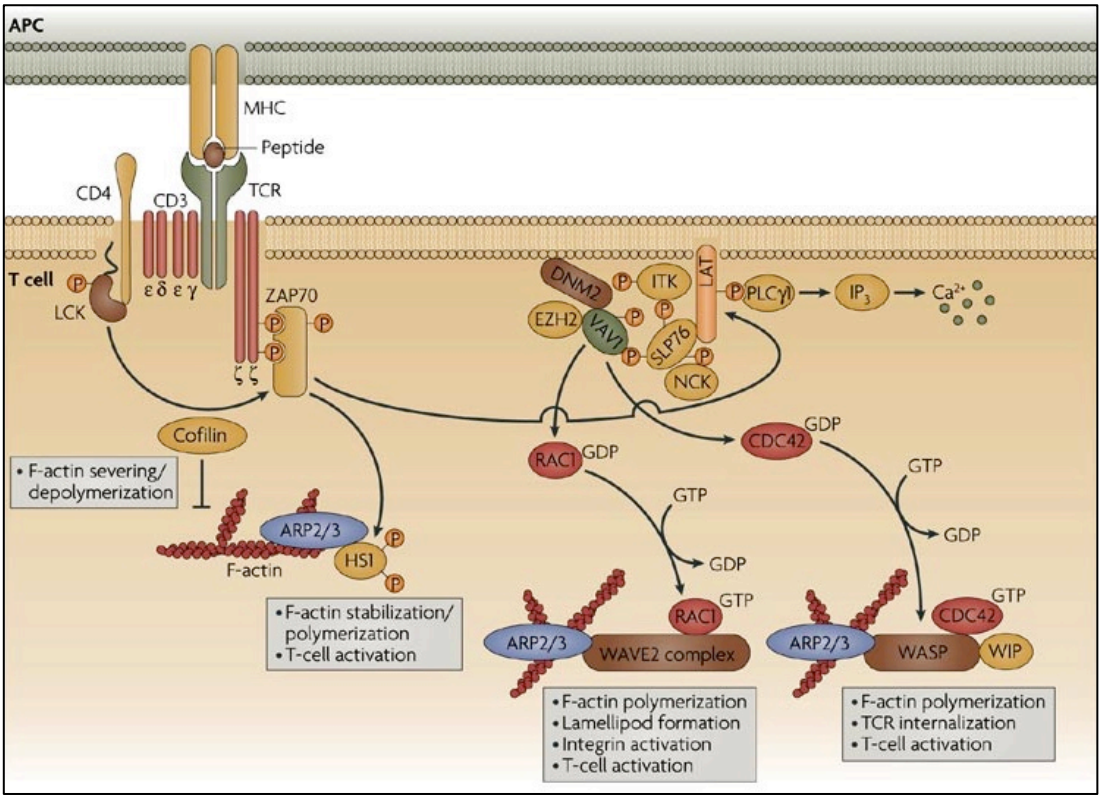

Figure 1.7: Regulation of F-actin polymerisation during the T cell-APC interaction. Following TCR ligation, LCK and ZAP70 are activated. LAT is then phosphorylated by ZAP70 and SLP76 is recruited by LAT. LAT and SLP76 serve as a scaffold for actin-regulatory proteins, PLCγ1, NCK1, ITK and VAV1. PLCγ1 activity leads to calcium mobilisation, which is essential for F-actin remodelling in T cells. VAV1 facilitates the exchange of GDP for GTP on the small Rho GTPases CDC42 and RAC1, thereby activating them. VAV1 might require an interaction with the methyltransferase EZH2 to regulate these GTPases and F-actin polymerisation. GTP-bound CDC42 activates WASP, which is recruited by NCK1. The binding of active CDC42 to WASP releases its auto-inhibition, thereby allowing WASP to polymerise F-actin through its association with the ARP2/3 complex. GTP-bound RAC1 interacts with the WAVE2 complex and is thought to either localise or activate WAVE2-mediated activation of ARP2/3 complex. Moreover, through an interaction with VAV1, dynamin-2 (DNM2) is localised to the immunological synapse where it participates in regulating F-actin reorganisation, and probably influences membrane dynamics and recruitment of additional actin regulators. HS1 is phosphorylated by TCR proximal kinases and stabilises newly generated actin filaments. Cofilin has a role in T cell actin dynamics through F-actin severing and depolymerising activity [Taken from (Billadeau et al., 2007)].

1.5 Myelodysplastic Syndrome

1.5.1 Background of Myelodysplastic Syndrome

Myelodysplastic syndromes (MDSs) are a heterogeneous group of clonal haematopoietic stem cell malignancies. Clinically, MDS patients are characterised by cytopenias, myeloid cell dysplasia and defective haematopoiesis (Adès et al., 2014; Corey et al., 2007; Nimer, 2008). This malignancy is generally associated with hypercellular dysplastic BM, although it can also be normocellular or hypocellular (Corey et al., 2007). If untreated, patients progress toward BM failure and develop fatal haematological complications. Moreover, approximately one-third of MDS patients also develop AML (Adès et al., 2014; Greenberg et al., 1997; Walter et al., 2012). Once thought relatively rare, MDS represents the most common haematological malignancies in the elderly (Corey et al., 2007).

1.5.2 Classification and Prognostic Scoring Systems of Myelodysplastic Syndrome

The World Health Organisation (WHO) classification system is currently used for stratification of the MDS patients. The WHO classification was developed in 2002 according to the previous classification system, French-American-British (FAB), 1982 (Vardiman et al., 2002). According to the WHO classification system, MDS patients can be grouped into eight categories based on their biological, genetic and morphological features (Table 1.1).

To predict the prognosis of MDS, the International Prognostic Scoring System (IPSS) was developed on the basis of findings in 816 patients with primary MDS (Greenberg et al., 1997). The IPSS relies on the primacy of blood cytopenias, cytogenetic abnormalities and percentage of blasts in BM as prognostic variables. The IPSS divides patients into four different risk groups: low, intermediate-1, intermediate-2 and high (Table 1.2).

In 2012, the IPSS was revised (IPSS-R) to address several limitations in the IPSS (Greenberg et al., 2012). Although IPSS-R retained the three basic IPSS parameters, which are cytopenias, cytogenetic abnormalities and percentage of BM blasts, it applied more specific cytogenetic subgroups where the rare abnormalities were included and the deletion of 7q was segregated from loss of whole chromosome 7. Also, IPSS-R segregated the <5% BM blast category into two groups, 0 - 2% and >2 - <5%, and the grouping of all patients with >10% blasts into the same category. In addition, it also separated cytopenias into haemoglobin, platelet count and absolute neutrophil count rather than based on the number of cytopenias, and categorised patients into five rather than four different risk groups: very low, low, intermediate, high and very high.

Table 1.1: WHO Classification of MDS (Vardiman et al., 2002)

Disease	Blood Findings	Bone Marrow Findings
Refractory anaemia (RA)	Anaemia No or rare blasts	Erythroid dysplasia only < 5% blasts < 15% ringed sideroblasts
Refractory anaemia with ringed sideroblasts (RARS)	Anaemia No blasts	Erythroid dysplasia only < 5% blasts ≥ 15% ringed sideroblasts
Refractory anaemia with multilineage dysplasia (RCMD)	Cytopenias (bicytopenia or pancytopenia) No or rare blasts No Auer rods < 1 x 10^9/L monocytes	Dysplasia in ≥ 10% of cells in two or more myeloid cell lines < 5% blasts No Auer rods < 15% ringed sideroblasts
Refractory anaemia with multilineage dysplasia and ringed sideroblasts (RCMD-RS)	Cytopenias (bicytopenia or pancytopenia) No or rare blasts No Auer rods < 1 x 10^9/L monocytes	Dysplasia in ≥ 10% of cells in two or more myeloid cell lines < 5% blasts No Auer rods ≥ 15% ringed sideroblasts
Refractory anaemia with excess blasts-1 (RAEB-1)	Cytopenias < 5% blasts No Auer rods < 1 x 10^9/L monocytes	Unilineage or multilineage dysplasia 5% to 9% blasts No Auer rods
Refractory anaemia with excess blasts-2 (RAEB-2)	Cytopenias 5% to 19% blasts Auer rods ± < 1 x 10^9/L monocytes	Unilineage or multilineage dysplasia 10% to 19% blasts Auer rods ±
MDS unclassified (MDS-U)	Cytopenias No or rare blasts No Auer rods	Unilineage dysplasia in granulocytes or megakaryocytes < 5% blasts No Auer rods
MDS associated with isolated del(5q)	Anaemia < 5% blasts Platelets normal or increased	Normal to increased megakaryocytes with hypolobulated nuclei < 5% blasts No Auer rods Isolated del(5q)

Table 1.2: IPSS for MDS (Greenberg et al., 1997)

(a) IPSS: Prognostic Variables

Prognostic Variable	Score				
	0	**0.5**	**1.0**	**1.5**	**2.0**
BM blasts (%)	<5	5-10	-	11-20	21-30
Cytogenetics*	Good	Intermediate	Poor	-	-
Cytopenias	0/1	2/3	-	-	-

*Good: normal, -Y, del(5q), del(20q); poor: complex (≥3 abnormalities) or chromosome 7 anomalies; intermediate: other abnormalities
- indicates not applicable

(b) IPSS: Risk Group and Clinical Outcomes

Risk Group	**Total Score**	**Median Survival (years)**	**25% AML Evolution (years)**
Low	0	5.7	9.4
Intermediate-1	0.5-1.0	3.5	3.3
Intermediate-2	1.5-2.0	1.2	1.1
High	≥2.5	0.4	0.2

1.5.3 Pathogenesis of Myelodysplastic Syndrome

To date, the exact mechanisms for the pathogenesis of MDS remains to be fully elucidated, owing to the heterogeneity and complexity of the disorder. However, MDS has been shown to be caused by several factors, which include cytogenetic abnormalities, genetic mutations, epigenetic alterations, immune dysregulation and miRNA dysregulation.

Cytogenetic abnormalities are major determinants of the pathogenesis, diagnosis and prognosis in MDS in addition to their importance in the selection of treatment for individual patients. Cytogenetic abnormalities are commonly observed in MDS, which have been demonstrated in approximately 50% of *de novo* MDS patients and 80% of therapy-related MDS cases. Unbalanced chromosomal abnormalities involving loss or gain of genetic materials are commonly seen in MDS patients while balanced abnormalities including translocations, inversions and insertions are less common (Garcia-Manero, 2015; Haase, 2008; Haase et al., 2007; Schanz et al., 2012). As MDS progresses, increased cytogenetic abnormalities are observed which is accompanied by the malignant transformation into AML (Greenberg et al., 1997). The three most common cytogenetic defects in MDS are del(5q), trisomy 8 and monosomy 7/ del(7q), with good, intermediate and poor prognosis, respectively (Greenberg et al., 1997; Haase, 2008; Haase et al., 2007).

Over the past decade, the development of single nucleotide polymorphism (SNP) array analysis and next generation sequencing has led to new insights into the genetic basis of MDS. According to recent large cohort studies of MDS, 72 - 90% of MDS patients carried at least one mutation, with an average of three per cases (Cazzola et al., 2013; Haferlach et al., 2014; Papaemmanuil et al., 2013). Although over 60 genes have recently been identified to be mutated in MDS, only six genes, *TET2*, *SF3B1*,

ASXL1, *SRSF2*, *DNMT3A* and *RUNX1*, are found to be consistently mutated in 10% or more of MDS patients (Cazzola et al., 2013; Haferlach et al., 2014; Kulasekararaj et al., 2013). Genes that are commonly mutated in MDS are involved in pathways important in epigenetic regulation (*TET2*, *DNMT3A*, *IDH1*, *IDH2*, *ASXL1* and *EZH2*), transcriptional regulation (*RUNX1*, *BCOR*, *ETV6*, *SETBP1* and *GATA6*), tumour suppressor (*TP53*), signal transduction (*JAK2*, *CBL*, *NRAS*, *FLT3*, *KIT* and *CSNK1A1*), RNA splicing machinery (*U2AF1*, *SRSF2*, *SF3B1* and *ZRSR2*) and the cohesin complex (*STAG1*, *STAG2*, *SMC3* and *RAD21*) [reviewed in (Kulasekararaj et al., 2013; Pellagatti and Boultwood, 2015; Zhang et al., 2015)].

Furthermore, accumulating evidence suggests that the alterations in the immune system play an important role in the pathogenesis of MDS. Immune dysregulation has been implicated in the defective haematopoiesis seen in MDS, owing to an abnormal susceptibility to apoptosis in haematopoietic precursors and limited responsiveness of these cells to growth factors (Ganan-Gomez et al., 2015). In accordance to this, many MDS patients seem to benefit from immunosuppressive therapy (Olnes and Sloand, 2011). Dysregulation of the expression and secretion of multiple cytokines has been reported in MDS including TNF-α, TRAIL, IFN-γ, TGF-β, IL-4, IL-6, IL-10 and IL-7 (Serio et al., 2014). Moreover, in MDS, cytotoxic ($CD8^+$) and helper ($CD4^+$) T cells are activated by MHC molecules on malignant MDS stem cells, which leads to T cell expansion in both peripheral blood (PB) and BM, in turn suppressing haematopoiesis [reviewed in (Glenthøj et al., 2016)]. In addition, the TLR signalling pathway is hyperactive in MDS, attributed to the upregulation of activators including *MYD88*, *TIRAP*, *IRAK1/4* and *TRAF*, coupled with the downregulation or allelic deletion of inhibitory factors such as *miR-145* and *miR-146a*. The TLR signalling activates NF-κB and MAPK pathways which

in turn induces the transcription of pro-inflammatory cytokines (Ganan-Gomez et al., 2015; Starczynowski et al., 2010). It has also been demonstrated that the immunosuppressive capacity of mesenchymal stem cells (MSC) is decreased in MDS patients and these cells failed to efficiently inhibit dendritic cell maturation in low risk MDS patients, suggesting that the functionality of MSC is altered in MDS and may favour the expansion of cytotoxic T cells in the early stages of the disease (Wang et al., 2013b). Intriguingly, Chen *et al.* demonstrated that myeloid-derived suppressor cell (MDSC), a group of inflammation-associated immature cells, are markedly expanded in the local BM of MDS patients. Increased numbers of MDSC causes defective myeloid and erythroid differentiation, coupled with reduction in T cell proliferation and functionality, as well as induces the secretion of suppressive cytokines including IL-10 and TGF-β, and inflammatory intermediates such as reactive oxygen species (ROS), arginase, cytokines and inducible nitric oxide synthase (iNOS), thereby inducing DNA instability and promoting the emergence of mutant MDS clones (Chen et al., 2013).

Additionally, a recent genomic analysis of AML and MDS cell lines found that approximately 77% (542 out of 706) of miRNAs are located in regions of leukaemia-associated cytogenetic changes, and 18% (99 out of 542) of these miRNAs are relevant in myeloid malignancies (Starczynowski et al., 2011). Moreover, miRNAs are essential regulators of the differentiation and development of haematopoietic stem cells (Georgantas et al., 2007; Liao et al., 2008). Therefore, alterations of miRNA could affect proliferation and differentiation of haematopoietic stem cells, contributing to the pathogenesis of haematological malignancies, including MDS (Lujambio and Lowe, 2012). There are several reviews summarising the findings of multiple studies on the differential expression of various miRNAs and the expression

pattern of specific miRNAs in MDS (Kuang et al., 2016; Milunović et al., 2016; Rhyasen and Starczynowski, 2012). Interestingly, there is only little overlap seen in the dysregulated miRNAs in MDS and the comparison between studies is difficult. This discrepancy might be due to different approaches, sample sources and size of patient cohorts used. As summarised in a review by Rhyasen *et al*., out of the 80 dysregulated miRNAs (30 downregulated and 50 upregulated miRNAs) in MDS, only 17 were commonly identified by more than a single study and only five of the miRNAs were common to four studies (Rhyasen and Starczynowski, 2012). However, progress has been made in our understanding of the involvement of miRNA dysregulation in the pathogenesis of MDS, but more extensive research is needed to clarify the role of this complex mechanism in MDS.

1.5.4 Differential Expression of *miR-181* in Myelodysplastic Syndrome

Aberrant expression of *miR-181* in MDS has been reported in several recent studies. Overexpression of *miR-181a* has been reported in advanced MDS patients and also their downregulation in early MDS cases. Besides that, the authors showed that the expression level of *miR-181a* increased steadily from healthy controls to MDS to AML (Pons et al., 2009). Furthermore, it has been shown that the four members of the *miR-181* family (*miR-181a*, *miR-181b*, *miR-181c* and *miR-181d*) are significantly upregulated in high risk MDS patients as compared with low risk patients. In addition, a decreased survival was observed in patients with elevated expression of *miR-181* in low risk MDS patients when compared to patients without increased *miR-181* levels. These findings indicate the pathogenetic overlap between high risk MDS and AML (Sokol et al., 2011). In a more recent study, interestingly, *miR-181a* has been shown to be downregulated in MSC from MDS patients when compared with normal controls (Santamaría et al., 2012).

1.6 Large Granular Lymphocytic Leukaemia

1.6.1 Background of Large Granular Lymphocytic Leukaemia

Large granular lymphocytic leukaemia (LGL leukaemia) embodies a spectrum of rare clonal lymphoproliferative disorders, which involve inappropriate expansion of large granular lymphocytes (LGLs), either cytotoxic T lymphocytes or NK cells (Lamy and Loughran, 2011; Watters et al., 2011). LGL leukaemia is an indolent disorder with good prognosis and characterised by cytopenia with neutropenia the most common, resulting in an increased frequency of bacterial infection (Loughran, 1993). LGL leukaemia is frequently associated with a wide array of autoimmune disorders such as rheumatoid arthritis (RA), pure red cell aplasia (PRCA) and immune thrombocytopenic purpura (ITP), as well as BM failure syndromes including aplastic anaemia (AA) and MDS (Bareau et al., 2010; Dhodapkar et al., 1994; Go et al., 2000; Kwong and Wong, 1998; Lamy and Loughran, 2011; Sauntharajah et al., 2001).

In 1985, the term LGL leukaemia was first introduced as a disorder involving clonal invasion of the PB, BM and spleen (Loughran et al., 1985). In 1993, the distinction between $CD3^+$ T cell and $CD3^-$ NK cell lineage subtypes of LGL (T-LGL and NK-LGL respectively) leukaemia was proposed (Loughran, 1993). In 1999, the WHO classification included T cell and NK cell LGL leukaemia in the mature peripheral T cell neoplasms subgroup (Harris et al., 1999). In 2008, a provisional entity of chronic NK cell lymphoproliferative disorder (CLPD-NK) was created by the WHO to separate it from the more aggressive NK-cell leukaemia (Swerdlow et al., 2008). The types of LGL leukaemia with their clinical features are shown in Table 1.3.

Table 1.3: Types of LGL Leukaemia (Steinway et al., 2014)

Type	Median Age	Clinical Features	Marker
T-LGL, indolent	60	Asymptomatic OR Symptomatic with - Neutropenia - Anaemia - Thrombocytopenia - Recurrent bacterial infections Autoimmune conditions - Rheumatoid arthritis - Pure red cell aplasia - Immune thrombocytopenic purpura	$CD3^+$ $CD8^+$ $CD16^+$ $CD56^-$ $CD57^+$ $TCR\alpha\beta^+$ (10% are $TCR\gamma\delta^+$)
T-LGL, aggressive (rare)	41	Cytopenias Acute B-symptoms Hepatosplenomegaly	$CD3^+$ $CD8^+$ $CD57^+$
CLPD-NK	39	Similar to T-LGL, indolent Less prevalent autoimmune disease	$CD3^-$ $CD16^+/CD56^+$ $CD57^+$
Aggressive NK-cell Leukaemia	58	Fulminant B symptoms Cytopenias Hepatosplenomegaly	$CD3^-$ $CD16^+$ $CD56^+$ $CD57^+$ EBV^+

1.6.2 Pathogenesis of Large Granular Lymphocytic Leukaemia

The understanding of the pathogenesis of LGL leukaemia is pivotal as it contributes to the development of drugs to combat the dysregulation of the disease. Several studies have demonstrated that LGL leukaemia is associated with dysregulation of the survival and apoptosis pathways including the Fas and Fas ligand (FasL), the interleukin-15 (IL-15), the platelet-derived growth factor (PDFG), the PI3K-AKT, the sphingolipid, the NF-κB, the RAS/MEK/ERK, and the JAK/STAT signalling pathways (Table 1.4) [reviewed in (Steinway et al., 2014; Zhang and Loughran, 2012)]. More recently, somatic mutations in the SH2 dimerisation and activation domain in the *STAT3* gene have been found to be associated with LGL leukaemia, further supporting the importance of STAT3 signalling in the pathogenesis of this disorder (Koskela et al., 2012).

Table 1.4: Known Dysregulated Signalling Pathways in LGL Leukaemia (Steinway et al., 2014; Zhang and Loughran, 2012)

Signalling Pathway	Function of Signalling Pathway	Dysregulation in LGL Leukaemia
Fas-FasL	Mediates apoptosis of activated CTL	Fas-FasL machinery is blocked by soluble Fas that is elevated in patient sera and is capable of blocking Fas-mediated cell death of leukaemia LGLs
IL-15	Promotes survival of T and NK cells	IL-15 prevents apoptosis of leukaemic LGLs by enhancing degradation of Bid, a critical apoptotic factor; higher level of soluble IL-15Rα may lower the IL-15 response threshold in leukaemic LGL cells
PDGF	Regulates cell growth and division	Elevated PDGF regulates long-term survival of leukaemic LGL cells through PI3K-AKT and MER/ERK pathways
PI3K-AKT	Promotes cell proliferation, survival and cancer progression	PI3K-AKT signalling is constitutively activated in T-LGL leukaemia, due to overactive Src family kinases, which leads to inhibition of pro-apoptotic signalling, promoting survival of T cells
Sphingolipid rheostat	Determines cell fate	Pro-apoptotic ceramide is decreased and anti-apoptotic sphingosine-1-phospshate (S1P) is elevated. S1P receptor 5 is overexpressed in leukaemic LGLs
NF-κB	Plays critical role in haematopoiesis and survival of immune cells	NF-κB has been shown to be activated in leukaemic LGLs downstream of AKT and promotes the expression of anti-apoptotic BCL-2 proteins
RAS/MEK/ERK	Regulates cell proliferation and differentiation in response to various growth factors	RAS and ERK are constitutively activated in NK-LGL leukaemic cells
JAK/STAT	Regulates cell proliferation, survival and immune response	Persistent activation of *STAT3* in LGL leukaemia; somatic activating mutations in the SH2 dimerisation and activation domain in the *STAT3* gene in 30-40% of NK and T-LGL patients

LGL: large granular lymphocyte; CTL: cytotoxic T lymphocyte

1.7 Association of Myelodysplastic Syndrome with T Cell Large Granular Lymphocytic Leukaemia

Clonal proliferations of T cell large granular lymphocytes (T-LGLs) have been documented in patients with BM failure syndromes including AA (Go et al., 2000), paroxysmal nocturnal hemoglobinuria (PNH) (Boyer et al., 2015; Karadimitris et al., 2001; Lamy and Loughran, 1999; Risitano et al., 2005) and MDS (Dhodapkar et al., 1994; Huh et al., 2009; Sauntharajah et al., 2001).

It is noted that clonal T-LGL proliferation associated with MDS is not uncommon and the coexistence of T-LGL and MDS has been reported by several studies. Dhodapkar and colleagues identified five patients with T-LGL and concomitant MDS out of 68 patients with T-LGL (Dhodapkar et al., 1994). Subsequently, Sauntharajah *et al.* described nine patients with coexistence of T-LGL and MDS (Sauntharajah et al., 2001). In addition, Huh *et al.* reported nine patients with T-LGL who also had MDS (Huh et al., 2009). Although the coexistence of T-LGL and MDS is rare, it seems likely that the simultaneous occurrence of T-LGL and MDS may be causally related rather than a chance event. Sauntharajah *et al.* have proposed two possible mechanisms of the association of T-LGL with MDS. Firstly, T-LGL might arise from a clonally rearranged MDS stem cell or alternatively, the T-LGL could represent an autoimmune response to an antigen presented by normal or MDS marrow cells (Sauntharajah et al., 2001). It has been suggested that T-LGL proliferation may have pathogenic roles in the development of cytopenias in MDS, in which the expanded cytotoxic $CD8^+$ T cells suppress the autologous progenitor cell growth *in vitro* (Molldrem et al., 1997). This is supported by a report which showed that a subgroup of MDS patients responded to immunosuppressive treatment with cyclosporine or anti-thymocyte globulin (ATG) (Sauntharajah et al., 2001). Several studies have reported the favourable factors in MDS patients associated with T-LGL,

which include BM hypocellularity, presence of HLA-DR15 expression, younger age, lower platelet count and blast percentage, and shorter duration of transfusion requirement (Epling-Burnette et al., 2007; Molldrem et al., 2002; Sauntharajah et al., 2002; Sauntharajah et al., 2003; Zhang et al., 2016). Nonetheless, the clinicopathological features as well as the prognostic and predictive value of the presence of T-LGL proliferation in MDS patients is still unclear and no treatment guideline has been established so far for these patients.

1.8 Project Aims

The *miR-181* family has been shown to be important in haematopoiesis including T cell development, differentiation, proliferation and activation, and hence its aberrant expression has been implicated in haematological malignancies. Therefore, the aim of this study was to identify biologically relevant targets of the *miR-181* family members using a functional assay, developed in-house (Gäken et al., 2012). We identified and validated one of the targets of *miR-181c* which was BRK1, a component of the WAVE complex that regulates actin polymerisation. Given the importance of *miR-181* family in T cell functions and the potential roles of BRK1 in the involvement of the WAVE complex and the regulation of actin dynamics in T cells, this study was subsequently aimed to delineate the influence of the *miR-181c*-BRK1 axis in T cell functions. In addition, as multiple studies reported the aberrant expression of the *miR-181* family in MDS and various leukaemia, we also aimed to investigate the expression level of *miR-181c* and its target BRK1 in MDS patients associated with T-LGL leukaemia.

2 Chapter 2 – Methods

2.1 PCR and Gel Electrophoresis

2.1.1 Design of Primers for miRNA Target Identification Functional Assay

The miRNA primers (for *miR-181a*, *miR-181b*, *miR-181c* and *miR-181d*) were designed based on the primary sequences which were obtained from miRBase web resource (http://www.mirbase.org/). The obtained miRNA sequences were aligned against human genomic DNA database in NCBI Nucleotide Blast (https://blast.ncbi.nlm.nih.gov/Blast.cgi) to obtain the complementary genomic region and sequences of approximately 4kb covering the miRNA sequences was selected. These selected sequences were further used to design primers using Primer 3 Software (http://primer3.ut.ee/). Primers amplifying *miR-181a*, *miR-181b*, *miR-181c/d* were designed, producing PCR products ranging from 600bp to 800bp in size. *miR-181c* and *miR-181d* were amplified by one pair of primers as they are located close to each other on chromosome 19. Restriction enzyme sites were incorporated in front of the primer sequences to facilitate the subsequent cloning experiments. Restriction sites were selected by using NEBcutter V2.0 (http://nc2.neb.com/NEBcutter2/) based on the criteria that there should be no internal restriction site in the PCR products. Sequences of the primers are listed in Appendix B1. Oligonucleotide primers were dissolved in nuclease free water to give a stock concentration of 100µM and stored at -20°C.

2.1.2 Standard PCR

PCR was carried out using GoTaq® Hot Start Colourless Master Mix (Promega) or DreamTaq PCR Master Mix (Thermo Scientific) and PCR reaction composition was set up as shown in Table 2.1. PCR reactions were run on a programmable thermal cycler (Applied Biosystems), with standard cycling conditions as shown in Table 2.2.

Table 2.1: Standard PCR Reaction Composition

Reagent	**Concentration**	**Volume (µl)**
Template DNA	10-100ng/µl	-
Go Taq or DreamTaq Master Mix	2×	10
Forward primer	10µM	0.2
Reverse primer	10µM	0.2
Nuclease free water	-	(up to 20µl)
Total	-	**20**

Table 2.2: Standard PCR Cycling Condition

Stage	**Temperature (°C)**	**Duration**	**Number of Cycle**
Initial Denaturation	95	2 min	1
Denaturation	95	30 sec	25-40
Annealing	As appropriate for the primers used	30 sec	
Extension	72	1 min	
Final Extension	72	5 min	1
Incubation	4	Infinity	1

2.1.3 Agarose Gel Electrophoresis

PCR products and other nucleic acid samples were separated by electrophoresis on a 0.8-1.0% agarose gel (Sigma-Aldrich) prepared in 100ml of 1× Tris Acetate-EDTA (TAE) buffer (Sigma-Aldrich), with 0.08mg/ml ethidium bromide (Sigma-Aldrich). 6× DNA Gel Loading Dye (Thermo Scientific) was added to the samples to give 1× final concentration and 10µl was loaded for electrophoresis. 5µl of Gene Ruler DNA Ladder Mix (Thermo Scientific) was run in parallel with samples as a marker to determine the size of the samples. Gels were run in 1× TAE buffer at 120V for 30-45 min and visualised under UV illumination using Syngene Gene Flash Bio Imaging Gel Documentation System.

2.1.4 Gel Extraction and Purification

Gel extraction and purification were carried out using QIAEX II® Gel Extraction Kit (Qiagen). In brief, DNA bands were excised from agarose gel with a clean, sharp scalpel under UV illumination. Three volumes of Buffer QX1 and 10µl of QIAEX II beads were added to the excised gel fragment and incubated at 50°C for 10 min to solubilise the agarose and bind the DNA. The tube was vortexed every 2 min to keep QIAEX II beads in suspension. The sample was then centrifuged for 1 min and supernatant was carefully removed with a pipette. After that, the pellet was washed once with 500µl Buffer QXI to remove residual agarose contaminants and twice with 500µl Buffer PE to remove residual salt contaminants. The pellet was air-dried for 15-30 min until it turns white. To elute DNA, the dried pellet was resuspended with 20µl of nuclease free water and incubated at room temperature for 5 min. Finally, the suspension was centrifuged at full speed for 1 min and the supernatant containing the purified DNA was carefully transferred to a clean tube. Purified DNA bands were stored at -20°C.

2.2 Cloning

2.2.1 Restriction Enzyme Digestion

Restriction enzyme digestion was carried out in a reaction containing 2µl of 10× NEB buffer (1, 2, 3 or 4; New England Biolabs), 0.5µl of restriction enzyme (5-10U; New England Biolabs), 2µl of 10× bovine serum albumin (BSA; when needed; New England Biolabs), 300-1000ng of DNA and nuclease free water in a total volume of 20µl. When two restriction enzymes were used simultaneously in a digestion reaction, the buffer indicating maximum activity for both enzymes was used or else a single digest was carried out initially with the enzyme requiring the lowest salt concentration followed by a second digest in the same mixture with the other

enzyme. 1M NaCl solution was added to adjust the concentration to the optimal salt concentration for the second enzyme digestion step. The reactions were incubated at 37°C or 50°C (depending on restriction enzyme) for 1 to 2 hours and heat inactivation of enzymes was carried out at 65°C for 20 min. Digested plasmid DNA was then analysed by agarose gel electrophoresis.

2.2.2 TOPO Cloning

TOPO cloning was performed using TOPO® TA Cloning® Kit, Dual Promoter, with pCR®II-TOPO® Vector (Life Technologies; vector map see Appendix A1). TOPO cloning was carried out in a reaction consisting 0.5-2µl of insert, 0.5µl of TOPO vector, 0.5µl of salt (200mM NaCl, 10mM $MgCl_2$) and nuclease free water in a total volume of 3µl and incubated at room temperature for 10 min followed by bacterial transformation.

2.2.3 Ligation

Ligations were performed with a vector:insert ratio of 1:1, 1:2 or 1:3, with 1µl of 400U T4 DNA ligase (New England Biolabs), 1µl of 1× ligase buffer (New England Biolabs) and nuclease free water in a total volume of 10µl. Reactions were either incubated at room temperature for 1 to 2 hours or at 4°C overnight. A vector only ligation was also performed as a control.

2.2.4 Transformation of Chemically Competent *E. coli*

Transformations were performed using One Shot® TOP10 Chemically Competent *E. coli* (Life Technologies). 25µl of cells were mixed with 1µl of ligation mixture and incubated on ice for 30 min. Reactions were then heat shocked at 42°C for 30 sec and returned to ice for a further 2 min before the addition of 400µl SOC medium (Life Technologies) and incubated at 37°C for an hour. 100µl of the cells were then

plated on LB agar plates containing 50µg/ml of carbenicillin (Bioline) and incubated at 37°C overnight. For blue-white screening, 50µl of 20mg/ml X-Gal (Melford) was spread on the surface of the LB agar prior to plating the transformed bacterial cells.

2.2.5 Small Scale Plasmid DNA Preparation

Bacteria from a single colony were cultured overnight in 2ml of LB broth, supplemented with 50µg/ml carbenicillin, at 37°C in a shaking incubator (200rpm). Bacterial cultures were pelleted for 5 min and plasmid DNA was extracted using Wizard® *Plus* SV Minipreps DNA Purification System (Promega) according to the manufacturer's instructions. In brief, cells were resuspended in 250µl of Cell Resuspension Solution before lysing in 250µl of Cell Lysis Solution and 10µl of Alkaline Protease Solution. After 5 min, the lysis reaction was stopped by the addition of 350µl Neutralization Solution. Protein and chromosomal DNA precipitate was pelleted (full speed, 10 min) and cleared supernatant was applied to a DNA binding Spin Column (full speed, 1 min). Columns were subsequently washed with 750µl of Wash Solution (full speed, 1 min) and again with 250µl of Wash Solution (full speed, 2 min). The plasmid DNA was then eluted from the column with 100µl of nuclease free water (full speed, 1 min) and stored at -20°C.

2.2.6 Large Scale Plasmid DNA Preparation

A starter culture was set up by culturing a single bacterial colony for 6-8 hours in 5ml of LB broth supplemented with 50µg/ml of carbenicillin, at 37°C with shaking. The starter culture was then diluted 1:500 or 1:1000 in 150ml of LB broth supplemented with 50µg/ml of carbenicillin and cultured for 12-16 hours at 37°C with shaking. The overnight culture was pelleted (5000×g, 10 min) and plasmid DNA was then extracted using GenElute™ HP Plasmid Maxiprep Kit (Sigma-Aldrich) according to the manufacturer's instructions. In brief, bacterial cells were

resuspended in 12ml of Resuspension Solution before lysing with 12ml of Lysis Solution at room temperature for 3-5 min. The lysis reaction was stopped with 12ml of chilled Neutralization Solution. 9ml of Binding Solution was added, mixed and the solution was poured into a filter syringe and was allowed to sit for 5 min to precipitate the protein. During the 5 min incubation, a GenElute HP Maxiprep Binding Column was placed into a 50ml collection tube and 12ml of Column Preparation Solution was added to the column and then centrifuged at 3000×g for 2 min. Half of the cleared lysates was expelled into the binding column by holding the filter syringe barrel over the binding column and gently applying pressure to the plunger and then centrifuged at 3000×g for 2 min. The rest of the cleared lysate was processed similarly. Columns were washed with 12ml of Wash Solution 1 (3000×g, 2 min) and with 12ml of Wash Solution 2 (3000×g, 5 min). The plasmid DNA was eluted with 3ml of Elution Solution (3000×g, 5 min). The plasmid solution was filter sterilised (0.2μm), aliquoted under sterile conditions and stored at -20°C.

2.3 Sanger Sequencing

Sanger sequencing was performed using BigDye® Terminator Cycle v3.1 Sequencing Kit (Applied Biosystems). Cycle sequencing was first carried out to amplify the insert on a programmable thermal cycler (Applied Biosystems). 300ng of plasmid DNA was used as template DNA and two reactions (one with forward primer and another with reverse primer; primer details see Appendix B5) were carried out for each plasmid DNA sample in order to obtain both forward and reverse sequences for each sample. The reaction composition and cycling protocol are shown in Table 2.3 and Table 2.4.

Table 2.3: Reaction Composition for Cycle Sequencing

Reagent	**Volume (µl)**
Plasmid DNA (300ng)	x
5× Sequencing Buffer	2
BigDye® Terminator v3.1 Ready Reaction Mix	0.5
Sequencing Primer (5ng/µl)	1
Nuclease free water	(up to 10µl)
Total	**10**

Table 2.4: Cycling Protocol for Cycle Sequencing

Stage	**Temperature (°C)**	**Time**	**Number of Cycle**
1	96	1 min	1
2	96	10 sec	15
	55	5 sec	
	60	1.15 min	
3	96	10 sec	5
	55	5 sec	
	60	1.30 min	
4	96	10 sec	5
	55	5 sec	
	60	2 min	
5	4	Infinity	1

After cycle sequencing, purification of the extension products was carried out using BigDye® XTerminator™ Purification Kit (Applied Biosystems) with shaking at 2000rpm for 30 min. The reagents used are shown in Table 2.5.

Table 2.5: Reagents for Purification of Extension Products in Sanger Sequencing

Reagent	**Volume (µl)**
Extension products from cycle sequencing	10
XTerminator™ solution	10
SAM™ solution	45
Total	**65**

Capillary electrophoresis was then performed on an ABI 3130XL Genetic Analyzer with appropriate run module selected in the Data Collection software. Results were analysed using ABI Sequencing Analysis 5.2 software and the sequences obtained were blast analysed using NCBI Nucleotide Blast.

2.4 Tissue Culture

2.4.1 Culture of Adherent Cell Lines

Adherent cell lines (MCF7, HeLa, HepG2, 293T and NIH/3T3) were cultured in Dulbecco's Modified Eagle medium (DMEM) (Life Technologies) supplemented with 10% foetal bovine serum (FBS; Sigma-Aldrich) and 1% L-Glutamine-Penicillin-Streptomycin solution (Sigma-Aldrich), under humidified conditions at 37°C in 5% CO_2. To passage and harvest the cells, DMEM medium was removed and an appropriate amount of 1× TrypLE^{TM} Express Enzyme (Life Technologies) was added, followed by incubation at 37°C for 5 min to detach the cells. The cell suspension was then centrifuged (300×g, 5 min) and the pellet was resuspended in an appropriate volume of medium and cells were either counted, seeded for expansion or collected for experiments.

2.4.2 Culture of Suspension Cell Lines

Suspension cell lines (Jurkat, K562, KG-1 NB-4, THP-1 and U937) were cultured in Roswell Park Memorial Institute (RPMI) 1640 medium (Life Technologies) supplemented with 10% FBS (Sigma-Aldrich) and 1% Penicillin-Streptomycin solution (Sigma-Aldrich), under humidified conditions at 37°C in 5% CO_2. Cells were passaged and harvested as described above but without trypsinisation.

2.4.3 Isolation of Peripheral Blood Mononuclear Cells and Primary T Cells

Isolation of peripheral blood mononuclear cells (PBMCs) from leukocyte cones was carried out by density gradient centrifugation using Ficoll Histopaque (Sigma-Aldrich). Blood sample from leukocyte cone was diluted with PBS containing 2% FBS up to a total of 40ml. The solution was slowly layered on top of the same volume of Ficoll Histopaque and then centrifuged at 560×g for 30 min. The interphase layer, which contains the PBMC, was carefully removed and washed with 50ml of PBS (400×g, 5 min). Washing steps were repeated twice with 50ml of 2% FBS in PBS (200×g, 5 min). Cells were counted and either cryopreserved in liquid nitrogen for future use, stimulated and cultured in the presence of IL-2 to obtain a primary T cell population, or $CD3^+$ T cells were isolated.

Isolated PBMC were stimulated with 1µg/ml of anti-human CD3 (clone OKT3; eBioscience) and anti-human CD28 (clone 28.2; eBioscience), cultured in X-Vivo^{TM}15 medium (Lonza) supplemented with 2% human AB serum (Sigma-Aldrich) in the presence of 100U/ml recombinant human IL-2 (Peprotech) for 48 hours. After stimulation and culture in the presence of human IL-2, the cell population consists mainly of T cells.

Alternatively, $CD3^+$ T cells were isolated from PBMC using Dynabeads® Untouched^{TM} Human T Cell Kit (Life Technologies). Briefly, isolated PBMC (5×10^8 cells) were resuspended in 5ml of ice-cold 2% FBS in PBS and 1ml of antibody mix (5µl of 1mg/ml HLA-DR antibody, Abcam was added) was added and incubated on roller at 4°C for 20 min. The cells were then washed with 9ml of 2% FBS in PBS (500×g, 8 min) and resuspended in 45ml of 2% FBS in PBS with 5ml of pre-washed Dynabeads® (Dynabeads® was washed twice with 5ml of 2% FBS in PBS). After incubation on roller at room temperature for 15 min, the tube was placed on a

magnetic stand for 2 min and the supernatant containing the untouched human T cells were collected and pelleted (200×g, 5 min). Cells were then resuspended in 1ml of supplemented X-Vivo^{TM}15 medium (Lonza) and proceeded to cell counting for subsequent experiments.

2.4.4 Culture of Primary T Cells

Primary T cells were cultured in X-Vivo^{TM}15 medium (Lonza) supplemented with 2% human AB serum (Sigma-Aldrich) and 100U/ml recombinant human IL-2 (Peprotech), under humidified conditions at 37°C in 5% CO_2. Cells were passaged and harvested as described in suspension cell lines above.

2.4.5 Counting of Cells

Cell suspensions were mixed with Trypan Blue (Lonza) in a 1:1 ratio and 10µl of the mixture was loaded onto Haemocytometer (Neubauer cell counting chamber, depth 0.1µl). For PBMC cell counting, 1% acetic acid was also added to lyse the erythrocytes. Only live unstained cells from four corner squares were counted and the cell number per ml was determined with the following calculation.

Cell Number/ml = Average Cell Count from 4 Squares × 10^4 × Dilution Factor

2.4.6 Cryopreservation of Cells

Suspension and adherent cell lines were resuspended in RPMI 1640 and DMEM freezing medium (containing 10% DMSO and 20% FBS) respectively at a density of 2×10^6 cell/ml in 2ml cryogenic vials. For PBMC and primary T cells, cells were resuspended in Synth-a-Freeze® Cryopreservative Medium (Life Technologies) at a density of 10×10^6 cell/ml. The cryogenic vials were frozen at -80°C in a Freezing Container (Nalgene Mr Frosty) overnight and then transferred to liquid nitrogen for long term storage.

2.5 Cell Transfection

2.5.1 Stable

Stable transfection of cells with plasmid DNA (pBabePuro expressing miRNA) were carried out by nucleofection using either Amaxa® Cell Line Nucleofector® Kit V (Lonza) or Ingenio® Electroporation Kit (Mirus Bio LLC). 2×10^6 cells (MCF7, HeLa or Jurkat T cells) were pelleted and resuspended in 100µl of nucleofection (Lonza) or electroporation (Mirus Bio LLC) solution and 2µg of plasmid DNA was added. The solution was transferred to a cuvette and electroporated using a cell line specific program on the Nucleofector II device (Lonza). The programs used were P-020 for MCF7, I-013 for HeLa and X-001 for Jurkat T cells. The transfected cells were immediately transferred to tissue culture flasks or plates depending on cell number and experimental requirements and allowed to recover for 48 hours. Selection for stable transfected cells was done with appropriate antibiotics based on the selectable marker present in the plasmid (2µg/ml of puromycin, InvivoGen; 500µg/ml of zeocin, InvivoGen; or 12µM of ganciclovir, InvivoGen) for 10-15 days when cells were harvested for subsequent analysis.

2.5.2 Transient

Transient transfection of cells with siGENOME small interfering RNA (siRNA) against *BRK1* (Dharmacon) or miRIDIAN miRNA hairpin inhibitors (Dharmacon) were performed by nucleofection as in the stable transfection described above. Sequences of siRNA and miRNA inhibitors are detailed in Appendix C2. 100nM of siRNA or miRNA inhibitors was used and transfected cells were cultured in 6-well plates before harvesting for further analysis at relevant time points (24h, 48h, 72h, 96h or 120h).

2.6 Short Hairpin RNA Lentivirus Production and Transduction

2.6.1 Oligonucleotide Annealing and Construction of pLKO.1-shBRK1 Plasmid

Long, complementary oligonucleotides encoding sequences of short hairpin RNA (shRNA) against *BRK1* (details in Appendix C) (Wang et al., 2013a) were annealed to create double stranded DNA molecules for cloning into the pLKO.1-TRC cloning vector (Addgene; vector map see Appendix A4). shBRK1 oligonucleotides were annealed by mixing 5µl of 20µM forward oligo, 5µl of 20µM reverse oligo, 5µl of 10× NEB buffer 2 and 35µl of nuclease free water. The mixture was incubated in a beaker with boiling water (98°C) and left to cool slowly to room temperature (2-3 hours). The annealed double stranded oligonucleotides had appropriate overhangs was cloned into pLKO.1-TRC cloning vector.

2.6.2 Lentivirus Production

shRNA lentivirus were generated by co-transfection of human embryonic kidney cell line HEK293T with four plasmids, pMDG (envelope plasmid encoding VSV-G), pRRE (packaging plasmid encoding Gag & Pol), pREV (packaging plasmid encoding REV) and the shRNA plasmids (pLKO.1-shBRK1_1, pLKO.1-shBRK1_2 or pLKO.1-scrambled shRNA) using Calcium Phosphate Transfection Kit (Life Technologies). 293T cells were seeded at a density of 1×10^7/1000cm in five layer flasks (T1000 flasks, Millipore) using DMEM medium supplemented with 10% FBS and 1% L-Glutamine-Penicillin-Streptomycin solution. The cells were incubated overnight at 37°C in 5% CO_2. Four plasmids mixture containing pMDG (55µg), pRRE (91µg), pREV (45µg) and pLKO.1-shRNA (182µg) were mixed and diluted to a total volume of 3.96ml with nuclease free water. 540µl of 2M $CaCl_2$ was then added to the mixture. Subsequently, the mixture was added drop wise to 4.5ml of 2× HEBS while vortexing and incubated at room temperature for 30 min in a total

volume of 9ml. The 9ml solution was mixed with 150ml of supplemented DMEM medium, added to the 293T cells in T1000 flasks and incubated for 16 hours at 37°C in 5% CO_2. The medium was replaced with 180ml of fresh supplemented DMEM medium and incubated at 37°C for a further 24 hours after which the supernatants containing the lentivirus were harvested and stored at 4°C. 100ml of fresh supplemented DMEM medium was added to the flasks and incubated for another 24 hours. The supernatant was again harvested and pooled with the 24 hours harvest. The pooled supernatant containing the lentivirus was concentrated by centrifugation at 8000rpm overnight at 6°C. The pellets were resuspended in 500µl of Opti-MEM®I Reduced Serum Medium (Life Technologies) and then aliquoted and stored at -80°C.

2.6.3 Lentivirus Titration

Titration of lentivirus (pLKO.1-scrambled shRNA, pLKO.1-shBRK1_1 and pLKO.1-shBRK1_2) was carried out by colony formation assay. HeLa cells were seeded at a density of 5×10^4/0.5ml per well in supplemented DMEM medium in 24-well plates. After 24 hours, 0.1, 0.01, 0.001 and 0.0001µl (which corresponds to a final concentration of 10^{-4}, 10^{-5}, 10^{-6} and 10^{-7} ml) of lentivirus were added to the HeLa cells in triplicate, supplemented with 8µg/ml of polybrene (Sigma-Aldrich). After 24 hours incubation, 0.5ml of fresh supplemented DMEM medium was added to dilute the lentivirus. 5µg/ml of puromycin (InvivoGen) was added after 24 hours and cells were selected for 15 days when the cells were washed with HEPES buffer solution (Life Technologies) and stained with Commassie Blue. The colonies were counted and lentivirus titre was calculated using following equation.

$$\text{Colony Forming Units/ml (CFU/ml)} = \text{Number of Colony} / \text{Final Concentration of Lentivirus Added}$$

2.6.4 Lentivirus Transduction

Cells were seeded in 24-well plates at a density of 6×10^5 (Jurkat T cells) or 1×10^6 (anti-CD3/CD28 stimulated primary T cells) per well in 1ml of culture medium (supplemented RPMI 1640 medium for Jurkat T cells; X-Vivo^{TM}15 medium supplemented with 10% AB serum and 100U/ml IL-2 for primary T cells). Lentivirus with a multiplicity of infection (MOI) of 24 for Jurkat T cells and MOI of 50 for primary T cells was added to the cells and supplemented with 4µg/ml of polybrene (Sigma-Aldrich). The plates were centrifuged at 800×g for 45 min at 32°C and incubated overnight. The next day, the plates were replaced with fresh supplemented culture medium. 2µg/ml of puromycin (InvivoGen) was added after 24 hours and selected for 5-15 days when the cells were harvested for further functional analysis. MOI of lentivirus used for transduction was calculated with the following equation.

Multiplicity of Infection (MOI) = Infectious Units (IFU) / Cell Number

Infectious Units/ml (IFU/ml) = CFU/ml × Volume of Lentivirus Used

2.7 DNA and RNA Extraction

2.7.1 Genomic DNA Extraction

Genomic DNA was extracted from cells using Quick-gDNA™ MiniPrep Kit (Zymo Research) according to the manufacturer's instructions. In brief, cells were pelleted (500×g, 5 min) and lysed with 500µl of Genomic Lysis Buffer for 5-10 min at room temperature. The cell lysate was added to a Zymo-Spin™ Column (10000×g, 1 min), the column was washed with 200µl of DNA Pre-Wash Buffer and 500µl of g-DNA Wash Buffer (10000×g, 1 min). DNA was eluted with 50µl of DNA Elution Buffer or water, incubated for 2-5 min at room temperature and spun for 30 sec. Eluted genomic DNA was stored at -20°C.

2.7.2 RNA Extraction with TRIzol

Total RNA was extracted from cells using TRIzol reagent (Life Technologies). 0.5-1×10^6 cells were pelleted and resuspended in 500µl of TRIzol reagent before adding 200µl of chloroform (Sigma-Aldrich) and mixing vigorously for 15 sec. After incubation for 2-3 min at room temperature, the sample was centrifuged at 12000×g for 15 min at 4°C and the upper colourless aqueous phase was carefully recovered in a fresh tube and mixed with 500µl of isopropanol (Sigma-Aldrich) and incubated for 10 min at room temperature to precipitate RNA. Following centrifugation at 12000×g for 10 min at 4°C, the pellet was washed with 1ml of 75% ethanol (7500×g, 5 min, 4°C) and air-dried. The RNA was resuspended in 25-50µl nuclease free water and stored at -80°C.

2.7.3 RNA Extraction with RNeasy Micro Kit

Total RNA was extracted from primary T cells using RNeasy® Micro Kit (Qiagen) according to the manufacturer's instructions. In brief, 5×10^5 cells were pelleted (300×g, 5 min), and disrupted and homogenised with 350µl of Buffer RLT by vortexing vigorously. Cell lysates were precipitated with 350µl of 70% ethanol and applied to RNeasy MinElute spin column (8000×g, 15 sec). Columns were washed with 350µl of Buffer RW1 (8000×g, 15 sec) and DNA contamination was removed by adding 80µl of DNase I incubation mix (10µl DNase I stock solution + 70µl Buffer RDD) directly to the column membrane and incubating at room temperature for 15 min. Columns were subsequently washed with 350µl of Buffer RW1 (8000×g, 15 sec), 500µl of Buffer RPE (8000×g, 15 sec) and 500µl of 80% ethanol (8000×g, 2 min) before 'dry' spinning the columns for 5 min to ensure all residual buffer was removed. RNA was eluted from the column with 14µl of RNase free water (full speed, 1 min) and stored at -80°C.

2.7.4 Nucleic Acid Quantification

DNA and RNA samples were quantified using a NanoDrop 8000 Spectrophotometer (Thermo Scientific). 1.5µl of neat sample was pipetted onto the Nanodrop pedestal which directly measures and calculates the concentration in ng/µl. The ratio of absorbance at 260nm and 280nm is used to assess the purity of DNA and RNA. A ratio of approximately 1.8 is generally accepted as "pure" for DNA while 2.0 as "pure" for RNA. If the ratio is appreciably lower in either case, it may indicate the presence of protein, phenol or other contaminants that absorb strongly at or near 280nm.

2.8 Quantitative Real Time PCR (qPCR)

2.8.1 qPCR – Probe Based Detection

First strand cDNA synthesis was performed using SuperScript® VILO™ cDNA Synthesis Kit (Life Technologies). Total RNA was used to prepare cDNA in 10µl reaction consisting of 500ng of RNA, 2µl of 5× Reaction Mix and 1µl of 10× Superscript Enzyme. The reaction was incubated at 25°C for 10 min and 42°C for 2 hours when the reaction was stopped by heat inactivating the reverse transcription (RT) enzyme at 85°C for 5 min. All cDNA samples were stored at -20°C.

Probe based detection qPCR was then carried out using the FastStart Universal Probe Master (ROX; Roche Diagnostics) and Universal Library Probes (Roche Diagnostics), according to the manufacturer's instructions. In brief, PCR reaction consisting 5µl of 1:50 diluted cDNA, 10µl of FastStart Universal Probe Master (ROX), 1µl of 20µM primer mix, 0.25µl of 25µM gene specific probe (primer and probe details in Appendix B3) and 3.75µl of nuclease free water was prepared in triplicate in MicroAmp^{TM} Fast Optical 96-Well Reaction Plates (Life Technologies). Reactions were run on a StepOnePlus Real-Time PCR machine (Applied

Biosystems) using the following cycling conditions: 95°C for 10 min; then 40 cycles of 95°C for 15 sec and 60°C for 1 min.

2.8.2 qPCR – DNA Dye Based Detection

Reverse transcription (RT) of miRNA was carried out using Universal cDNA Synthesis Kit II (Exiqon). Total RNA was used to prepare cDNA in 10µl reaction consisting of 100ng of RNA, 2µl of 5× Reaction Buffer and 1µl of Enzyme Mix. The reaction was then incubated at 42°C for an hour before the reaction was stopped by heat inactivating the RT enzyme at 95°C for 5 min. All cDNA samples were stored at -20°C.

DNA dye based detection qPCR was then carried out using ExiLENT SYBR® Green Master Mix (Exiqon) according to the manufacturer's instructions. In brief, PCR reaction consisting 4µl of 20× diluted cDNA, 5µl of PCR Master Mix and 1µl of miRNA specific primer mix (details in Appendix B4) was prepared in triplicate in MicroAmp™ Fast Optical 96-Well Reaction Plate (Life Technologies). Reactions were run on a StepOnePlus Real-Time PCR machine (Applied Biosystems) using the following cycling condition: 95°C for 10 min; then 40 cycles of 95°C for 10 sec and 60°C for 1 min. Melting curve analysis was included.

2.8.3 qPCR Analysis – Relative Quantification

Fluorescence signals were first normalised to that of the passive reference dye ROX™, included within the PCR master mix, to give a reporter normalised (Rn) value for each cycle of the reaction (no reference dye in DNA dye based detection). Next, a baseline signal was determined to account for background fluorescence and the Rn values baseline corrected to give ΔRn values. Finally, amplification curves were plotted using log (ΔRn) against cycle number and a threshold ΔRn value set to

intersect the exponential (or geometric) phase of the curves. The point of intersection determines the threshold cycle (Ct) number which is used as the basic measure of relative target concentration within the PCR. The Ct values for experimental and control samples were then used in subsequent calculations to achieve relative target quantification. Relative quantities were determined using the comparative Ct method described by Applied Biosystems. The amount of target was normalised to the *GAPDH* (probe based detection), *miR-103a* (DNA dye based detection, as recommended by Exiqon) or U6 (DNA dye based detection) reference and calculated relative to a designated calibrator sample using only Ct values in the mathematical formula $2^{-\Delta\Delta Ct}$ as follows.

$\Delta\Delta Ct = \Delta Ct_{target} - \Delta Ct_{calibrator}$

$\Delta Ct_{target} = Ct_{target} - Ct_{reference}$

$\Delta Ct_{calibrator} = Ct_{calibrator} - Ct_{reference}$

Relative quantity = $2^{-\Delta\Delta Ct}$

2.9 Immunoblotting

2.9.1 Protein Extraction

Whole cell protein extracts were prepared using Radio-Immunoprecipitation Assay (RIPA) Lysis Buffer (Santa Cruz Biotechnology) containing 1× TBS, 1% Nonidet P-40, 0.5% sodium deoxycholate, 0.1% SDS and 0.004% sodium azide (NaN_3), supplemented with 10µl of 200mM phenylmethylsulfonyl fluoride (PMSF) solution, 10µl of 100mM sodium orthovanadate solution and 10µl of protease inhibitor cocktail solution. Cell pellets were lysed with 100µl of 1× RIPA lysis buffer and incubated on ice for 30 min. Cellular debris was pelleted (300×g, 5 min, 4°C) and supernatant containing the protein lysates were stored at -80°C.

2.9.2 Protein Assay

Protein concentrations were measured using DC™ Protein Assay (Bio-Rad) according to the manufacturer's instructions. BSA Protein Standard II (Bio-Rad) was used to create a standard curve by serial dilution from 1.4 to 0.175mg/ml. 5µl of BSA standards and 1:10 diluted protein lysates were first mixed with 25µl of working reagent A (20µl of reagent S has been added to each ml of reagent A), then 200µl of reagent B and incubated at room temperature for 15 min. Colour change was measured by absorbance at 750nm on a microplate reader (BioTek ELx808) and protein concentration was calculated against the standard curve.

2.9.3 Western Blotting

Protein samples (typically 15-20µg) were prepared by addition of 1× NuPAGE® LDS Sample Buffer (Life Technologies) and 10% 1M dithiothreitol (DTT; Sigma-Aldrich), and denatured at 100°C for 5 min. Samples were then loaded alongside a Spectra™ Multicolor Broad Range Protein Ladder (Thermo Scientific) on NuPAGE™ Novex™ 4-12% Bis-Tris Protein Gel (1.0 mm; 10, 12 or 15 wells; Life Technologies) and run at a constant voltage of 200V for 40-50 min in 1× NuPAGE® MES SDS Running Buffer (Life Technologies). To transfer proteins from the gel to a PVDF membrane, the gel was placed under an immunoblot PVDF membrane (Bio-Rad) and then sandwiched between blot paper (Bio-Rad) and nylon pads. Proteins were transferred from the gel to the membrane at 25V for 90-120 min at 4°C in 1× NuPAGE® Transfer Buffer (Life Technologies) after which the membrane was incubated in 5ml of blocking buffer (5% non-fat dried milk in 0.1% Tween 20/PBS buffer) for at least an hour to reduce non-specific antibody binding. An appropriate dilution of the primary antibody (details in Appendix D) was prepared in blocking buffer and added to the membrane and incubated overnight at 4°C. Membranes were

subsequently washed three times in 0.1% Tween 20/PBS buffer for 15 min before incubating with an appropriate dilution of horseradish peroxidase (HRP)-conjugated secondary antibody (details in Appendix D) in blocking buffer, for an hour at room temperature. Membranes were washed three times in 0.1% Tween 20/PBS buffer for 15 min. The membranes were incubated in Pierce™ ECL Western Blotting Substrate (Thermo Scientific) for 5 min, sealed in Saran wrap and secured in developing cassette. Proteins were exposed to CL-Xposure™ Clear Blue X-ray Film (Thermo Scientific) for the preferable time using Photon Imaging Systems SRX-101A. Alternatively, images were acquired using Chemiluminescent Western Blot Imaging System (Azure Biosystems c300). The protein expression was then quantified by Image Studio™ Lite Version 5 software (LI-COR) against loading control according to the band intensity.

2.10 Flow Cytometry

2.10.1 Cell Cycle Analysis

Cell pellets (1×10^6) were washed once with PBS and fixed in 1ml of 70% ice-cold ethanol for 30 min on ice. Fixed cells were then stained in 400µl of staining solution containing 40µg/ml of propidium iodide (PI) solution (Sigma-Aldrich) and 100µg/ml of RNase A (Sigma-Aldrich) in PBS for 30 min at 37°C before analysing using flow cytometry.

2.10.2 Annexin V Staining

Cell pellets (5×10^5) were washed with ice-cold PBS and 1× Cell-based Assay Annexin V Binding Buffer (Cayman Chemical Company) before staining with 2.5µl of APC Annexin V (BioLegend) and 2.5µl of PI staining solution (BioLegend) in 50µl of 1× Binding Buffer at room temperature for 15 min in the dark. Stained cells

were subsequently washed twice with 1× Binding Buffer (300×g, 5 min) and resuspended in 400µl of 1× Binding Buffer before analysing using flow cytometry.

2.10.3 T Cell Stimulation

Prior to CD69, CD154 and F-actin staining, both Jurkat and primary T cells were stimulated, and results were analysed by comparison between unstimulated and stimulated cells. For Jurkat T cells, stimulation was performed with 10µg/ml of plate bound anti-human CD3 (clone OKT3; eBioscience) and 25ng/ml of Phorbol 12-Myristate 13-Acetate (PMA; Sigma-Aldrich) in 24-well plates with 0.5×10^6 cells per well. Primary T cells were stimulated with 2µg/ml of plate bound anti-human CD3 (clone OKT3; eBioscience) and 2µg/ml of soluble anti-human CD28 (clone 28.2; eBioscience) in 24-well plates with 1×10^6 cells per well.

2.10.4 CD69 and CD154 Staining

0.5×10^6 (Jurkat T cells) or 1×10^6 (primary T cells) cells were pelleted and washed with 1ml of FACS buffer (2.5% FBS in PBS). After washing, Jurkat T cells were stained with 5µl of anti-human CD69 PE (clone FN50; eBioscience) while primary T cells were stained with 5µl of Pacific Blue™ anti-human CD69 (clone FN50; BioLegend) and anti-human CD154 PE (clone 24-31; eBioscience) in FACS buffer for 30 min at room temperature in the dark. Primary T cells were also stained with 5µl of APC anti-Human CD3 (clone OKT3; BioLegend) in addition to the T cell activation markers (CD69 and CD154) in order to confirm the T cell population. Stained cells were washed with 1ml of FACS buffer and resuspended in 400µl of FACS buffer before analysing the CD69 and CD154 expressions using flow cytometry.

2.10.5 F-actin Staining

Cell pellets (1×10^6) were washed with 1ml of FACS buffer (2.5% FBS in PBS) and fixed with 200µl of 2% paraformaldehyde (Sigma-Aldrich) for 15 min at room temperature. Fixed cells were permeabilised with 100µl of 0.05% saponin (Sigma-Aldrich) and 10% FBS in PBS for 30 min at room temperature before staining with 5µl of rhodamine phalloidin (Life Technologies) for 30 min at room temperature in the dark. Stained cells were subsequently washed with 1ml of FACS buffer and resuspended in 400µl of FACS buffer. Total cellular F-actin content was then analysed using flow cytometry.

2.10.6 Flow Cytometry – Data Acquisition and Analysis

Samples were analysed on a BD FACSCanto II (BD Biosciences) flow cytometer using BD FACSDiva™ software v6.1.3 (BD Biosciences). PI, anti-CD69 PE, anti-CD154 PE and rhodamine phalloidin stains were detected using the PE (blue) channel; anti-CD3 APC and APC Annexin V using the APC (red) channel; and Pacific Blue anti-CD69 using the BV421 (violet) channel. 10000 events were acquired for each sample and all data was collected from the side scatter (SSC) and forward scatter (FSC) as well as PE, APC or BV421 channels depending on experiment types for later analysis. FlowJo Version 9.7.7 or Version 10.1 software (Tree Star) was used to perform post acquisition analysis.

2.11 Immunofluorescence Microscopy

2.11.1 Spreading Assay

24 hours prior to the spreading assay, each well of a 8-well chamber culture slide (BD Falcon) was coated with 200µl of 0.01% poly-L-lysine solution (Sigma-Aldrich) for 15 min at room temperature, rinsed with sterile water and dried at room temperature for at least 2 hours. The wells were subsequently coated with 150µl of

10µg/ml anti-human CD3 (clone OKT3; Bioscience) overnight at 4°C. The wells were washed three times with 500µl PBS and two times with 500µl of Chamber Buffer (10% FBS, 1% L-Glutamine-Penicillin-Streptomycin solution and 25mM HEPES buffer solution in RPMI 1640 medium without phenol red). 150µl of Chamber Buffer was placed in each well and the slide was pre-warmed at 37°C. 0.5×10^6 (for 1 min of spreading) or 0.2×10^6 (for 3 and 5 min of spreading) cells were pelleted (300×g, 5 min) and resuspended in 50µl of Chamber Buffer. The cell suspensions were plated gently onto the slides by placing the pipette tip at the base of the well and expelling the cells in a single smooth motion onto the bottom of the well. The cells were allowed to spread for 1, 3 or 5 min and fixed with 200µl of 4% paraformaldehyde for 30 min. After rinsing three times with 500µl of PBS/FBS/NaN_3 staining buffer (10% FBS and 0.02% sodium azide in PBS), fixed cells were permeabilised with 300µl of 0.1% Triton X-100 (Calbiochem) in PBS for 5 min at room temperature and then again rinsed three times with 500µl of PBS/FBS/NaN_3 staining buffer. Subsequently, it was blocked with 300µl of 5% goat serum (Sigma-Aldrich) in PBS/FBS/NaN_3 staining buffer for an hour at room temperature before staining with 5µl of rhodamine phalloidin (Life Technologies) for 30 min at room temperature in the dark. Stained cells were then washed three times with 500µl of PBS/FBS/NaN_3 staining buffer before mounting with one drop of Vectashield Mounting Medium with DAPI (Vector Laboratories) and a coverslip was carefully placed on top of the slide. The slides were analysed using fluorescence microscope (Leica DM4500B) with a 100× oil objective, and images were acquired using Leica DFC365 FX monochrome digital camera and Leica LAS AF software. Percentage of spreading was calculated by counting at least 100 cells per

experimental condition. Cells that form a F-actin ring at the cell periphery were scored as positive while cells without an F-actin ring were scored as negative.

2.11.2 Immunological Synapse Assay

MEC-1 B cells were first stained with CellTracker Blue CMAC (Life Technologies) according to the manufacturer's instructions and pulsed with 2μg/mL of a cocktail of staphylococcal superantigens (sAgs; SEA and SEB; Sigma-Aldrich) for 30 min at 37°C. B cells (1×10^6) were centrifuged at 200×g for 5 min with an equal number of T cells (Jurkat or primary T cells) and incubated at 37°C for 15 min. Cells were transferred onto microscope slides (Menzel-Glaser Polysine slides; Thermo Scientific) using a cell concentrator (Cytofuge 2) and fixed with 3% methanol-free formaldehyde (TABB Laboratories) in PBS for 15 min at room temperature. Subsequently, cells were permeabilised with 0.3% Triton X-100 (Calbiochem) in PBS for 5 min and treated with blocking buffer (0.1% BSA in PBS) for 10 min. F-actin was stained with 5μl of rhodamine phalloidin (Life Technologies). After washing, the cell specimens were sealed with 22mm×32mm coverslips using fluorescent mounting medium (Dako). Medial optical section images were captured by A1R (Nikon) confocal microscope using a 60×/1.40 oil objective with NIS-elements imaging software (Nikon). Detectors were set to detect an optimal signal below saturation limits. Fluorescence was acquired sequentially to prevent passage of fluorescence from other channels (Multi-Track). Image sets to be compared were acquired during the same session using identical acquisition settings. Blinded confocal images were analysed using NIS-elements imaging software (Nikon). T cell-B cell conjugates were identified only when T cells were in direct contact interaction with B cells (blue fluorescent channel) and the total area (in square micrometre) of F-actin (red fluorescent channel) accumulation at all T cell contact

sites and synapses with B cell (minimum n=16; maximum n=30 per experimental condition) was measured.

2.12 Migration Assay

Migration assay of Jurkat T cells was performed using 96-well Boyden Chamber Chemotaxis Plate (5µm polycarbonate membrane, 3.2mm diameter; Receptor Technologies Ltd). Cells were harvested and incubated in migration medium (25mM HEPES buffer solution and 0.1% BSA in RPMI 1640 medium without phenol red, serum free) for 30 min at 37°C to starve the cells. Starved cells were stained with 5µM of Calcein AM (Life Technologies) for 30 min at 37°C and washed twice with migration medium before resuspension at a density of 4×10^6 cells/0.5ml in migration medium. 25µl containing 2×10^5 cells were loaded on the upper chamber of the Boyden chamber in triplicate. In the lower chamber, 29µl of medium with serum (20% FBS, 25mM HEPES buffer solution and 0.1% BSA in RPMI 1640 medium without phenol red) was loaded. 25µl of migration medium was also loaded into lower chamber in triplicate as blank. Besides that, eight standards (ranging from 1562.5 to 2×10^5 cells in 25µl) were also prepared using wild-type cells to generate a standard curve and 25µl of each standard was loaded into the lower chamber in triplicate. The plate was incubated at 37°C in 5% CO_2 for 4 hours to allow the cells to migrate through the membrane to the lower chamber. The filter was wiped gently with cotton swab and flushed with PBS to remove any attached cells before centrifuging the plate at 400×g for 10 min to pull all the cells to the bottom of the well. Fluorescence intensity was measured with a fluorescence microplate reader (Tecan GENios Pro Multifunction Multimode Microplate Reader) with excitation wavelength of 485nm and emission wavelength of 535nm and cell number was

subsequently calculated against standard curve. The percentage of migration was estimated using the following equation.

Percentage of Migration (%) = Number of Migrated Cell in Lower Chamber / Total Number of Cell

Total Number of Cell = Number of Non-migrated and Migrated Cells = 2×10^5

2.13 Patient Samples

BM derived $CD3^+$ samples from five MDS patients associated with T-LGL leukaemia were obtained from King's College London Haemato-Oncology Tissue Bank (Human Tissue Authority Licence Number 12223). The samples were collected, stored and used in accordance with donor consent given under the auspices of ethics approval, provided by the UK National Research Ethics Service (NRES) (Approval Reference 08/H0906/94).

2.14 Statistical Analysis

Statistical analysis was performed using Prism Version 5 software (GraphPad Software Inc). Statistical significance was calculated by *P* values using nonparametric, two tailed, unpaired t test.

3 Chapter 3 – Identification and Validation of *miR-181c/d* Target Genes

3.1 Introduction

miRNAs are short endogenous non-coding RNAs of 18-25 nucleotides in length which influence gene expression either by promoting mRNA degradation or translational inhibition (Ambros, 2001; Bartel, 2004). miRNAs have been shown to play pivotal roles in a diverse range of biological events in both normal and cancer cells [reviewed in (Ambros, 2004; Ghildiyal and Zamore, 2009)].

Our study focused on the *miR-181* family which has been demonstrated to play crucial roles in haematopoiesis. The expression of *miR-181a* and *miR-181b* has been reported to be upregulated during erythroid differentiation in human cord blood-derived $CD34^+$ cells (Choong et al., 2007; Lu et al., 2005). Overexpression of *miR-181* in both K562 cells and human cord blood-derived $CD34^+$ progenitor cells was found to promote megakaryocytic differentiation by repressing *Lin28* expression, disrupting the *Lin28-Let-7* reciprocal regulatory loop and in turn upregulating *Let-7* (Li et al., 2012a). This finding is in contrast to a study performed by Garzon and colleagues where they reported that *miR-181b* and *miR-181c* were downregulated during *in vitro* megakaryocytic differentiation in $CD34^+$ BM progenitors (Garzon et al., 2006). Furthermore, it has been shown that the *miR-181* family inhibits granulocytic and macrophage-like differentiation in HL-60 cells and $CD34^+$ HSPC by reducing the expression of *PRKCD*, *CTDSPL* and *CAMKK1* (Su et al., 2015). Moreover, computational algorithms predicted that *miR-181a* regulates genes that are critical to very early steps in erythroid (*MYB*, *CREBBP* and *AGTR2*), myeloid (*ERI-1*, *ETS*, *MEIS-1* and *HOXA5*) and lymphoid (*PU.1*, *MEF*, *SPI-B* and *MYB*) differentiation, suggesting that *miR-181a* might be important in the early steps of

haematopoiesis (Georgantas et al., 2007). In addition, *miR-181* was found to be preferentially expressed in B lymphoid cells in mouse BM and overexpression of *miR-181* in HSPC caused an elevation in the fraction of B lineage cells both *in vitro* and *in vivo*, suggesting that *miR-181* is a positive regulator of B cell differentiation (Chen et al., 2004a). Moreover, it has been demonstrated that *miR-181a* and *miR-181b* promote the development of NK cells (Cichocki et al., 2011; Henao-Mejia et al., 2013). *miR-181a/b*-deficient mice were found to develop haematological defects including T cell proliferation and development as well as early B cell development (Henao-Mejia et al., 2013). Additionally, *miR-181a* has been shown to increase the TCR signalling strength and the sensitivity of T cells to antigens by repressing the expression of multiple negative regulators in the TCR signalling pathway (phosphatases *PTPN22*, *SHP-2*, *DUSP5* and *DUSP6*) and increasing the basal level of LCK and ERK activation, thereby augmenting the TCR-mediated T cell activation (Li et al., 2007). Moreover, ectopic expression of *miR-181c* decreased both T cell activation and proliferation by reducing the expression of *IL-2*, suggesting that *miR-181c* modulates T cell activation and proliferation (Xue et al., 2011). Taken together, multiple previous studies have shown that the *miR-181* family plays an important role in haematopoietic development as well as T cell functions.

Various computational algorithms have been developed to identify miRNA target genes in order to gain insight into the functions of miRNAs (Bentwich, 2005). However, a major drawback of these prediction models is an inevitable bias due to reliance on the complementarity between miRNA and target gene, resulting in a substantial false positive rate (Didiano and Hobert, 2006). Multiple studies showed that perfectly matched miRNA seed sequence with 3'UTR of target mRNA is not necessary for miRNA target gene regulation. miRNAs could bind to the 5'UTR of

target mRNA (Lytle et al., 2007) and also mRNA binding sites are present in the central region (Shin et al., 2010) or the 3' end of miRNA (Grimson et al., 2007; Lal et al., 2009).

As current miRNA target identification methods are often associated with a lack of sensitivity and specificity, we utilised a functional screening assay which has been developed in-house (Gäken et al., 2012) in this study to identify novel downstream targets of the *miR-181* family members. This is a selection-based functional assay which allows rapid and specific detection of targets for a given miRNA. This strategy makes no assumptions based on previously identified sequences, but relies directly on downregulation, by a miRNA, of a thymidine kinase-zeocin (TKzeo) fusion gene expressed upstream of a cDNA library (Sigma-Aldrich, MREH01). This cDNA library, derived from multiple human tissues and 10 human cell lines, contains 16,923 unique genes. The main advantage of this assay is that it identifies miRNA targets that are downregulated either by mRNA degradation or translational repression and not merely relies on the binding of miRNA to putative targets. This assay predicts miRNA targets that are regulated by miRNA without seed-match pairing. Moreover, only targets that are significantly downregulated could be identified due to the nature of the assay and therefore the predicted targets are considered to be the most crucial targets of the investigated miRNA. Accordingly, the number of targets identified by this assay will be considerably smaller than predicted by computational algorithms.

We aimed to identify possible downstream targets of the *miR-181* family using this functional assay to elucidate the role of *miR-181* in normal haematopoiesis. Our study started with the identification of *miR-181c/d* target genes in the first instance and an overview of the novel functional assay principle is illustrated in Figure 3.1.

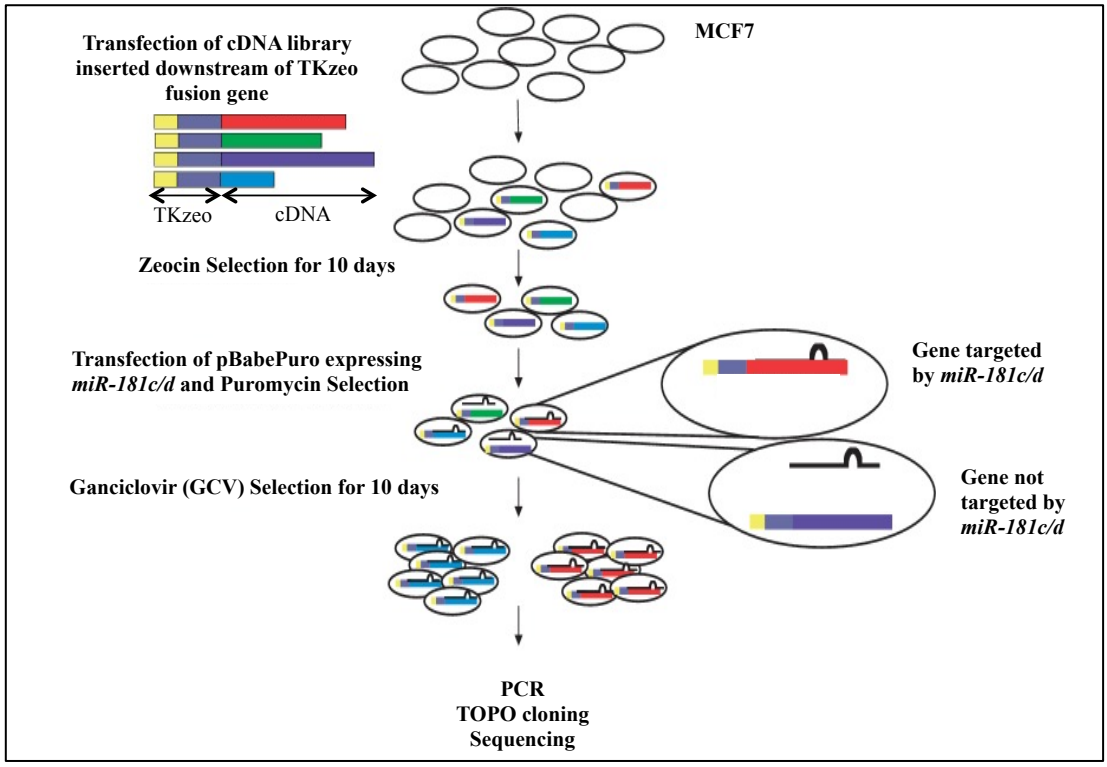

Figure 3.1: Principal of functional assay for *miR-181c/d*-mediated target genes identification. Human breast adenocarcinoma MCF7 cells which express low levels of *miR-181c* and *miR-181d* are first transfected with a cDNA library inserted downstream of a TKzeo fusion gene in the p3'TKzeo dual selection plasmid. During recovery period, constructs can integrate into the genome and express the encoded transcript and then zeocin selection results in a population of cells that express the TKzeo fusion gene from stably integrated library constructs. These cells are resistance to zeocin but sensitive to ganciclovir (GCV). Zeocin resistant cells are subsequently transfected with pBabePuro vector expressing *miR-181c/d*. After selection for stable integration with puromycin and cell expansion, cells are treated with GCV. Cells expressing TKzeo fusion gene that are not targeted by *miR-181c/d* will die, while cells that have downregulated the TKzeo fusion gene expression (cells containing library constructs which are targeted by *miR-181c/d*) either by translational repression or mRNA degradation will survive under GCV selection. Genomic DNA is then isolated from the GCV resistant cells and the cDNA containing *miR-181c/d* target sites is PCR amplified. PCR products are subjected to sequencing and sequences obtained are aligned against human genome to identify the putative *miR-181c/d* target genes [Adapted from (Gäken et al., 2012)].

3.2 Identification of *miR-181c/d* Targets Using A Functional Assay

3.2.1 Construction of pBabePuro Plasmids Expressing *miR-181a*, *miR-181b* and *miR-181c/d*

miR-181a (Figure 3.2a), *miR-181b* (Figure 3.2a) and *miR-181c/d* (Figure 3.2b) were first amplified from genomic DNA isolated from HeLa cells by PCR using designed primers (primer details in Appendix B1). *miR-181c* and *miR-181d* were amplified with a single primer pair as they are located close to each other at the chromosome. Due to the unspecific amplification (~400bp band) for *miR-181c/d*, we utilised the ApoI restriction site within the fragment of 808bp product to confirm the correct fragment was isolated. After digestion, two bands (~200bp and ~600bp) were shown (Figure 3.2c), confirming the correct amplification of *miR-181c/d*.

Subsequently, *miR-181* amplicons were cloned into TOPO vector to generate TOPO-*miR-181a*, TOPO-*miR-181b* and TOPO-*miR-181c/d* plasmids, and then verified with EcoRI enzyme digestion, generating two fragments, ~4kb (TOPO vector) and ~700bp (PCR products of *miR-181a*, *miR-181b* and *miR-181c/d*) (Figure 3.3). In addition, TOPO-*miR-181* plasmids were also validated by sequencing using M13 primers (Life Technologies; primer details in Appendix B5).

Next, the *miR-181* was subcloned into pBabePuro retroviral vector (vector map see Appendix A2), a mammalian retroviral vector conferring puromycin resistance (Morgenstern and Land, 1990), using BamHI and EcoRI restriction sites to generate pBabe-*miR-181a*, pBabe-*miR-181b* and pBabe-*miR-181c/d* plasmids. Digestion of the plasmids with EcoRI and BamHI enzymes to check for the insertion of *miR-181* in the pBabePuro vector generated two fragments, ~5kb (pBabePuro vector) and ~700bp (*miR-181* inserts) (Figure 3.4). The plasmids were also verified by sequencing with designed primers (primer details in Appendix B5).

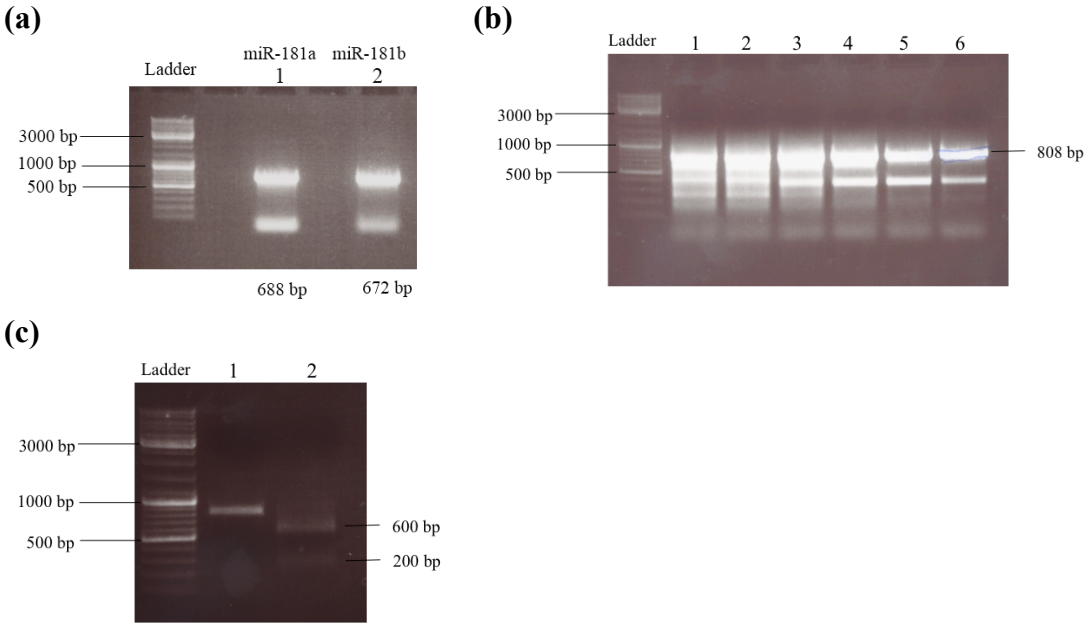

Figure 3.2: PCR amplification of *miR-181a*, *miR-181b* and *miR-181c/d*. (a) Gel image shows the PCR products of *miR-181a* (688bp, lane 1) and *miR-181b* (672bp, lane 2). (b) Gel image shows the PCR amplification of *miR-181c/d* using increasing annealing temperature (lane 1-6). The most specific amplified *miR-181c/d* (808bp, lane 6) was used in subsequent cloning. (c) Gel image shows the ApoI enzyme digestion of *miR-181c/d* PCR product. Lane 1: undigested product of 808bp; Lane 2: digested product with 200bp and 600bp bands.

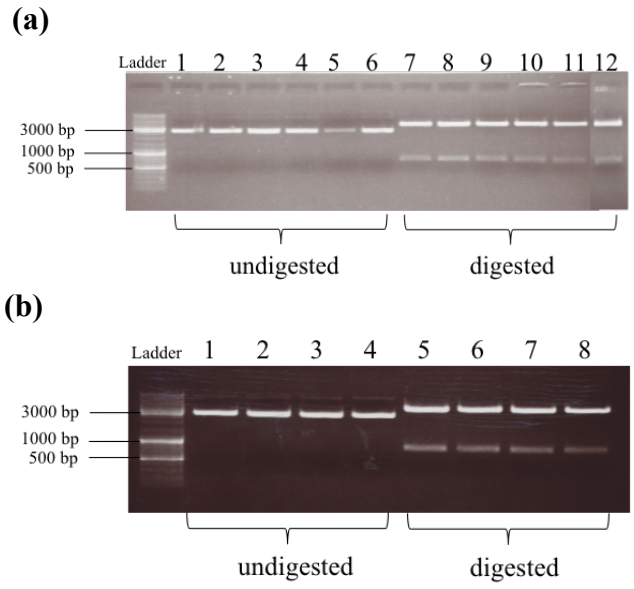

Figure 3.3: EcoRI enzyme digestion of TOPO-*miR-181* plasmids. (a) Gel image shows the EcoRI enzyme digestion of TOPO-*miR-181a* and TOPO-*miR-181b* plasmids. Lane 1-3: undigested TOPO-*miR-181a* plasmids; Lane 4-6: undigested TOPO-*miR-181b* plasmids; Lane 7-9: digested TOPO-*miR-181a* plasmids; Lane 10-12: digested TOPO-*miR-181b* plasmids. (b) Gel image shows the EcoRI enzyme digestion of TOPO-*miR-181c/d* plasmids. Lane 1-4: undigested TOPO-*miR-181c/d* plasmids; Lane 5-8: digested TOPO-*miR-181c/d* plasmids.

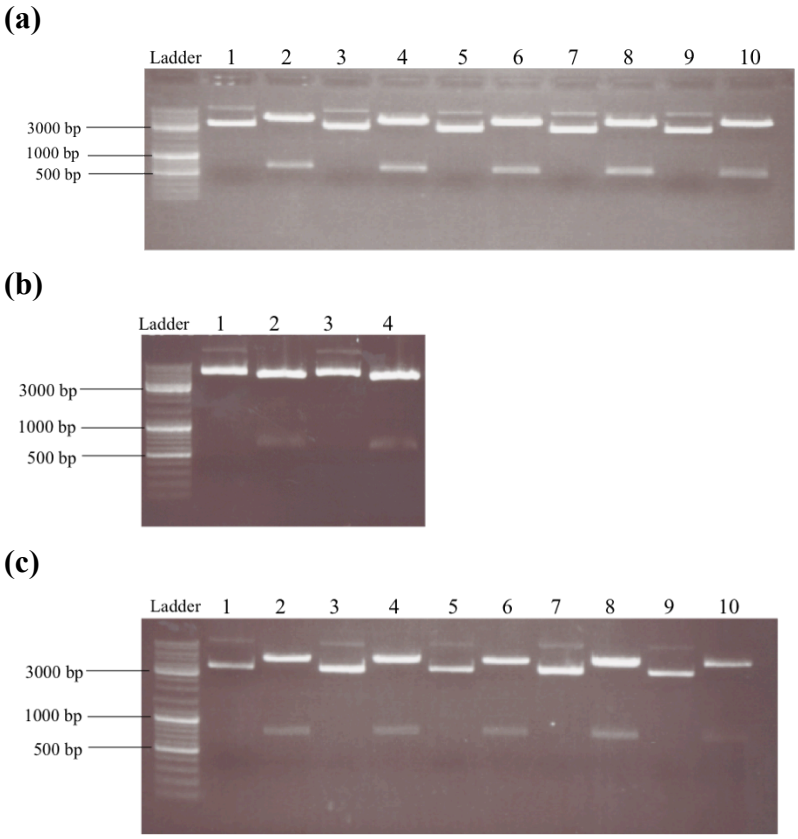

Figure 3.4: EcoRI and BamHI enzyme digestion of pBabe-*miR-181* plasmids. (a) Gel image shows the EcoRI and BamHI enzyme digestion of pBabe-*miR-181a* plasmids. Lane 1, 3, 5, 7 and 9: undigested plasmids; Lane 2, 4, 6, 8 and 10: digested plasmids. (b) Gel image shows the EcoRI and BamHI enzyme digestion of pBabe-*miR-181b* plasmids. Lane 1 and 3: undigested plasmids; Lane 2 and 4: digested plasmids. (c) Gel image shows the EcoRI and BamHI enzyme digestion of pBabe-*miR-181c/d* plasmids. Lane 1, 3, 5, 7 and 9: undigested plasmids; Lane 2, 4, 6, 8 and 10: digested plasmids.

3.2.2 Transfection of MCF7 Cells with p3'TKzeo-library Plasmid and pBabePuro Plasmid Expressing *miR-181c/d*

A panel of nine cell lines have previously been screened in-house for the expression levels of about 600 miRNAs and the MCF7 cell line expressed only low levels of *miR-181c* and *miR-181d* (Appendix F). Therefore, liquid nitrogen stock of MCF7 cells transfected with p3'TKzeo-library (cDNA library from Sigma-Aldrich, MREH01 inserted between SfiI sites in the p3'TKzeo vector, vector map see Appendix A3) which have previously been produced in-house (by Dr Joop Gäken, Dr Heba Alkhatabi and Dr Austin Kulasekararaj) was used in subsequent miRNA transfection. Cells were first selected under zeocin for transfected cells but also remove silenced integrants and cDNAs targeted by endogenous miRNAs in essence self-cleaning the system. Subsequently, a large scale transfection, by electroporation, of the zeocin-selected MCF7 cells containing p3'TKzeo-library with pBabe-*miR-181c/d* plasmid was perfomed (24 transfections with 2×10^6 cells per transfection). After transfection, cells were puromycin selected and after 48 hours, GCV was added for 10 days. Under GCV selection, cells expressing TKzeo fusion gene that are not targeted by *miR-181c/d* will die while cells downregulated the TKzeo fusion gene expression due to *miR-181c/d* targeting will survive. A total of 45 GCV resistant colonies was obtained from the 24 transfections and the colonies were expanded and then genomic DNA was extracted for target identification.

3.2.3 Targets Amplification and Detection

PCR was carried out on the genomic DNA isolated from GCV resistant cells in order to amplify genes that are targeted by *miR-181c/d*, using p3'TKzeo specific primers flanking the SfiI cloning site (primer details in Appendix B2). Optimisation of the primer pairs showed that the primer pair of 3F and 10RTT was the most specific as other primer pairs showed amplification on negative control. Potential targets of *miR-181c/d* were amplified using primer pair of 3F and 10RTT (Figure 3.5). No template control and genomic DNA extracted from MCF7 cells transfected with empty pBabePuro vector were used as negative control during PCR amplification while genomic DNA extracted from MCF7 cells carrying cDNA library transfected with empty pBabePuro vector was used as positive control. There was no amplification in no template control as no DNA was present and also there were no bands observed in the negative control as there was no cDNA library present in the cells. The positive control showed a smear indicative of the amplification of the cDNA library.

A total of 12 amplified bands were purified from the gel, cloned into TOPO vector and sequenced. Sequences were aligned against human genome and transcripts database in NCBI Nucleotide Blast and two transcripts with high homology were identified which are *DHTKD1* and *BRK1* (Appendix G). The detected targets (*DHTKD1* and *BRK1*) are indicated in the gel image in Figure 3.5.

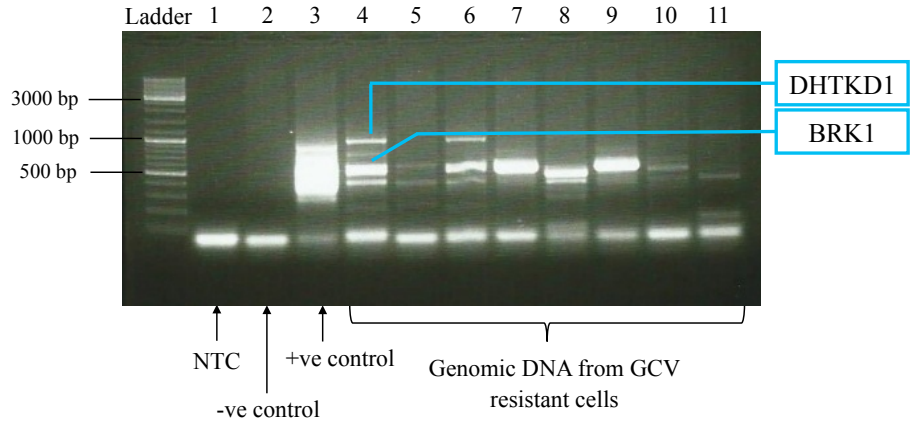

Figure 3.5: Putative targets of *miR-181c/d* amplified by PCR. Gel image shows the PCR amplification of the genomic DNA isolated from GCV resistant cells. Lane 1: no template control (NTC); Lane 2: negative control (genomic DNA from MCF7 cells transfected with empty pBabePuro vector); Lane 3: positive control (genomic DNA from MCF7 cells carrying p3'TKzeo-library transfected with empty pBabePuro vector); Lane 4-11: genomic DNA from GCV resistant cells.

3.3 Prediction of *miR-181c/d* Targets by Computational Algorithms

There are many prediction programs available that can be used to predict miRNA targets *in silico*. In this study, miRecords (http://c1.accurascience.com/miRecords/) which predict targets based on 11 prediction programs (DIANA, MicroInspector, miRanda, MirTarget2, miTarget, NBmiRTar, PicTar, PITA, Rna22, RNAhybrid and TargetScan) was used to predict the targets of *hsa-miR-181c* and *hsa-miR-181d*. More than 30 thousands predicted targets were found using all the 11 programs. Therefore, we filtered the results by reducing the number of prediction programs used. A total of 151 target genes for *miR-181c* were predicted by at least six programs, which are miRanda, MirTarget2, PicTar, PITA, RNAhybrid and TargetScan (Appendix H1). For *miR-181d*, a total of 222 targets were predicted by at least five programs, which include miRanda, MirTarget2, PITA, RNAhybrid and TargetScan (Appendix H2). Interestingly, the targets identified by our functional assay (*DHTKD1* and *BRK1*) were not in the filtered lists for both *miR-181c* and *miR-181d*.

3.4 Validation of the Identified Targets of *miR-181c/d*

3.4.1 Minimum Free Energy by RNAhybrid

RNAhybrid (https://bibiserv2.cebitec.uni-bielefeld.de/rnahybrid) was used to determine the likelihood of *miR-181c* and *miR-181d* targeting *DHTKD1* and *BRK1*. RNAhybrid is a computational algorithm that examines the degree of complementarity between miRNA and its target mRNA by determining the minimum free energy (mfe) of hybridisation between them. The lower the mfe values, the higher the degree of complementarity between miRNA and its target mRNA, indicating the increasing likeliness of the mRNA to be a target of the miRNA of interest. The hybridisation between mature *miR-181c* or *miR-181d* and *DHTKD1* or *BRK1* and their mfe values are shown in Figure 3.6. Interestingly, there is no seed-match pairing between *miR-181c* or *miR-181d* with both of their targets.

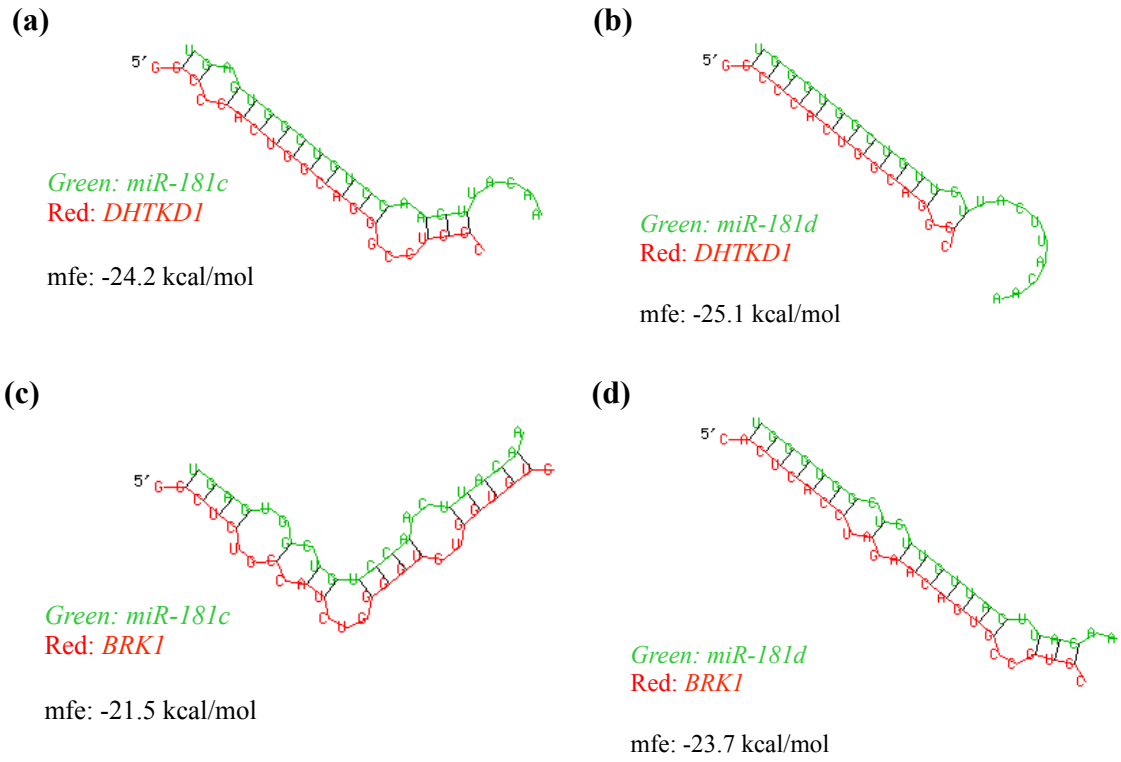

Figure 3.6: Predicted hybridisation between *miR-181c* and *miR-181d* with their putative target genes, *DHTKD1* and *BRK1* by RNAhybrid. Hybridisation between (a) *miR-181c* and *DHTKD1*, (b) *miR-181d* and *DHTKD1*, (c) *miR-181c* and *BRK1* as well as (d) *miR-181d* and *BRK1*. Green represents mature miRNA sequences and red represents target mRNAs. The predicted minimum free energy (mfe) values of the hybridisation are indicated.

3.4.2 Overexpression and Inhibition of *miR-181c* and *miR-181d*

In order to select cell lines to perform validation experiments, the expression levels of endogenous *miR-181c* and *miR-181d* were examined in different cell lines, including HepG2, 293T, NIH/3T3, MCF7, HeLa, Jurkat, K562, KG1, NB4, THP-1 and U937. Leukemic cell lines (Jurkat, K562, KG1, NB4, THP-1 and U937) have a relatively low expression of *miR-181c* and *miR-181d* as compared to adherent cell lines (HepG2, 293T, NIH/3T3, MCF7 and HeLa) (Figure 3.7). Two adherent cell lines, MCF7 and HeLa, which express lower level of *miR-181c* and *miR-181d* compared to other adherent cell lines, and one leukemic cell line, Jurkat T cells were chosen to perform validation experiments.

Overexpression of *miR-181c/d* in MCF7, HeLa and Jurkat T cells was performed by transfecting pBabe-*miR-181c/d* plasmid using electroporation. As experimental controls, cells were mock transfected or transfected with empty pBabePuro vector. Relative to controls, *miR-181c* and *miR-181d* expression levels were increased by approximately 50 and 20 fold respectively in *miR-181c/d* overexpressing MCF7 cells, almost 60 and 40 fold respectively in HeLa cells, and approximately 2000 and 700 fold respectively in Jurkat T cells (Figure 3.8). Surprisingly, following ectopic expression of *miR-181c/d*, there were no changes in both the *BRK1* and *DHTKD1* mRNA levels in all the three cell lines as compared to controls (Figure 3.9).

Inhibition of *miR-181c* and *miR-181d* was also performed in *miR-181c/d* overexpressing MCF7, HeLa and Jurkat T cells by transfecting the cells with miRIDIAN hsa-miR-181c-5p-Hairpin Inhibitor and miRIDIAN hsa-miR-181d-5p-Hairpin Inhibitor (Dharmacon; details see Appendix C2). Mock transfection and transfection using miRIDIAN Hairpin Inhibitor Negative Control (Dharmacon) were used as experimental controls. For *DHTKD1* mRNA level, inconsistent results were

found between the three cell lines, where an increase in *DHTKD1* mRNA level was seen in MCF7 cells following *miR-181d* inhibition, an decrease *DHTKD1* mRNA expression was observed in HeLa cells following *miR-181c* and *miR-181d* inhibition, whereas the mRNA level of *DHTKD1* remained unaltered in Jurkat T cells following both *miR-181c* and *miR-181d* inhibition (Figure 3.10a). However, *BRK1* mRNA expression level remained unchanged following *miR-181c* or *miR-181d* inhibition in all the three cell lines, similar to *miR-181c/d* overexpression (Figure 3.10b).

Given that overexpression and inhibition of *miR-181c* and *miR-181d* had no impact on the mRNA expression level of the target genes, we hypothesised that *miR-181c* and *miR-181d* might regulate the target genes by repressing their translation rather than by mRNA degradation and therefore the protein expressions were examined. Indeed, protein levels of BRK1 and DHTKD1 were substantially downregulated in *miR-181c/d* overexpressing MCF7, HeLa and Jurkat T cells as compared to controls (Figure 3.11a). The reduced protein expression of BRK1 and DHTKD1 in *miR-181c/d* overexpressing cells could be reversed by *miR-181c* inhibition where a marked increase in DHTKD1 and BRK1 protein levels were observed (Figure 3.11b). Interestingly, inhibition of *miR-181d* had no impact on the protein expression of BRK1 and DHTKD1 (Figure 3.11b), indicating that BRK1 and DHTKD1 protein expressions are regulated by *miR-181c* instead of *miR-181d*.

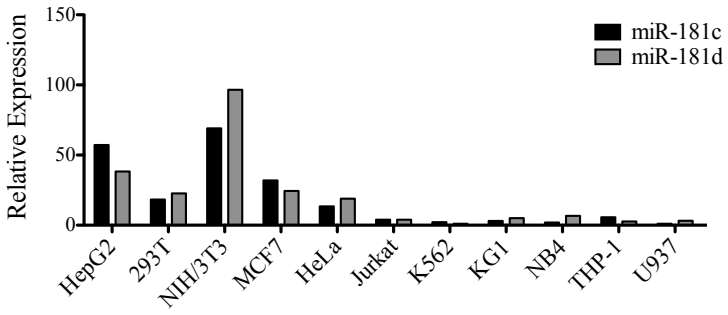

Figure 3.7: Endogenous expression of *miR-181c* and *miR-181d* in different cell lines. Figure shows qPCR analysis of *miR-181c* and *miR-181d* expression in HepG2, 293T, NIH/3T3, MCF7, HeLa, Jurkat, K562, KG1, NB4, THP-1 and U937 cell lines. Expression levels of *miR-181c* and *miR-181d* are normalised to endogenous control *miR-103a.*

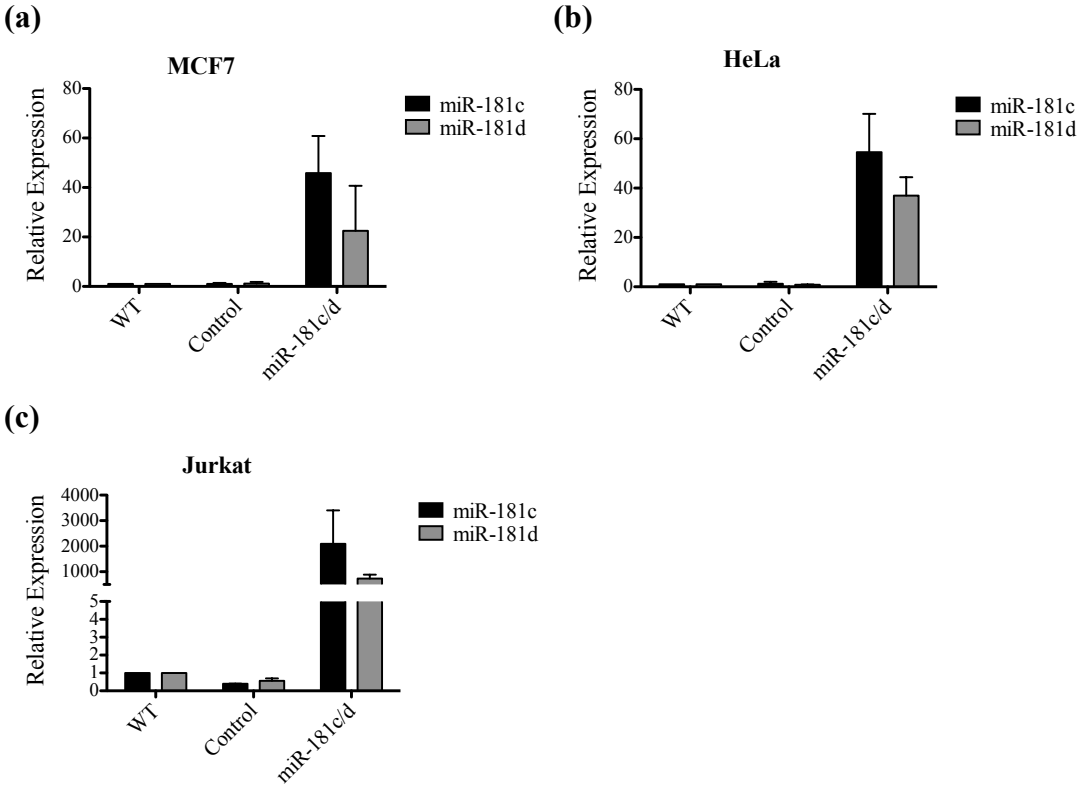

Figure 3.8: Expression of *miR-181c* and *miR-181d* following *miR-181c/d* overexpression. Figures show qPCR analysis of *miR-181c* and *miR-181d* expression in (a) MCF7, (b) HeLa and (c) Jurkat T cells transfected with pBabe-*miR-181c/d* plasmid (miR-181c/d) and empty pBabePuro vector (Control) as well as mock transfection (WT). Expression levels of *miR-181c* and *miR-181d* are calibrated to mock transfection and normalised to endogenous control *miR-103a*. Error bars represent mean ± SD of 3 independent experiments.

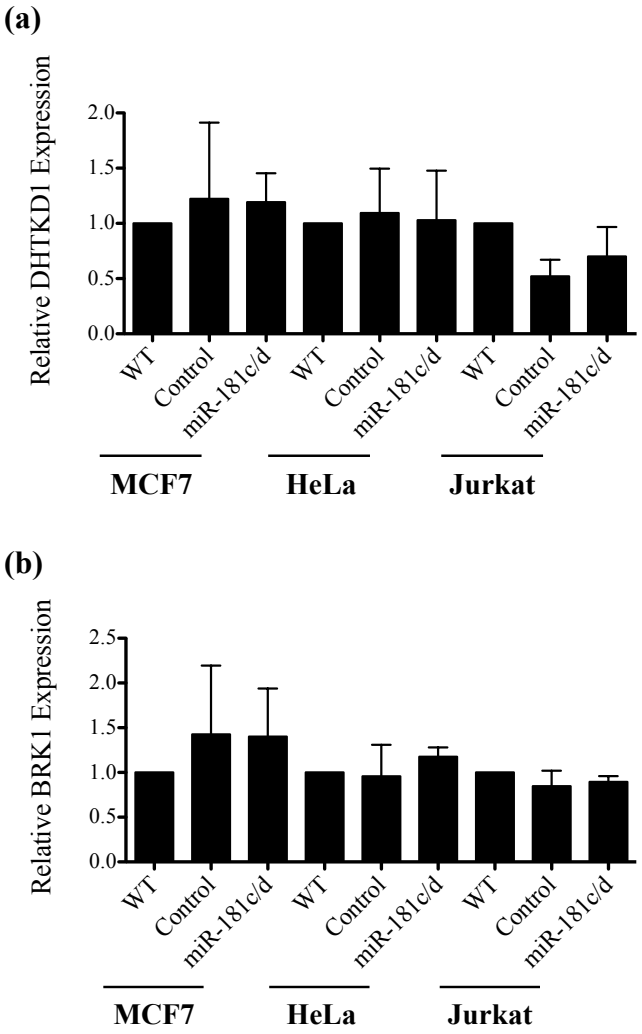

Figure 3.9: mRNA expression levels of *DHTKD1* and *BRK1* following *miR-181c/d* overexpression. Figures show qPCR analysis of (a) *DHTKD1* and (b) *BRK1* mRNA expressions in MCF7, HeLa and Jurkat T cells following *miR-181c/d* overexpression. Relative *DHTKD1* and *BRK1* expression levels are calibrated to mock transfection and normalised to endogenous control *GAPDH*. Error bars represent mean ± SD of 3 independent experiments.

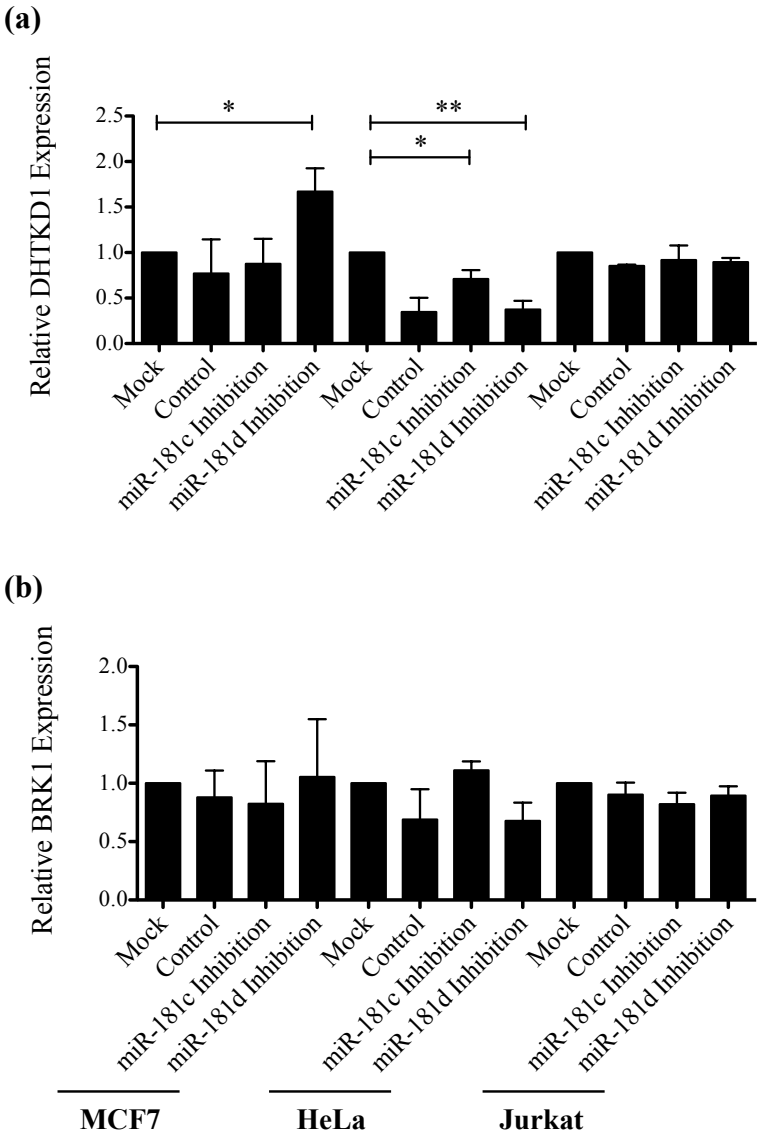

Figure 3.10: mRNA expression levels of *DHTKD1* and *BRK1* following *miR-181c* and *miR-181d* inhibition. Figures show qPCR analysis of (a) *DHTKD1* and (b) *BRK1* mRNA expressions in *miR-181c/d* overexpressing MCF7, HeLa and Jurkat T cells following *miR-181c* and *miR-181d* inhibition. Relative *DHTKD1* and *BRK1* expressions are calibrated to mock transfection and normalised to endogenous control *GAPDH*. Error bars represent mean ± SD of 3 independent experiments.

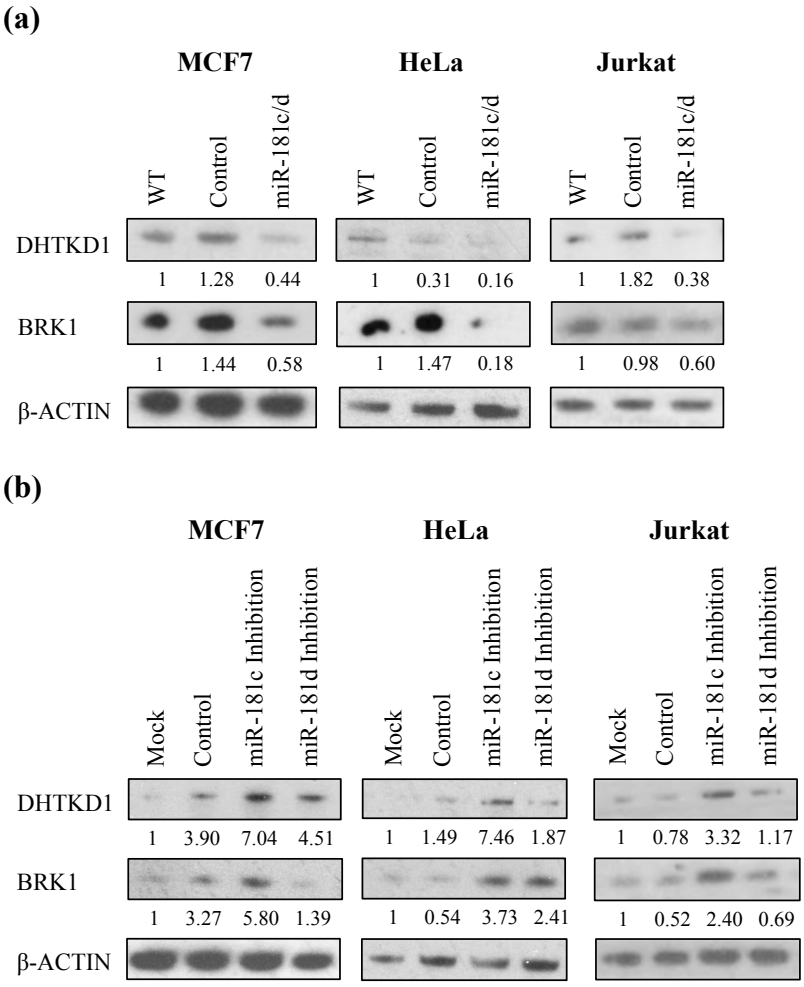

Figure 3.11: Protein expression of DHTKD1 and BRK1 following *miR-181c* and *miR-181d* overexpression and inhibition. (a) Western blot analysis of the protein expression of DHTKD1 and BRK1 in *miR-181c/d* overexpressing MCF7, HeLa and Jurkat T cells. (b) Western blot analysis of the protein expression of DHTKD1 and BRK1 in *miR-181c/d* overexpressing MCF7, HeLa and Jurkat T cells following *miR-181c* and *miR-181d* inhibition. β-ACTIN level is used as a loading control and numbers represent the densitometric quantification of DHTKD1 and BRK1 protein expression levels normalised to β-ACTIN. Blot shown is representative of 3 independent experiments.

3.5 Discussion

Since the discovery of the first miRNA in 1993 (Lee et al., 1993), there have been rapid advances in the development of computational algorithms to predict miRNA targets, which have contributed to the identification of new miRNAs and a large number of predicted targets. The main obstacle in miRNA research is the accurate detection of target genes and it remains difficult and challenging to date due to the binding of miRNA to target with incomplete homology. Increasing evidence shows that base pairing between the miRNA seed region with the 3'UTR of target mRNA is not always required for miRNA regulation (Grimson et al., 2007; Lal et al., 2009; Lu et al., 2010; Lytle et al., 2007; Shin et al., 2010). In addition, the small size of miRNA provides only limited sequence information for their specificity. Moreover, a single miRNA is likely to influence the expression of a large number of mRNAs and also multiple miRNAs can act together to control an individual mRNA, which has further complicated the identification of miRNA target genes.

Nevertheless, several miRNA target identification methods including computational algorithms, expression array and proteomic approaches have been developed and applied in miRNA studies. Undeniably, each of these approaches has their own benefits and limitations. Computational algorithms have been developed to predict the miRNA target sites *in silico*, predominantly based on the base pairing interactions between miRNA and target mRNAs. The commonly accepted rule for computational programs is the complementary pairing between 5' seed sequence of miRNA and 3'UTR of target mRNA, which results in a high rate of false positive results (Didiano and Hobert, 2006). Given that individual miRNAs have the ability to regulate a number of genes, several experimental assays have evolved with the intention of screening a set of target genes, targeted by a specific miRNA. These

assays predict miRNA targets based on their differential expression at mRNA or protein level following overexpression or repression of the miRNA under investigation (Lewis et al., 2003; Thomson et al., 2011). The most widely used technique at the mRNA level is the gene expression profiling using expression array (microarray) or next generation sequencing. One of the caveats of using differential gene expression to identify miRNA targets is that it is unable to distinguish between direct and indirect targets (Lim et al., 2005) and it is associated with a false positive rate resulting from mishybridisation (Chiang et al., 2010; Thomson et al., 2004). In addition, this analysis is incapable to detect targets that are predominantly repressed by miRNA at the translational level. Thus, proteomic approaches such as stable isotope labelling with amino acids in cell culture (SILAC) are used to identify targets resulting from translational inhibition by a specific miRNA. SILAC is a high throughput method for quantitative proteomics in which relative protein abundance is measured by mass spectrometry of samples labelled with different isotopes. The drawbacks of SILAC assay are that this assay is expensive, very time-consuming and unable to distinguish between direct and indirect targets (Baek et al., 2008). Furthermore, co-immunoprecipitation of the RISC component, AGO has also been applied to identify miRNA targets (Hendrickson et al., 2008). This technique uses epitope-tagged AGO to co-immunoprecipitate the associated miRNA/mRNA pairs followed by microarray or high-throughput sequencing to identify the targets. The main limitation of this assay is that it may co-immunoprecipitate mRNA that interacts with AGO protein due to cell lysis, contributing to false positive results. Besides that, this method is technically challenging as it depends on the stable binding between miRNA/mRNA pairs and AGO protein (Mili and Steitz, 2004). Moreover, molecular techniques such as western blot, RT-qPCR and luciferase

reporter assay, are commonly used in validating individual targets of miRNA (Kuhn et al., 2008). Following overexpression or inhibition of a specific miRNA, western blot and RT-qPCR analysis are used to examine differential expression of target genes at protein and mRNA levels respectively. These methods are able to determine whether the regulation of miRNA on their targets is through translational repression or mRNA degradation. The disadvantages of these methods are that they only investigate a single miRNA target at a time and are unable to discriminate between direct and indirect targets (Zhang et al., 2007). On the other hand, the luciferase reporter assay is able to determine the direct target genes of a miRNA. This assay is dependent upon the cloning of binding sites of putative targets downstream of a luciferase reporter gene. Binding of endogenous or introduced miRNAs to the cloned target sequence will result in downregulation of luciferase expression. However, this technique requires prior knowledge about the correct target site and might involve a large amount of cloning work and therefore it might be time-consuming (Kong et al., 2008; Lytle et al., 2007). Despite progress made within the field, many targets of miRNA have not been identified and experimentally validated due to the lack of highly sensitive and specific techniques.

In the present study, the application of our functional assay allows an efficient identification of miRNA targets where miRNAs interact with or without a seed sequence with their target mRNAs. This assay has the potential to identify downregulated targets at both mRNA and protein levels and the identified number of putative targets by this assay is smaller than the number of targets predicted by computational algorithms, expression arrays or proteomic approaches. Besides that, this assay isolates only the targets that are significantly downregulated and therefore the identified targets are likely to be the most crucial targets. This functional assay

relies on using a large cDNA library, representing approximately 77% of the human transcriptome, inserted downstream of a fusion gene (TKzeo). The presence of this large library will increase the possibility of identifying many targets for many miRNAs (Gäken et al., 2012). Using this functional assay, we identified two target genes of *miR-181c/d* which are *BRK1* and *DHTKD1*. The chromosomal location and functions of *BRK1* and *DHTKD1* are shown in Table 3.1.

Using RNAhybrid, we further strengthened the possibility that *BRK1* and *DHTKD1* are targeted by *miR-181c/d*. We found that the mfe values of hybridisation between *miR-181c* and *BRK1*, *miR-181c* and *DHTKD1*, *miR-181d* and *BRK1* as well as *miR-181d* and *DHTKD1* ranged from -21.5 to -25.1 kcal/mol. These mfe values are lower than the mfe value for hybridisation between *miR-10a* and its validated target, *HOXA1* (-19.8 kcal/mol) as reported by a previous study (Garzon et al., 2006). Therefore, our data suggests that *BRK1* and *DHTKD1* are likely to be targeted by *miR-181c/d* based on the degree of complementarity predicted by mfe values using RNAhybrid.

Besides validating the identified targets by RNAhybrid, *BRK1* and *DHTKD1* were also validated experimentally by examining their expression levels following overexpression and inhibition of *miR-181c* and *miR-181d*. To avoid differences in genetic background of the cell lines which may interfere with miRNA regulation of its target, we used three independent cell lines, MCF7, HeLa and Jurkat T cells in the validation experiments. Interestingly, our validation experiments showed that *BRK1* and *DHTKD1* are regulated by *miR-181c* instead of *miR-181d* as inhibition of *miR-181d* had no impact on the BRK1 and DHTKD1 protein expression levels. In addition, overexpression and inhibition of *miR-181c* had no impact on the mRNA expression but did in fact modulate protein expression, suggesting that *miR-181c*

regulates BRK1 expression by blocking the translation rather than by degrading the mRNA.

According to literature reviews and miRTarBase Release 6.0 (http://mirtarbase.mbc.nctu.edu.tw/), there are a number of *miR-181c* target genes which were validated experimentally by reporter assay, western blot or RT-qPCR analysis. Using RT-qPCR and western blotting analysis, Liu *et al.* showed that lower expression level of *miR-181c* in glioblastoma cells decreased *PCAF* expression, suggesting the role of *miR-181c* in reduction of the activation of major tumour suppressive pathways in glioblastoma (Liu et al., 2007a). Ruan *et al.* utilised the same methods, RT-qPCR and western blot and showed that *miR-181c* negatively regulates *NOTCH2* in glioma cells (Ruan et al., 2015). Furthermore, Hashimoto *et al.* reported that epigenetically-silenced *miR-181c* plays an important role in the pathogenesis of gastric carcinomas through its target genes, *NOTCH4*, *KRAS* and *MECP2*, as identified by cDNA microarray analysis and validated by RT-PCR and western blot analysis in gastric carcinoma KATOIII cell line (Hashimoto et al., 2010; Hashimoto et al., 2013). Moreover, *miR-181c* was also found to negatively modulate T cell activation by targeting *IL-2*, as validated by luciferase reporter assay (Xue et al., 2011). Another study also utilised luciferase reporter assay and identified *TRIM2*, *SIRT1* and *BTBD3* as putative target genes of *miR-181c*, suggesting the potential function of *miR-181c* in brain homeostasis and disease pathogenesis (Schonrock et al., 2012). In addition, Zhang *et al.* showed that *miR-181c* directly targets the 3'UTR of *TNF-α* mRNA using luciferase reporter assay, and *miR-181c* regulates both TNF-α mRNA and protein expressions using RT-qPCR and western blot analysis in BV-2 microglial cell line, suggesting the regulation of *TNF-α* by *miR-181c* after ischemia/hypoxia and microglia-mediated neuronal injury (Zhang et

al., 2012). *miR-181c* was also found to regulate *PDPK1* expression in brain endothelial cells using microarray analysis and it was validated by RT-qPCR and western blot analysis (Tominaga et al., 2015). Additionally, Ji *et al.* found that the *miR-181* family directly targets *CDX2*, *GATA6* and *NLK*, which are known regulators of hepatic cell differentiation in hepatocellular carcinomas using western blot analysis and luciferase reporter assay in Hep3B and HuH1 hepatocellular carcinoma cell lines (Ji et al., 2009). Zhu *et al.* reported that *miR-181* family plays a key role in the development of multidrug resistance in both SGC7901 gastric and A549 lung cancer cell lines by modulation of apoptosis via regulation of *BCL2,* as validated by luciferase reporter assay (Zhu et al., 2010). Besides that, using luciferase reporter assay, RT-qPCR and western blot analysis, She *et al.* found that the *miR-181* family targets *RAP1B* in glioblastoma U251 cell line (She et al., 2014). Moreover, it has also been recently shown that the *miR-181* family inhibits granulocytic and macrophage-like differentiation of HL-60 and $CD34^+$ HSPC by directly targeting *PRKCD*, *CTDSPL* and *CAMKK1,* as validated using luciferase reporter assay, RT-qPCR and western blot analysis (Su et al., 2015).

However, none of these validated targets was identified by our functional assay in the present study. This might be attributed to the nature of the functional assay which is only able to identify targets that are significantly downregulated. The validated targets described above might not be downregulated sufficiently to be detected by this functional assay. In addition, the validated target genes of *miR-181c* might not be present in the cDNA library that we transfected into the MCF7 cells in this functional assay. Moreover, it might be due to the lower number of sequencing reads of these genes in the cDNA library. The number of sequencing reads in the cDNA library, obtained from Sigma-Aldrich's website, for both the validated targets and the

targets detected in our study are shown in Table 3.2. The validated target genes of *miR-181c* which have low sequencing reads in the cDNA library include *CDX2*, *GATA6*, *NOTCH4*, *BTBD3*, *RAP1B* and *PRKCD* and hence there is a lower chance to identify these targets with the functional assay.

Collectively, we confirm that BRK1 is a novel downstream target of *miR-181c.* We also showed that *miR-181c* regulates BRK1 by translational repression.

Table 3.1: Chromosomal Location and Functions of *BRK1* and *DHTKD1*.

Gene	***BRK1***	***DHTKD1***
Chromosomal Location	3p25.3	10p14
Subcellular Location	Extracellular Cytoskeleton Cytosol	Mitochondrion Nucleus Cytosol Endoplasmic reticulum
Molecular Function (Gene Ontology)	Contributes to Rac GTPase binding	*No Data Available*
Molecular Function (UniProtKB)	Involved in regulation of actin and microtubule organisation Part of a WAVE complex that activates the ARP2/3 complex	The 2-oxoglutarate dehydrogenase complex catalyses the overall conversion of 2-oxoglutarate to succinyl-CoA and CO(2).
Biological Processes (Gene Ontology)	In utero embryonic development Small GTPase-mediated signal transduction RAC protein signal transduction Innate immune response Vascular factor receptor signalling pathway	Glycolytic process Metabolic process Oxidation-reduction process
Pathways	Regulation of actin dynamics for phagocytic cup formation Regulation of actin cytoskeleton Immune system Signalling by Rho GTPases Interleukin-3, 5 and GM-CSF signalling	Glyoxylate metabolism and glycine degradation Metabolism Viral mRNA translation Integrated breast cancer pathway

(Adapted from http://www.genecards.org/)

Table 3.2: Number of Sequencing Reads of Validated and Detected Targets in cDNA Library (Adapted from Sigma-Aldrich)

Validated Targets	**Number of Reads**
PCAF	3813
NOTCH2	644
NOTCH4	90
KRAS	1334
MECP2	2099
TRIM2	1097
SIRT1	335
BTBD3	26
PDPK1	531
CDX2	2
GATA6	11
NLK	704
BCL2	583
RAP1B	11
PRKCD	29
CTDSPL	673
CAMKK1	276
Detected Targets	**Number of Reads**
DHTKD1	1881
BRK1	337

4 Chapter 4 – Roles of *miR-181c*-BRK1 Axis in T Cell Function

4.1 Introduction

Reorganisation of the actin cytoskeleton is a requisite event in controlling T cell activation and it is important for multiple aspects in T cell function (Holsinger et al., 1998). The ability of T cells to polymerise actin is critical from the very first step of TCR triggering to the completion of a successful T cell activation. During T cell activation, multiple cellular processes including cellular polarisation, receptor sequestration and signalling, integrin-mediated adhesion, immunological synapse formation, and releases of cytokines and lytic granules are all dependent upon the proper regulated actin dynamics in T cells (Billadeau et al., 2007; Burkhardt et al., 2008; Kumari et al., 2014; Yu et al., 2013).

The *miR-181* family has been demonstrated to be involved in T cell development, differentiation, proliferation and activation. *miR-181a* regulates T cell differentiation at a very early stage in human lymphopoiesis. *miR-181a* was found to regulate genes that are important in lymphoid differentiation including *PU.1*, *MEF*, *SPI-B*, *MYB* and *CXCR4*, suggesting that *miR-181a* might block the T cell differentiation in very early steps of haematopoiesis (Georgantas et al., 2007). Furthermore, *miR-181a* is an intrinsic modulator of the TCR signalling strength and the sensitivity of T cells to antigens during T cell development and function. *miR-181a* represses the expression of multiple negative regulators in the TCR signalling pathway such as phosphatases *PTPN22*, *SHP-2*, *DUSP5* and *DUSP6*, and increases the basal level of LCK and ERK activation, thus reducing the amount of signal that is required for achieving full LCK and ERK activation upon antigen stimulation. This enhances the TCR signalling strength and sensitivity of T cells to antigens, thereby augmenting the

TCR-mediated T cell activation (Li et al., 2007). In addition, *miR-181a* and *miR-181b* influence T cell proliferation and development as *miR-181a/b*-deficient mice showed reduced proliferative capacity and total number of T cells. This defect was found to be associated with impaired PI3K signalling pathway through modulation of the phosphatase *PTEN* expression by *miR-181a* and *miR-181b* (Henao-Mejia et al., 2013). Moreover, *miR-181c* modulates T cell activation and proliferation by regulating the expression of *IL-2*. *miR-181c* was found to target *IL-2* and ectopic expression of *miR-181c* reduced both T cell activation and proliferation (Xue et al., 2011). Although the *miR-181* family has been demonstrated to be important in T cells, its role in actin polymerisation during T cell activation is still unknown.

WAVE protein is a member of the WASP family that regulates actin cytoskeletal dynamics (Campellone and Welch, 2010; Padrick and Rosen, 2010; Pollitt and Insall, 2009b). Among the three isoforms of WAVE, WAVE2 has been shown to be the major isoform expressed in T cells (Nolz et al., 2006; Zipfel et al., 2007) and increasing data indicate that it is an essential regulator of multiple actin cytoskeleton-dependent processes during T cell activation (Nolz et al., 2006; Nolz et al., 2007; Nolz et al., 2008; Zipfel et al., 2007). Suppression of *WAVE2* in Jurkat T cells has been shown to reduce the F-actin accumulation at the immunological synapse and decrease conjugate formation (Nolz et al., 2006; Zipfel et al., 2007). In addition, loss of *WAVE2* also led to defect in stable lamellipodia generation and impairment in the regulation of Ca^{2+} in T cells (Nolz et al., 2006). Furthermore, depletion of WAVE2 also caused reduction in IL-2 promoter activity (Nolz et al., 2007; Nolz et al., 2008) and defective integrin-mediated adhesion in response to TCR activation (Nolz et al., 2006; Nolz et al., 2007; Nolz et al., 2008).

BRK1, a subunit of WAVE regulatory complex, has been found to be a downstream target of *miR-181c* in our study (see Chapter 3). BRK1 is a small protein of 9kDa with a presumed coiled-coil region that has been shown to be important in the stability and integrity of WAVE complex as loss of *BRK1* led to degradation of the complex in both mammalian cell lines (Cai et al., 2009; Derivery et al., 2008; Escobar et al., 2010) and *Drosophila* (Kunda et al., 2003; Qurashi et al., 2007). Although much remains unknown regarding the functions of *BRK1* in T cells, accumulating evidence indicate its important role in the actin cytoskeleton-dependent cellular processes. In HeLa cells, *BRK1* was shown to be required for lamellipodia formation (Derivery et al., 2008; Eden et al., 2002). Moreover, suppression of *BRK1* in PG NSCLC cell line caused actin filament reorganisation, inhibited pseudopodia formation and blocked cell migration (Cai et al., 2009). Loss of *BRK1* in SN12C and U031 renal cell carcinoma cell lines as well as U2OS osteosarcoma cell lines also resulted in defective directional migration and invasive growth, coupled with reduced cell proliferation (Escobar et al., 2010). Furthermore, *BRK1* is also essential in actin dynamics and cell survival during embryo development as genetic ablation of *Brk1* in mice resulted in dramatic defects in embryo compaction and development (Escobar et al., 2010). In addition, *BRK1* also regulates actin dynamics during the processes of neurite outgrowth in human IMR-32 neuroblastoma cell line and primary rat hippocampal neurons (Wang et al., 2013a).

Given the importance of the *miR-181* family in T cells and the crucial roles of BRK1 in the involvement of WAVE protein and in the regulation of actin reorganisation, we therefore focused our study on delineating the potential roles of *miR-181c*-BRK1 axis in T cell functions.

4.2 Primary T Cell Activation Resulted in Downregulation of *miR-181c* Expression and Upregulation of BRK1 Protein Expression

To investigate whether the regulation of BRK1 by *miR-181c* correlates with T cell activation, we examined the *miR-181c* expression and the BRK1 protein expression level in $CD3^+$ T cells isolated from PBMC, before and after co-stimulation with CD3 and CD28 antibodies. After stimulation, *miR-181c* expression was significantly reduced (*P* value=0.00038) (Figure 4.1a) while BRK1 protein expression was substantially elevated (Figure 4.1b) in $CD3^+$ cells. This finding further strengthens our hypothesis that the *miR-181c*-BRK1 axis maybe important in T cell activation.

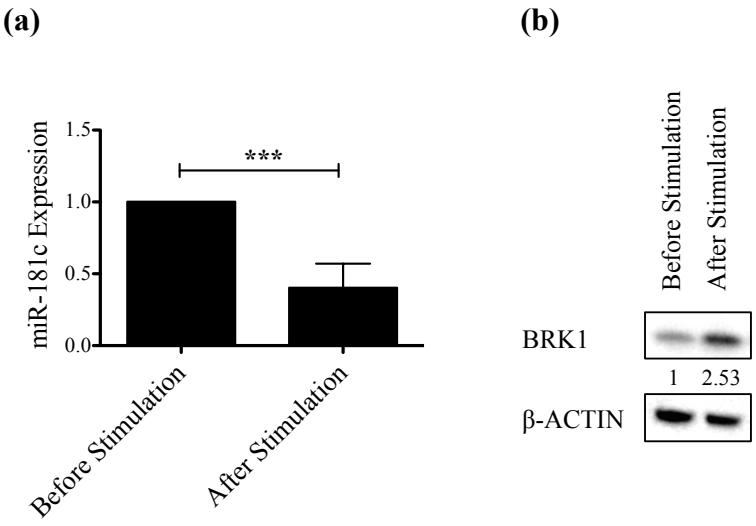

Figure 4.1: Reduced *miR-181c* expression and increased BRK1 protein expression following primary T cell activation. (a) Figure shows the qPCR analysis of *miR-181c* expression in PBMC derived $CD3^+$ T cells before and after stimulation. Co-stimulation of $CD3^+$ cells was performed with 2µg/ml of plate-bound anti-human CD3 and soluble anti-human CD28 antibodies for 24h. Expression of *miR-181c* is normalised to endogenous control *miR-103a*. Error bars represent mean ± SD of 4 independent experiments. *** $P \leq 0.001$. (b) Western blot analysis of BRK1 protein expression in PBMC derived $CD3^+$ T cells before and after stimulation. β-ACTIN level is used as a loading control and numbers represent the densitometric quantification of BRK1 protein expression level normalised to β-ACTIN. Blot shown is representative of 3 independent experiments.

4.3 Effects of *miR-181c* Overexpression in Jurkat T Cells

4.3.1 Overexpression of *miR-181c* in Jurkat T Cells

In order to study the roles of *miR-181c* in T cell function, we overexpressed *miR-181c* in Jurkat T cells by transfecting the cells with pBabePuro plasmid expressing exogenous *miR-181c* (plasmid will be indicated as pBabe-*miR-181c* in the following text). The cloning of *miR-181c* into pBabePuro expression vector was carried out similar to the cloning of *miR-181c/d* into pBabePuro vector for miRNA target identification functional assay (see Chapter 2 and 3). Mock transfection and cells transfected with empty pBabePuro vector were used as experimental controls.

Following transfection, an upregulation of *miR-181c* by approximately 600 fold in Jurkat T cells transfected with pBabe-*miR-181c* plasmid was observed when compared to controls (Figure 4.2). *miR-181c* overexpressing Jurkat T cells were used in subsequent functional assays.

4.3.2 Overexpression of *miR-181c* in Jurkat T Cells Led to Reduced BRK1 and WAVE2 Protein Expressions

Before studying the roles of *miR-181c* in T cells, we examined the protein expression levels of BRK1 and WAVE2 following *miR-181c* overexpression in Jurkat T cells. As a result of *miR-181c* overexpression, BRK1 protein level was decreased as compared to controls (Figure 4.3), indicating that BRK1 is indeed a downstream target of *miR-181c* as identified and validated in Chapter 3. In addition, loss of BRK1 as a result of *miR-181c* overexpression also led to reduced WAVE2 protein expression (Figure 4.3), suggesting that BRK1 plays an important role in stabilising the WAVE2 regulatory complex.

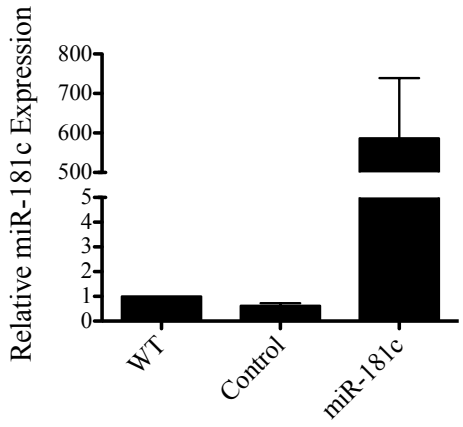

Figure 4.2: Overexpression of *miR-181c* in Jurkat T Cells. Figure shows the qPCR analysis of *miR-181c* expression in Jurkat T cells transfected with pBabe-*miR-181c* plasmid (miR-181c), pBabePuro empty vector (Control) and mock transfected cells (WT). The data are calibrated to mock transfection and normalised to endogenous control *miR-103a*. Error bars represent mean ± SD of 3 independent experiments.

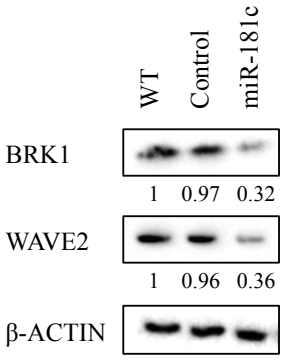

Figure 4.3: Overexpression of *miR-181c* in Jurkat T cells resulted in reduced BRK1 and WAVE2 protein expressions. Western blot analysis of BRK1 and WAVE2 protein expressions following *miR-181c* overexpression in Jurkat T cells. β-ACTIN level is used as a loading control and numbers represent the densitometric quantification of protein expression levels normalised to β-ACTIN. Blot shown is representative of 2 independent experiments.

4.3.3 Overexpression of *miR-181c* in Jurkat T Cells Had No Impact on Cell Proliferation, Cell Cycle and Cell Viability

To assess the effects of *miR-181c* overexpression on cell proliferation in Jurkat T cells, we used trypan blue exclusion to score the total number of cell at regular intervals. Trypan blue does not stain live cells with intact cell membrane but it traverses the cell membrane of dead cells, giving a distinctive blue colour under the microscope. The trypan blue exclusion results showed nearly identical cell counts in the controls and *miR-181c* overexpressing cells at all the time points (day1 to day6) (Figure 4.4a), suggesting that ectopic expression of *miR-181c* in Jurkat T cells has no influence on cell proliferation.

Furthermore, we also examined the effect of *miR-181c* overexpression in Jurkat T cells on the changes of kinetics of cell cycle entry by flow cytometry analysis using propidium iodide (PI) staining. The percentage of cells in each cell cycle phase (G1, S and G2-M) was studied post-transfection. There was no substantial difference in the percentage of cells in the three phases of cell cycle between *miR-181c* overexpressing cells and controls (Figure 4.4b).

In addition, the effect of *miR-181c* overexpression in Jurkat T cells on the cell viability was examined by Annexin V and PI staining. There was no difference in the percentages of live (~90% of Annexin V^- PI^- cells), early apoptotic (~6% of Annexin V^+ PI^- cells) and late apoptotic cells (~2% of Annexin V^+ PI^+ cells) between *miR-181c* overexpressing cells and controls (Figure 4.4c).

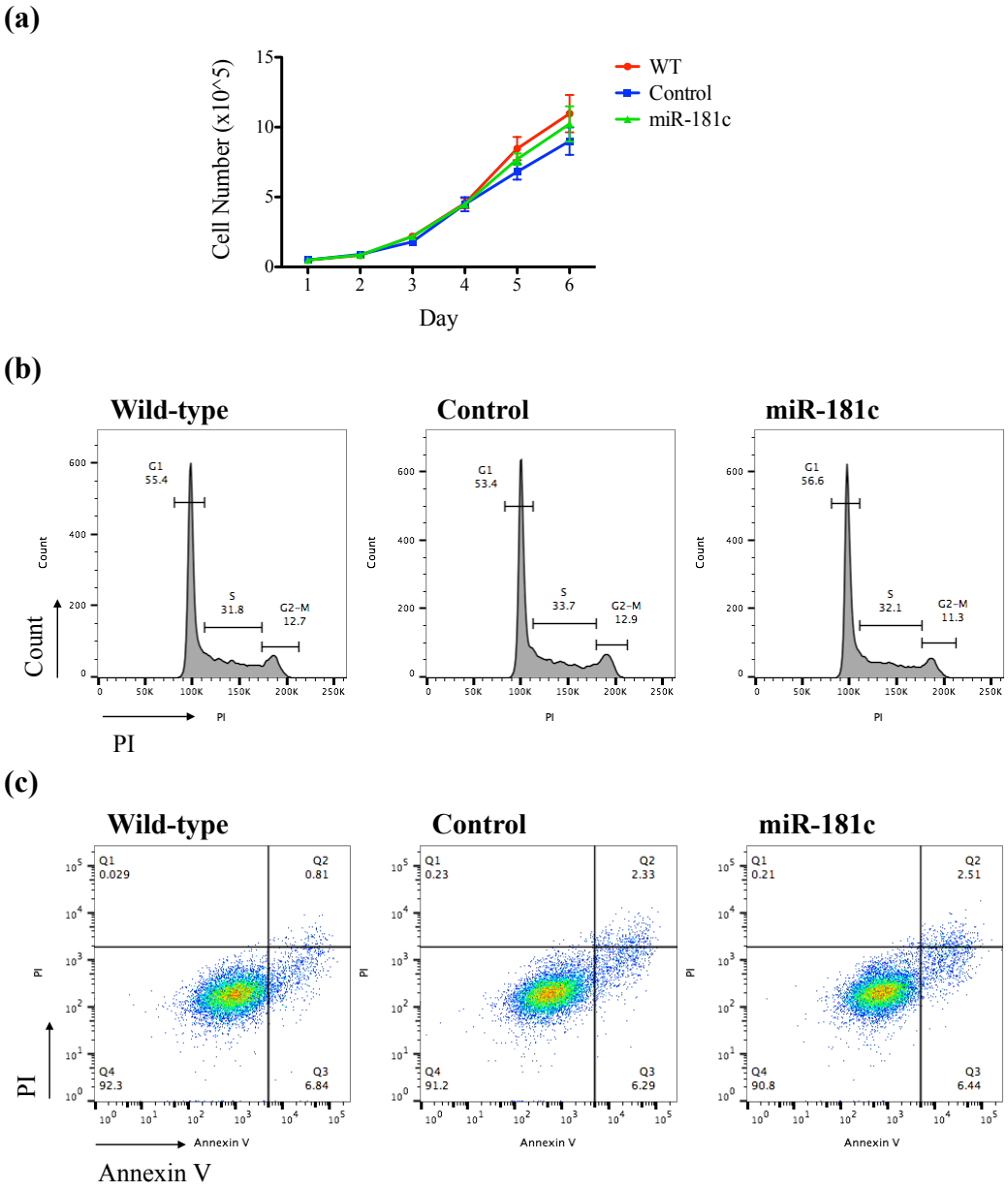

Figure 4.4: Overexpression of *miR-181c* in Jurkat T cells had no impact on cell proliferation, cell cycle and cell viability. (a) Plot shows the cell proliferation of *miR-181c* overexpressing cells (green), mock-transfected (WT, red) and empty pBabePuro vector-transfected cells (Control, blue). Cells were seeded and cultured in a 24-well plate and counted every day for 6 days post-transfection. Error bars represent mean ± SEM of 3 independent experiments. (b) Cell cycle profiles of Jurkat T cells overexpressing with *miR-181c* and controls. Samples were fixed with 70% ethanol, stained with PI and analysed by flow cytometry. Y-axis indicates cell number and x-axis indicates PI staining. Plots are representative of 3 independent experiments. (c) APC Annexin V and PI staining of Jurkat T cells following *miR-181c* overexpression. The percentage of live (Q4 = double negative for Annexin V and PI), early apoptotic (Q3 = positive Annexin V and negative PI) and late apoptotic (Q2 = double positive for Annexin V and PI) cells were analysed by flow cytometry. Y-axis indicates log fluorescence intensity of PI staining and x-axis indicates log fluorescence intensity of APC Annexin V staining.

4.3.4 Overexpression of *miR-181c* Repressed Jurkat T Cell Activation

Since there was no effect on cell proliferation, cell cycle profile and cell viability following *miR-181c* overexpression in Jurkat T cells, we next investigated the influence of *miR-181c* in T cell activation. The expression of CD69, a marker for T cell activation, was examined by flow cytometry analysis, before and after co-stimulation with CD3 antibody and PMA. After stimulation, the expression of CD69 on the surface of Jurkat T cells in mock, empty pBabePuro vector and pBabe-*miR-181c* transfections, were all elevated as compared to those before stimulation (Figure 4.5). However, the upregulation of CD69 expression was lower in the cells overexpressed with *miR-181c* (72.6% $CD69^+$ cells) than in mock transfected (90.3% $CD69^+$ cells) and empty vector transfected cells (92.8% $CD69^+$ cells) (Figure 4.5). This data indicates that enforced expression of *miR-181c* partially represses Jurkat T cell activation.

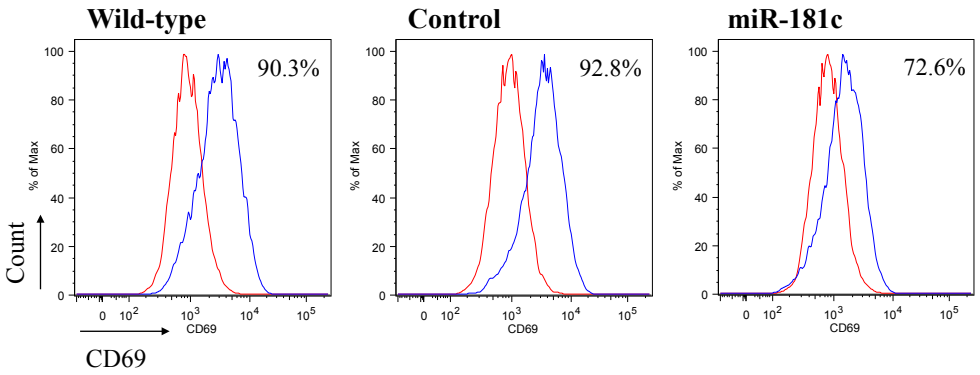

Figure 4.5: Overexpression of *miR-181c* in Jurkat T cells repressed T cell activation. CD69 expression in *miR-181c* overexpressing Jurkat T cells and controls before (red) and after (blue) stimulation. Jurkat T cells were stimulated with 10µg/ml plate-bound anti-human CD3 antibody and 25ng/ml PMA for 24h. Y-axis indicates cell number and x-axis indicates log fluorescence intensity of CD69-PE staining. Plots are representative of 3 independent experiments.

4.3.5 Overexpression of *miR-181c* in Jurkat T Cells Reduced Actin Polymerisation During Lamellipodia Generation and Immunological Synapse Formation

Reorganisation of the actin cytoskeleton is requisite in the control of T cell activation (Holsinger et al., 1998). The finding of reduced T cell activation as a result of *miR-181c* overexpression has led us to examine whether F-actin polymerisation during T cell activation is altered in *miR-181c* overexpressing cells. We assessed the ability of the cells to cap actin in response to T cell stimulation in order to define the roles of *miR-181c* in dynamic cytoskeletal regulation in Jurkat T cells.

Firstly, the total cellular F-actin content was quantified by flow cytometry with the staining of F-actin using phalloidin, before and after stimulation with anti-CD3 and PMA. In controls, the total cellular F-actin content in the cells increased after stimulation while in miR-*181c* overexpressing cells, the total cellular F-actin content remained unaltered (Figure 4.6). To quantitatively determine the effect of *miR-181c* overexpression on actin polymerisation, the mean fluorescence intensity (MFI) was analysed, indicative of the total cellular F-actin content. After stimulation, *miR-181c* overexpressing Jurkat T cells had a significantly lower MFI as compared to the controls (Figure 4.6). This result indicates that ectopic expression of *miR-181c* in Jurkat T cells causes a marked reduction in actin polymerisation in response to stimulation.

The generation of lamellipodia in T cells requires properly regulated actin dynamics and thus we next studied whether *miR-181c* overexpression reduces actin polymerisation during lamellipodia formation. Spreading of T cells on anti-TCR coated slide requires the formation of stable actin structures and the generation of lamellipodia (Bunnell et al., 2001). Therefore, we analysed the effect of *miR-181c* overexpression on the ability of Jurkat T cells to spread onto anti-CD3 coated slides

by performing a spreading assay. Cells were allowed to spread on anti-CD3 coated slides for 1, 3 and 5 minutes and then stained using phalloidin to visualise F-actin. During the spreading process, *miR-181*c overexpressing cells failed to spread whilst control cells were able to spread in a highly ordered fashion, forming a round lamellipodial interface containing radially-arrayed F-actin-rich structures at the periphery of the cells (Figure 4.7). At 1 minute, the percentages of spreading for all three experimental conditions were all very low (11.1%, 4.5% and 7.0% respectively for mock, empty vector and *miR-181c* transfected cells) as the cells have not started to spread yet. However, after 3 and 5 minutes of spreading, a significantly lower percentage of cells that have spread was observed in *miR-181c* overexpression (11.7% at 3 minutes and 14.6% at 5 minutes) as compared to mock (75.7% at 3 minutes and 84.7% at 5 minutes) and empty vector (76.2% at 3 minutes and 92.4% at 5 minutes) transfections (Figure 4.7). This data suggests that ectopic expression of *miR-181c* leads to defects in lamellipodia formation in response to TCR stimulation.

The mutual recognition of T cell and APC results in the engagement and clustering of the TCR, and the formation of the T cell-APC interface, known as the immunological synapse. Regulation of actin polymerisation at the immunological synapse is crucial to initiate and sustain T cell activation. Hence, we next assessed whether *miR-181c* overexpression could impair actin polymerisation at the immunological synapse (T cell-B cell contact site). Our results showed that overexpression of *miR-181c* in Jurkat T cells led to severe impairment in actin polymerisation in response to stimulation with superantigen-pulsed MEC-1 B cells. A marked reduction of F-actin staining (red) at the T cell-B cell contact site was observed in *miR-181c* overexpressing Jurkat T cells in comparison to controls (Figure 4.8). To quantitatively determine the effect of *miR-181c* overexpression on

immunological synapse formation, we measured the total area (in square micrometre) of F-actin accumulation at the T cell contact sites and synapses with B cells. There was a significant reduction in the total area of F-actin accumulation at T cell-B cell contact site in *miR-181c* overexpressing cells as compared to cells in mock transfection (*P* value=0.0002) and cells transfected with empty vector (*P* value=0.0009) (Figure 4.8). This data suggests that in Jurkat T cells, *miR-181c* is essential for immunological synapse formation, a process that is highly dependent on proper regulation of actin cytoskeleton dynamics at the T cell-B cell conjugation site.

4.3.6 Overexpression of *miR-181c* Had No Impact on Cell Migration in Jurkat T Cells

To study whether ectopic expression of *miR-181c* in Jurkat T cells has an impact on migration, a process dependent upon actin polymerisation, we examined the ability of the cells to migrate towards a serum-rich condition. Our results showed that there was no difference in migration between cells overexpressed with *miR-181c* and the controls (Figure 4.9), indicating that enforced expression of *miR-181c* does not affect Jurkat T cell migration.

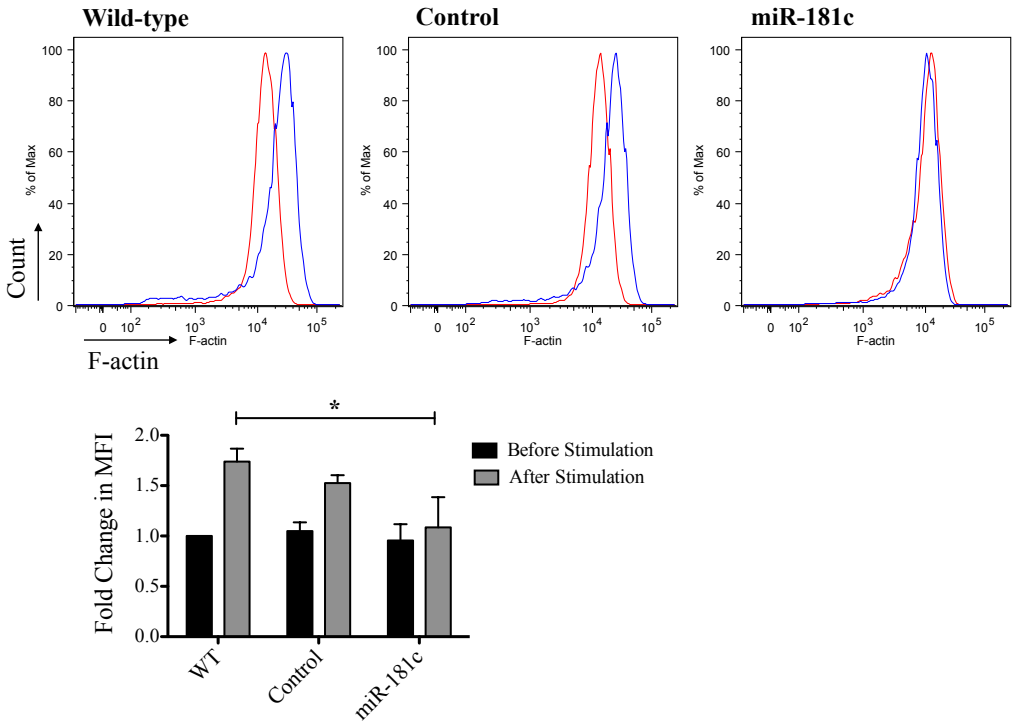

Figure 4.6: Overexpression of *miR-181c* in Jurkat T cells reduced actin polymerisation. F-actin staining of *miR-181c* overexpressing Jurkat T cells and controls, before (red) and after (blue) stimulation. Jurkat T cells were stimulated with 10µg/ml plate-bound anti-human CD3 antibody and 25ng/ml PMA for 24h. Y-axis indicates cell number and x-axis indicates log fluorescence intensity of F-actin (rhodamine phalloidin) staining. Results are representative of 3 independent experiments. Chart shows the quantification of fold change in MFI before and after stimulation. Error bars represent mean ± SD of 3 independent experiments. * $P \leq 0.05$.

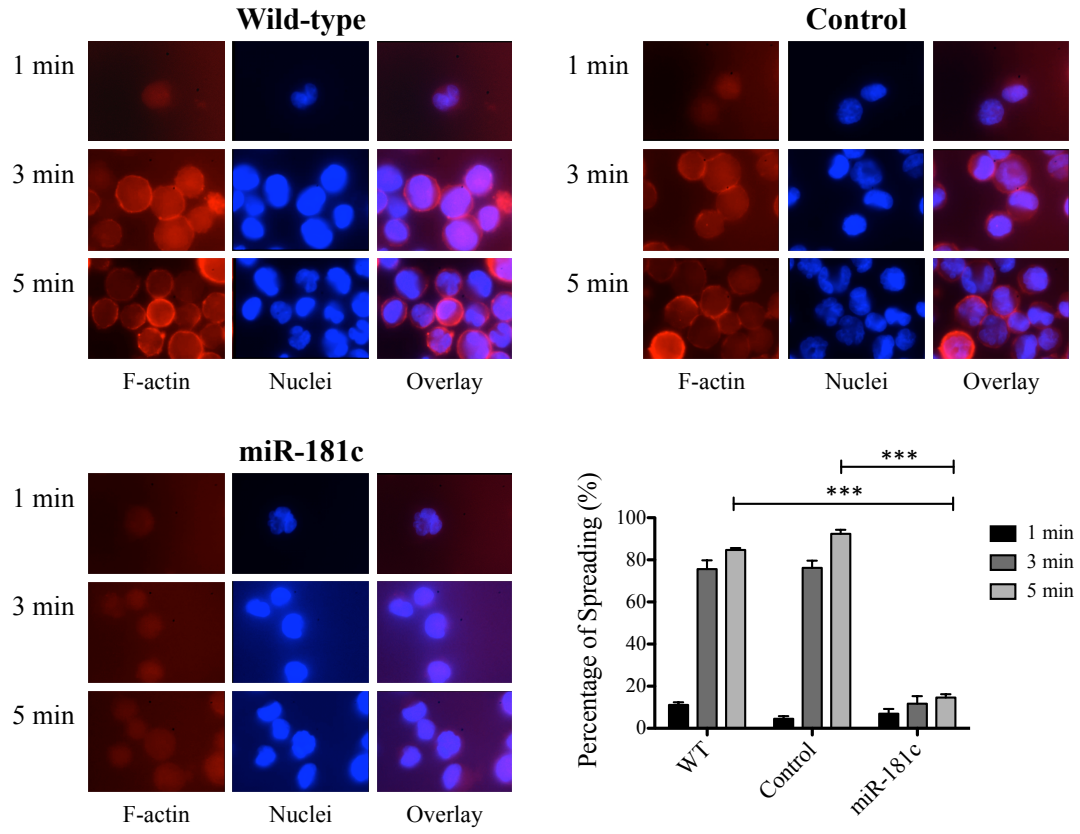

Figure 4.7: Overexpression of *miR-181c* in Jurkat T cells caused defective lamellipodia formation in response to TCR stimulation during cell spreading. Microscopy images show the lamellipodia formation in *miR-181c* transfected Jurkat T cells and controls during cell spreading at 1, 3 and 5 min. Cells were fixed, permeabilised, blocked and stained with rhodamine phalloidin (red) and DAPI (blue), followed by analysis using fluorescence microscopy with a 100× objective. Images shown are representative of 3 independent experiments. Chart shows the percentage of spreading at 1, 3 and 5 min of spreading. Percentage of spreading was calculated by counting at least 100 cells per experimental condition. Cells that form a F-actin ring at the cell periphery were scored as positive while cells without an F-actin ring were scored as negative. Statistical analysis is performed at 5 min time point. Error bars represent mean ± SEM of 3 independent experiments. *** $P \leq 0.001$.

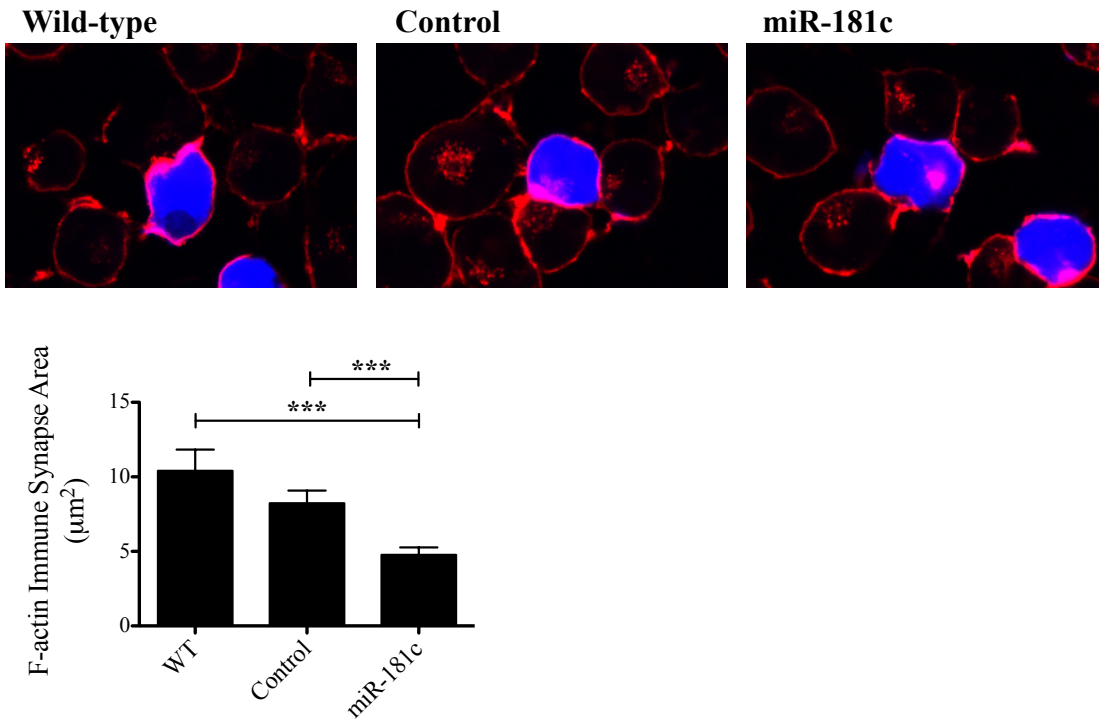

Figure 4.8: Overexpression of *miR-181c* in Jurkat T cells impaired immunological synapse formation. Confocal images show the immunological synapse formation between transfected Jurkat T cells (unstained) and superantigen-pulsed MEC-1 B cells (blue). Equal number of Jurkat T cells and superantigen-pulsed MEC-1 B cells were centrifuged, incubated, transferred to microscope slides, fixed, permeabilised and blocked. F-actin was stained using rhodamine phalloidin (red) and slides were analysed by confocal microscopy using a 60×/1.40 oil objective. Chart shows the quantification of the total area of F-actin at the T cell-B cell contact site (minimum conjugate measured n=16; maximum n=21) by NIS-elements imaging software and error bars represent mean ± SEM. *** $P \leq 0.001$.

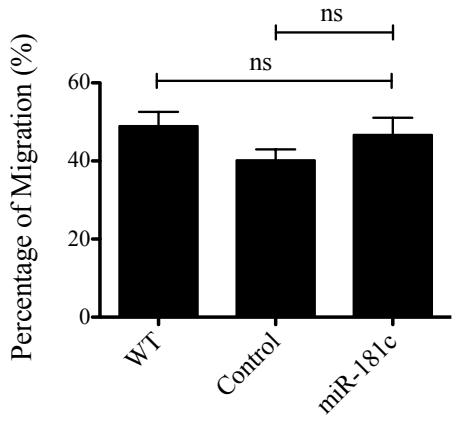

Figure 4.9: Overexpression of *miR-181c* in Jurkat T cells had no impact on cell migration. Percentage of migration in *miR-181c* overexpressing Jurkat T cells and controls. Cells were serum-starved, stained with Calcien AM, allowed to migrate towards serum-rich medium for 4h in a Boyden chamber. Number of migrated cells was determined by fluorescence intensity of Calcien AM using microplate reader and percentage of migration was calculated by the number of migrated cells relative to the total number of cells (non-migrated and migrated cells). Error bars represent mean ± SEM of 3 independent experiments. ns: not significant.

4.4 Effects of Transient *BRK1* Knockdown in Jurkat T Cells

4.4.1 Transient Knockdown of *BRK1* in Jurkat T Cells

Our previous results showed that *miR-181c* plays a crucial role in T cell activation and actin polymerisation-dependent T cell functions including lamellipodia generation and immunological synapse formation. We therefore focused our study on ascertaining the roles of *BRK1*, a *miR-181c* target, in T cell functions. In order to evaluate the roles of *BRK1* in T cell functions, a pool of four siRNAs targeting *BRK1* (Dharmacon; details see Appendix C2) was used to knockdown *BRK1* in Jurkat T cells. siRNA negative control and mock transfections were used as experimental controls. Both mRNA and protein expression of BRK1 were assessed at 24, 48, 72, 96 and 120 hours post-transfection. Successful reduction of *BRK1* mRNA expression was achieved using siRNA in Jurkat T cells. The reduction of *BRK1* expression was sustained for up to 120 hours post-transfection and the level of knockdown gradually reduced over this period, where 94.1% knockdown was achieved at 24 hours, 93.5% at 48 hours, 88.9% at 72 hours, 83% at 96 hours and 80.1% at 120 hours post-transfection (Figure 4.10a). Similarly, the BRK1 protein levels were substantially reduced in the siRNA-treated samples from 24 to 120 hours post-transfection (Figure 4.10b). Given that siBRK1 was able to silence *BRK1* in Jurkat T cells up to 120 hours post-transfection, we next examined the influence of *BRK1* knockdown in T cell functions.

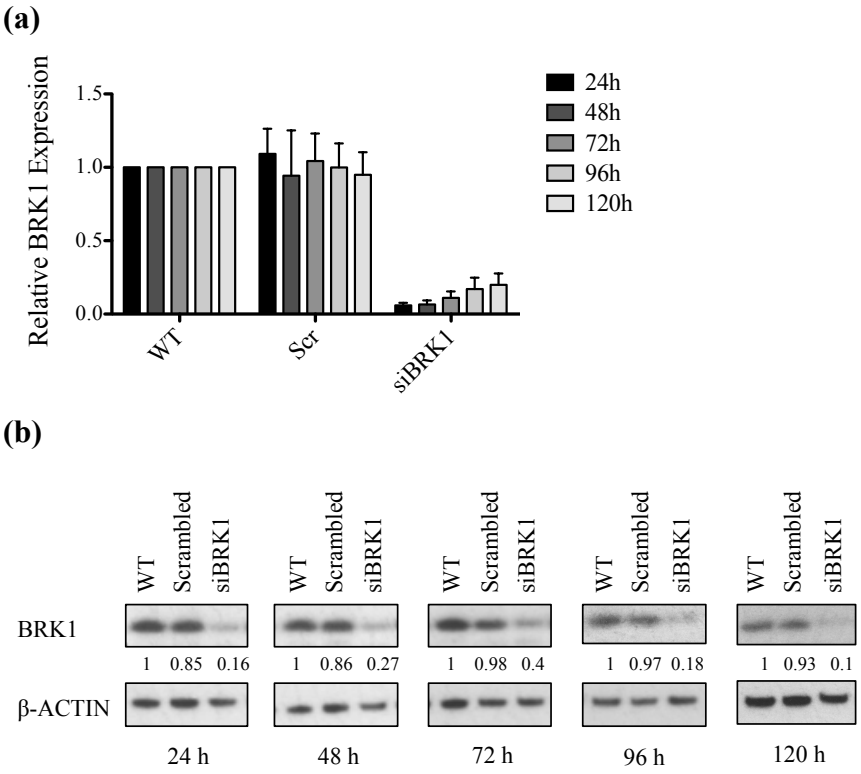

Figure 4.10: Transient knockdown of *BRK1* in Jurkat T cells. (a) Figure shows the qPCR analysis of relative *BRK1* expression in Jurkat T cells transfected with siRNA targeting *BRK1* (siBRK1), siRNA negative control (Scr) and mock transfected cells (WT). mRNA expression of *BRK1* was assessed at indicated time points after transfection. The data are calibrated to mock transfection and normalised to endogenous control *GAPDH*. Error bars represent mean ± SD of 3 independent experiments. (b) Western blot analysis of BRK1 protein expression in siBRK1-transfected Jurkat T cells and controls. Total protein lysates were prepared at the indicated time points after transfection. β-ACTIN level is used as a loading control and numbers represent the densitometric quantification of BRK1 protein expression level normalised to β-ACTIN. Blot shown is representative of 3 independent experiments.

4.4.2 Transient Knockdown of *BRK1* in Jurkat T Cells Had No Impact on Cell Cycle Profile

We next examined the effect of transient *BRK1* knockdown in Jurkat T cells on the changes of kinetics of cell cycle entry. Similarly to *miR-181c* overexpression, there was no significant difference in the percentage of cells in the three phases of cell cycle (G1, S and G2-M) between the siBRK1-treated cells and the controls at the three time points measured (24, 48 and 72 hours post-transfection) (Figure 4.11).

4.4.3 Transient Knockdown of *BRK1* Had Mild Impact on Jurkat T Cell Activation

To investigate whether *BRK1* knockdown influences T cell activation as in *miR-181c* overexpression, the expression of CD69 in *BRK1*-suppressed Jurkat T cells was examined, before and after co-stimulation with CD3 antibody and PMA. After stimulation, the expression of CD69 on the surface of Jurkat T cells in mock, siRNA negative control and siBRK1 transfections, were all increased when compared to those before stimulation. However, similarly to ectopic expression of *miR-181c*, the upregulation of CD69 expression was slightly lower in the *BRK1*-knockdown cells (79.7% $CD69^+$ cells) than in mock transfected (83.4% $CD69^+$ cells) and siRNA negative control transfected cells (84.9% $CD69^+$ cells) (Figure 4.12). This data indicates that in Jurkat T cells, consistent with *miR-181c* overexpression, transient *BRK1* knockdown slightly represses T cell activation.

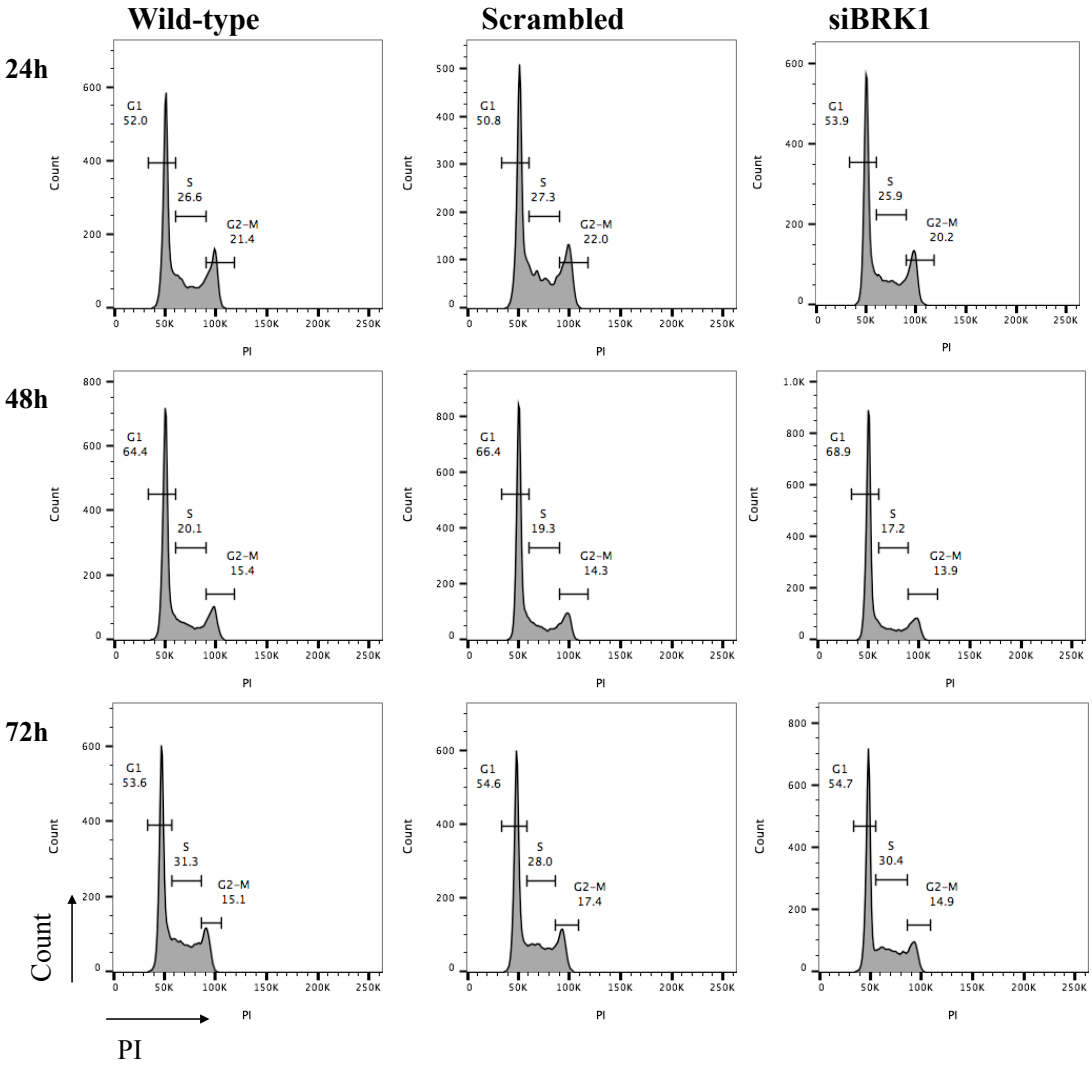

Figure 4.11: Transient *BRK1* knockdown had no impact on cell cycle profile in Jurkat T cells. Cell cycle profile of Jurkat T cells following siRNA-mediated knockdown of *BRK1*. Samples were fixed with 70% ethanol, stained with PI and analysed at 24, 48 and 72 hours post-transfection. Y-axis indicates cell number and x-axis indicates PI staining. Plots shown are representative of 3 independent experiments.

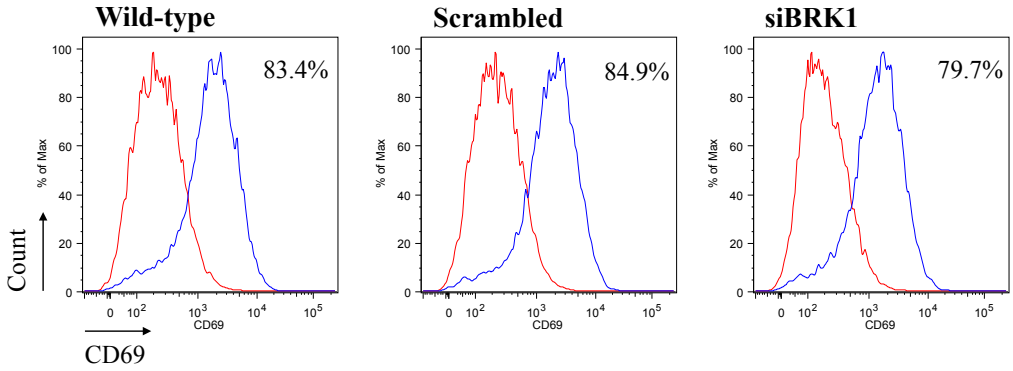

Figure 4.12: Transient *BRK1* knockdown had mild impact on Jurkat T cell activation. CD69 expression in siRNA-mediated *BRK1* knockdown Jurkat T cells, before (red) and after (blue) stimulation. Jurkat T cells was stimulated at 48h post-transfection with 10µg/ml plate-bound anti-human CD3 antibody and 25ng/ml PMA for 24h. Y-axis indicates cell number and x-axis indicates log fluorescence intensity of CD69-PE staining. Plots are representative of 3 independent experiments.

4.4.4 Transient Knockdown of *BRK1* Caused Defective Lamellipodia Formation in Jurkat T Cells

Due to our finding of impaired lamellipodia formation following *miR-181c* overexpression in Jurkat T cells and previous reports from other groups which showed that WAVE2 protein is implicated in regulating the generation of lamellipodia in T cells (Nolz et al., 2006), we next analysed the effect of *BRK1* suppression on the ability of Jurkat T cells to spread onto anti-CD3 coated slides by performing a spreading assay. Consistent with *miR-181c* overexpression, *BRK1*-knockdown cells failed to spread properly while in controls, cells were able to spread in a highly ordered fashion, forming a round lamellipodial interface containing radially-arrayed F-actin-rich structures at the cell periphery (Figure 4.13). At 1 minute of spreading, the percentage of spreading for all experimental conditions were all very low while at 3 and 5 minute, a reduced percentage of spreading was observed in cells transfected with siBRK1 as compared to controls (Figure 4.13). This data suggests that in Jurkat T cells, similar to ectopic expression of *miR-181c*, transient *BRK1* knockdown also results in defective lamellipodia generation in response to TCR stimulation.

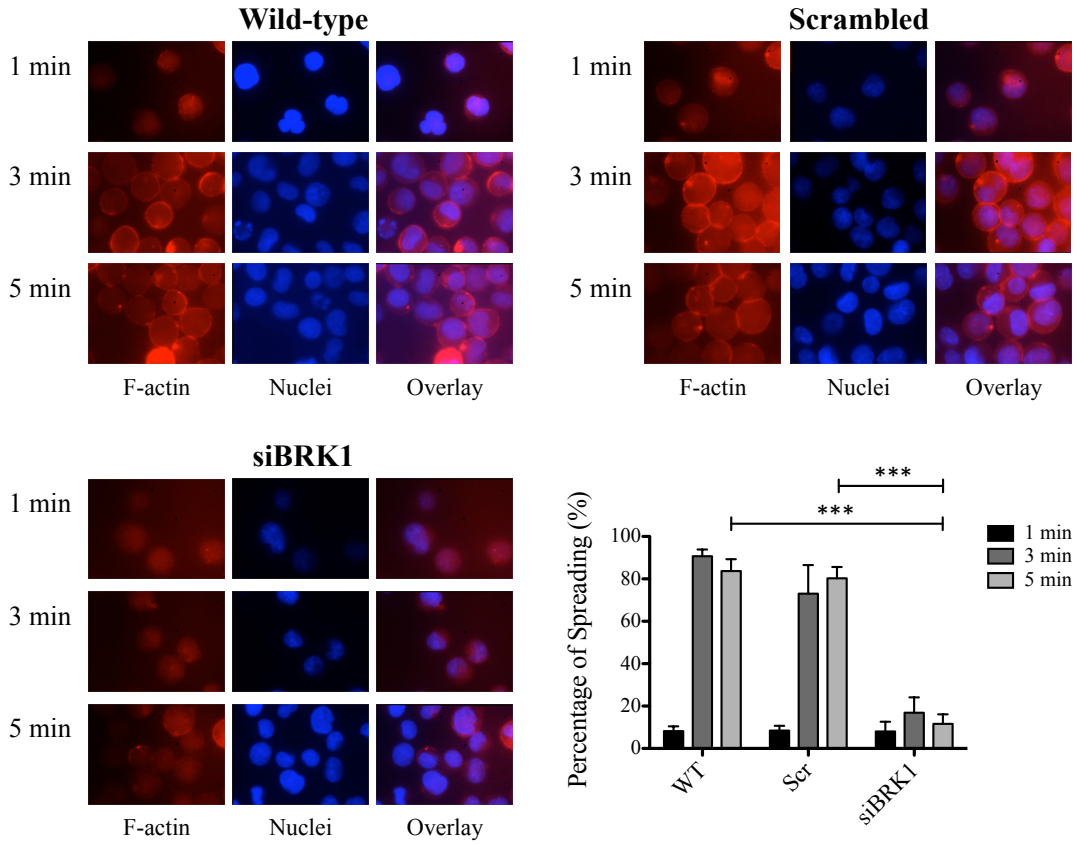

Figure 4.13: Transient *BRK1* knockdown in Jurkat T cells resulted in defects in lamellipodia formation in response to TCR stimulation during cell spreading. Microscopy images show the lamellipodia formation in Jurkat T cells following siRNA-mediated *BRK1* knockdown at 1, 3 and 5 min of cell spreading. Cells were fixed, permeabilised, blocked and stained with rhodamine phalloidin (red) and DAPI (blue), followed by analysis using fluorescence microscopy with a 100× objective. Images shown are representative of 3 independent experiments. Chart shows the percentage of spreading at 1, 3 and 5 min. Percentage of spreading was calculated by counting at least 100 cells per experimental condition. Cells that form a F-actin ring at the cell periphery were scored as positive while cells without an F-actin ring were scored as negative. Statistical analysis is performed at 5 min time point. Error bars represent mean ± SEM of 3 independent experiments. *** $P \leq 0.001$.

4.5 Effects of Stable *BRK1* Knockdown in T Cells

4.5.1 Stable Knockdown of *BRK1* in T Cells

Several limitations of using siRNA targeting *BRK1* to achieve gene silencing have been faced in performing functional assays in T cells. Therefore, we employed lentiviral shRNA targeting *BRK1* in the subsequent studies. The main reason of switching from siRNA to shRNA was the much higher number of cells required for various T cell functional assays, making the use of siRNA very costly. Furthermore, we found that there was poor consistency between experimental replicates using siRNA. In addition, we observed a high level of cell death after siRNA electroporation.

Two lentiviral vectors targeting *BRK1*, pLKO.1-shBRK1_1 and pLKO.1-shBRK1_2 were used to knockdown *BRK1* in Jurkat and primary T cells. Scrambled shRNA (pLKO.1-scrambled shRNA, Addgene, plasmid #1864) and mock transduction were used as experimental controls. The lentiviral vectors were first titrated using colony formation assay in HeLa cells in order to calculate the amount of virus to be used in Jurkat and primary T cells transduction (Figure 4.14). Colony forming units/ml (CFU/ml) was calculated from number of colony as follows.

Colony forming units/ml (CFU/ml) = Number of colony / Final concentration of lentivirus added

For scrambled shRNA,
CFU/ml (for 10^{-6} final concentration) = $12.3/10^{-6} = 1.23\times10^{7}$
CFU/ml (for 10^{-7} final concentration) = $2/10^{-7} = 2\times10^{7}$
Average of CFU/ml from 2 concentrations = 1.615×10^{7}

For shBRK1_1,
CFU/ml (for 10^{-7} final concentration) = $9.7/10^{-7} = 9.7\times10^{7}$

For shBRK1_2,
CFU/ml (for 10^{-7} final concentration) = $16/10^{-7} = 1.6\times10^{8}$

Jurkat T cells were transduced with lentivirus with an MOI of 24 to achieve a constitutive knockdown of *BRK1*. The *BRK1* mRNA expression was drastically reduced in cells transduced with the two shBRK1 lentiviral vectors as compared to the controls. However, shBRK1_1 showed higher knockdown as compared to shBRK1_2, where *BRK1* mRNA expression was reduced to less than 4% for the shBRK1_1 and 22% for the shBRK1_2 (Figure 4.15a). Similarly to *BRK1* mRNA expression, BRK1 protein level was markedly reduced in both of the shBRK1-treated samples when compared to the controls (Figure 4.15b).

To transduce primary T cells, lentivirus with an MOI of 50 was used to achieve constitutive *BRK1* knockdown. Following transduction, mRNA and protein level of BRK1 were examined before and after stimulation with CD3 and CD28 antibodies. Comparable to Jurkat T cells, the *BRK1* mRNA expression was decreased in both of the shBRK1-treated cells, before and after stimulation, as compared to the controls. The shBRK1_1 showed higher knockdown as compared to shBRK1_2. Before stimulation, *BRK1* expression was reduced to less than 9% for the shBRK1_1 and 33% for the shBRK1_2 while after stimulation, the percentage of *BRK1* knockdown with shBRK1_1 was 92.26% and with shBRK1_2 was 60.84% (Figure 4.16a). Consistent with *BRK1* mRNA expression, protein expression level of BRK1 was also substantially decreased in both shBRK1-treated samples before and after stimulation (Figure 4.16b).

Given that we achieved good constitutive knockdown of *BRK1* in both Jurkat and primary T cells, we next evaluated the influence of *BRK1* suppression on several T cell functions.

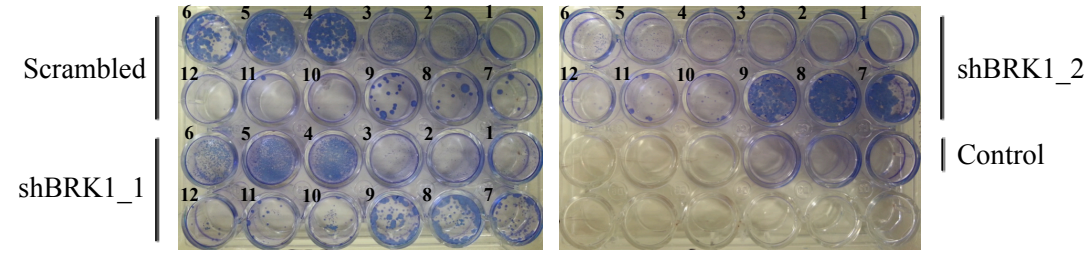

Figure 4.14: Lentivirus titration by colony formation assay. Figure shows the number of colony formed in HeLa cells transduced with the three lentiviral vectors (scrambled shRNA, shBRK1_1 and shBRK1_2). Cells were treated with puromycin to select for colonies with stable integration of lentiviral vectors. For scrambled shRNA, number of colony was counted from wells with 10^{-6} and 10^{-7} final concentrations while for shBRK1_1 and shBRK1_2, number of colony was counted from wells with 10^{-7} final concentration. Number of colony was scored from triplicate wells for each condition. Well 1, 2 and 3: 0.1µl of lentivirus added (final concentration 10^{-4}); well 4, 5 and 6: 0.01µl of lentivirus added (final concentration 10^{-5}); well 7, 8 and 9: 0.001µl of lentivirus added (final concentration 10^{-6}); well 10, 11 and 12: 0.0001µl of lentivirus added (final concentration 10^{-7}). Control: no lentivirus added.

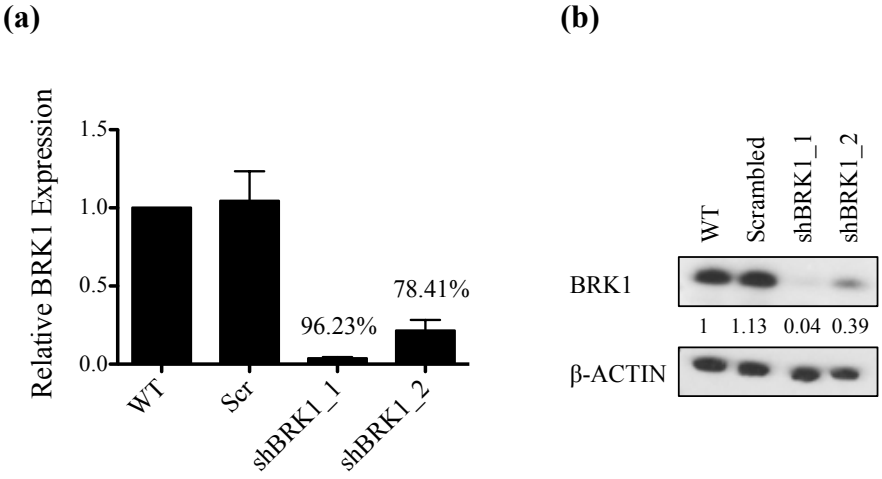

Figure 4.15: Stable knockdown of *BRK1* in Jurkat T cells. (a) Figure shows the qPCR analysis of relative *BRK1* expression in Jurkat T cells following transduction with two independent shRNA targeting *BRK1* (shBRK1_1 and shBRK1_2). The data are calibrated to mock transduction and normalised to endogenous control *GAPDH*. Numbers above the bar are indicative of the percentage of *BRK1* knockdown. Error bars represent mean ± SD of 5 independent experiments. (b) Western blot analysis of BRK1 protein expression in Jurkat T cells transduced with shBRK1. β-ACTIN level is used as a loading control and numbers represent the densitometric quantification of BRK1 protein expression level normalised to β-ACTIN. Blot shown is representative of 5 independent experiments.

(a)

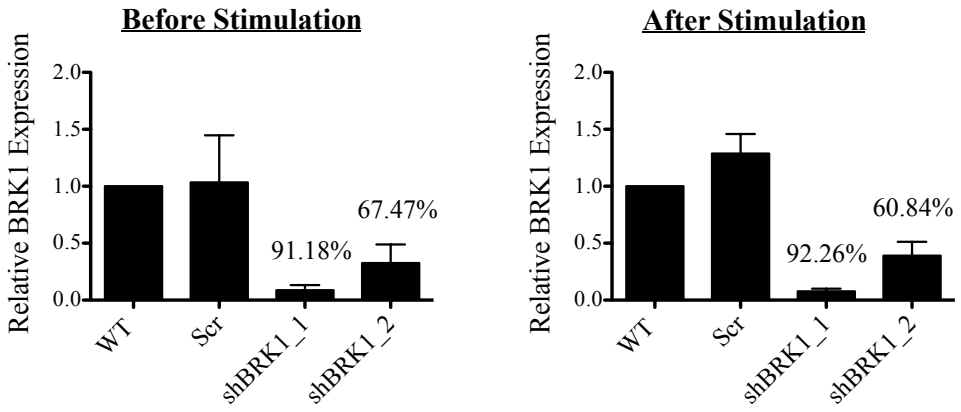

(b)

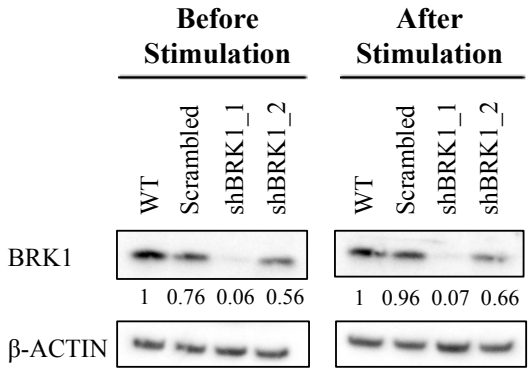

Figure 4.16: Stable knockdown of *BRK1* in primary T cells. (a) Figures show the qPCR analysis of relative *BRK1* expression in primary T cells transduced with shRNA targeting *BRK1* (shBRK1_1 and shBRK1_2) before and after stimulation. Primary T cells were stimulated with 2μg/ml of plate bound anti-human CD3 and soluble anti-human CD28 for 24h. The data are calibrated to mock transduction and normalised to endogenous control *GAPDH*. Numbers above the bar are indicative of the percentage of *BRK1* knockdown. Error bars represent mean ± SD of 4 independent experiments. (b) Western blot analysis of BRK1 protein expression in shBRK1-transduced primary T cells before and after stimulation. β-ACTIN level is used as a loading control and numbers represent the densitometric quantification of BRK1 protein expression level normalised to β-ACTIN. Blot shown is representative of 4 independent experiments.

4.5.2 Stable Knockdown of *BRK1* Led to Reduced Expressions of Other Proteins in the WAVE2 Complex

Before studying the impact of *BRK1* knockdown in T cells, we explored the role of *BRK1* in the stability and integrity of WAVE2 protein in both Jurkat and primary T cells. Following *BRK1* silencing in Jurkat and primary T cells, the stability of WAVE2 protein was investigated by examining the protein expressions of other members in the WAVE2 complex, including WAVE2, ABI1, SRA1 and HEM1. In addition, protein expression of ARP2 and ARP3, which have been shown to bind to the activated WAVE2 protein to carry out actin nucleation (Goley and Welch, 2006; Takenawa and Suetsugu, 2007), were also studied. Upon knockdown of *BRK1* in both Jurkat and primary T cells, the protein expressions of WAVE2, ABI1 and SRA1 were reduced as compared to controls while HEM1, ARP2 and ARP3 protein expression levels remained unchanged (Figure 4.17). This data suggests that BRK1 protein is important in the stability of the WAVE2 regulatory complex in T cells.

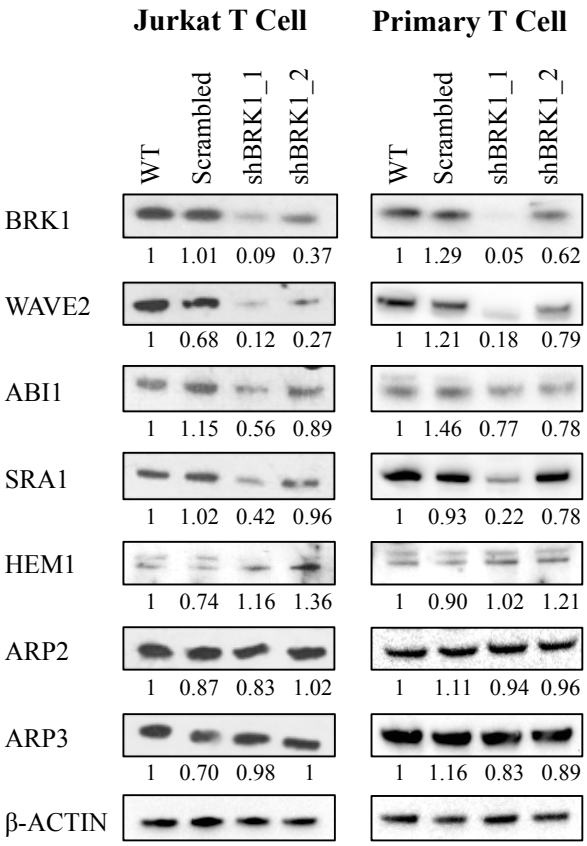

Figure 4.17: Stable *BRK1* knockdown in T cells reduced protein expressions of other members in the WAVE2 complex. Western blot analysis of BRK1, WAVE2, ABI1, SRA1, HEM1, ARP2 and ARP3 protein expressions in both Jurkat and primary T cells following shRNA-mediated *BRK1* knockdown. β-ACTIN level is used as a loading control and numbers represent the densitometric quantification of protein expression levels normalised to β-ACTIN. Blot shown is representative of 2 independent experiments.

4.5.3 Stable Knockdown of *BRK1* in T Cells Had Mild Impact on Cell Proliferation But Had No Impact on Cell Cycle and Cell Viability

Trypan blue exclusion result showed that *BRK1* knockdown had only a relatively mild impact on the proliferation with a slight reduction in total cell number at day 6 as compared to controls, although the difference was not statistically significance (Figure 4.18).

Moreover, we also examined the effect of *BRK1* suppression in T cells on the changes of kinetics of cell cycle entry. In Jurkat T cells, cell cycle profiles showed that there was no change in the percentage of cells in the three phases of cell cycle (G1, S and G2-M) between shBRK1-treated cells and cells in the controls (Figure 4.19a). The cell cycle of primary T cells was analysed before and after co-stimulation with CD3 and CD28 antibodies. After stimulation, there was no change in the cell cycle profiles in cells with reduced expression of *BRK1*, as in Jurkat T cells. Before stimulation, there were not many cells detected in S and G2-M phases, indicating that the cells do not enter the cell cycle unless they are stimulated (Figure 4.19b).

In addition, the effect of *BRK1* knockdown on cell viability was also examined in both Jurkat and primary T cells. In Jurkat T cells, there was no difference in the percentage of live (85-90% of Annexin V^- PI^- cells), early apoptotic (6-11% of Annexin V^+ PI^- cells) and late apoptotic cells (~3% of Annexin V^+ PI^+ cells) between *BRK1*-knockdown cells and controls (Figure 4.20a). Similarly to Jurkat T cells, there was no variation observed in the percentages of live, early apoptotic and late apoptotic cells between *BRK1*-knockdown primary T cells and controls, both before and after stimulation with CD3 and CD28 antibodies (Figure 4.20b).

Consistent with the results observed with the overexpression of *miR-181c* in Jurkat T cells, constitutive knockdown of *BRK1* in both Jurkat and primary T cells did not influence cell proliferation, cell cycle profile and cell viability.

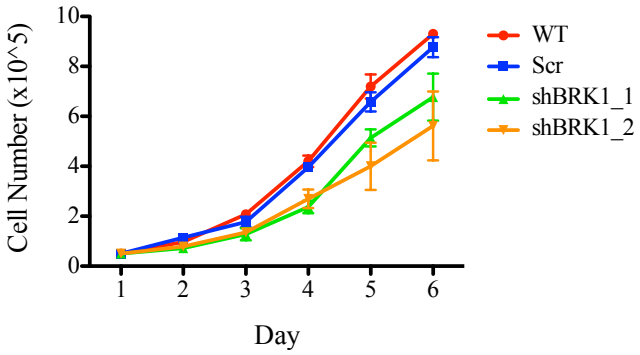

Figure 4.18: Stable knockdown of *BRK1* had mild impact on Jurkat T cell proliferation. Plot shows the cell proliferation of *BRK1*-knockdown Jurkat T cells (green and orange), mock transduced (WT, red) and scrambled shRNA transduced cells (Scr, blue). Cells were seeded and cultured in a 24-well plate and counted every day for 6 days. Error bars represent mean ± SEM of 3 independent experiments.

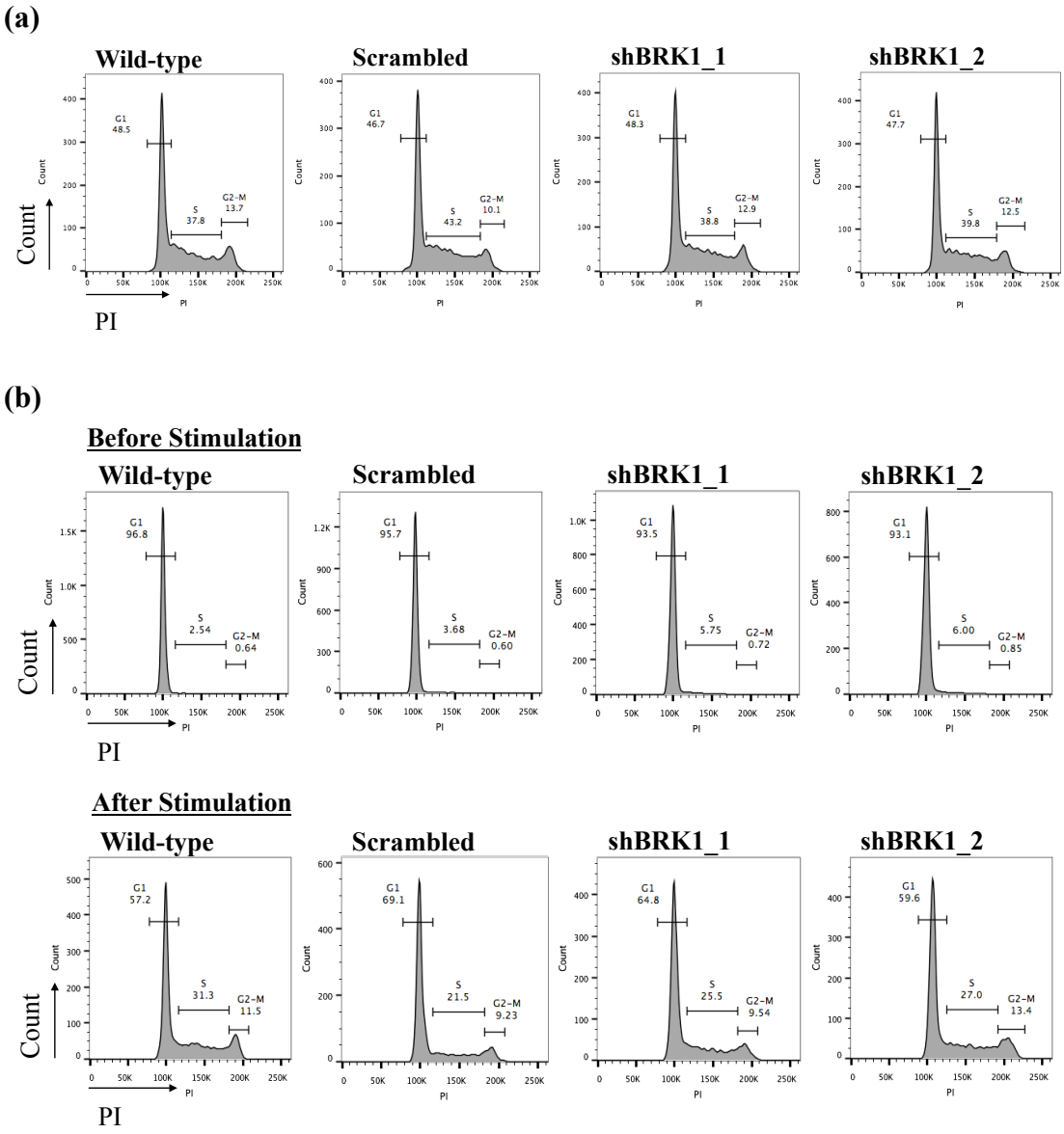

Figure 4.19: Stable *BRK1* knockdown in Jurkat and primary T cells had no impact on cell cycle profile. Cell cycle profile of (a) Jurkat and (b) primary T cells following shRNA-mediated *BRK1* knockdown. Samples were fixed with 70% ethanol, stained with PI and analysed by flow cytometry. For primary T cells, cell cycle profile was analysed before and after stimulation. Primary T cells were stimulated with 2µg/ml of plate bound anti-human CD3 and soluble anti-human CD28 antibodies for 24h. Y-axis indicates cell number and x-axis indicates PI staining. Plots are representative of 3 independent experiments.

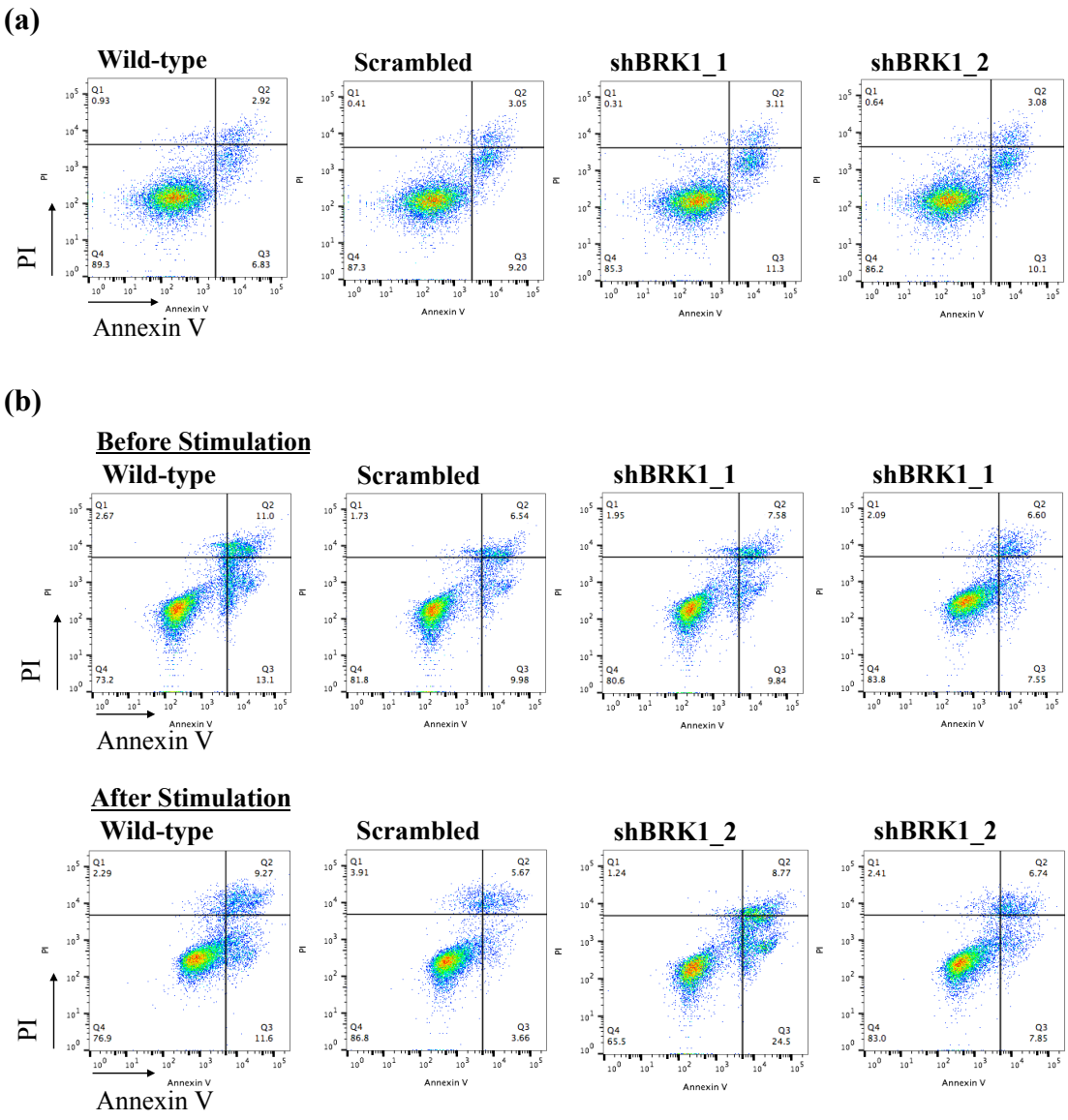

Figure 4.20: Stable *BRK1* knockdown in Jurkat and primary T cells had no impact on cell viability. APC Annexin V and PI staining of (a) Jurkat and (b) primary T cells following shRNA-mediated *BRK1* knockdown. The percentage of live (Q4 = double negative for Annexin V and PI), early apoptotic (Q3 = positive Annexin V and negative PI) and late apoptotic (Q2 = double positive for Annexin V and PI) cells were analysed by flow cytometry. In primary T cells, Annexin V and PI staining were analysed before and after stimulation. Primary T cells were stimulated with 2µg/ml of plate bound anti-human CD3 and soluble anti-human CD28 for 24h. Y-axis indicates log fluorescence intensity of PI staining and x-axis indicates log fluorescence intensity of APC Annexin V staining.

4.5.4 Stable Knockdown of *BRK1* Repressed T Cell Activation

We next investigated the effects of *BRK1* suppression on T cell activation. The surface expression of T cell activation markers, CD69 and CD154 were analysed by flow cytometry analysis. The levels of CD69 and CD154 were examined before and after stimulation with CD3 antibody and PMA for Jurkat T cells, and CD3 and CD28 antibodies for primary T cells. Upon stimulation, the expression of CD69 on the surface of Jurkat T cells in mock, scrambled shRNA and shBRK1 transductions were all increased. However, the increase in CD69 expression was markedly reduced in the *BRK1*-knockdown cells (46.8% $CD69^+$ cells for shBRK1_1 and 35.2% for shBRK1_2) as compared to mock transduced (86.3% $CD69^+$ cells) and scrambled shRNA transduced cells (78.9% $CD69^+$ cells) (Figure 4.21a). Consistent with the results observed in Jurkat T cells, the expression level of CD69 in primary T cells in all experimental conditions were elevated after stimulation as compared to before stimulation, but the increase of CD69 expression was lower in the *BRK1*-knockdown cells in comparison to controls (Figure 4.21b). To confirm the finding that *BRK1* knockdown causes reduction in primary T cell activation as shown by CD69 expression, the expression of another T cell activation marker, CD154 was also examined in primary T cells. Similar results were observed and the increase in CD154 expression upon stimulation was lower in *BRK1*-suppressed cells (61.4% $CD154^+$ cells for shBRK1_1 and 49.8% for shBRK1_2) as compared to mock transduced (85.3% of $CD154^+$ cells) and scrambled shRNA transduced cells (80.9% of $CD154^+$ cells) (Figure 4.21c). These data and the *miR-181c* overexpression studies suggest that the *miR-181c*-BRK1 axis plays an important role in regulation of T cell activation.

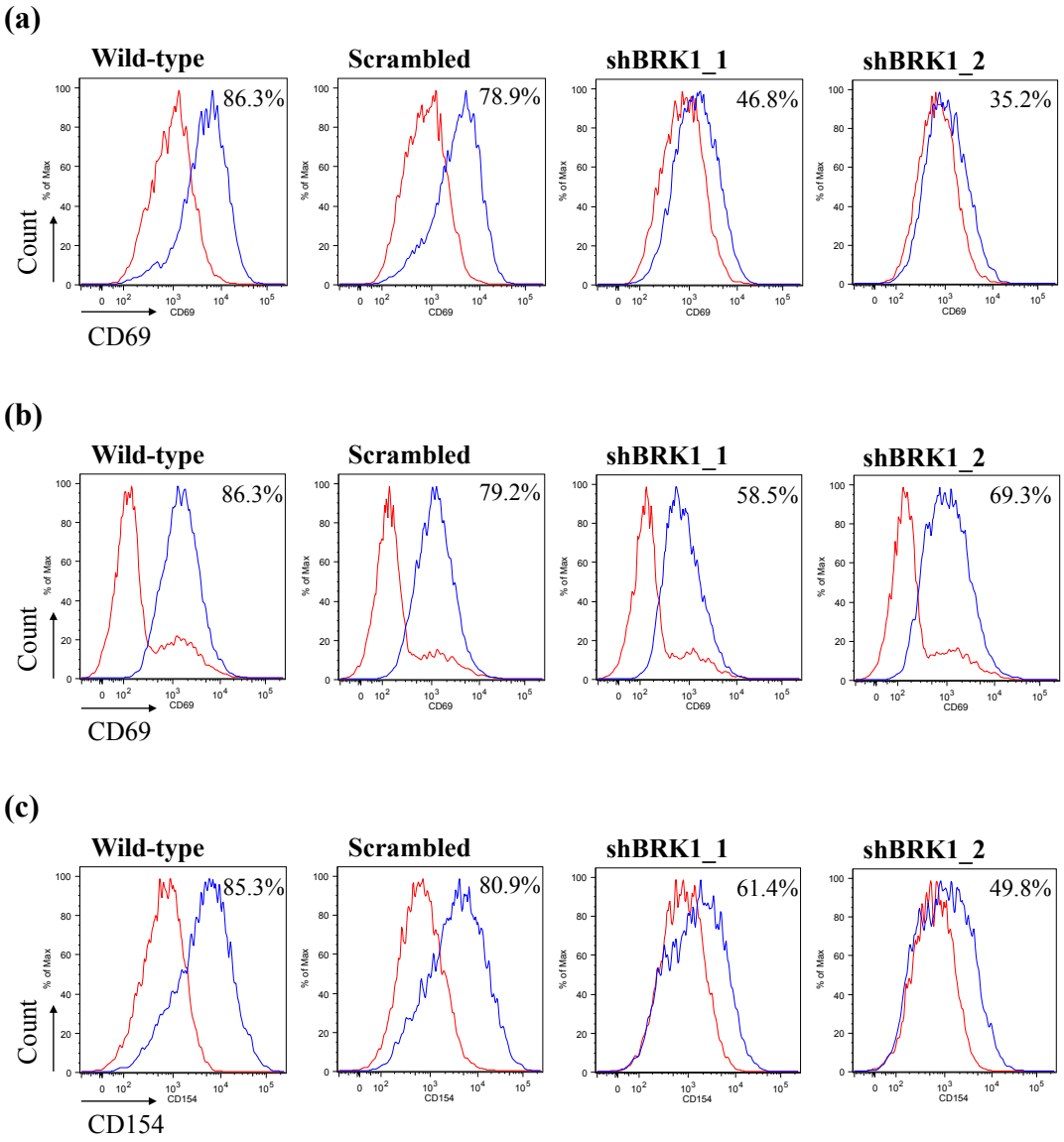

Figure 4.21: Stable *BRK1* knockdown in Jurkat and primary T cells repressed T cell activation. (a) CD69 expression in Jurkat T cells transduced with shRNA against *BRK1* before (red) and after (blue) stimulation. Jurkat T cells were stimulated with 10µg/ml plate-bound anti-human CD3 antibody and 25ng/ml PMA for 24h. Y-axis indicates cell number and x-axis indicates log fluorescence intensity of CD69-PE staining. (b) CD69 expression in primary T cells following shBRK1 transduction before (red) and after (blue) stimulation. Primary T cells were stimulated with 2µg/ml plate-bound anti-human CD3 and soluble anti-human CD28 antibodies for 24h. Y-axis indicates cell number and x-axis indicates log fluorescence intensity of Pacific Blue CD69 staining. (c) CD154 expression in primary T cells following shRNA-mediated *BRK1* knockdown, before (red) and after (blue) stimulation. Y-axis indicates cell number and x-axis indicates log fluorescence intensity of CD154-PE staining. Results are representative of 3 independent experiments.

4.5.5 Stable Knockdown of *BRK1* Decreased Actin Polymerisation During Lamellipodia and Immunological Synapse Formation in T Cells

Owing to the importance of reorganisation of the actin cytoskeleton in T cell activation (Holsinger et al., 1998) and our findings on the pivotal role of the *miR-181c*-BRK1 axis in T cell activation, we next assessed whether *BRK1* silencing in T cells has a similar effect as *miR-181c* overexpression on the regulation of actin polymerisation. As in *miR-181c* overexpression, total cellular F-actin content was first quantified in both *BRK1*-knockdown Jurkat and primary T cells, before and after stimulation. In both Jurkat (Figure 4.22a) and primary T cells (Figure 4.22b), the total F-actin content remained unaltered in *BRK1*-knockdown cells (shBRK1_1 and shBRK1_2) while in controls, the total cellular F-actin content increased after stimulation as compared to those before stimulation, as quantified by MFI. This data is consistent with those obtained with *miR-181c* overexpression, implying that *miR-181c*-BRK1 axis is required for maximal actin polymerisation in T cells.

The influence of *miR-181c* and its target BRK1 on the total cellular F-actin content upon stimulation have led us to determine whether constitutive knockdown of *BRK1* in T cells also has an effect on lamellipodia formation as in *miR-181c* overexpression. Generation of lamellipodia occurs during cell spreading upon TCR stimulation and it requires actin reorganisation. Therefore, as in *miR-181c* overexpression and transient *BRK1* knockdown, spreading assay was performed to examine the ability of the cells to spread onto anti-CD3 coated slides following constitutive *BRK1* knockdown. Our results were consistent with the findings in *miR-181c* overexpression and transient *BRK1* knockdown where we found that downregulation of *BRK1* in both Jurkat (Figure 4.23a) and primary T cells (Figure 4.23b) resulted in a defect in lamellipodia formation. Similar to *miR-181c* overexpression and transient knockdown of *BRK1*, no difference was seen at 1

minute of spreading between *BRK1*-knockdown T cells and controls while significant differences were observed at 3 and 5 minutes of spreading where depletion of *BRK1* had significant impact on the cell ability to spread in response to anti-CD3 stimulation (Figure 4.23). This data suggests that the *miR-181c*-BRK1 axis is required for the generation of lamellipodia in response to TCR stimulation, a phenomenon requiring proper regulated actin polymerisation.

Subsequently, we also examined whether *BRK1* is required for actin polymerisation at the T cell-B cell contact site by performing immunological synapse assay following constitutive *BRK1* knockdown in both Jurkat and primary T cells. Consistent with findings in the *miR-181c* overexpression studies, our results demonstrated that in both Jurkat (Figure 4.24a) and primary T cells (Figure 4.24b), knockdown of *BRK1* resulted in a severe impairment in actin polymerisation in response to stimulation with superantigen-pulsed MEC-1 B cells as shown by significantly reduced F-actin staining (red) and total area of F-actin accumulation at the T cell-B cell contact site. Hence, consistent with *miR-181c* overexpression, this data indicates that reduced expression of *BRK1* in T cells induced a defect in F-actin accumulation at the immunological synapse, suggesting that the *miR-181c*-BRK1 axis is important in immunological synapse formation, a process that is highly dependent on proper actin reorganisation in T cells.

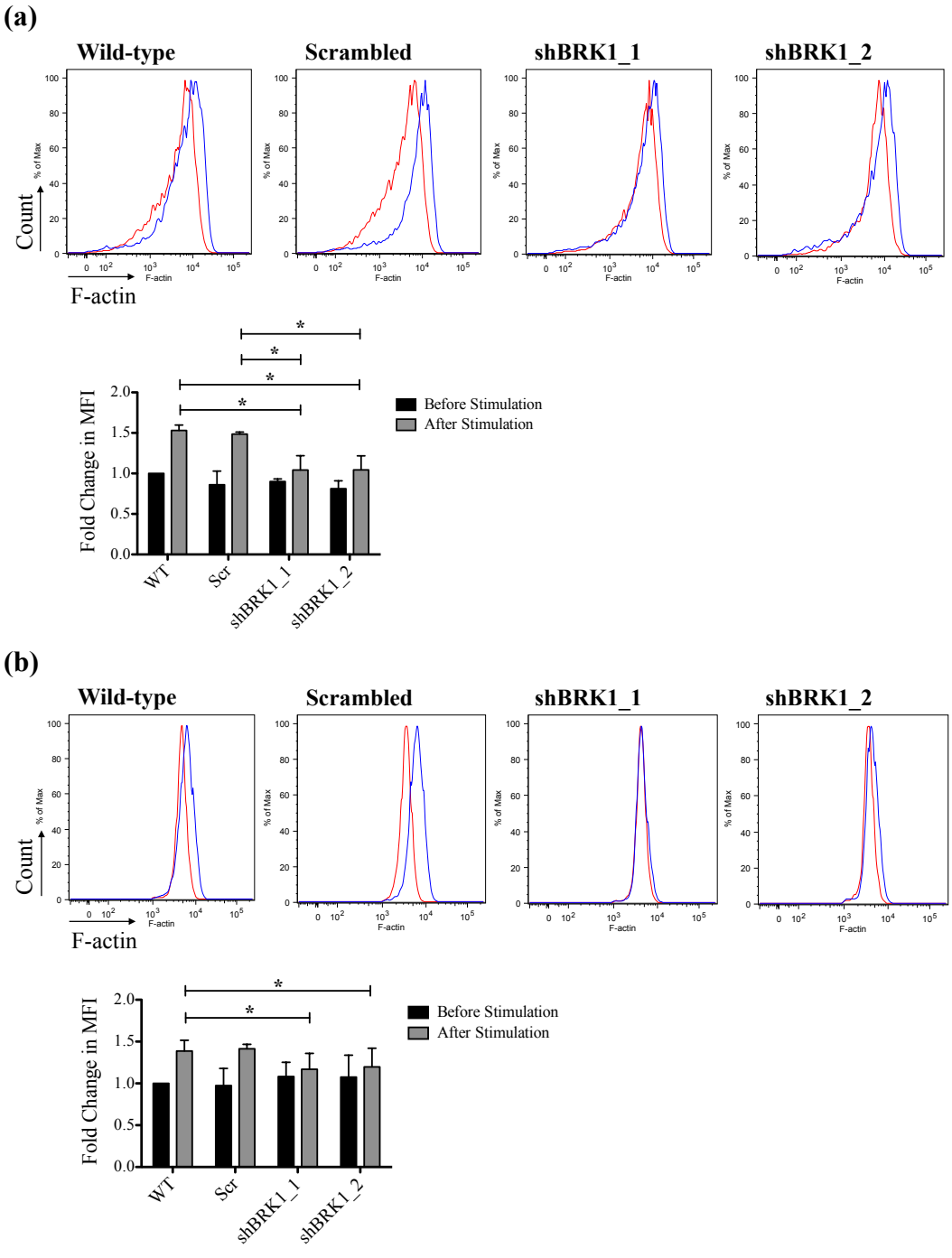

Figure 4.22: Stable *BRK1* knockdown in Jurkat and primary T cells reduced actin polymerisation. F-actin staining of (a) Jurkat and (b) primary T cells following *BRK1* suppression before (red) and after (blue) stimulation. Jurkat T cells were stimulated with 10µg/ml plate-bound anti-human CD3 antibody and 25ng/ml PMA for 24h while primary T cells with 2µg/ml plate-bound anti-human CD3 and soluble anti-human CD28 antibodies for 24h. Y-axis indicates cell number and x-axis indicates log fluorescence intensity of F-actin (rhodamine phalloidin) staining. Plots are representative of 3 independent experiments. Charts show the quantification of fold change in MFI before and after stimulation. Error bars represent mean ± SD of 3 independent experiments. * $P \leq 0.05$.

(a)

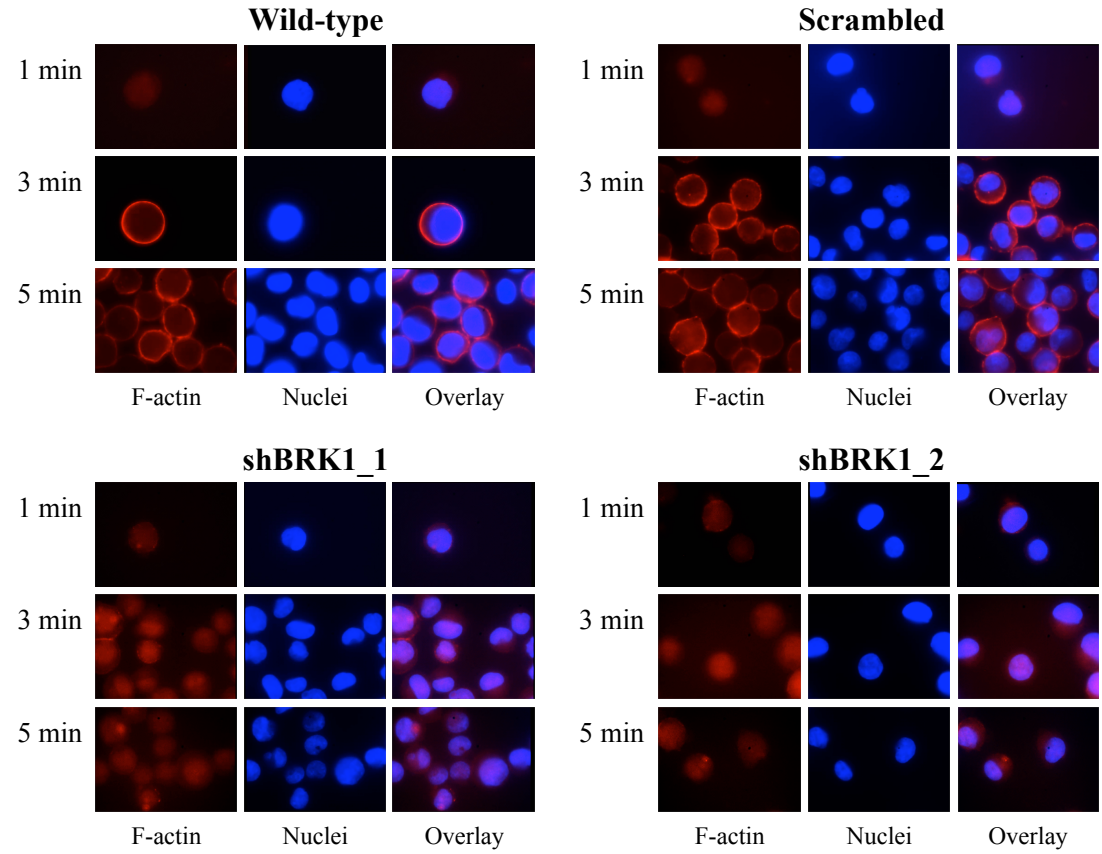
Wild-type
Scrambled
shBRK1_1
shBRK1_2
1 min
3 min
5 min
F-actin
Nuclei
Overlay

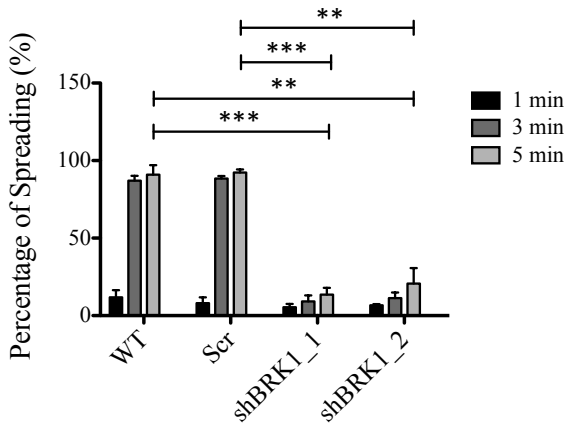
Percentage of Spreading (%)
150
100
50
0
**
***
**
***
1 min
3 min
5 min
WT
Scr
shBRK1_1
shBRK1_2

(b)

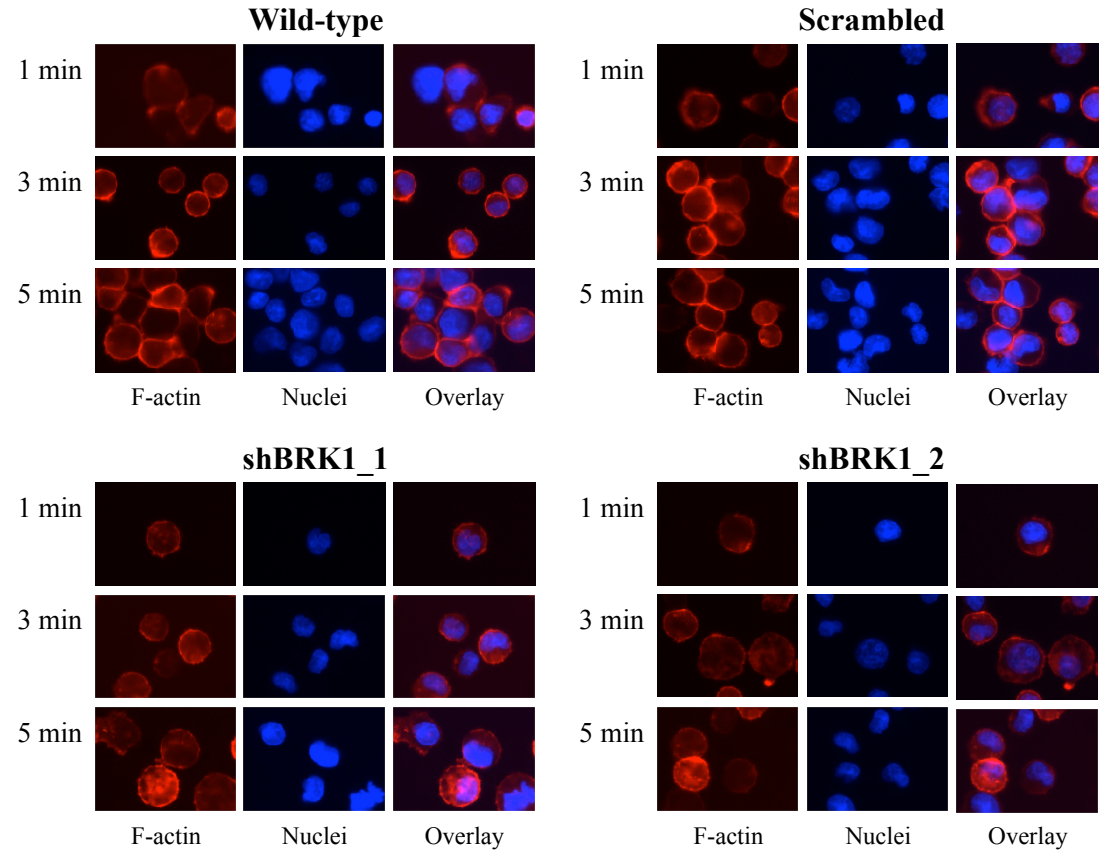

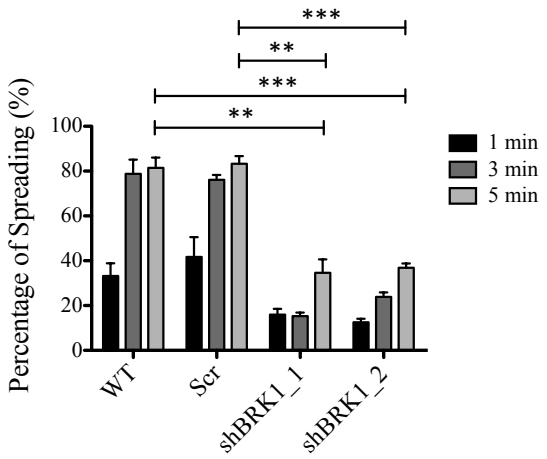

Figure 4.23: Stable *BRK1* knockdown in Jurkat and primary T cells led to defective lamellipodia formation in response to TCR stimulation during cell spreading. Microscopy images show the lamellipodia formation in (a) Jurkat and (b) primary T cells following *BRK1* suppression at 1, 3 and 5 min of cell spreading. Cells were fixed, permeabilised, blocked and stained with rhodamine phalloidin (red) and DAPI (blue), followed by analysis using fluorescence microscopy with a 100× objective. Images shown are representative of 3 independent experiments. Charts show the percentage of spreading at 1, 3 and 5 min of spreading. Statistical analysis is performed at 5 min time point. Error bars represent mean ± SEM of 3 independent experiments. ** $P \leq 0.01$, *** $P \leq 0.001$.

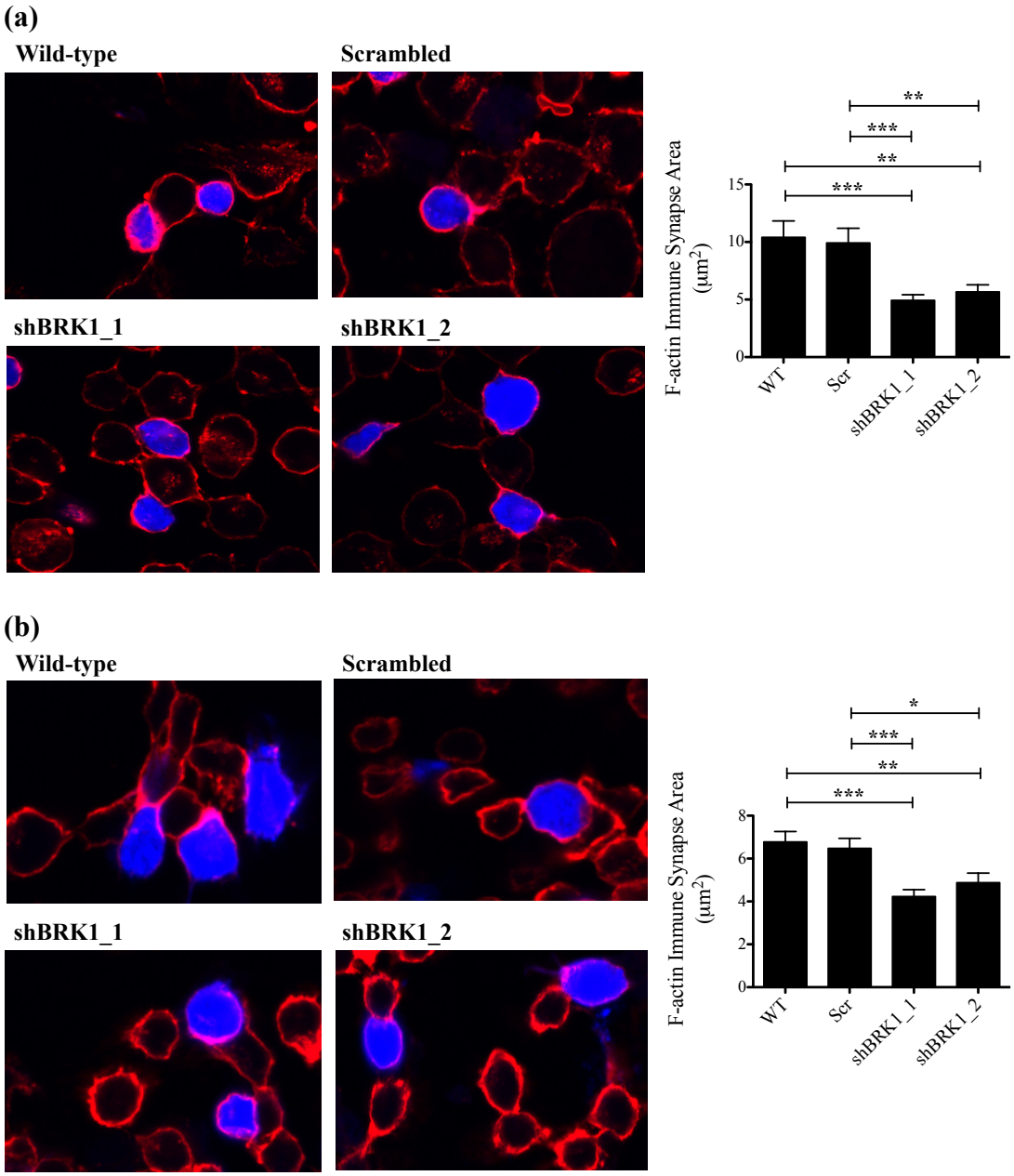

Figure 4.24: Stable *BRK1* knockdown in Jurkat and primary T cells impaired immunological synapse formation. Confocal images show the immunological synapse formation between *BRK1*-knockdown (a) Jurkat or (b) primary T cells (unstained) and superantigen-pulsed MEC-1 B cells (blue). Equal number of T cells and superantigen-pulsed MEC-1 B cells were centrifuged, incubated, transferred to microscope slides, fixed, permeabilised and blocked. F-actin was stained using rhodamine phalloidin (red) and slides were analysed by confocal microscopy using a 60×/1.40 oil objective. Charts show the quantification of the total area of F-actin accumulation at the T cell-B cell contact site (minimum conjugate measured n=16; maximum n=21 for Jurkat T cells and minimum n=14; maximum n=30 for primary T cells) by NIS-elements imaging software and error bars represent mean ± SEM. * $P \leq 0.05$, ** $P \leq 0.01$, *** $P \leq 0.001$.

4.5.6 Stable Knockdown of *BRK1* Had No Impact on Cell Migration in Jurkat T Cells

To study the impact of *BRK1* knockdown on migration of Jurkat T cells, a cellular process depending on actin cytoskeleton, the ability of the cells to migrate towards a serum-rich condition was examined. As in the *miR-181c* overexpression studies, constitutive *BRK1* knockdown in Jurkat T cells did not influence cell migration because there was no difference in the percentage of migration between *BRK1*-knockdown cells and controls (Figure 4.25).

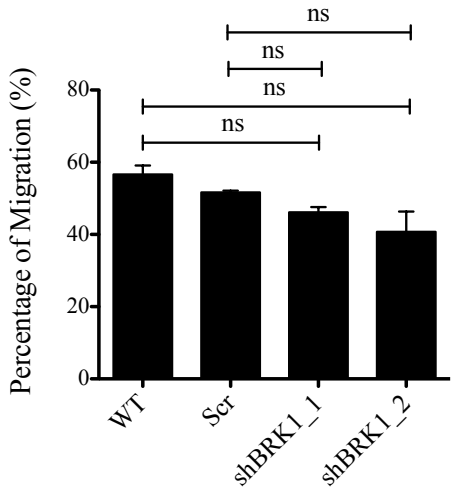

Figure 4.25: Stable knockdown of *BRK1* had no impact on Jurkat T cell migration. Chart shows the percentage of migration in Jurkat T cells following *BRK1* knockdown. Cells were serum-starved, stained with Calcien AM, allowed to migrate towards serum-rich medium for 4h. Number of migrated cells was determined by fluorescence intensity using microplate reader and percentage of migration was calculated by the number of migrated cells relative to the total number of cells (non-migrated and migrated cells). Error bars represent mean ± SEM of 2 independent experiments. ns: not significant.

4.6 Discussion

Regulation of actin reorganisation is critical in T cell activation and multiple previous studies have suggested that actin-regulatory proteins are involved in this process. These include TCR-proximal signalling molecules such as PLCγ1, NCK1, ITK and VAV1 (Fuller et al., 2003); activator of ARP2/3 complex such as WASP (Cannon and Burkhardt, 2004; Sims et al., 2007; Snapper et al., 1998; Zhang et al., 1999), WAVE2 (Nolz et al., 2006; Nolz et al., 2007; Nolz et al., 2008; Zipfel et al., 2007), WASH (Gomez et al., 2012) and HS1(Gomez et al., 2006; Taniuchi et al., 1995); actin severing proteins such as cofilin (Eibert et al., 2004) and coronin-1 (Föger et al., 2006) as well as dynamin-2 (Gomez et al., 2005) and EZH2 (Su et al., 2005).

WAVE protein is a member of the WASP family that plays an important role in regulating actin cytoskeletal dynamics (Campellone and Welch, 2010; Padrick and Rosen, 2010; Pollitt and Insall, 2009b). It is well known that at the N-terminal of WAVE protein, it forms a WAVE regulatory complex consists of WAVE1/2/3, ABI1/2/3, SRA1, HEM1/2 and BRK1 (Chen et al., 2010; Gautreau et al., 2004). The integrity and stability of WAVE regulatory complex is dependent upon each of the members in the complex. Elimination of any of the members in the WAVE regulatory complex causes subsequent degradation of the complex in *Dictyostelium* (Blagg et al., 2003; Ibarra et al., 2006; Linkner et al., 2011; Pollitt and Insall, 2008; Pollitt and Insall, 2009a), *Drosophila* (Bogdan et al., 2004; Kunda et al., 2003; Qurashi et al., 2007; Rogers et al., 2003; Schenck et al., 2004), mammalian cell lines (Cai et al., 2009; Derivery et al., 2008; Escobar et al., 2010; Grove et al., 2004; Nolz et al., 2006; Steffen et al., 2004; Weiner et al., 2006) and mouse models (Dubielecka et al., 2011; Park et al., 2008; Rakeman and Anderson, 2006). In the present study, to

evaluate the importance of *BRK1* in the stability and integrity of the WAVE2 complex in T cells, we suppressed its expression in both Jurkat and primary T cells. Our data showed that silencing of *BRK1* led to reduced protein expressions of WAVE2, SRA1 and ABI1, suggesting that BRK1 is required for the stability of other proteins in the WAVE2 complex in T cells. This finding is consistent with several previous studies which also showed that loss of *BRK1* led to degradation of other proteins in the WAVE complex in *Dictyostelium* (Pollitt and Insall, 2009a), *Drosophila* (Kunda et al., 2003; Qurashi et al., 2007) and mammalian cell lines (Cai et al., 2009; Derivery et al., 2008; Escobar et al., 2010). In HeLa cells, Derivery and colleagues showed that siRNA knockdown of *BRK1* caused reduction in the protein expressions of WAVE2, SRA1, NAP1 and ABI1 (Derivery et al., 2008) while in lung cancer PG cell line, Cai *et al.* reported that loss of *BRK1* resulted in decreased expression of WAVE2 protein (Cai et al., 2009). Suppression of *BRK1* in osteosarcoma U2OS cell line also contributed to decreased protein expressions of ABI1, WAVE1 and WAVE2 (Escobar et al., 2010). In Jurkat T cells, elimination of *WAVE2* led to subsequent degradation of other members in the WAVE2 complex including HEM1, SRA1 and ABI2. Similarly, *HEM1* suppression in Jurkat T cells also induced reduction in WAVE2, SRA1 and ABI2 protein expressions (Nolz et al., 2006). In addition, thymocytes and T lymphocytes from *Hem1*-knockout mice also showed reduced protein expressions of WAVE2, ABI1, ABI2 and SRA1 (Park et al., 2008). However, data published by Zipfel *et al*. contradicts our and multiple previous findings. In the Zipfel *et al*. study, knockdown of *ABI1*, *ABI2*, or both *ABI1* and *ABI2* in Jurkat T cells had no impact on the stability of NAP1/HEM1/HEM2, SRA1, WAVE1 and WAVE2 proteins. The protein expression levels of NAP1/HEM1/HEM2, SRA1, WAVE1 and WAVE2 in primary thymocytes derived

from *Abi1*$^{+/-}$*Abi2*$^{-/-}$ mice were also unchanged. Besides that, knockdown of WAVE proteins in Jurkat T cells also did not affect the ABI1 and ABI2 protein expressions (Zipfel et al., 2007). Interestingly, in our study, HEM1 protein level was not affected by *BRK1* knockdown in both Jurkat and primary T cells. This might be due to the fact that BRK1 does not interact directly with HEM1. Previous studies have shown that BRK1 is a precursor in the assembly of WAVE-ABI-BRK1 heterotrimeric complex and in the subsequent binding of the heterotrimer to the SRA1-HEM1 dimer in order to form a functional WAVE regulatory complex. The binding of WAVE-ABI-BRK1 heterotrimer to SRA1-HEM1 dimer is mainly via interaction between BRK1 and SRA1 (Chen et al., 2010; Derivery et al., 2008; Linkner et al., 2011). Thus, during the assembly of a WAVE regulatory complex, BRK1 interacts directly with WAVE, ABI and SRA1 proteins but not HEM1 protein. Furthermore, we also found that the ARP2 and ARP3 protein levels were not altered following suppression of *BRK1*, a expected result because ARP2/3 complex only interacts with activated WAVE2 protein at its C-terminal end (Goley and Welch, 2006; Takenawa and Suetsugu, 2007). Taken together, our results strongly suggest that BRK1 is an important component in regulating the stability of the WAVE2 regulatory complex.

In this study, BRK1, a component of the WAVE protein, was identified as novel target of *miR-181c*. Although much is known about the importance of WAVE2 complex in T cell activation, the role of BRK1 in the regulation of actin reorganisation in T cells is unknown. WAVE2 has been shown to be required for lamellipodia formation, immunological synapse formation, integrin activation, CRAC-mediated calcium entry and IL-2 production in T cells (Nolz et al., 2006; Nolz et al., 2007; Nolz et al., 2008; Zipfel et al., 2007). The *miR-181* family has previously been reported to play pivotal roles in T cell functions including T cell

development, differentiation, proliferation and activation (Georgantas et al., 2007; Henao-Mejia et al., 2013; Li et al., 2007; Xue et al., 2011). Therefore, given the important role of the *miR-181* family in T cell functions and the potential role of BRK1 in the regulation of actin polymerisation in T cells via its interaction with the WAVE2 complex, we investigated the influence of the *miR-181c*-BRK1 axis in T cell functions in this study. We found that upon stimulation of $CD3^+$ T cells, the expression of *miR-181c* was significantly reduced but the protein expression of BRK1 was markedly elevated. This finding further strengthens our hypothesis that the *miR-181c*-BRK1 axis might be important in T cell activation. Our data is in agreement with another previous study which showed that Jurkat and PBMC derived $CD4^+$ T cell activation resulted in the downregulation of *miR-181c* expression (Xue et al., 2011).

In order to assess the impact of the *miR-181c*-BRK1 axis on T cell activation, we downregulated *BRK1* and overexpressed *miR-181c* in Jurkat and primary T cells. Although suppression of *BRK1* and overexpression of *miR-181c* had no impact on cell proliferation, cell cycle profile and cell viability in T cells, we have demonstrated that the *miR-181c*-BRK1 axis plays pivotal roles in regulating the actin polymerisation-dependent processes in T cells. We showed that *BRK1* suppression repressed T cell activation with reduced expressions of CD69 and CD154 in *BRK1*-knockdown cells. Subsequently, to investigate whether *BRK1* negatively regulates T cell activation through modulation of actin polymerisation in T cells, we examined the total cellular F-actin content. Indeed, reduced total cellular F-actin content was seen in cells with *BRK1* depletion following stimulation. We therefore studied whether *BRK1* regulates processes in T cells that are dependent on actin cytoskeleton, including lamellipodia generation, immunological synapse formation

and cell migration. In fact, silencing of *BRK1* contributed to defects in the generation of stable lamellipodia as the *BRK1*-suppressed cells failed to accumulate F-actin at the leading edge of spreading T cell. Moreover, *BRK1*-knockdown cells also failed to accumulate F-actin at the T cell-B cell conjugation site, indicating that reduced expression of *BRK1* in T cells results in impairment in immunological synapse formation. Nonetheless, suppression of *BRK1* in Jurkat T cells did not influence cell migration. This finding is in contrast to published data which showed that in solid tumour cell lines, suppression of *BRK1* in NSCLC cell line (Cai et al., 2009) as well as renal cell carcinoma and osteosarcoma cell lines (Escobar et al., 2010) resulted in defective cell migration. This discrepancy might be attributed to the different cell types where *BRK1* might not play a role in cell migration in haematopoietic cells. Together, our data demonstrated that suppression of *BRK1* is important in T cell activation and specifically disrupts the processes in T cells that are dependent on actin reorganisation, including lamellipodia generation and immunological synapse formation.

To date, there are no published studies on the role of BRK1 in actin polymerisation-mediated T cell activities and our data demonstrated these important roles of BRK1 in T cells. Nevertheless, BRK1 is known to participate in the WAVE2 complex which has been shown to be important in T cell activation by regulating the actin cytoskeletal remodelling in T cells. The first published study on the roles of WAVE2 in regulating multiple pathways leading to T cell activation was by Nolz and colleagues. Their data revealed that WAVE2 protein is a critical component in the actin regulatory machinery in T cells (Nolz et al., 2006). They showed that *WAVE2* suppression led to reduction in the conjugation formation and the F-actin accumulation at the T cell-B cell site. This is consistent with our finding where we

showed that *BRK1* suppression also impaired immunological synapse formation. Furthermore, in their study, they demonstrated that WAVE2 was required for the generation of stable lamellipodia in response to anti-TCR ligation and this is in line with our results showing that silencing of *BRK1* induced defects in lamellipodia formation in spreading T cells in response to TCR stimulation (Nolz et al., 2006). A year later, another study reported a novel mechanism of ABI/WAVE complex in the regulation of TCR-mediated T cell activation (Zipfel et al., 2007). They showed that ABI proteins localise to the sites of dynamic actin polymerisation, which include the leading edge of spreading T cells (lamellipodia) and the T cell-B cell conjugation site (immunological synapse). In addition, WAVE proteins (WAVE1 and WAVE2) also co-localised with ABI proteins and F-actin at the T cell-B cell conjugation site. Furthermore, they also showed that primary T cells derived from *Abi1/Abi2*-deficient mice exhibited a reduction in actin polymerisation after T cell activation (Zipfel et al., 2007) and this is in agreement with our finding in *BRK1*-suppressed Jurkat and primary T cells where decreased total cellular F-actin content was observed following T cell stimulation. Besides that, the other two members of the WAVE2 complex, ABI2 and HEM1, have also been found to be essential for conjugate formation. Previous study showed that ABI2 and HEM1 are recruited to the immunological synapse site together with WAVE2 and F-actin (Nolz et al., 2006). Moreover, *Hem1* deficiency in mice has been shown to result in impaired T cell activation, adhesion and development as well as defective F-actin polymerisation and actin cap formation in lymphocytes (Park et al., 2008). Our findings on the roles of BRK1 in T cells together with multiple previous studies on the other members of the WAVE complex have demonstrated that BRK1 and WAVE2 complex are important in the regulation of actin polymerisation-mediated T cell functions.

We also revealed the indispensable role of *miR-181c* in actin polymerisation-mediated T cell functions. The impact of ectopic expression of *miR-181c* in Jurkat T cells on disruption of the T cell functions that are dependent on actin reorganisation phenocopy the impact seen in *BRK1* suppression studies. Similar to downregulation of *BRK1*, overexpression of *miR-181c* in Jurkat T cells also contributed to reduction in T cell activation and actin polymerisation coupled with defects in lamellipodia generation and immunological synapse formation, hence confirming the important roles of the *miR-181c*-BRK1 axis in T cell activation. Our finding on repressed T cell activation as a result of *miR-181c* overexpression is consistent with data published by Xue *et al*. who reported that *miR-181c* mimics were able to reduce CD25, CD69 and CD154 expressions in Jurkat and $CD4^+$ T cells, indicating the reduction in T cell activation (Xue et al., 2011). Although the role of *miR-181c* in the regulation of actin reorganisation in T cells is poorly studied, there are a few previous studies which showed that the *miR-181* family is involved in T lymphocyte development, differentiation, proliferation and activation. *miR-181a* acts as an intrinsic modulator in TCR signalling pathways through the downregulation of different phosphatases such as *PTPN22*, *SHP-2*, *DUSP5* and *DUSP6* that dampen LCK and ERK signalling, in turn enhancing the T cell activation (Li et al., 2007). Moreover, *miR-181a* is highly expressed at the $CD4^+CD8^+$ stage of thymocyte maturation in comparison with previous $CD4^-CD8^-$ stages or mature $CD4^+$ or $CD8^+$ T cells (Neilson et al., 2007). Furthermore, Georgantas *et al.* also predicted, using computational algorithms, that *miR-181a* regulates molecules such as *PU.1*, *MEF*, *SPI-B* and *MYB* as well as regulating *CXCR4* as shown by a reporter assay. These molecules are critical to very early steps in haematopoiesis and thus *miR-181a* might inhibit T lymphocytes differentiation through modulation of these molecules (Georgantas et

al., 2007). In addition, reduced proliferative capacity and total number of T cells were seen in *miR-181a/b*-deficient mice suggesting that *miR-181a* and *miR-181b* might be important in T cell proliferation and development (Henao-Mejia et al., 2013). Besides that, Xue *et al*. showed that overexpression of *miR-181c* in Jurkat and $CD4^+$ T cells reduced T cell activation and proliferation by reducing the expression of *IL-2* (Xue et al., 2011). Collectively, these data suggest that *miR-181* plays essential roles in T cells and in the present study, we demonstrated that *miR-181c* is indeed an important mediator of actin reorganisation during T cell activation by modulating the expression of *BRK1*.

5 Chapter 5 – Correlation of *miR-181c* and BRK1 in Myelodysplastic Syndromes with T Cell Large Granular Lymphocytic Leukaemia

5.1 Introduction

MDS is a heterogeneous group of clonal haematopoietic stem cell malignancies, characterised by cytopenias, myeloid cell dysplasia and defective haematopoiesis (Adès et al., 2014; Corey et al., 2007; Nimer, 2008). Several studies have reported the association of MDS with T-LGL leukaemia, a rare and indolent disorder involving inappropriate expansion of the large granular cytotoxic T lymphocytes (Bassan et al., 1987; Dhodapkar et al., 1994; Huh et al., 2009; Sauntharajah et al., 2001; Zhang et al., 2016). Dhodapkar and colleagues identified five patients with the coexistence of MDS and T-LGL (Dhodapkar et al., 1994) while Sauntharajah *et al.* and Huh *et al.* described nine patients each (Huh et al., 2009; Sauntharajah et al., 2001). More recently, Zhang *et al.* showed that MDS patients with T-LGL cell proliferation exhibit more frequent BM hypocellularity and lineage hypoplasia, particularly erythroid hypoplasia, as compared to MDS patients without T-LGL proliferation (Zhang et al., 2016). Although increasing evidence indicate that T-LGL leukaemia is frequently associated with BM failure syndromes including MDS (Bassan et al., 1987; Dhodapkar et al., 1994; Huh et al., 2009; Sauntharajah et al., 2001; Zhang et al., 2016), but there is limited data on the clinicopathological features of T-LGL cell proliferation in MDS patients, and the mechanism of the interference between T-LGL cells and the BM haematopoietic and stromal niches.

The *miR-181* family plays essential roles in haematopoiesis and its aberrant expression has been implicated in haematological malignancies including MDS. Expression of *miR-181a* was upregulated in advanced MDS cases but downregulated in early MDS. In addition, the expression level of *miR-181a* was found to increase

steadily from controls to MDS to AML (Pons et al., 2009). Furthermore, the expression of *miR-181* family members was significantly elevated in high risk MDS patients as compared to low risk patients. Moreover, elevated expression levels of *miR-181* family members were found to be associated with shorter survival in low risk MDS patients (Sokol, et al., 2011). On the contrary, the expression of *miR-181a* was reported to be decreased in MSC from MDS patients when compared with normal controls (Santamaría et al., 2012).

However, there are no published studies on the expression of *miR-181* family in MDS patients associated with T-LGL leukaemia. Our data on the important role of the *miR-181c*-BRK1 axis in T cell functions as well as previous findings by other groups on differential expression of *miR-181* family members in MDS have led us to analyse the *miR-181c* expression and BRK1 protein expression in BM derived $CD3^+$ T cells from MDS patients associated with T-LGL leukaemia in order to study the correlation of *miR-181c* and BRK1 in this specific group of MDS patients.

5.2 Clinical Features of MDS Patients with T-LGL Leukaemia

Five MDS patients associated with T-LGL leukaemia were analysed for their *miR-181c* and BRK1 expression levels. Both samples in TRIzol and cell pellets of BM derived $CD3^+$ cells were obtained from the King's College London Haemato-Oncology Tissue Bank (Human Tissue Authority Licence Number 12223). The samples were collected, stored and used in accordance with donor consent given under the auspices of ethics approval, provided by the UK National Research Ethics Service (NRES) (Approval Reference 08/H0906/94).

The median age of the patient group was 60 and two of the five patients were male. All five patients were classified as RCMD according to the MDS WHO classification system. Moreover, all of the patients had a normal karyotype and none of them had a *STAT3* mutation. BM cellularity was normal in three patients and decreased in two patients. One of the patients had anaemia, neutropenia and thrombocytopenia, three patients had anaemia and neutropenia; and another patient had anaemia only. In addition, lymphocytosis was seen in three of the five patients. One of the five patients had mild splenomegaly and associated with coeliac disease. The immunophenotyping of the T-LGL population is shown in Table 5.1.

Table 5.1: Clinical Characteristics of MDS Patients Associated with T-LGL Leukaemia

Patient	Age	Sex	Diagnosis	Immunophenotype of T-LGL population
P1	79	M	RCMD	$CD2^+$ $CD3^+$ $CD8^+$ $CD16^+$ $CD56^-$ $CD57^-$
P2	60	M	RCMD	$CD2^+$ $CD3^+$ $CD8^+$ $CD16^+$ $CD56^-$ $CD57^{(weak)}$
P3	72	F	RCMD	$CD2^+$ $CD3^+$ $CD8^+$ $CD7^{(weak)}$ $CD56^-$ $CD57^-$
P4	36	F	RCMD	$CD2^+$ $CD3^+$ $CD8^+$ $CD16^+$ $CD56^+$ $CD57^-$
P5	37	F	RCMD	$CD2^+$ $CD3^+$ $CD8^+$ $CD7^+$ $CD56^-$ $CD57^-$

5.3 Increased *miR-181c* and Decreased BRK1 Protein Expressions in MDS Patients with T-LGL Leukaemia

To study the correlation of *miR-181c* and BRK1 in MDS patients associated with T-LGL leukaemia, we examined the *miR-181c* expression and BRK1 protein expression in the BM derived $CD3^+$ cells from five patients using qPCR and western blot analysis respectively. In comparison to three healthy controls, four out of five patients had increased expression of *miR-181c* (Figure 5.1a). However, the difference was not statistically significant (*P* value=0.2407) and this might be due to the small number of samples studied.

For BRK1 protein expression analysis, one of the samples (P4) was degraded and protein was undetectable by western blot and was excluded from further western blot analysis. A significant decrease in the protein expression level of BRK1 (*P* value=0.0302) was detected in all four patient samples, as compared to three healthy controls (Figure 5.1b). Given that BRK1 is a component of the WAVE2 complex, WAVE2 protein level was also examined in these patients to assess whether reduced BRK1 expression would have an impact on WAVE2. Indeed, significant reduction in the WAVE2 protein expression (*P* value=0.0002) was detected in all of the four patient samples in comparison to three healthy controls (Figure 5.1b).

Subsequently, we studied the correlation of *miR-181c* expression with BRK1 and WAVE2 protein expression levels by performing Pearson correlation analysis. *miR-181c* expression level was found to be negatively correlated with protein expression levels of BRK1 (r = -0.6848) and WAVE2 (r = -0.7323) (Figure 5.1c). Nonetheless, the correlation between *miR-181c* expression and BRK1 (*P* value=0.0896) as well as WAVE2 (*P* value=0.0587) protein expressions were not statistically significant owing to the small sample size.

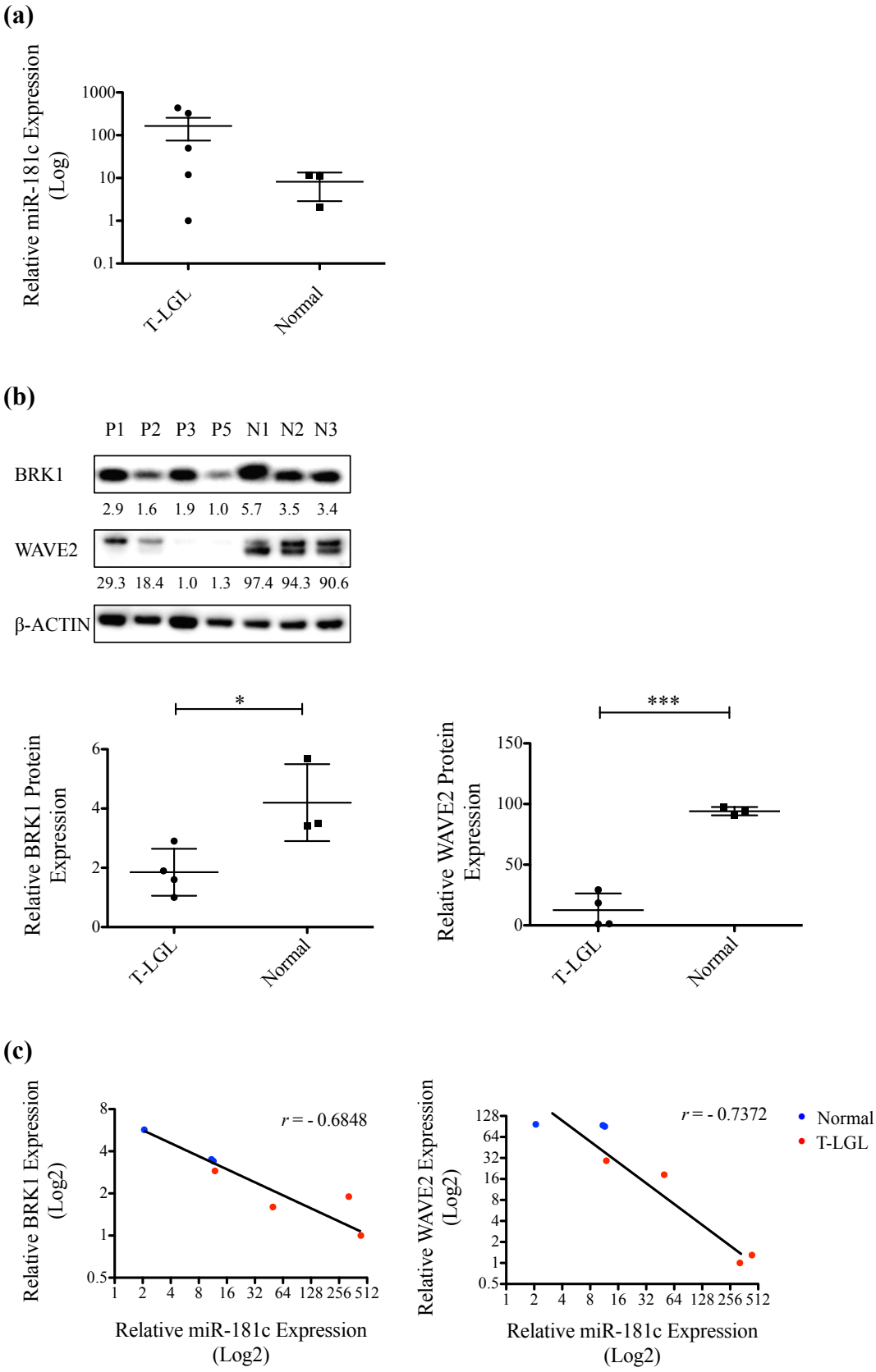
(a)
Relative miR-181c Expression (Log)
1000
100
10
1
0.1
T-LGL
Normal
(b)
P1 P2 P3 P5 N1 N2 N3
BRK1
2.9 1.6 1.9 1.0 5.7 3.5 3.4
WAVE2
29.3 18.4 1.0 1.3 97.4 94.3 90.6
β-ACTIN
*
Relative BRK1 Protein Expression
6
4
2
0
T-LGL
Normal
***
Relative WAVE2 Protein Expression
150
100
50
0
T-LGL
Normal
(c)
Relative BRK1 Expression (Log2)
r = - 0.6848
8
4
2
1
0.5
1 2 4 8 16 32 64 128 256 512
Relative miR-181c Expression (Log2)
Relative WAVE2 Expression (Log2)
r = - 0.7372
128
64
32
16
8
4
2
1
0.5
1 2 4 8 16 32 64 128 256 512
Relative miR-181c Expression (Log2)
Normal
T-LGL

Figure 5.1: Increased *miR-181c* but decreased BRK1 protein expression levels in BM derived $CD3^+$ T cells from MDS patients with T-LGL leukaemia. (a) Figure shows the qPCR analysis of relative *miR-181c* expression in five MDS patients with T-LGL leukaemia (T-LGL) and three healthy controls (normal). RNA was extracted from the TRIzol stock of BM derived $CD3^+$ cells, reversed transcribed to cDNA and analysed by qPCR. *miR-181c* expression is normalised to endogenous control U6 and error bars represent mean ± SEM. (b) Western blot analysis of BRK1 and WAVE2 protein expressions in four MDS patients with T-LGL leukaemia (P1-P3, P5) and three healthy controls (N1-N3). Total protein lysates were obtained from the cell pellets of BM derived $CD3^+$ cells. β-ACTIN level is used as a loading control and numbers represent the densitometric quantification of BRK1 and WAVE2 protein expression levels normalised to β-ACTIN. Data are presented in charts and error bars represent mean ± SD. * $P \leq 0.05$, *** $P \leq 0.001$. (c) Scatter plots show the Pearson correlation analysis of *miR-181c* expression with BRK1 and WAVE2 protein expressions. Blue dots represent healthy controls while red dots represent MDS patients associated with T-LGL leukaemia. The Pearson correlation coefficient *r* was calculated and indicated at the plots.

5.4 Discussion

To date, the mechanism of the occurrence of T-LGL leukaemia in MDS remains elusive. Nonetheless, Sauntharajah *et al.* have proposed two possible mechanisms of the association of T-LGL with MDS where the T-LGL might arise from a clonally rearranged MDS stem cell or alternatively, the T-LGL could represent an autoimmune response to an antigen presented by normal or MDS marrow cells (Sauntharajah et al., 2001). We focused on analysing the expression patterns of *miR-181c* and its target BRK1 in MDS patients associated with T-LGL leukaemia, because we anticipated that this analysis might provide new information relating to the disease pathogenesis and development. Indeed, our data demonstrated that the expression of *miR-181c* was increased but the protein expression levels of BRK1 and WAVE2 were decreased in BM derived $CD3^+$ cells from MDS patients associated with T-LGL leukaemia.

There are several publications reporting the aberrant expression of *miR-181* in MDS patients. However, these studies involved MDS patients without focus on a specific group of patients and also different cell types were used. For instance, Pons and colleagues evaluated the expression of 25 mature miRNAs in BM mononuclear cells of 25 MDS patients and 12 healthy controls by using RT-qPCR analysis and found that *miR-181a* was downregulated in early MDS but upregulated in advanced MDS (Pons et al., 2009). Similarly, Sokol *et al.* also used BM mononuclear cells from 44 MDS patients and 17 normal controls to examine miRNA expression by microarray profiling. They reported the upregulation of *miR-181a*, *miR-181b*, *miR-181c* and *miR-181d* in high risk MDS patients in comparison to low risk patients as validated by RT-qPCR analysis (Sokol, et al., 2011). Intriguingly, Santamaria *et al.* profiled the miRNA expression in MSC from 21 low risk MDS with the use of low density

arrays and found that the expression of *miR-181a* was reduced in MSC from MDS patients when compared with normal controls (Santamaría et al., 2012).

In this study, we also showed that the *miR-181c* expression was negatively correlated with protein expressions of BRK1 and WAVE2 in $CD3^+$ T cells from both patients and healthy controls. This data confirms our finding on the negative regulation of BRK1 expression by *miR-181c* at the translational level and suggests the negative correlation of *miR-181c* and BRK1 expression in a proportion of RCMD patients with T-LGL leukaemia.

Taken together, we demonstrated that in a proportion of RCMD patients with T-LGL leukaemia, the *miR-181c* and BRK1 expression was negatively correlated where the *miR-181c* expression was upregulated but the BRK1 protein expression was downregulated. Despite the small sample size, our finding provides insight into the possible implication of *miR-181c* in the disease mechanism via the regulation of its novel target, BRK1, which requires further evaluation and investigation.

6 Chapter 6 – Conclusion

6.1 Conclusion

This study aimed to identify the target genes of *miR-181* family members and to study its biological functions in order to provide insight into the roles of *miR-181* in haematopoiesis and haematological malignancies. Currently available miRNA target identification methods lack sensitivity and specificity as most of the target identification methods rely predictive algorithms that mainly concentrate on the complementary binding between the miRNA seed sequence and the 3'UTR of target mRNA (Didiano and Hobert, 2006). Therefore, a functional assay based on an optimised and enriched cDNA library and a dual selection strategy which has previously been developed in-house (Gäken et al., 2012), was applied in this study to identify biologically relevant targets of the *miR-181* family members. This method makes no assumptions on previously identified sequences, but relies directly on miRNA mediated downregulation of a thymidine kinase-zeocin (TKzeo) fusion gene upstream of a cDNA library which act as 3'UTR. This assay is able to identify miRNA targets that are downregulated by mRNA degradation or translational repression and not merely relies on the complementary binding of miRNA to putative targets. In this project, we focused on the identification of *miR-181c/d*-regulated target genes. One such target was BRK1, a component of the WAVE2 complex that has been shown to play a pivotal role in actin polymerisation (Takenawa and Suetsugu, 2007). Subsequent validation experiments showed that *BRK1* was regulated by *miR-181c* but not *miR-181d*. Overexpression and inhibition of *miR-181c* had no impact on *BRK1* mRNA expression but did in fact alter the protein expression levels, suggesting that BRK1 is modulated by *miR-181c* through translational repression. In addition, in MDS patients associated with T-LGL

leukaemia, the expression of *miR-181c* was negatively correlated with protein expression of BRK1 in BM derived $CD3^+$ T cells. Increased expression of *miR-181c* and decreased BRK1 protein expression were observed in these cells, suggesting the modulation of BRK1 protein expression by *miR-181c* in this group of MDS patients.

It has previously been demonstrated that the *miR-181* family plays a key role in T cell development, differentiation, proliferation and activation (Georgantas et al., 2007; Henao-Mejia et al., 2013; Li et al., 2007; Xue et al., 2011). Nevertheless, the role of *miR-181c* in actin polymerisation in T cells is still unknown. In addition, the role of BRK1 in the regulation of actin dynamics in T cells remains to be elucidated. Multiple studies have shown that the WAVE2 complex plays a crucial role in regulation of the actin cytoskeleton in T cells. The WAVE2 complex regulates immunological synapse formation, lamellipodia formation, calcium entry, integrin adhesion and IL-2 production in T cells (Nolz et al., 2006; Nolz et al., 2007; Nolz et al., 2008; Zipfel et al., 2007). Given the important role *miR-181* plays in T cell activity and the potential role of BRK1 in the involvement in WAVE2 complex and actin polymerisation in T cells, we next focused our study on ascertaining the influence of the *miR-181c*-BRK1 axis in several T cell functions. In order to study the role of *miR-181c* and its target BRK1, we overexpressed *miR-181c* in Jurkat T cells and downregulated *BRK1* by shRNA in Jurkat and primary T cells. Although ectopic expression of *miR-181c* and suppression of *BRK1* had no impact on T cell proliferation, cell cycle profile and cell viability, we showed that the *miR-181c*-BRK1 axis did in fact regulate actin polymerisation-dependent processes during T cell activation. Firstly, we showed that upon stimulation of $CD3^+$ T cells derived from PBMC by CD3 and CD28 antibodies, the expression of *miR-181c* was reduced but the protein expression of BRK1 was upregulated. This data further strengthens

our hypothesis that the *miR-181c*-BRK1 axis might be important in T cell activation. Subsequently, we showed that overexpression of *miR-181c* in Jurkat T cells repressed T cell activation as indicated by decreased expression of CD69. In addition, we observed no increase in total cellular F-actin content in *miR-181c* overexpressing cells upon stimulation, indicating the involvement of *miR-181c* in actin polymerisation in T cells. Moreover, *miR-181c* overexpressing cells also failed to accumulate F-actin at the leading edge of spreading T cells, indicating the defective formation of lamellipodia, a process highly dependent upon actin reorganisation. Ectopic expression of *miR-181c* in Jurkat T cells also resulted in reduction in the F-actin accumulation at the T cell-B cell conjugation site, suggesting an impairment in immunological synapse formation. Similarly to *miR-181c* overexpression, we found that knockdown of *BRK1* in both Jurkat and primary T cells led to reduction in T cell activation as shown by decreased expression of CD69 and CD154. Depletion of *BRK1* in Jurkat and primary T cells also contributed to a reduction in total cellular F-actin content upon stimulation, decreased F-actin accumulation at the T cell-B cell conjugation site, and impaired lamellipodia formation during T cell spreading on anti-CD3 coated slides. Additionally, our data in Jurkat and primary T cells showed that suppression of *BRK1* resulted in decreased protein expressions of WAVE2, ABI1 and SRA1, suggesting that BRK1 has additional functions in regulating the stability of the proteins involved in the WAVE2 complex. This is in concordance with previous studies which demonstrated that loss of *BRK1* led to degradation of other proteins in the WAVE complex in *Dictyostelium* (Pollitt and Insall, 2009a), *Drosophila* (Kunda et al., 2003; Qurashi et al., 2007) and mammalian cell lines (Cai et al., 2009; Derivery et al., 2008; Escobar et al., 2010).

In conclusion, we have identified BRK1 as a novel target of *miR-181c* and validated that *miR-181c* regulates BRK1 by repressing its translation. In addition, we have highlighted the important role of the *miR-181c*-BRK1 axis in impaired actin polymerisation-dependent T cell functions and T cell activation. Furthermore, we showed the deregulation of *miR-181c*-BRK1 axis in a proportion of MDS patients with T-LGL leukaemia, suggesting the potential role of *miR-181c*-BRK1 axis in the development of T-LGL leukaemia in MDS, through a still unknown mechanism.

References

Acuto, O., Di Bartolo, V., and Michel, F. (2008). Tailoring T-cell receptor signals by proximal negative feedback mechanisms. Nature Reviews Immunology *8*, 699-712.

Adès, L., Itzykson, R., and Fenaux, P. (2014). Myelodysplastic syndromes. The Lancet *383*, 2239-2252.

Almeida, M. I., Reis, R. M., and Calin, G. A. (2011). MicroRNA history: Discovery, recent applications, and next frontiers. Mutation Research/Fundamental and Molecular Mechanisms of Mutagenesis *717*, 1-8.

Ambros, V. (2001). microRNAs: tiny regulators with great potential. Cell *107*, 823-826.

Ambros, V. (2004). The functions of animal microRNAs. Nature *431*, 350-355.

Artyomov, M. N., Lis, M., Devadas, S., Davis, M. M., and Chakraborty, A. K. (2010). CD4 and CD8 binding to MHC molecules primarily acts to enhance Lck delivery. Proceedings of the National Academy of Sciences *107*, 16916-16921.

Baek, D., Villén, J., Shin, C., Camargo, F. D., Gygi, S. P., and Bartel, D. P. (2008). The impact of microRNAs on protein output. Nature *455*, 64-71.

Bareau, B., Rey, J., Hamidou, M., Donadieu, J., Morcet, J., Reman, O., Schleinitz, N., Tournilhac, O., Roussel, M., Fest, T., and Lamy, T. (2010). Analysis of a French cohort of patients with large granular lymphocyte leukemia: a report on 229 cases. Haematologica *95*, 1534-1541.

Bartel, D. P. (2004). MicroRNAs: Genomics, Biogenesis, Mechanism, and Function. Cell *116*, 281-297.

Bartel, D. P. (2009). MicroRNAs: target recognition and regulatory functions. Cell *136*, 215-233.

Bassan, R., Marini, B., Allavena, P., Pirelli, A., and Barbui, T. (1987). RAEB in Patient with Chronic Granulated T-lymphocytosis. British Journal of Haematology *65*, 503-504.

Bentwich, I. (2005). Prediction and validation of microRNAs and their targets. FEBS Letters *579*, 5904-5910.

Billadeau, D. D., and Burkhardt, J. K. (2006). Regulation of cytoskeletal dynamics at the immune synapse: new stars join the actin troupe. Traffic *7*, 1451-1460.

Billadeau, D. D., Nolz, J. C., and Gomez, T. S. (2007). Regulation of T-cell activation by the cytoskeleton. Nature Reviews Immunology *7*, 131-143.

Blagg, S. L., Stewart, M., Sambles, C., and Insall, R. H. (2003). PIR121 Regulates Pseudopod Dynamics and SCAR Activity in Dictyostelium. Current Biology *13*, 1480-1487.

Bogdan, S., Grewe, O., Strunk, M., Mertens, A., and Klämbt, C. (2004). Sra-1 interacts with Kette and Wasp and is required for neuronal and bristle development in Drosophila. Development *131*, 3981-3989.

Borchert, G. M., Lanier, W., and Davidson, B. L. (2006). RNA polymerase III transcribes human microRNAs. Nature Structural & Molecular Biology *13*, 1097-1101.

Boyer, T., Grardel, N., Copin, M.-C., Roumier, C., Touzart, A., Buchdahl, A.-L., Corm, S., de Latour, R. P., Preudhomme, C., and Terriou, L. (2015). Paroxysmal nocturnal hemoglobinuria (PNH) and T cell large granular lymphocyte (LGL) leukemia-an unusual association: another cause of cytopenia in PNH. Annals of Hematology *94*, 1759-1760.

Brownlie, R. J., and Zamoyska, R. (2013). T cell receptor signalling networks: branched, diversified and bounded. Nature Reviews Immunology *13*, 257-269.

Bunnell, S. C., Kapoor, V., Trible, R. P., Zhang, W., and Samelson, L. E. (2001). Dynamic Actin Polymerization Drives T Cell Receptor-Induced Spreading: A Role for The Signal Transduction Adaptor LAT. Immunity *14*, 315-329.

Burkhardt, J. K., Carrizosa, E., and Shaffer, M. H. (2008). The Actin Cytoskeleton in T Cell Activation. Annual Review of Immunology *26*, 233-259.

Butrym, A., Rybka, J., Baczyńska, D., Poręba, R., Mazur, G., and Kuliczkowski, K. (2016). Expression of microRNA-181 determines response to treatment with azacitidine and predicts survival in elderly patients with acute myeloid leukaemia. Oncology Letters *12*, 2296-2300.

Cai, X., Xiao, T., James, S. Y., Da, J., Lin, D., Liu, Y., Zheng, Y., Zou, S., Di, X., Guo, S.*, et al.* (2009). Metastatic potential of lung squamous cell carcinoma associated with HSPC300 through its interaction with WAVE2. Lung Cancer *65*, 299-305.

Calvez, R., Lafouresse, F., DeMeester, J., Galy, A., Valitutti, S., and Dupré, L. (2011). The Wiskott-Aldrich syndrome protein permits the assembly of a focused immunological synapse enabling sustained TCR signalling. Haematologica *96*, 1415-1423.

Campellone, K. G., and Welch, M. D. (2010). A nucleator arms race: cellular control of actin assembly. Nature Reviews Molecular Cell Biology *11*, 237-251.

Cannon, J. L., and Burkhardt, J. K. (2004). Differential Roles for Wiskott-Aldrich Syndrome Protein in Immune Synapse Formation and IL-2 Production. The Journal of Immunology *173*, 1658-1662.

Carrizosa, E., Gomez, T. S., Labno, C. M., Dehring, D. A. K., Liu, X., Freedman, B. D., Billadeau, D. D., and Burkhardt, J. K. (2009). Hematopoietic lineage cell-specific protein 1 is recruited to the immunological synapse by IL-2-inducible T cell kinase and regulates phospholipase Cγ1 Microcluster dynamics during T cell spreading. The Journal of Immunology *183*, 7352-7361.

Cascón, A., Escobar, B., Montero-Conde, C., Rodríguez-Antona, C., Ruiz-Llorente, S., Osorio, A., Mercadillo, F., Letón, R., Campos, J. M., García-Sagredo, J. M., *et al.* (2007). Loss of the actin regulator HSPC300 results in clear cell renal cell carcinoma protection in Von Hippel-Lindau patients. Human Mutation *28*, 613-621.

Cazzola, M., Della Porta, M. G., and Malcovati, L. (2013). The genetic basis of myelodysplasia and its clinical relevance. Blood *122*, 4021-4034.

Cheloufi, S., Dos Santos, C. O., Chong, M. M., and Hannon, G. J. (2010). A dicer-independent miRNA biogenesis pathway that requires Ago catalysis. Nature *465*, 584-589.

Chen, C.-Z., Li, L., Lodish, H. F., and Bartel, D. P. (2004a). MicroRNAs Modulate Hematopoietic Lineage Differentiation. Science *303*, 83-86.

Chen, G., Zeng, W., Miyazato, A., Billings, E., Maciejewski, J. P., Kajigaya, S., Sloand, E. M., and Young, N. S. (2004b). Distinctive gene expression profiles of CD34 cells from patients with myelodysplastic syndrome characterized by specific chromosomal abnormalities. Blood *104*, 4210-4218.

Chen, X., Eksioglu, E. A., Zhou, J., Zhang, L., Djeu, J., Fortenbery, N., Epling-Burnette, P., Van Bijnen, S., Dolstra, H., Cannon, J., *et al.* (2013). Induction of myelodysplasia by myeloid-derived suppressor cells. The Journal of Clinical Investigation *123*, 4595-4611.

Chen, Z., Borek, D., Padrick, S. B., Gomez, T. S., Metlagel, Z., Ismail, A. M., Umetani, J., Billadeau, D. D., Otwinowski, Z., and Rosen, M. K. (2010). Structure and control of the actin regulatory WAVE complex. Nature *468*, 533-538.

Chendrimada, T. P., Gregory, R. I., Kumaraswamy, E., Norman, J., Cooch, N., Nishikura, K., and Shiekhattar, R. (2005). TRBP recruits the Dicer complex to Ago2 for microRNA processing and gene silencing. Nature *436*, 740-744.

Cheng, A. M., Byrom, M. W., Shelton, J., and Ford, L. P. (2005). Antisense inhibition of human miRNAs and indications for an involvement of miRNA in cell growth and apoptosis. Nucleic Acids Research *33*, 1290-1297.

Chiang, H. R., Schoenfeld, L. W., Ruby, J. G., Auyeung, V. C., Spies, N., Baek, D., Johnston, W. K., Russ, C., Luo, S., and Babiarz, J. E. (2010). Mammalian microRNAs: experimental evaluation of novel and previously annotated genes. Genes & Development *24*, 992-1009.

Choong, M. L., Yang, H. H., and McNiece, I. (2007). MicroRNA expression profiling during human cord blood-derived CD34 cell erythropoiesis. Experimental Hematology *35*, 551-564.

Cianferoni, A., Massaad, M., Feske, S., Miguel, A., Gallego, L., Ramesh, N., and Geha, R. S. (2005). Defective nuclear translocation of nuclear factor of activated T cells and extracellular signal-regulated kinase underlies deficient IL-2 gene expression in Wiskott-Aldrich syndrome. Journal of Allergy and Clinical Immunology *116*, 1364-1371.

Cichocki, F., Felices, M., McCullar, V., Presnell, S. R., Al-Attar, A., Lutz, C. T., and Miller, J. S. (2011). Cutting edge: microRNA-181 promotes human NK cell development by regulating Notch signaling. The Journal of Immunology *187*, 6171-6175.

Corey, S. J., Minden, M. D., Barber, D. L., Kantarjian, H., Wang, J. C. Y., and Schimmer, A. D. (2007). Myelodysplastic syndromes: the complexity of stem-cell diseases. Nature Reviews Cancer *7*, 118-129.

Cotta-de-Almeida, V., Westerberg, L., Maillard, M. H., Onaldi, D., Wachtel, H., Meelu, P., Chung, U.-i., Xavier, R., Alt, F. W., and Snapper, S. B. (2007). Wiskott-Aldrich syndrome protein (WASP) and N-WASP are critical for T cell development. Proceedings of the National Academy of Sciences *104*, 15424-15429.

Debernardi, S., Skoulakis, S., Molloy, G., Chaplin, T., Dixon-McIver, A., and Young, B. D. (2007). MicroRNA miR-181a correlates with morphological sub-class of acute myeloid leukaemia and the expression of its target genes in global genome-wide analysis. Leukemia *21*, 912-916.

Dehring, D. A. K., Clarke, F., Ricart, B. G., Huang, Y., Gomez, T. S., Williamson, E. K., Hammer, D. A., Billadeau, D. D., Argon, Y., and Burkhardt, J. K. (2011). Hematopoietic lineage cell-specific protein 1 functions in concert with the Wiskott-Aldrich syndrome protein to promote podosome array organization and chemotaxis in dendritic cells. The Journal of Immunology *186*, 4805-4818.

Deindl, S., Kadlecek, T. A., Brdicka, T., Cao, X., Weiss, A., and Kuriyan, J. (2007). Structural basis for the inhibition of tyrosine kinase activity of ZAP-70. Cell *129*, 735-746.

Delon, J., Bercovici, N., Liblau, R., and Trautmann, A. (1998). Imaging antigen recognition by naive CD4+ T cells: compulsory cytoskeletal alterations for the triggering of an intracellular calcium response. European Journal of Immunology *28*, 716-729.

Denli, A. M., Tops, B. B., Plasterk, R. H., Ketting, R. F., and Hannon, G. J. (2004). Processing of primary microRNAs by the Microprocessor complex. Nature *432*, 231-235.

Derivery, E., Fink, J., Martin, D., Houdusse, A., Piel, M., Stradal, T. E., Louvard, D., and Gautreau, A. (2008). Free Brick1 is a trimeric precursor in the assembly of a functional wave complex. PLoS One *3*, e2462.

Derivery, E., Lombard, B., Loew, D., and Gautreau, A. (2009). The Wave complex is intrinsically inactive. Cell Motility and The Cytoskeleton *66*, 777-790.

Dhodapkar, M., Li, C., Lust, J., Tefferi, A., and Phyliky, R. (1994). Clinical spectrum of clonal proliferations of T-large granular lymphocytes: a T-cell clonopathy of undetermined significance? Blood *84*, 1620-1627.

Didiano, D., and Hobert, O. (2006). Perfect seed pairing is not a generally reliable predictor for miRNA-target interactions. Nature Structural & Molecular Biology *13*, 849-851.

Djakovic, S., Dyachok, J., Burke, M., Frank, M. J., and Smith, L. G. (2006). BRICK1/HSPC300 functions with SCAR and the ARP2/3 complex to regulate epidermal cell shape in Arabidopsis. Development *133*, 1091-1100.

Dombroski, D., Houghtling, R. A., Labno, C. M., Precht, P., Takesono, A., Caplen, N. J., Billadeau, D. D., Wange, R. L., Burkhardt, J. K., and Schwartzberg, P. L. (2005). Kinase-independent functions for Itk in TCR-induced regulation of Vav and the actin cytoskeleton. The Journal of Immunology *174*, 1385-1392.

Dower, N. A., Stang, S. L., Bottorff, D. A., Ebinu, J. O., Dickie, P., Ostergaard, H. L., and Stone, J. C. (2000). RasGRP is essential for mouse thymocyte differentiation and TCR signaling. Nature Immunology *1*, 317-321.

Dubielecka, P. M., Ladwein, K. I., Xiong, X., Migeotte, I., Chorzalska, A., Anderson, K. V., Sawicki, J. A., Rottner, K., Stradal, T. E., and Kotula, L. (2011). Essential role for Abi1 in embryonic survival and WAVE2 complex integrity. Proceedings of the National Academy of Sciences *108*, 7022-7027.

Dustin, M. L., and Cooper, J. A. (2000). The immunological synapse and the actin cytoskeleton: molecular hardware for T cell signaling. Nature Immunology *1*, 23-29.

Ebinu, J. O., Bottorff, D. A., Chan, E. Y., Stang, S. L., Dunn, R. J., and Stone, J. C. (1998). RasGRP, a Ras guanyl nucleotide-releasing protein with calcium-and diacylglycerol-binding motifs. Science *280*, 1082-1086.

Ebinu, J. O., Stang, S. L., Teixeira, C., Bottorff, D. A., Hooton, J., Blumberg, P. M., Barry, M., Bleakley, R. C., Ostergaard, H. L., and Stone, J. C. (2000). RasGRP links T-cell receptor signaling to Ras. Blood *95*, 3199-3203.

Eden, S., Rohatgi, R., Podtelejnikov, A. V., Mann, M., and Kirschner, M. W. (2002). Mechanism of regulation of WAVE1-induced actin nucleation by Rac1 and Nck. Nature *418*, 790-793.

Egan, S. E., Giddings, B. W., Brooks, M. W., Buday, L., Sizeland, A. M., and Weinberg, R. A. (1993). Association of Sos Ras exchange protein with Grb2 is implicated in tyrosine kinase signal transduction and transformation. Nature *363*, 45-51.

Eibert, S. M., Lee, K.-H., Pipkorn, R., Sester, U., Wabnitz, G. H., Giese, T., Meuer, S. C., and Samstag, Y. (2004). Cofilin peptide homologs interfere with immunological synapse formation and T cell activation. Proceedings of the National Academy of Sciences *101*, 1957-1962.

Epler, J. A., Liu, R., Chung, H., Ottoson, N. C., and Shimizu, Y. (2000). Regulation of β1 integrin-mediated adhesion by T cell receptor signaling involves ZAP-70 but differs from signaling events that regulate transcriptional activity. The Journal of Immunology *165*, 4941-4949.

Epling-Burnette, P. K., Painter, J. S., Rollison, D. E., Ku, E., Vendron, D., Widen, R., Boulware, D., Zou, J. X., Bai, F., and List, A. F. (2007). Prevalence and clinical association of clonal T-cell expansions in Myelodysplastic Syndrome. Leukemia *21*, 659-667.

Escobar, B., de Cárcer, G., Fernández-Miranda, G., Cascón, A., Bravo-Cordero, J. J., Montoya, M. C., Robledo, M., Cañamero, M., and Malumbres, M. (2010). Brick1 Is an Essential Regulator of Actin Cytoskeleton Required for Embryonic Development and Cell Transformation. Cancer Research *70*, 9349-9359.

Fabian, M. R., and Sonenberg, N. (2012). The mechanics of miRNA-mediated gene silencing: a look under the hood of miRISC. Nature Structural & Molecular Biology *19*, 586-593.

Fei, J., Li, Y., Zhu, X., and Luo, X. (2012). miR-181a post-transcriptionally downregulates oncogenic RalA and contributes to growth inhibition and apoptosis in chronic myelogenous leukemia (CML). PLoS One *7*, e32834.

Finco, T. S., Kadlecek, T., Zhang, W., Samelson, L. E., and Weiss, A. (1998). LAT is required for TCR-mediated activation of PLCγ1 and the Ras pathway. Immunity *9*, 617-626.

Föger, N., Rangell, L., Danilenko, D. M., and Chan, A. C. (2006). Requirement for coronin 1 in T lymphocyte trafficking and cellular homeostasis. Science *313*, 839-842.

Frank, M. J., and Smith, L. G. (2002). A Small, Novel Protein Highly Conserved in Plants and Animals Promotes the Polarized Growth and Division of Maize Leaf Epidermal Cells. Current Biology *12*, 849-853.

Franke, G., Bausch, B., Hoffmann, M. M., Cybulla, M., Wilhelm, C., Kohlhase, J., Scherer, G., and Neumann, H. P. H. (2009). Alu-Alu recombination underlies the vast majority of large VHL germline deletions: Molecular characterization and genotype-phenotype correlations in VHL patients. Human Mutation *30*, 776-786.

Friedman, R. C., Farh, K. K.-H., Burge, C. B., and Bartel, D. P. (2009). Most mammalian mRNAs are conserved targets of microRNAs. Genome Research *19*, 92-105.

Fuller, C. L., Braciale, V. L., and Samelson, L. E. (2003). All roads lead to actin: the intimate relationship between TCR signaling and the cytoskeleton. Immunological Reviews *191*, 220-236.

Gäken, J., Mohamedali, A. M., Jiang, J., Malik, F., Stangl, D., Smith, A. E., Chronis, C., Kulasekararaj, A. G., Thomas, N. S. B., Farzaneh, F*., et al.* (2012). A functional assay for microRNA target identification and validation. Nucleic Acids Research *40*, e75.

Ganan-Gomez, I., Wei, Y., Starczynowski, D. T., Colla, S., Yang, H., Cabrero-Calvo, M., Bohannan, Z. S., Verma, A., Steidl, U., and Garcia-Manero, G. (2015). Deregulation of innate immune and inflammatory signaling in myelodysplastic syndromes. Leukemia *29*, 1458-1469.

Garcia-Manero, G. (2015). Myelodysplastic syndromes: 2015 Update on diagnosis, risk-stratification and management. American Journal of Hematology *90*, 831-841.

Garzon, R., Pichiorri, F., Palumbo, T., Iuliano, R., Cimmino, A., Aqeilan, R., Volinia, S., Bhatt, D., Alder, H., and Marcucci, G. (2006). MicroRNA fingerprints during human megakaryocytopoiesis. Proceedings of the National Academy of Sciences of the United States of America *103*, 5078-5083.

Gautreau, A., Ho, H.-y. H., Li, J., Steen, H., Gygi, S. P., and Kirschner, M. W. (2004). Purification and architecture of the ubiquitous Wave complex. Proceedings of the National Academy of Sciences of the United States of America *101*, 4379-4383.

Genot, E., and Cantrell, D. A. (2000). Ras regulation and function in lymphocytes. Current Opinion in Immunology *12*, 289-294.

Georgantas, R. W., Hildreth, R., Morisot, S., Alder, J., Liu, C.-g., Heimfeld, S., Calin, G. A., Croce, C. M., and Civin, C. I. (2007). CD34+ hematopoietic stem-progenitor cell microRNA expression and function: A circuit diagram of differentiation control. Proceedings of the National Academy of Sciences *104*, 2750-2755.

Ghildiyal, M., and Zamore, P. D. (2009). Small silencing RNAs: an expanding universe. Nature Reviews Genetics *10*, 94-108.

Glenthøj, A., Ørskov, A. D., Hansen, J. W., Hadrup, S. R., O'Connell, C., and Grønbæk, K. (2016). Immune Mechanisms in Myelodysplastic Syndrome. International Journal of Molecular Sciences *17*, 944.

Go, R. S., Tefferi, A., Li, C.-Y., Lust, J. A., and Phyliky, R. L. (2000). Lymphoproliferative disease of granular T lymphocytes presenting as aplastic anemia. Blood *96*, 3644-3646.

Goley, E. D., and Welch, M. D. (2006). The ARP2/3 complex: an actin nucleator comes of age. Nature Reviews Molecular Cell Biology *7*, 713-726.

Gomez, T. S., and Billadeau, D. D. (2009). A FAM21-containing WASH complex regulates retromer-dependent sorting. Developmental Cell *17*, 699-711.

Gomez, T. S., Gorman, J. A., de Narvajas, A. A.-M., Koenig, A. O., and Billadeau, D. D. (2012). Trafficking defects in WASH-knockout fibroblasts originate from collapsed endosomal and lysosomal networks. Molecular Biology of the Cell *23*, 3215-3228.

Gomez, T. S., Hamann, M. J., McCarney, S., Savoy, D. N., Lubking, C. M., Heldebrant, M. P., Labno, C. M., McKean, D. J., McNiven, M. A., Burkhardt, J. K., and Billadeau, D. D. (2005). Dynamin 2 regulates T cell activation by controlling actin polymerization at the immunological synapse. Nature Immunology *6*, 261-270.

Gomez, T. S., Kumar, K., Medeiros, R. B., Shimizu, Y., Leibson, P. J., and Billadeau, D. D. (2007). Formins regulate the actin-related protein 2/3 complex-independent polarization of the centrosome to the immunological synapse. Immunity *26*, 177-190.

Gomez, T. S., McCarney, S. D., Carrizosa, E., Labno, C. M., Comiskey, E. O., Nolz, J. C., Zhu, P., Freedman, B. D., Clark, M. R., Rawlings, D. J.*, et al.* (2006). HS1 Functions as an Essential Actin-Regulatory Adaptor Protein at the Immune Synapse. Immunity *24*, 741-752.

Greenberg, P., Cox, C., LeBeau, M. M., Fenaux, P., Morel, P., Sanz, G., Sanz, M., Vallespi, T., Hamblin, T., Oscier, D.*, et al.* (1997). International Scoring System for Evaluating Prognosis in Myelodysplastic Syndromes. Blood *89*, 2079-2088.

Greenberg, P. L., Tuechler, H., Schanz, J., Sanz, G., Garcia-Manero, G., Solé, F., Bennett, J. M., Bowen, D., Fenaux, P., Dreyfus, F.*, et al.* (2012). Revised International Prognostic Scoring System for Myelodysplastic Syndromes. Blood *120*, 2454-2465.

Gregory, R. I., Yan, K.-p., Amuthan, G., Chendrimada, T., Doratotaj, B., Cooch, N., and Shiekhattar, R. (2004). The Microprocessor complex mediates the genesis of microRNAs. Nature *432*, 235-240.

Grimson, A., Farh, K. K.-H., Johnston, W. K., Garrett-Engele, P., Lim, L. P., and Bartel, D. P. (2007). MicroRNA Targeting Specificity in Mammals: Determinants beyond Seed Pairing. Molecular Cell *27*, 91-105.

Grove, M., Demyanenko, G., Echarri, A., Zipfel, P. A., Quiroz, M. E., Rodriguiz, R. M., Playford, M., Martensen, S. A., Robinson, M. R., Wetsel, W. C.*, et al.* (2004). Abi2-Deficient Mice Exhibit Defective Cell Migration, Aberrant Dendritic Spine Morphogenesis, and Deficits in Learning and Memory. Molecular and Cellular Biology *24*, 10905-10922.

Ha, M., and Kim, V. N. (2014). Regulation of microRNA biogenesis. Nature Reviews Molecular Cell Biology *15*, 509-524.

Haase, D. (2008). Cytogenetic features in myelodysplastic syndromes. Annals of Hematology *87*, 515-526.

Haase, D., Germing, U., Schanz, J., Pfeilstöcker, M., Nösslinger, T., Hildebrandt, B., Kundgen, A., Lübbert, M., Kunzmann, R., Giagounidis, A. A. N.*, et al.* (2007). New insights into the prognostic impact of the karyotype in MDS and correlation with subtypes: evidence from a core dataset of 2124 patients. Blood *110*, 4385-4395.

Haferlach, T., Nagata, Y., Grossmann, V., Okuno, Y., Bacher, U., Nagae, G., Schnittger, S., Sanada, M., Kon, A., and Alpermann, T. (2014). Landscape of genetic lesions in 944 patients with myelodysplastic syndromes. Leukemia *28*, 241-247.

Han, J., Lee, Y., Yeom, K.-H., Kim, Y.-K., Jin, H., and Kim, V. N. (2004). The Drosha-DGCR8 complex in primary microRNA processing. Genes & Development *18*, 3016-3027.

Han, J., Shui, J.-W., Zhang, X., Zheng, B., Han, S., and Tan, T.-H. (2005). HIP-55 is important for T-cell proliferation, cytokine production, and immune responses. Molecular and Cellular Biology *25*, 6869-6878.

Harris, N. L., Jaffe, E. S., Diebold, J., Flandrin, G., Muller-Hermelink, H. K., Vardiman, J., Lister, T. A., and Bloomfield, C. D. (1999). The World Health Organization Classification of Neoplastic Diseases of the Hematopoietic and Lymphoid Tissues: Report of the Clinical Advisory Committee Meeting, Airlie House, Virginia, November, 1997. Annals of Oncology *10*, 1419-1432.

Hashimoto, Y., Akiyama, Y., Otsubo, T., Shimada, S., and Yuasa, Y. (2010). Involvement of epigenetically silenced microRNA-181c in gastric carcinogenesis. Carcinogenesis *31*, 777-784.

Hashimoto, Y., Akiyama, Y., and Yuasa, Y. (2013). Multiple-to-Multiple Relationships between MicroRNAs and Target Genes in Gastric Cancer. PLoS One *8*, e62589.

Henao-Mejia, J., Williams, A., Goff, Loyal A., Staron, M., Licona-Limón, P., Kaech, Susan M., Nakayama, M., Rinn, John L., and Flavell, Richard A. (2013). The MicroRNA miR-181 Is a Critical Cellular Metabolic Rheostat Essential for NKT Cell Ontogenesis and Lymphocyte Development and Homeostasis. Immunity *38*, 984-997.

Hendrickson, D. G., Hogan, D. J., Herschlag, D., Ferrell, J. E., and Brown, P. O. (2008). Systematic identification of mRNAs recruited to argonaute 2 by specific microRNAs and corresponding changes in transcript abundance. PLoS One *3*, e2126.

Hickey, C. J., Schwind, S., Radomska, H. S., Dorrance, A. M., Santhanam, R., Mishra, A., Wu, Y.-Z., Alachkar, H., Maharry, K., Nicolet, D.*, et al.* (2013). Lenalidomide-mediated enhanced translation of C/EBPα-p30 protein up-regulates expression of the antileukemic microRNA-181a in acute myeloid leukemia. Blood *121*, 159-169.

Hogg, N., Patzak, I., and Willenbrock, F. (2011). The insider's guide to leukocyte integrin signalling and function. Nature Reviews Immunology *11*, 416-426.

Holsinger, L. J., Graef, I. A., Swat, W., Chi, T., Bautista, D. M., Davidson, L., Lewis, R. S., Alt, F. W., and Crabtree, G. R. (1998). Defects in actin-cap formation in Vav-deficient mice implicate an actin requirement for lymphocyte signal transduction. Current Biology *8*, 563-573.

Huang, J., Brameshuber, M., Zeng, X., Xie, J., Li, Q.-j., Chien, Y.-h., Valitutti, S., and Davis, M. M. (2013). A single peptide-major histocompatibility complex ligand triggers digital cytokine secretion in CD4+ T cells. Immunity *39*, 846-857.

Huh, Y. O., Medeiros, L. J., Ravandi, F., Konoplev, S., Jorgensen, J. L., and Miranda, R. N. (2009). T-Cell Large Granular Lymphocyte Leukemia Associated With Myelodysplastic Syndrome. A Clinicopathologic Study of Nine Cases. American Journal of Clinical Pathology *131*, 347-356.

Ibarra, N., Blagg, S. L., Vazquez, F., and Insall, R. H. (2006). Nap1 Regulates Dictyostelium Cell Motility and Adhesion through SCAR-Dependent and -Independent Pathways. Current Biology *16*, 717-722.

Isken, F., Steffen, B., Merk, S., Dugas, M., Markus, B., Tidow, N., Zühlsdorf, M., Illmer, T., Thiede, C., and Berdel, W. E. (2008). Identification of acute myeloid leukaemia associated microRNA expression patterns. British Journal of Haematology *140*, 153-161.

Ismail, A. M., Padrick, S. B., Chen, B., Umetani, J., and Rosen, M. K. (2009). The WAVE regulatory complex is inhibited. Nature Structural & Molecular Biology *16*, 561-563.

Ji, J., Yamashita, T., Budhu, A., Forgues, M., Jia, H. L., Li, C., Deng, C., Wauthier, E., Reid, L. M., and Ye, Q. H. (2009). Identification of microRNA-181 by genome-wide screening as a critical player in EpCAM-positive hepatic cancer stem cells. Hepatology *50*, 472-480.

Jonas, S., and Izaurralde, E. (2015). Towards a molecular understanding of microRNA-mediated gene silencing. Nature Reviews Genetics *16*, 421-433.

Karadimitris, A., Li, K., Notaro, R., Araten, D. J., Nafa, K., Thertulien, R., Ladanyi, M., Stevens, A. E., Rosenfeld, C. S., Roberts, I. A. G., and Luzzatto, L. (2001). Association of clonal T-cell large granular lymphocyte disease and paroxysmal nocturnal haemoglobinuria (PNH): further evidence for a pathogenetic link between T cells, aplastic anaemia and PNH. British Journal of Haematology *115*, 1010-1014.

Karp, X., and Ambros, V. (2005). Encountering MicroRNAs in Cell Fate Signaling. Science *310*, 1288-1289.

Kim, Y. K., and Kim, V. N. (2007). Processing of intronic microRNAs. The EMBO Journal *26*, 775-783.

Kong, Y. W., Cannell, I. G., de Moor, C. H., Hill, K., Garside, P. G., Hamilton, T. L., Meijer, H. A., Dobbyn, H. C., Stoneley, M., Spriggs, K. A.*, et al.* (2008). The mechanism of micro-RNA-mediated translation repression is determined by the promoter of the target gene. Proceedings of the National Academy of Sciences *105*, 8866-8871.

Koscianska, E., Starega-Roslan, J., and Krzyzosiak, W. J. (2011). The role of Dicer protein partners in the processing of microRNA precursors. PLoS One *6*, e28548.

Koskela, H. L., Eldfors, S., Ellonen, P., Van Adrichem, A. J., Kuusanmäki, H., Andersson, E. I., Lagström, S., Clemente, M. J., Olson, T., and Jalkanen, S. E. (2012). Somatic STAT3 mutations in large granular lymphocytic leukemia. New England Journal of Medicine *366*, 1905-1913.

Krawczyk, C., Oliveira-dos-Santos, A., Sasaki, T., Griffiths, E., Ohashi, P. S., Snapper, S., Alt, F., and Penninger, J. M. (2002). Vav1 controls integrin clustering and MHC/peptide-specific cell adhesion to antigen-presenting cells. Immunity *16*, 331-343.

Kuang, X., Chi, J., and Wang, L. (2016). Deregulated microRNA expression and its pathogenetic implications for myelodysplastic syndromes. Hematology *21*, 1-10.

Kuhn, D. E., Martin, M. M., Feldman, D. S., Terry Jr, A. V., Nuovo, G. J., and Elton, T. S. (2008). Experimental validation of miRNA targets. Methods *44*, 47-54.

Kulasekararaj, A. G., Mohamedali, A. M., and Mufti, G. J. (2013). Recent advances in understanding the molecular pathogenesis of myelodysplastic syndromes. British Journal of Haematology *162*, 587-605.

Kumari, S., Curado, S., Mayya, V., and Dustin, M. L. (2014). T cell antigen receptor activation and actin cytoskeleton remodeling. Biochimica et Biophysica Acta (BBA) - Biomembranes *1838*, 546-556.

Kunda, P., Craig, G., Dominguez, V., and Baum, B. (2003). Abi, Sra1, and Kette Control the Stability and Localization of SCAR/WAVE to Regulate the Formation of Actin-Based Protrusions. Current Biology *13*, 1867-1875.

Kurisu, S., and Takenawa, T. (2009). The WASP and WAVE family proteins. Genome Biology *10*, 226.1-226.9.

Kwong, Y. L., and Wong, K. F. (1998). Association of pure red cell aplasia with T large granular lymphocyte leukaemia. Journal of Clinical Pathology *51*, 672-675.

Labno, C. M., Lewis, C. M., You, D., Leung, D. W., Takesono, A., Kamberos, N., Seth, A., Finkelstein, L. D., Rosen, M. K., and Schwartzberg, P. L. (2003). Itk functions to control actin polymerization at the immune synapse through localized activation of Cdc42 and WASP. Current Biology *13*, 1619-1624.

Lagos-Quintana, M., Rauhut, R., Lendeckel, W., and Tuschl, T. (2001). Identification of Novel Genes Coding for Small Expressed RNAs. Science *294*, 853-858.

Lal, A., Navarro, F., Maher, C. A., Maliszewski, L. E., Yan, N., O'Day, E., Chowdhury, D., Dykxhoorn, D. M., Tsai, P., and Hofmann, O. (2009). miR-24 Inhibits cell proliferation by targeting E2F2, MYC, and other cell-cycle genes via binding to "seedless" 3' UTR microRNA recognition elements. Molecular Cell *35*, 610-625.

Lamy, T., and Loughran, T. P. (1999). Current concepts: large granular lymphocyte leukemia. Blood Reviews *13*, 230-240.

Lamy, T., and Loughran, T. P. (2011). How I treat LGL leukemia. Blood *117*, 2764-2774.

Le Bras, S., Foucault, I., Foussat, A., Brignone, C., Acuto, O., and Deckert, M. (2004). Recruitment of the actin-binding protein HIP-55 to the immunological synapse regulates T cell receptor signaling and endocytosis. Journal of Biological Chemistry *279*, 15550-15560.

Le, J., Mallery, E. L., Zhang, C., Brankle, S., and Szymanski, D. B. (2006). Arabidopsis BRICK1/HSPC300 Is an Essential WAVE-Complex Subunit that Selectively Stabilizes the Arp2/3 Activator SCAR2. Current Biology *16*, 895-901.

Lebensohn, A. M., and Kirschner, M. W. (2009). Activation of the WAVE Complex by Coincident Signals Controls Actin Assembly. Molecular Cell *36*, 512-524.

Lee, R. C., Feinbaum, R. L., and Ambros, V. (1993). The C. elegans heterochronic gene lin-4 encodes small RNAs with antisense complementarity to lin-14. Cell *75*, 843-854.

Lee, Y., Ahn, C., Han, J., Choi, H., Kim, J., Yim, J., Lee, J., Provost, P., Rådmark, O., and Kim, S. (2003). The nuclear RNase III Drosha initiates microRNA processing. Nature *425*, 415-419.

Lee, Y., Hur, I., Park, S. Y., Kim, Y. K., Suh, M. R., and Kim, V. N. (2006). The role of PACT in the RNA silencing pathway. The EMBO Journal *25*, 522-532.

Lee, Y., Kim, M., Han, J., Yeom, K. H., Lee, S., Baek, S. H., and Kim, V. N. (2004). MicroRNA genes are transcribed by RNA polymerase II. The EMBO Journal *23*, 4051-4060.

Lewis, B. P., Shih, I.-h., Jones-Rhoades, M. W., Bartel, D. P., and Burge, C. B. (2003). Prediction of mammalian microRNA targets. Cell *115*, 787-798.

Li, M., Ling, B., Xiao, T., Tan, J., An, N., Han, N., Guo, S., Cheng, S., and Zhang, K. (2014). Sp1 transcriptionally regulates BRK1 expression in non-small cell lung cancer cells. Gene *542*, 134-140.

Li, Q.-J., Chau, J., Ebert, P. J., Sylvester, G., Min, H., Liu, G., Braich, R., Manoharan, M., Soutschek, J., and Skare, P. (2007). miR-181a is an intrinsic modulator of T cell sensitivity and selection. Cell *129*, 147-161.

Li, X., Zhang, J., Gao, L., McClellan, S., Finan, M., Butler, T., Owen, L., Piazza, G., and Xi, Y. (2012a). MiR-181 mediates cell differentiation by interrupting the Lin28 and let-7 feedback circuit. Cell Death & Differentiation *19*, 378-386.

Li, Z., Huang, H., Li, Y., Jiang, X., Chen, P., Arnovitz, S., Radmacher, M. D., Maharry, K., Elkahloun, A., Yang, X.*, et al.* (2012b). Up-regulation of a HOXA-PBX3 homeobox-gene signature following down-regulation of miR-181 is associated with adverse prognosis in patients with cytogenetically abnormal AML. Blood *119*, 2314-2324.

Liao, R., Sun, J., Zhang, L., Lou, G., Chen, M., Zhou, D., Chen, Z., and Zhang, S. (2008). MicroRNAs play a role in the development of human hematopoietic stem cells. Journal of Cellular Biochemistry *104*, 805-817.

Lim, L. P., Lau, N. C., Garrett-Engele, P., Grimson, A., Schelter, J. M., Castle, J., Bartel, D. P., Linsley, P. S., and Johnson, J. M. (2005). Microarray analysis shows that some microRNAs downregulate large numbers of target mRNAs. Nature *433*, 769-773.

Lin, S., and Gregory, R. I. (2015). MicroRNA biogenesis pathways in cancer. Nature Reviews Cancer *15*, 321-333.

Lin, S., Pan, L., Guo, S., Wu, J., Jin, L., Wang, J.-C., and Wang, S. (2013). Prognostic role of microRNA-181a/b in hematological malignancies: a meta-analysis. PLoS One *8*, e59532.

Linkner, J., Witte, G., Stradal, T., Curth, U., and Faix, J. (2011). High-Resolution X-Ray Structure of the Trimeric Scar/WAVE-Complex Precursor Brk1. PLoS One *6*, e21327.

Liu, G., Min, H., Yue, S., and Chen, C.-Z. (2008). Pre-miRNA loop nucleotides control the distinct activities of mir-181a-1 and mir-181c in early T cell development. PLoS One *3*, e3592.

Liu, T., Papagiannakopoulos, T., Puskar, K., Qi, S., Santiago, F., Clay, W., Lao, K., Lee, Y., Nelson, S. F., Kornblum, H. I.*, et al.* (2007a). Detection of a MicroRNA Signal in an In Vivo Expression Set of mRNAs. PLoS One *2*, e804.

Liu, Y., Sun, W., Zhang, K., Zheng, H., Ma, Y., Lin, D., Zhang, X., Feng, L., Lei, W., Zhang, Z.*, et al.* (2007b). Identification of genes differentially expressed in human primary lung squamous cell carcinoma. Lung Cancer *56*, 307-317.

Loughran, J. T. P., Kadin, M. E., Starkebaum, G., Abkowitz, J. L., Clark, E. A., Disteche, C., Lum, L. G., and Slichter, S. J. (1985). Leukemia of Large Granular Lymphocytes: Association with Clonal Chromosomal Abnormalities and Autoimmune Neutropenia, Thrombocytopenia, and Hemolytic Anemia. Annals of Internal Medicine *102*, 169-175.

Loughran, T. J. (1993). Clonal diseases of large granular lymphocytes. Blood *82*, 1-14.

Lu, F., Zhang, J., Ji, M., Li, P., Du, Y., Wang, H., Zang, S., Ma, D., Sun, X., and Ji, C. (2014). miR-181b increases drug sensitivity in acute myeloid leukemia via targeting HMGB1 and Mcl-1. International Journal of Oncology *45*, 383-392.

Lu, J., Getz, G., Miska, E. A., Alvarez-Saavedra, E., Lamb, J., Peck, D., Sweet-Cordero, A., Ebert, B. L., Mak, R. H., Ferrando, A. A.*, et al.* (2005). MicroRNA expression profiles classify human cancers. Nature *435*, 834-838.

Lu, L.-F., Boldin, M. P., Chaudhry, A., Lin, L.-L., Taganov, K. D., Hanada, T., Yoshimura, A., Baltimore, D., and Rudensky, A. Y. (2010). Function of miR-146a in controlling Treg cell-mediated regulation of Th1 responses. Cell *142*, 914-929.

Lujambio, A., and Lowe, S. W. (2012). The microcosmos of cancer. Nature *482*, 347-355.

Lund, E., Güttinger, S., Calado, A., Dahlberg, J. E., and Kutay, U. (2004). Nuclear export of microRNA precursors. Science *303*, 95-98.

Lytle, J. R., Yario, T. A., and Steitz, J. A. (2007). Target mRNAs are repressed as efficiently by microRNA-binding sites in the 5' UTR as in the 3' UTR. Proceedings of the National Academy of Sciences *104*, 9667-9672.

Macián, F., García-Cózar, F., Im, S.-H., Horton, H. F., Byrne, M. C., and Rao, A. (2002). Transcriptional mechanisms underlying lymphocyte tolerance. Cell *109*, 719-731.

MacRae, I. J., Zhou, K., and Doudna, J. A. (2007). Structural determinants of RNA recognition and cleavage by Dicer. Nature Structural & Molecular Biology *14*, 934-940.

Manz, B. N., Jackson, B. L., Petit, R. S., Dustin, M. L., and Groves, J. (2011). T-cell triggering thresholds are modulated by the number of antigen within individual T-cell receptor clusters. Proceedings of the National Academy of Sciences *108*, 9089-9094.

Maranchie, J. K., Afonso, A., Albert, P. S., Kalyandrug, S., Phillips, J. L., Zhou, S., Peterson, J., Ghadimi, B. M., Hurley, K., Riss, J.*, et al.* (2004). Solid renal tumor severity in von Hippel Lindau disease is related to germline deletion length and location. Human Mutation *23*, 40-46.

Marcucci, G., Maharry, K., Radmacher, M. D., Mrózek, K., Vukosavljevic, T., Paschka, P., Whitman, S. P., Langer, C., Baldus, C. D., Liu, C.-G.*, et al.* (2008a). Prognostic Significance of, and Gene and MicroRNA Expression Signatures Associated With, CEBPA Mutations in Cytogenetically Normal Acute Myeloid Leukemia With High-Risk Molecular Features: A Cancer and Leukemia Group B Study. Journal of Clinical Oncology *26*, 5078-5087.

Marcucci, G., Radmacher, M. D., Maharry, K., Mrózek, K., Ruppert, A. S., Paschka, P., Vukosavljevic, T., Whitman, S. P., Baldus, C. D., Langer, C.*, et al.* (2008b). MicroRNA Expression in Cytogenetically Normal Acute Myeloid Leukemia. New England Journal of Medicine *358*, 1919-1928.

McNeill, A., Rattenberry, E., Barber, R., Killick, P., MacDonald, F., and Maher, E. R. (2009). Genotype-phenotype correlations in VHL exon deletions. American Journal of Medical Genetics Part A *149A*, 2147-2151.

Ménasché, G., Kliche, S., Bezman, N., and Schraven, B. (2007). Regulation of T-cell antigen receptor-mediated inside-out signaling by cytosolic adapter proteins and Rap1 effector molecules. Immunological Reviews *218*, 82-91.

Miki, H., Yamaguchi, H., Suetsugu, S., and Takenawa, T. (2000). IRSp53 is an essential intermediate between Rac and WAVE in the regulation of membrane ruffling. Nature *408*, 732-735.

Mili, S., and Steitz, J. A. (2004). Evidence for reassociation of RNA-binding proteins after cell lysis: implications for the interpretation of immunoprecipitation analyses. Rna *10*, 1692-1694.

Milunović, V., Mandac Rogulj, I., Planinc-Peraica, A., Bulycheva, E., and Kolonić Ostojić, S. (2016). The role of microRNA in myelodysplastic syndromes: beyond DNA methylation and histone modification. European Journal of Haematology *96*, 553-563.

Molina, I., Sancho, J., Terhorst, C., Rosen, F., and Remold-O'Donnell, E. (1993). T cells of patients with the Wiskott-Aldrich syndrome have a restricted defect in proliferative responses. The Journal of Immunology *151*, 4383-4390.

Molldrem, J. J., Caples, M., Mavroudis, D., Plante, M., Young, N. S., and Barrett, A. J. (1997). Antithymocyte globulin for patients with myelodysplastic syndrome. British Journal of Haematology *99*, 699-705.

Molldrem, J. J., Leifer, E., Bahceci, E., Saunthararajah, Y., Rivera, M., Dunbar, C., Liu, J., Nakamura, R., Young, N. S., and Barrett, A. J. (2002). Antithymocyte Globulin for Treatment of the Bone Marrow Failure Associated with Myelodysplastic Syndromes. Annals of Internal Medicine *137*, 156-163.

Monks, C. R., Freiberg, B. A., Kupfer, H., Sciaky, N., and Kupfer, A. (1998). Three-dimensional segregation of supramolecular activation clusters in T cells. Nature *395*, 82-86.

Morgenstern, J. P., and Land, H. (1990). Advanced mammalian gene transfer: high titre retroviral vectors with multiple drug selection markers and a complementary helper-free packaging cell line. Nucleic Acids Research *18*, 3587-3596.

Morlando, M., Ballarino, M., Gromak, N., Pagano, F., Bozzoni, I., and Proudfoot, N. J. (2008). Primary microRNA transcripts are processed co-transcriptionally. Nature Structural & Molecular Biology *15*, 902-909.

Mosakhani, N., Mustjoki, S., and Knuutila, S. (2013). Down-regulation of miR-181c in imatinib-resistant chronic myeloid leukemia. Molecular Cytogenetics *6*, 27-27.

Nanbakhsh, A., Visentin, G., Olive, D., Janji, B., Mussard, E., Dessen, P., Meurice, G., Zhang, Y., Louache, F., Bourhis, J.-H., and Chouaib, S. (2015). miR-181a modulates acute myeloid leukemia susceptibility to natural killer cells. Oncoimmunology *4*, e996475.

Neilson, J. R., Zheng, G. X., Burge, C. B., and Sharp, P. A. (2007). Dynamic regulation of miRNA expression in ordered stages of cellular development. Genes & Development *21*, 578-589.

Nimer, S. D. (2008). Myelodysplastic syndromes. Blood *111*, 4841-4851.

Nolz, J. C., Gomez, T. S., Zhu, P., Li, S., Medeiros, R. B., Shimizu, Y., Burkhardt, J. K., Freedman, B. D., and Billadeau, D. D. (2006). The WAVE2 Complex Regulates Actin Cytoskeletal Reorganization and CRAC-Mediated Calcium Entry during T Cell Activation. Current Biology *16*, 24-34.

Nolz, J. C., Medeiros, R. B., Mitchell, J. S., Zhu, P., Freedman, B. D., Shimizu, Y., and Billadeau, D. D. (2007). WAVE2 Regulates High-Affinity Integrin Binding by Recruiting Vinculin and Talin to the Immunological Synapse. Molecular and Cellular Biology *27*, 5986-6000.

Nolz, J. C., Nacusi, L. P., Segovis, C. M., Medeiros, R. B., Mitchell, J. S., Shimizu, Y., and Billadeau, D. D. (2008). The WAVE2 complex regulates T cell receptor signaling to integrins via Abl- and CrkL–C3G-mediated activation of Rap1. The Journal of Cell Biology *182*, 1231-1244.

O'Donoghue, G. P., Pielak, R. M., Smoligovets, A. A., Lin, J. J., and Groves, J. T. (2013). Direct single molecule measurement of TCR triggering by agonist pMHC in living primary T cells. Elife *2*, e00778.

Oda, A., and Eto, K. (2013). WASPs and WAVEs: From molecular function to physiology in hematopoietic cells. Seminars in Cell & Developmental Biology *24*, 308-313.

Oh-Hora, M., and Rao, A. (2008). Calcium signaling in lymphocytes. Current Opinion in Immunology *20*, 250-258.

Oikawa, T., Yamaguchi, H., Itoh, T., Kato, M., Ijuin, T., Yamazaki, D., Suetsugu, S., and Takenawa, T. (2004). PtdIns(3,4,5)P3 binding is necessary for WAVE2-induced formation of lamellipodia. Nature Cell Biology *6*, 420-426.

Olnes, M. J., and Sloand, E. M. (2011). Targeting immune dysregulation in myelodysplastic syndromes. JAMA *305*, 814-819.

Padrick, S. B., and Rosen, M. K. (2010). Physical mechanisms of signal integration by WASP family proteins. Annual Review of Biochemistry *79*, 707-735.

Papaemmanuil, E., Gerstung, M., Malcovati, L., Tauro, S., Gundem, G., Van Loo, P., Yoon, C. J., Ellis, P., Wedge, D. C., and Pellagatti, A. (2013). Clinical and biological implications of driver mutations in myelodysplastic syndromes. Blood *122*, 3616-3627.

Park, H., Staehling-Hampton, K., Appleby, M. W., Brunkow, M. E., Habib, T., Zhang, Y., Ramsdell, F., Liggitt, H. D., Freie, B., Tsang, M.*, et al.* (2008). A point mutation in the murine Hem1 gene reveals an essential role for Hematopoietic Protein 1 in lymphopoiesis and innate immunity. The Journal of Experimental Medicine *205*, 2899-2913.

Pekarsky, Y., Santanam, U., Cimmino, A., Palamarchuk, A., Efanov, A., Maximov, V., Volinia, S., Alder, H., Liu, C.-G., Rassenti, L.*, et al.* (2006). Tcl1 Expression in Chronic Lymphocytic Leukemia Is Regulated by miR-29 and miR-181. Cancer Research *66*, 11590-11593.

Pellagatti, A., and Boultwood, J. (2015). The molecular pathogenesis of the myelodysplastic syndromes. European Journal of Haematology *95*, 3-15.

Pollitt, A. Y., and Insall, R. H. (2008). Abi Mutants in Dictyostelium Reveal Specific Roles for the SCAR/WAVE Complex in Cytokinesis. Current Biology *18*, 203-210.

Pollitt, A. Y., and Insall, R. H. (2009a). Loss of Dictyostelium HSPC300 causes a scar-like phenotype and loss of SCAR protein. BMC Cell Biology *10*, 1-7.

Pollitt, A. Y., and Insall, R. H. (2009b). WASP and SCAR/WAVE proteins: the drivers of actin assembly. Journal of Cell Science *122*, 2575-2578.

Pons, A., Nomdedeu, B., Navarro, A., Gaya, A., Gel, B., Diaz, T., Valera, S., Rozman, M., Belkaid, M., Montserrat, E., and Monzo, M. (2009). Hematopoiesis-related microRNA expression in myelodysplastic syndromes. Leukemia & Lymphoma *50*, 1854-1859.

Qurashi, A., Sahin, H. B., Carrera, P., Gautreau, A., Schenck, A., and Giangrande, A. (2007). HSPC300 and its role in neuronal connectivity. Neural Development *2*, 18.

Raab, M., Wang, H., Lu, Y., Smith, X., Wu, Z., Strebhardt, K., Ladbury, J. E., and Rudd, C. E. (2010). T cell receptor "inside-out" pathway via signaling module SKAP1-RapL regulates T cell motility and interactions in lymph nodes. Immunity *32*, 541-556.

Rakeman, A. S., and Anderson, K. V. (2006). Axis specification and morphogenesis in the mouse embryo require Nap1, a regulator of WAVE-mediated actin branching. Development *133*, 3075-3083.

Reinhart, B. J., Slack, F. J., Basson, M., Pasquinelli, A. E., Bettinger, J. C., Rougvie, A. E., Horvitz, H. R., and Ruvkun, G. (2000). The 21-nucleotide let-7 RNA regulates developmental timing in Caenorhabditis elegans. Nature *403*, 901-906.

Rhyasen, G. W., and Starczynowski, D. T. (2012). Deregulation of microRNAs in myelodysplastic syndrome. Leukemia *26*, 13-22.

Risitano, A. M., Maciejewski, J. P., Muranski, P., Wlodarski, M., O'Keefe, C., Sloand, E. M., and Young, N. S. (2005). Large granular lymphocyte (LGL)-like clonal expansions in paroxysmal nocturnal hemoglobinuria (PNH) patients. Leukemia *19*, 217-222.

Rodriguez, A., Griffiths-Jones, S., Ashurst, J. L., and Bradley, A. (2004). Identification of mammalian microRNA host genes and transcription units. Genome Research *14*, 1902-1910.

Rogers, S. L., Wiedemann, U., Stuurman, N., and Vale, R. D. (2003). Molecular requirements for actin-based lamella formation in Drosophila S2 cells. The Journal of Cell Biology *162*, 1079-1088.

Roncagalli, R., Hauri, S., Fiore, F., Liang, Y., Chen, Z., Sansoni, A., Kanduri, K., Joly, R., Malzac, A., and Lähdesmäki, H. (2014). Quantitative proteomics analysis of signalosome dynamics in primary T cells identifies the surface receptor CD6 as a Lat adaptor-independent TCR signaling hub. Nature Immunology *15*, 384-392.

Roose, J. P., Mollenauer, M., Gupta, V. A., Stone, J., and Weiss, A. (2005). A diacylglycerol-protein kinase C-RasGRP1 pathway directs Ras activation upon antigen receptor stimulation of T cells. Molecular and Cellular Biology *25*, 4426-4441.

Ruan, J., Lou, S., Dai, Q., Mao, D., Ji, J., and Sun, X. (2015). Tumor suppressor miR-181c attenuates proliferation, invasion, and self-renewal abilities in glioblastoma. Neuroreport *26*, 66-73.

Ruby, J. G., Jan, C. H., and Bartel, D. P. (2007). Intronic microRNA precursors that bypass Drosha processing. Nature *448*, 83-86.

Santamaría, C., Muntión, S., Rosón, B., Blanco, B., López-Villar, O., Carrancio, S., Sánchez-Guijo, F. M., Díez-Campelo, M., Alvarez-Fernández, S., and Sarasquete, M. E. (2012). Impaired expression of DICER, DROSHA, SBDS and some microRNAs in mesenchymal stromal cells from myelodysplastic syndrome patients. Haematologica *97*, 1218-1224.

Sauntharajah, Y., Molldrem, J. J., Rivera, M., Williams, A., Stetler-Stevenson, M., Sorbara, L., Young, N. S., and Barrett, J. A. (2001). Coincident myelodysplastic syndrome and T-cell large granular lymphocytic disease: clinical and pathophysiological features. British Journal of Haematology *112*, 195-200.

Sauntharajah, Y., Nakamura, R., Nam, J.-M., Robyn, J., Loberiza, F., Maciejewski, J. P., Simonis, T., Molldrem, J., Young, N. S., and Barrett, A. J. (2002). HLA-DR15 (DR2) is overrepresented in myelodysplastic syndrome and aplastic anemia and predicts a response to immunosuppression in myelodysplastic syndrome. Blood *100*, 1570-1574.

Sauntharajah, Y., Nakamura, R., Wesley, R., Wang, Q. J., and Barrett, A. J. (2003). A simple method to predict response to immunosuppressive therapy in patients with myelodysplastic syndrome. Blood *102*, 3025-3027.

Savignac, M., Mellström, B., and Naranjo, J. R. (2007). Calcium-dependent transcription of cytokine genes in T lymphocytes. Pflügers Archiv-European Journal of Physiology *454*, 523-533.

Schanz, J., Tüchler, H., Solé, F., Mallo, M., Luño, E., Cervera, J., Granada, I., Hildebrandt, B., Slovak, M. L., Ohyashiki, K.*, et al.* (2012). New Comprehensive Cytogenetic Scoring System for Primary Myelodysplastic Syndromes (MDS) and Oligoblastic Acute Myeloid Leukemia After MDS Derived From an International Database Merge. Journal of Clinical Oncology *30*, 820-829.

Schenck, A., Qurashi, A., Carrera, P., Bardoni, B., Diebold, C., Schejter, E., Mandel, J.-L., and Giangrande, A. (2004). WAVE/SCAR, a multifunctional complex coordinating different aspects of neuronal connectivity. Developmental Biology *274*, 260-270.

Schonrock, N., Humphreys, D. T., Preiss, T., and Götz, J. (2012). Target Gene Repression Mediated by miRNAs miR-181c and miR-9 Both of Which Are Down-regulated by Amyloid-β. Journal of Molecular Neuroscience *46*, 324-335.

Schulze-Luehrmann, J., and Ghosh, S. (2006). Antigen-receptor signaling to nuclear factor κB. Immunity *25*, 701-715.

Schwind, S., Maharry, K., Radmacher, M. D., Mrózek, K., Holland, K. B., Margeson, D., Whitman, S. P., Hickey, C., Becker, H., Metzeler, K. H., *et al.* (2010). Prognostic Significance of Expression of a Single MicroRNA, miR-181a, in Cytogenetically Normal Acute Myeloid Leukemia: A Cancer and Leukemia Group B Study. Journal of Clinical Oncology *28*, 5257-5264.

Serio, B., Risitano, A., Giudice, V., Montuori, N., and Selleri, C. (2014). Immunological derangement in hypocellular myelodysplastic syndromes. Translational Medicine@ UniSa *8*, 31-42.

She, X., Yu, Z., Cui, Y., Lei, Q., Wang, Z., Xu, G., Luo, Z., Li, G., and Wu, M. (2014). miR-181 subunits enhance the chemosensitivity of temozolomide by Rap1B-mediated cytoskeleton remodeling in glioblastoma cells. Medical Oncology *31*, 1-10.

Shin, C., Nam, J.-W., Farh, K. K.-H., Chiang, H. R., Shkumatava, A., and Bartel, D. P. (2010). Expanding the microRNA targeting code: functional sites with centered pairing. Molecular Cell *38*, 789-802.

Sims, T. N., Soos, T. J., Xenias, H. S., Dubin-Thaler, B., Hofman, J. M., Waite, J. C., Cameron, T. O., Thomas, V. K., Varma, R., and Wiggins, C. H. (2007). Opposing effects of PKCθ and WASp on symmetry breaking and relocation of the immunological synapse. Cell *129*, 773-785.

Smith-Garvin, J. E., Koretzky, G. A., and Jordan, M. S. (2009). T Cell Activation. Annual Review of Immunology *27*, 591-619.

Snapper, S. B., Rosen, F. S., Mizoguchi, E., Cohen, P., Khan, W., Liu, C.-H., Hagemann, T. L., Kwan, S.-P., Ferrini, R., and Davidson, L. (1998). Wiskott-Aldrich syndrome protein-deficient mice reveal a role for WASP in T but not B cell activation. Immunity *9*, 81-91.

Sokol, L., Caceres, G., Volinia, S., Alder, H., Nuovo, G. J., Liu, C.-G., McGraw, K., Clark, J. A., Sigua, C. A., Chen, D.-T., *et al.* (2011). Identification of a risk dependent microRNA expression signature in myelodysplastic syndromes. British Journal of Haematology *153*, 24-32.

Starczynowski, D. T., Kuchenbauer, F., Argiropoulos, B., Sung, S., Morin, R., Muranyi, A., Hirst, M., Hogge, D., Marra, M., Wells, R. A., *et al.* (2010). Identification of miR-145 and miR-146a as mediators of the 5q- syndrome phenotype. Nature Medicine *16*, 49-58.

Starczynowski, D. T., Morin, R., McPherson, A., Lam, J., Chari, R., Wegrzyn, J., Kuchenbauer, F., Hirst, M., Tohyama, K., Humphries, R. K., *et al.* (2011). Genome-wide identification of human microRNAs located in leukemia-associated genomic alterations. Blood *117*, 595-607.

Steffen, A., Rottner, K., Ehinger, J., Innocenti, M., Scita, G., Wehland, J., and Stradal, T. E. (2004). Sra-1 and Nap1 link Rac to actin assembly driving lamellipodia formation. The EMBO Journal *23*, 749-759.

Steinway, S. N., LeBlanc, F., and Loughran Jr, T. P. (2014). The pathogenesis and treatment of large granular lymphocyte leukemia. Blood Reviews *28*, 87-94.

Stroynowska-Czerwinska, A., Fiszer, A., and Krzyzosiak, W. J. (2014). The panorama of miRNA-mediated mechanisms in mammalian cells. Cellular and Molecular Life Sciences *71*, 2253-2270.

Su, I.-h., Dobenecker, M.-W., Dickinson, E., Oser, M., Basavaraj, A., Marqueron, R., Viale, A., Reinberg, D., Wülfing, C., and Tarakhovsky, A. (2005). Polycomb group protein ezh2 controls actin polymerization and cell signaling. Cell *121*, 425-436.

Su, R., Lin, H. S., Zhang, X. H., Yin, X. L., Ning, H. M., Liu, B., Zhai, P. F., Gong, J. N., Shen, C., Song, L.*, et al.* (2015). MiR-181 family: regulators of myeloid differentiation and acute myeloid leukemia as well as potential therapeutic targets. Oncogene *34*, 3226-3239.

Suetsugu, S., Kurisu, S., Oikawa, T., Yamazaki, D., Oda, A., and Takenawa, T. (2006). Optimization of WAVE2 complex-induced actin polymerization by membrane-bound IRSp53, PIP3, and Rac. The Journal of Cell Biology *173*, 571-585.

Suetsugu, S., Miki, H., and Takenawa, T. (1999). Identification of Two Human WAVE/SCAR Homologues as General Actin Regulatory Molecules Which Associate with the Arp2/3 Complex. Biochemical and Biophysical Research Communications *260*, 296-302.

Sun, W., Zhang, K., Zhang, X., Lei, W., Xiao, T., Ma, J., Guo, S., Shao, S., Zhang, H., Liu, Y.*, et al.* (2004). Identification of differentially expressed genes in human lung squamous cell carcinoma using suppression subtractive hybridization. Cancer Letters *212*, 83-93.

Swerdlow, S., Campo, E., Harris, N., Jaffe, E., Pileri, S., and Stein, H. (2008). WHO Classification of Tumours of Haematopoietic and Lymphoid Tissues. WHO Classification of Tumours IARC *2*.

Szymanski, D. B. (2005). Breaking the WAVE complex: the point of Arabidopsis trichomes. Current Opinion in Plant Biology *8*, 103-112.

Takenawa, T., and Suetsugu, S. (2007). The WASP-WAVE protein network: connecting the membrane to the cytoskeleton. Nature Reviews Molecular Cell Biology *8*, 37-48.

Taniuchi, I., Kitamura, D., Maekawa, Y., Fukuda, T., Kishi, H., and Watanabe, T. (1995). Antigen-receptor induced clonal expansion and deletion of lymphocytes are impaired in mice lacking HS1 protein, a substrate of the antigen-receptor-coupled tyrosine kinases. The EMBO Journal *14*, 3664.

Thomson, D. W., Bracken, C. P., and Goodall, G. J. (2011). Experimental strategies for microRNA target identification. Nucleic Acids Research *39*, 6845-6853.

Thomson, J. M., Parker, J., Perou, C. M., and Hammond, S. M. (2004). A custom microarray platform for analysis of microRNA gene expression. Nature Methods *1*, 47-53.

Tominaga, N., Kosaka, N., Ono, M., Katsuda, T., Yoshioka, Y., Tamura, K., Lötvall, J., Nakagama, H., and Ochiya, T. (2015). Brain metastatic cancer cells release microRNA-181c-containing extracellular vesicles capable of destructing blood-brain barrier. Nature Communications *6*, 1-12.

Turner, M., and Billadeau, D. D. (2002). VAV proteins as signal integrators for multi-subunit immune-recognition receptors. Nature Reviews Immunology *2*, 476-486.

Vardiman, J. W., Harris, N. L., and Brunning, R. D. (2002). The World Health Organization (WHO) classification of the myeloid neoplasms. Blood *100*, 2292-2302.

Verduci, L., Azzalin, G., Gioiosa, S., Carissimi, C., Laudadio, I., Fulci, V., and Macino, G. (2015). microRNA-181a enhances cell proliferation in acute lymphoblastic leukemia by targeting EGR1. Leukemia Research *39*, 479-485.

Visone, R., Rassenti, L. Z., Veronese, A., Taccioli, C., Costinean, S., Aguda, B. D., Volinia, S., Ferracin, M., Palatini, J., Balatti, V.*, et al.* (2009). Karyotype-specific microRNA signature in chronic lymphocytic leukemia. Blood *114*, 3872-3879.

Voinnet, O. (2009). Origin, Biogenesis, and Activity of Plant MicroRNAs. Cell *136*, 669-687.

Walter, M. J., Shen, D., Ding, L., Shao, J., Koboldt, D. C., Chen, K., Larson, D. E., McLellan, M. D., Dooling, D., and Abbott, R. (2012). Clonal architecture of secondary acute myeloid leukemia. New England Journal of Medicine *366*, 1090-1098.

Wang, G., Zhao, R. A. N., Zhao, X., Chen, X. I., Wang, D., Jin, Y., Liu, X. I., Zhao, C. I., Zhu, Y., Ren, C.*, et al.* (2015). MicroRNA-181a enhances the chemotherapeutic sensitivity of chronic myeloid leukemia to imatinib. Oncology Letters *10*, 2835-2841.

Wang, J.-L., Tong, C.-W., Chang, W.-T., and Huang, A. M. (2013a). Novel genes FAM134C, C3orf10 and ENOX1 are regulated by NRF-1 and differentially regulate neurite outgrowth in neuroblastoma cells and hippocampal neurons. Gene *529*, 7-15.

Wang, Z., Tang, X., Xu, W., Cao, Z., Sun, L., Li, W., Li, Q., Zou, P., and Zhao, Z. (2013b). The different immunoregulatory functions on dendritic cells between mesenchymal stem cells derived from bone marrow of patients with low-risk or high-risk myelodysplastic syndromes. PLoS One *8*, e57470.

Wardenburg, J. B., Fu, C., Jackman, J. K., Flotow, H., Wilkinson, S. E., Williams, D. H., Johnson, R., Kong, G., Chan, A. C., and Findell, P. R. (1996). Phosphorylation of SLP-76 by the ZAP-70 protein-tyrosine kinase is required for T-cell receptor function. Journal of Biological Chemistry *271*, 19641-19644.

Watters, R. J., Liu, X., and Loughran, T. P. (2011). T-cell and natural killer-cell large granular lymphocyte leukemia neoplasias. Leukemia & Lymphoma *52*, 2217-2225.

Weiner, O. D., Rentel, M. C., Ott, A., Brown, G. E., Jedrychowski, M., Yaffe, M. B., Gygi, S. P., Cantley, L. C., Bourne, H. R., and Kirschner, M. W. (2006). Hem-1 Complexes Are Essential for Rac Activation, Actin Polymerization, and Myosin Regulation during Neutrophil Chemotaxis. PLoS Biology *4*, e38.

Wightman, B., Ha, I., and Ruvkun, G. (1993). Posttranscriptional regulation of the heterochronic gene lin-14 by lin-4 mediates temporal pattern formation in C. elegans. Cell *75*, 855-862.

Xue, Q., Guo, Z.-Y., Li, W., Wen, W.-H., Meng, Y.-L., Jia, L.-T., Wang, J., Yao, L.-B., Jin, B.-Q., Wang, T., and Yang, A.-G. (2011). Human activated CD4+ T lymphocytes increase IL-2 expression by downregulating microRNA-181c. Molecular Immunology *48*, 592-599.

Yu, Y., Smoligovets, A. A., and Groves, J. T. (2013). Modulation of T cell signaling by the actin cytoskeleton. Journal of Cell Science *126*, 1049-1058.

Zanette, D., Rivadavia, F., Molfetta, G., Barbuzano, F., Proto-Siqueira, R., Falcão, R., Zago, M., and Silva-Jr, W. (2007). miRNA expression profiles in chronic lymphocytic and acute lymphocytic leukemia. Brazilian Journal of Medical and Biological Research *40*, 1435-1440.

Zeng, R., Cannon, J. L., Abraham, R. T., Way, M., Billadeau, D. D., Bubeck-Wardenberg, J., and Burkhardt, J. K. (2003). SLP-76 coordinates Nck-dependent Wiskott-Aldrich syndrome protein recruitment with Vav-1/Cdc42-dependent Wiskott-Aldrich syndrome protein activation at the T cell-APC contact site. The Journal of Immunology *171*, 1360-1368.

Zhang, B., Pan, X., Cobb, G. P., and Anderson, T. A. (2007). microRNAs as oncogenes and tumor suppressors. Developmental Biology *302*, 1-12.

Zhang, D., and Loughran, T. P. (2012). Large granular lymphocytic leukemia: molecular pathogenesis, clinical manifestations, and treatment. ASH Education Program Book *2012*, 652-659.

Zhang, J., Shehabeldin, A., da Cruz, L. A. G., Butler, J., Somani, A.-K., McGavin, M., Kozieradzki, I., dos Santos, A. O., Nagy, A., Grinstein, S.*, et al.* (1999). Antigen Receptor–Induced Activation and Cytoskeletal Rearrangement Are Impaired in Wiskott-Aldrich Syndrome Protein-Deficient Lymphocytes. The Journal of Experimental Medicine *190*, 1329-1342.

Zhang, L., Dong, L.-Y., Li, Y.-J., Hong, Z., and Wei, W.-S. (2012). The microRNA miR-181c controls microglia-mediated neuronal apoptosis by suppressing tumor necrosis factor. Journal of Neuroinflammation *9*, 1-12.

Zhang, L., Padron, E., and Lancet, J. (2015). The molecular basis and clinical significance of genetic mutations identified in myelodysplastic syndromes. Leukemia Research *39*, 6-17.

Zhang, W., Sloan-Lancaster, J., Kitchen, J., Trible, R. P., and Samelson, L. E. (1998). LAT: the ZAP-70 tyrosine kinase substrate that links T cell receptor to cellular activation. Cell *92*, 83-92.

Zhang, X., Sokol, L., Bennett, J. M., Moscinski, L. C., List, A., and Zhang, L. (2016). T-cell large granular lymphocyte proliferation in myelodysplastic syndromes: Clinicopathological features and prognostic significance. Leukemia Research *43*, 18-23.

Zhu, D.-X., Zhu, W., Fang, C., Fan, L., Zou, Z.-J., Wang, Y.-H., Liu, P., Hong, M., Miao, K.-R., Liu, P.*, et al.* (2012). miR-181a/b significantly enhances drug sensitivity in chronic lymphocytic leukemia cells via targeting multiple anti-apoptosis genes. Carcinogenesis *33*, 1294-1301.

Zhu, W., Shan, X., Wang, T., Shu, Y., and Liu, P. (2010). miR-181b modulates multidrug resistance by targeting BCL2 in human cancer cell lines. International Journal of Cancer *127*, 2520-2529.

Zipfel, P. A., Bunnell, S. C., Witherow, D. S., Gu, J. J., Chislock, E. M., Ring, C., and Pendergast, A. M. (2007). Role for the Abi/Wave Protein Complex in T Cell Receptor-Mediated Proliferation and Cytoskeletal Remodeling. Current Biology *16*, 35-46.

Appendix

Appendix A: Vectors

A1: pCR®II-TOPO® Vector (Adapted from Life Technologies)

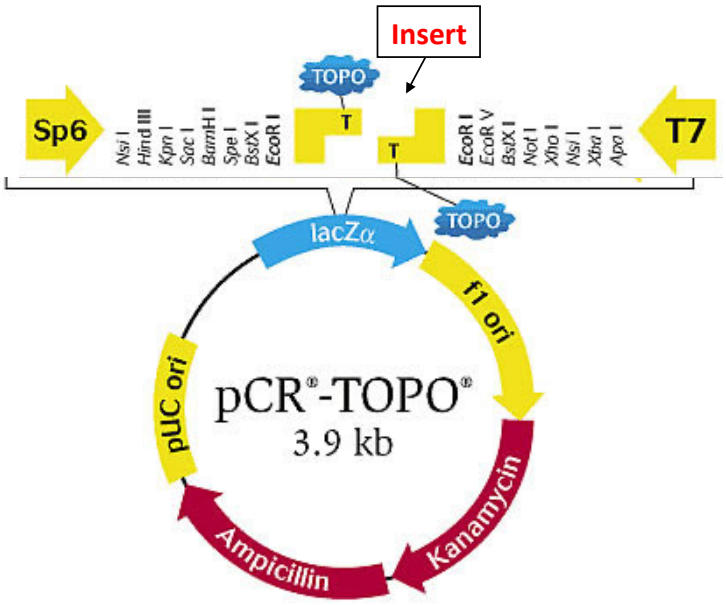

A2: pBabePuro Vector

The *miR-181* was inserted into pBabePuro vector via its restriction sites of BamHI and EcoRI.

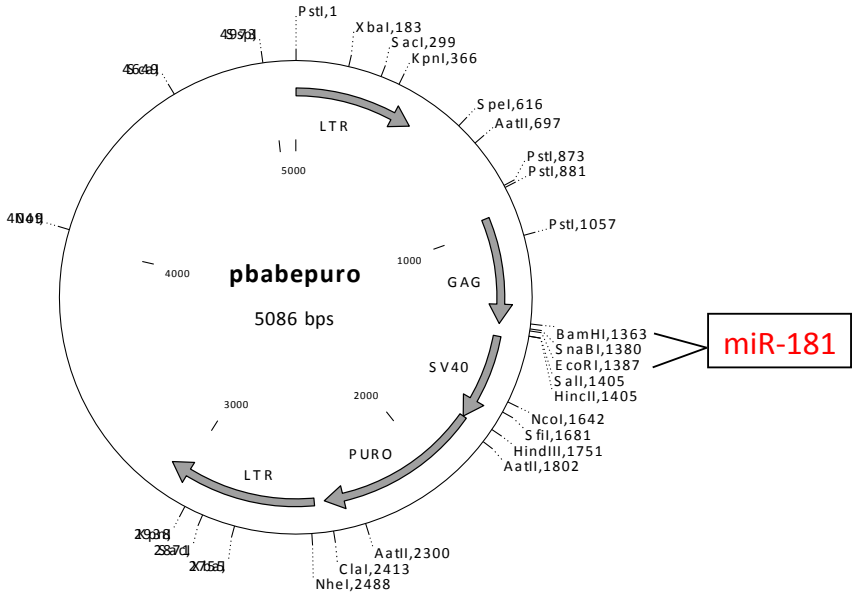

A3: p3'TKzeo Dual Selection Vector (Adapted from Sigma-Aldrich)

The human cDNA library was inserted directionally downstream of a TKzeo fusion gene via two SfiI sites that are different in their interpalindromic sequence.

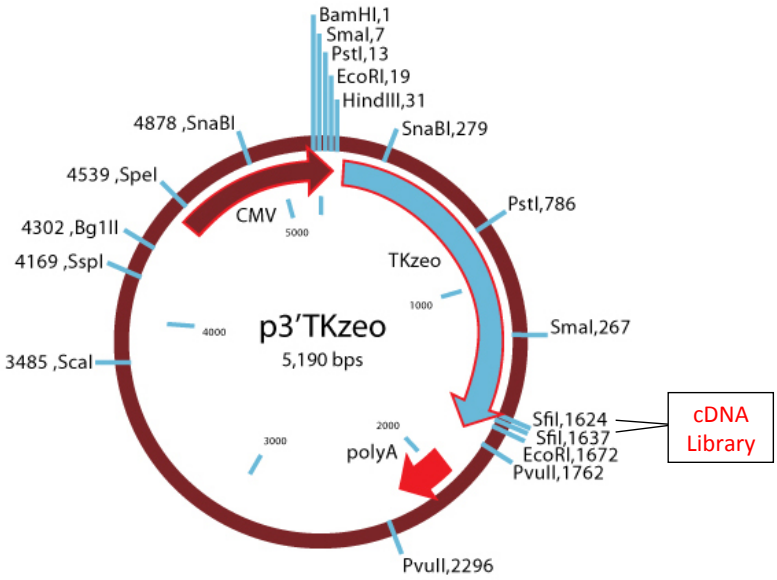

A4: pLKO.1-TRC Cloning Vector (Taken from Addgene)

The shRNA against *BRK1* was inserted into pLKO.1-TRC cloning vector via its restriction sites of AgeI and EcoRI.

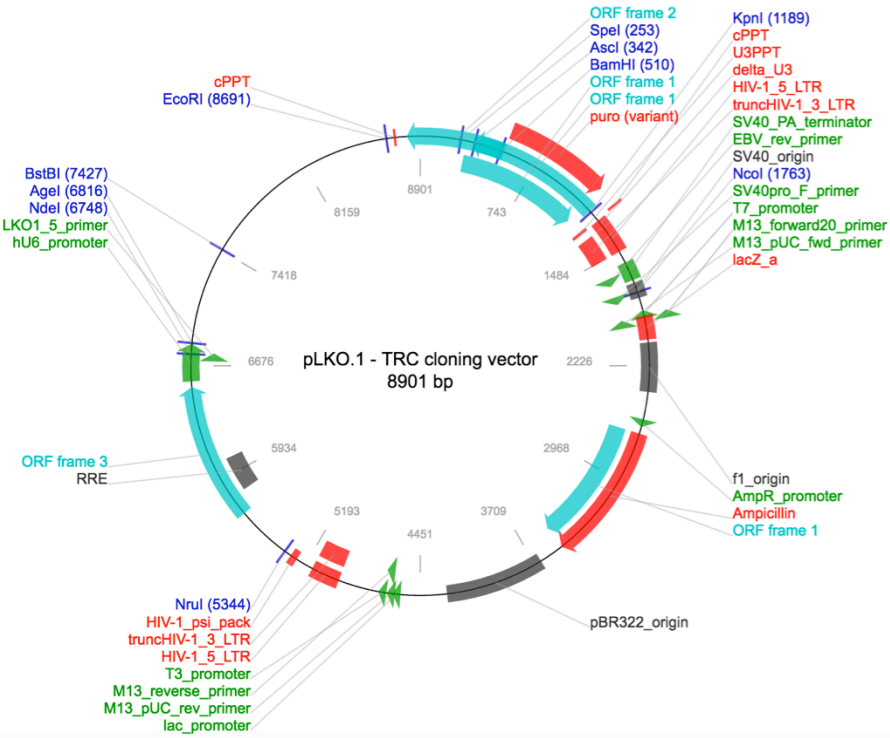

Appendix B: Oligonucleotides

B1: Oligonucleotides used to amplify *miR-181* from human genomic DNA

Oligo	Sequence 5'-3'	Incorporated Restriction Site at 5' End
miR-181a_F	CGGATCCTCAGGAAAATGTGGGTTGTTGA	BamHI
miR-181a_R	AGAATTCGACTGCTCCTTACCTTGTTGA	EcoRI
miR-181b_F	CGGATCCTCCAAGCACTCCTTCCTTCT	BamHI
miR-181b_R	AGAATTCCCGAGGAAATGGATTGCAGA	EcoRI
miR-181c/d_F	CGGATCCTACTTAAGGAGCGGGCTTGA	BamHI
miR-181c/d_R	AGAATTCGAGCTGAGATTGGGCCACT	EcoRI
miR-181c_F	CGGATCCTACTTAAGGAGCGGGCTTGA	BamHI
miR-181c_R	CGAATTCCTGGAAGGTCAGAGTCACCG	EcoRI

B2: Oligonucleotides used to amplify putative targets of *miR-181c/d*

Several primers designed to flank the SfiI sites in the p3'TKzeo vector were used in optimisation of amplification of putative *miR-181c/d* target genes.

Oligo	**Sequence 5'-3'**	**Annealing Temperature (°C)**
3 Forward (3F)	GGGTCGACCTCGAATCCTTA	62
9 Forward (9F)	CAAGTTGACCAGTGCCGTTC	61
11 Forward (11F)	CCTTAGGCCATTAAGGCC	61
14 Forward (14 F)	TCGACCTCGAATCCTTAG	56
15 Forward (15 F)	GGGTCGACCTCGAATCC	55
10 Reverse (10RTTT)	CGAGGCGGCCGACATGTTT	55, 56, 61 or 62 (depending on forward primer)

Primers Alignment in p3'UTR of TKzeo Vector

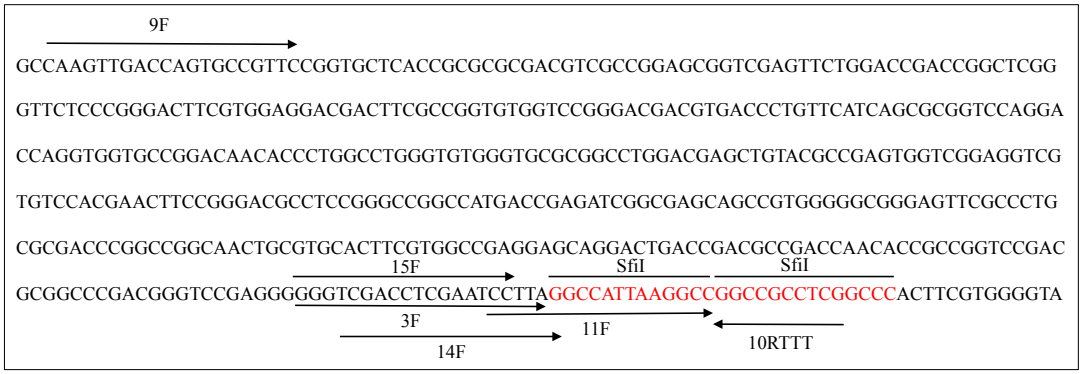

Reverse Primer of 10RTTT

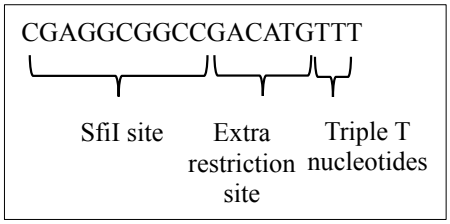

Reverse primer of 10RTTT has an extra restriction site and triple T nucleotides

B3: Oligonucleotides for qPCR (Probe Based Detection)

Oligo	Sequence 5'-3'	Probe
GAPDH_F	AGCCACATC GCTCAGACAC	60
GAPHD_R	GCCCAATACGACCAAATCC	60
BRK1_F	AGTACATTGAAGCTCGGGTGA	3
BRK1_R	GGCCTGTGTTGTGTAAAGCA	3
DHTKD1_F	TGTCGAAACTAATGCTGGAATC	49
DHTKD1_R	TCCATATCGCTTCACTGTCG	49

B4: Oligonucleotides for qPCR (DNA Dye Based Detection – SYBR® Green)

Oligo	Target Sequence 5'-3'
hsa-miR-103a-3p	AGCAGCAUUGUACAGGGCUAUGA
hsa-miR-181c-5p	AACAUUCAACCUGUCGGUGAGU
hsa-miR-181d	AACAUUCAUUGUUGUCGGUGGGU
U6	GUGCUCGCUUCGGCAGCACAUAUACUAAAAUUGG AACGAUACAGAGAAGAUUAGCAUGGCCCCUGCGC AAGGAUGACACGCAAAUUCGUGAAGCGUUCCAU AUUUUU

B5: Oligonucleotides for Sanger Sequencing

Oligo	Sequence 5'-3'
pLKO.1_Seq	CAAGGCTGTTAGAGAGATAATTGGA
M13 Forward (-20)	GTAAAACGACGGCCAG
M13 Reverse	CAGGAAACAGCTATGAC
pBabe_Seq_F1	TCGATCCTCCCTTTATCCAGC
pBabe_Seq_R1	CGGGACTATGGTTGCTGACT
pBabe_Seq_F2	TCTTCCTCCATCCGCCC
pBabe_Seq_R2	CACACCTGGTTGCTGACT

Appendix C:

C1: Oligonucleotides of shRNA Directed Against *BRK1*

Oligo	Sequence 5'-3'
shBRK1_1_F	CCGGGACTTTCTCAACTCGTTCGATCTCGAGATCGAACGAGTTGAGAAAGTCTTTTTG
shBRK1_1_R	AATTCAAAAAGACTTTCTCAACTCGTTCGATCTCGAGATCGAACGAGTTGAGAAAGTC
shBRK1_2_F	CCGGCTTGTCGTTCAAGACTTGCAACTCGAGTTGCAAGTCTTGAACGACAAGTTTTTG
shBRK1_2_R	AATTCAAAAACTTGTCGTTCAAGACTTGCAACTCGAGTTGCAAGTCTTGAACGACAAG

C2: Sequences of miRNA Inhibitors, siRNA and shRNA

miRNA Inhibitors	**Mature miRNA Sequence**	**Supplier**
miRIDIAN microRNA Hairpin Inhibitor Negative Control #1	NA	Dharmacon (IN-001005-01-05)
miRIDIAN microRNA Human hsa-miR-181c-5p-Hairpin Inhibitor	AACAUUCAACCUGUCGGUGAGU	Dharmacon (IH-300556-05-0002)
miRIDIAN microRNA Human hsa-miR-181d-5p-Hairpin Inhibitor	AACAUUCAUUGUUGUCGGUGGGU	Dharmacon (IH-300766-06-0002)
siRNA	**Target Sequence**	**Supplier**
siGENOME Non-Targeting siRNA Pool #1	UAGCGACUAAACACAUCAA, UAAGGCUAUGAAGAGAUAC, AUGUAUUGGCCUGUAUUAG, AUGAACGUGAAUUGCUCAA	Dharmacon (D-001206-13-05)
siGENOME Human BRK1 siRNA-SMARTpool	CGAUAUGUCUUGUCGUUCA, GAACGGAGAAUAGAGUACA, ACACUAAACGAGAAAUUGA, GGGCUAACCGGGAGUACAU	Dharmacon (M-017711-01-0005)
shRNA	**Target Sequence**	**Supplier**
shBRK1_1	GACTTTCTCAACTCGTTCGAT	NA
shBRK1_2	CTTGTCGTTCAAGACTTGCAA	NA
Scrambled shRNA	CCTAAGGTTAAGTCGCCCTCG	Addgene

NA: not applicable

Appendix D: Antibodies for Western Blotting

Primary Antibody	**Description**	**Source (Cat No)**	**Working Dilution**
Anti-β-ACTIN	Mouse monoclonal	Abcam (ab8226)	1:1000
Anti-DHTKD1	Rabbit polyclonal antibody	Abgent (AP10715c)	1:500
Anti-BRK1	Mouse monoclonal	Generous gift from Professor Stradal Theresia	1:3
Anti-WAVE2 (H-110)	Rabbit polyclonal antibody	Santa Cruz Biotechnology (sc-33548)	1:500
Anti-ABI1 (C-1)	Mouse monoclonal antibody	Santa Cruz Biotechnology (sc-398554)	1:500
Anti-PIR121-1/Sra-1	Rabbit polyclonal IgG	Millipore (07-531)	1:500
Anti-HEM1 (Q-12)	Goat polyclonal antibody	Santa Cruz Biotechnology (sc-107591)	1:200
Anti-ARP2 (H-84)	Rabbit polyclonal antibody	Santa Cruz Biotechnology (sc-15389)	1:500
Anti-ARP3	Rabbit immunoaffinity purified IgG	Millipore (07-272)	1:500
Secondary Antibody	**Description**	**Source (Cat No)**	**Working Dilution**
Anti-rabbit IgG	HRP-linked antibody	Cell Signaling Technology (7074)	1:1000
Anti-mouse IgG	HRP-linked antibody	Promega (W4021)	1:1000 or 1:5000
Rabbit anti-goat IgG	Polyclonal HRP-linked antibody	Dako (P044901-2)	1:1000

Appendix E

E1: Plasmids

Plasmid	Source
pBabePuro	Dr Joop Gäken
pMDG (envelope plasmid encoding VSVG)	Dr David Darling
pREV (packaging plasmid encoding REV)	Dr David Darling
pRRE (packaging plasmid encoding Gag & Pol)	Dr David Darling
p3'TKzeo-library	Dr Joop Gäken
pLKO.1-scrambled shRNA	Addgene (plasmid #1864)
pLKO.1-TRC cloning vector	Addgene (plasmid #10878)

E2: Cell Lines

Cell Line	Cell Source	Provider
MCF7	Breast adenocarcinoma	Dr Joop Gäken
HeLa	Cervical adenocarcinoma	Dr Joop Gäken
Jurkat	Acute T cell leukaemia	Dr Terry Gaymes
HepG2	Hepatocellular carcinoma	Dr Joop Gäken
293T	Human embryonic kidney	Dr David Darling
NIH/3T3	Mouse embryo fibroblast	Dr Joop Gäken
K562	Chronic myelogenous leukaemia	Dr David Darling
KG-1	Acute myelogenous leukaemia	Dr Terry Gaymes
NB-4	Acute promyelocytic leukaemia	Dr Terry Gaymes
THP-1	Acute monocytic leukaemia	Dr Terry Gaymes
U937	Histiocytic lymphoma	Dr Terry Gaymes
MEC-1	Chronic B cell leukaemia	Dr Alan Ramsay

Appendix F: miRNA Profiling of Cell Lines

Cell Line	***miR-181c* Expression**	***miR-181d* Expression**
293T	2966.093018	75.01759338
HeLa	10684.79199	60.73740768
CHO	894.2407837	370.772583
MCF7	1155.665527	1
COS7	7059.505371	41.21817398
NIH/3T3	1782.085938	344.5409851
TE761	935.8190918	8.6062603
HepG2	387.5531311	1
Saos2	6478.030273	326.6053162

miRNA profiling was performed using Illumina bead assay by the company Geneservice. Normalised expression levels of miRNA were between 1 (no expression) and 60,000. A 500 fold change was used as the cut-off point where expression below 500 was considered low while above 500 was considered high. This was based on the qPCR results of the miRNA expression, which have shown a strong correlation between the qPCR and the array profiling data. This work was performed by Dr Joop Gäken before the start of this project.

Appendix G: Alignment of forward and reverse sequences against human genome and transcripts database in NCBI Nucleotide Blast

G1.1: Forward sequence that aligned to *DHTKD1* mRNA transcript

Score	Expect	Identities	Gaps	Strand
649 bits(351)	0.0	356/358(99%)	1/358(0%)	Plus/Plus

```
Query  1     gggtggggtggcacatgcctgtaatcccagcactttgggaggccaaggctggtggatcac  60
             ||||||||||||||||||||||||||||||||||||||||||||||||||||||||||||
Sbjct  2931  GGGTGGGGTGGCACATGCCTGTAATCCCAGCACTTTGGGAGGCCAAGGCTGGTGGATCAC  2990

Query  61    ctgaggtcaggagttcgagaccagcctggccaacacggtgaaaccccgcctctactaaaa  120
             ||||||||||||||||||||||||||||||||||||||||||||||||||||||||||||
Sbjct  2991  CTGAGGTCAGGAGTTCGAGACCAGCCTGGCCAACACGGTGAAACCCCGCCTCTACTAAAA  3050

Query  121   atacaaaaaatagccgggtgtggtggtgggcacctgtgatcccagcttcctgggaggctg  180
             ||||||||||||||||||||||||||||||||||||||||||||||||||||||||||||
Sbjct  3051  ATACAAAAAATAGCCGGGTGTGGTGGTGGGCACCTGTGATCCCAGCTTCCTGGGAGGCTG  3110

Query  181   aggcaagagaatcgcttgaatctgggggggcggaggttgcagtgagccaggatcacaccat  240
             |||||||||||||||||||||||||| ||||||||||||||||||||||||||||||||||
Sbjct  3111  AGGCAAGAGAATCGCTTGAATCTGGGAGGCGGAGGTTGCAGTGAGCCAGGATCACACCAT  3170

Query  241   tgctgtccagcctgggtgacagagcaagactgcgtttcaaaaaaaaaaaaaaaaaaaCCC  300
             ||||||||||||||||||||||||||||||||||||||||||||||||||||||||||||
Sbjct  3171  TGCTGTCCAGCCTGGGTGACAGAGCAAGACTGCGTTTCAAAAAAAAAAAAAAAAAAACCC  3230

Query  301   ATTAAAAGAGGCCTCCTTCCTCCACTCTCTCAACCCCTCTGTTGGGGTAACATGAAAA  358
             |||||||||||||||||||||||||||||||||||||||||| ||||||||||
Sbjct  3231  ATTAAAAGAGGCCTCCTTCCTCCACTCTCTCAACCCCTCTGTTGGG-TAACATGAAAA  3287
```

G1.2: Reverse sequence that aligned to *DHTKD1* mRNA transcript

Score	Expect	Identities	Gaps	Strand
610 bits(330)	8e-172	465/528(88%)	18/528(3%)	Plus/Minus

```
Query  5     ttttttttttttttttttttttttttttttttttttccctatttctaccatcacACCTTC  64
             ||| ||||||| || || ||||| |||| || |||||| ||||||||||||||||||||||
Sbjct  3459  TTTCTTTTTTTGTTATTGTTTTTCTTTTGTTGTTTTCC-TATTTCTACCATCACACCTTC  3401

Query  65    AAGGAAAAATTTGCTGGTTGCATTCACATATTCATAACCAGTTCCCCTGGTTATTCCACC  124
             ||||| ||||||||||||||||||||||||||||||||||||||||||||||||||||||
Sbjct  3400  AAGGATAAATTTGCTGGTTGCATTCACATATTCATAACCAGTTCCCCTGGTTATTCCACC  3341

Query  125   TATTGCAAATTAAATCACGTATATCAATCCCAACATCTTAAAGGAATACAGTCTTTTCAT  184
             ||||||| ||||||||||||||||||||||||||||| ||||||||||||||||||||||
Sbjct  3340  TATTGCAGATTAAATCACGTATATCAATCCCAACATCTTAGAGGAATACAGTCTTTTCAT  3281

Query  185   GTTACCCAACAAAGGGGTTGAAAAAGGGGAGGAAGGAGGCCTCTTTTAAGGGGttttttt  244
             |||||||||| |||||||| | || ||||||||||||||||||||| ||||||||||
Sbjct  3280  GTTACCCAACAGAGGGGTTGAGAGAGTGGAGGAAGGAGGCCTCTTTTAATGGGTTTTTTT  3221

Query  245   ttttttttttttgaa-cgcaatcttggtctgtcacccagggtgggcagcaagggtgtgaa  303
             ||||||||||||||| |||| ||||| |||||||||||||| ||| |||||| |||||||
Sbjct  3220  TTTTTTTTTTTTGAAACGCAGTCTTGCTCTGTCACCCAGGCTGGACAGCAATGGTGTGA-  3162

Query  304   tctttgctcatggaaacctc-gcccccaagattcaagcgattctcttgcctcagcctccc  362
             || | |||||  | |||||| ||| || ||||||||||||||||||||||||||||||||
Sbjct  3161  TCCTGGCTCACTGCAACCTCCGCCTCCCAGATTCAAGCGATTCTCTTGCCTCAGCCTCCC  3102

Query  363   aggaagctgggatcacaggtgccccccac-acacccggctattttt-gtttttatagaaa  420
             |||||||||||||||||||||| |||| |||||||||||||||| || ||| ||| |
Sbjct  3101  AGGAAGCTGGGATCACAGGTGCCCACCACCACACCCGGCTATTTTTTGTATTTTTAGTAG  3042

Query  421   ag-cgggg-ttcaccgtgggggggcaggggggggctcga-ctcc-gaacttaggtgatc-ac  475
             || ||||| |||||||||  || ||||  || ||||| |||| || || |||||||| ||
Sbjct  3041  AGGCGGGGTTTCACCGTGTTGGCCAGGCTGGTCTCGAACTCCTGACCTCAGGTGATCCAC  2982

Query  476   -agtcttggc-tctcaaag--ctgtgat-acagAAA-GTGTCCACCCC  517
              || |||||| || |||||  ||| ||| ||||  | ||| |||||||
Sbjct  2981  CAGCCTTGGCCTCCCAAAGTGCTGGGATTACAGGCATGTG-CCACCCC  2935
```

G2.1: Forward sequence that aligned to *BRK1* mRNA transcript

Score	Expect	Identities	Gaps	Strand
771 bits(417)	0.0	424/427(99%)	1/427(0%)	Plus/Minus

```
Query  31   agagcccaaaggccacacttttgaaaaaagaaaaaCAAGAATAAGCCCTGTTGCTCTTTA  90
            ||||||||||||||||||||||||||||||||||||||||||||||||||||||||||||
Sbjct  432  AGAGCCCAAAGGCCACACTTTTGAAAAAAGAAAAACAAGAATAAGCCCTGTTGCTCTTTA  373

Query  91   AGGAGAAAGGAAGGAGCTGAAGGCTGCTGGGGCCTTTCCCATGTGGCCTGTGTTGTGTAA  150
            ||||||||||||||||||||||||||||||||||||||||||||||||||||||||||||
Sbjct  372  AGGAGAAAGGAAGGAGCTGAAGGCTGCTGGGGCCTTTCCCATGTGGCCTGTGTTGTGTAA  313

Query  151  AGCAACTTCCCAGCAGCAGCACGGCACTGTTCTAGGTGAGTGTCTCACCTTTTGTCACCC  210
            ||||||||||||||||||||||||||||||||||||||||||||||||||||||||||||
Sbjct  312  AGCAACTTCCCAGCAGCAGCACGGCACTGTTCTAGGTGAGTGTCTCACCTTTTGTCACCC  253

Query  211  GAGCTTCAATGCACTCTATTCTCCGTTCAAGGGCTGTCAATTTCTCGTTTAGTGTTGCAA  270
            |||||||||||  ||||||||||||||||||||||||||||||||||||||||||||||
Sbjct  252  GAGCTTCAATGTACTCTATTCTCCGTTCAAGGGCTGTCAATTTCTCGTTTAGTGTTGCAA  193

Query  271  GTCTTGAACGACAAGACATATCGAACGAGTTGAGAAAGTCTGCGATTTTCTTGATGCTGC  330
            ||||||||||||||||||||||||||||||||||||||||||||||||||||||||||||
Sbjct  192  GTCTTGAACGACAAGACATATCGAACGAGTTGAGAAAGTCTGCGATTTTCTTGATGCTGC  133

Query  331  TGGTGATTATCTCAATGTACTCCCGGTTAGCCCAGTCCTGGTGAATCTCCCGCTGCACCG  390
            ||||||||||||||||||||||||||||||||||||||||||||||||||||||||||||
Sbjct  132  TGGTGATTATCTCAATGTACTCCCGGTTAGCCCAGTCCTGGTGAATCTCCCGCTGCACCG  73

Query  391  GATCCTCCTGTCCCGCCATGGCCGCCGCCTGAGGAAAAGCGACTGCGCAGGCGCCCCGAC  450
            ||||||||||||||||||||||||||||||||||||| ||||||||||||||||||||||
Sbjct  72   GATCCTCCTGTCCCGCCATGGCCGCCGCCTGAGGAAGAGCGACTGCGCAGGCGCCCCGAC  13

Query  451  C-TACAG  456
            | |||||
Sbjct  12   CCTACAG  6
```

G2.2: Reverse sequence that aligned to *BRK1* mRNA transcript

Score	Expect	Identities	Gaps	Strand
782 bits(423)	0.0	429/432(99%)	0/432(0%)	Plus/Plus

```
Query  5    GAGGACTGTAGGGTCGGGGCGCCTGCGCAGTCGCTTTTCCTCAGGCGGCGGCCATGGCGG  64
            |||| |||||||||||||||||||||||||||||| |||||||||||||||||||||||||
Sbjct  1    GAGGCCTGTAGGGTCGGGGCGCCTGCGCAGTCGCTCTTCCTCAGGCGGCGGCCATGGCGG  60

Query  65   GACAGGAGGATCCGGTGCAGCGGGAGATTCACCAGGACTGGGCTAACCGGGAGTACATTG  124
            ||||||||||||||||||||||||||||||||||||||||||||||||||||||||||||
Sbjct  61   GACAGGAGGATCCGGTGCAGCGGGAGATTCACCAGGACTGGGCTAACCGGGAGTACATTG  120

Query  125  AGATAATCACCAGCAGCATCAAGAAAATCGCAGACTTTCTCAACTCGTTCGATATGTCTT  184
            ||||||||||||||||||||||||||||||||||||||||||||||||||||||||||||
Sbjct  121  AGATAATCACCAGCAGCATCAAGAAAATCGCAGACTTTCTCAACTCGTTCGATATGTCTT  180

Query  185  GTCGTTCAAGACTTGCAACACTAAACGAGAAATTGACAGCCCTTGAACGGAGAATAGAGT  244
            ||||||||||||||||||||||||||||||||||||||||||||||||||||||||||||
Sbjct  181  GTCGTTCAAGACTTGCAACACTAAACGAGAAATTGACAGCCCTTGAACGGAGAATAGAGT  240

Query  245  GCATTGAAGCTCGGGTGACAAAAGGTGAGACACTCACCTAGAACAGTGCCGTGCTGCTGC  304
             ||||||||||||||||||||||||||||||||||||||||||||||||||||||||||||
Sbjct  241  ACATTGAAGCTCGGGTGACAAAAGGTGAGACACTCACCTAGAACAGTGCCGTGCTGCTGC  300

Query  305  TGGGAAGTTGCTTTACACAACACAGGCCACATGGGAAAGGCCCCAGCAGCCTTCAGCTCC  364
            ||||||||||||||||||||||||||||||||||||||||||||||||||||||||||||
Sbjct  301  TGGGAAGTTGCTTTACACAACACAGGCCACATGGGAAAGGCCCCAGCAGCCTTCAGCTCC  360

Query  365  TTCCTTTCTCCTTAAAGAGCAACAGGGCTTATTCTTGttttttcttttttcaaaagtgtgg  424
            ||||||||||||||||||||||||||||||||||||||||||||||||||||||||||||
Sbjct  361  TTCCTTTCTCCTTAAAGAGCAACAGGGCTTATTCTTGTTTTTTCTTTTTTCAAAAGTGTGG  420

Query  425  cctttgggctct  436
            ||||||||||||
Sbjct  421  CCTTTGGGCTCT  432
```

Appendix H: Predicted Targets of *miR-181c* and *miR-181d* Using miRecords

H1: A list of 151 *miR-181c* targets predicted by miRanda, MirTarget2, PicTar, PITA, RNAhybrid and TargetScan

Symbol	Description	Symbol	Description
SENP1	SUMO1/sentrin specific peptidase 1	ESR1	estrogen receptor 1
PI4K2B	phosphatidylinositol 4-kinase type 2 beta	ATP2B1	ATPase, Ca++ transporting, plasma membrane 1
CTTNBP2 NL	CTTNBP2 N-terminal like	EIF4A2	eukaryotic translation initiation factor 4A, isoform 2
PCDHAC1	protocadherin alpha subfamily C, 1	ETV6	ets variant gene 6 (TEL oncogene)
PCDHAC2	protocadherin alpha subfamily C, 2	ACSL1	acyl-CoA synthetase long-chain family member 1
PCDHA1	protocadherin alpha 1	HLF	hepatic leukemia factor
PCDHA12	protocadherin alpha 12	ITGA3	integrin, alpha 3 (antigen CD49C, alpha 3 subunit of VLA-3 receptor)
PCDHA13	protocadherin alpha 13	ITGB8	integrin, beta 8
PCDHA2	protocadherin alpha 2	KPNA1	karyopherin alpha 1 (importin alpha 5)
PCDHA3	protocadherin alpha 3	KPNB1	karyopherin (importin) beta 1
PCDHA4	protocadherin alpha 4	LBR	lamin B receptor
PCDHA5	protocadherin alpha 5	MAP2K1	mitogen-activated protein kinase kinase 1
PCDHA7	protocadherin alpha 7	PTPN9	protein tyrosine phosphatase, non-receptor type 9
PCDHA8	protocadherin alpha 8	RBBP7	retinoblastoma binding protein 7
SLC38A2	solute carrier family 38, member 2	CLIP1	CAP-GLY domain containing linker protein 1
CCNJ	cyclin J	STC1	stanniocalcin 1
PCNP	PEST proteolytic signal containing nuclear protein	UBE2B	ubiquitin-conjugating enzyme E2B (RAD6 homolog)
FLJ20160	FLJ20160 protein	ATP1B1	ATPase, Na+/K+ transporting, beta 1 polypeptide
INOC1	INO80 complex homolog 1 (S. cerevisiae)	ACVR2A	activin A receptor, type IIA
FAM13B1	family with sequence similarity 13, member B1	CYR61	cysteine-rich, angiogenic inducer, 61
KIAA0182	KIAA0182	NR3C1	nuclear receptor subfamily 3, group C, member 1 (glucocorticoid receptor)
TOX	thymocyte selection-associated high mobility group box	ATXN1	ataxin 1
DAZAP2	DAZ associated protein 2	TIMP3	TIMP metallopeptidase inhibitor 3 (Sorsby fundus dystrophy, pseudoinflammatory)
KIAA0528	KIAA0528	IL1A	interleukin 1, alpha
GLS	glutaminase	PAM	peptidylglycine alpha-amidating monooxygenase
BTBD3	BTB (POZ) domain containing 3	ATP2B2	ATPase, Ca++ transporting, plasma membrane 2
USP33	ubiquitin specific peptidase 33	LMO3	LIM domain only 3 (rhombotin-like 2)
KIAA0423	KIAA0423	C16orf87	chromosome 16 open reading frame 87

Symbol	Description	Symbol	Description
HIC2	hypermethylated in cancer 2	AFTPH	Aftiphilin
GPD1L	glycerol-3-phosphate dehydrogenase 1-like	OSBPL8	oxysterol binding protein-like 8
KANK1	KN motif and ankyrin repeat domains 1	LIN28B	lin-28 homolog B (C. elegans)
DNAJC13	DnaJ (Hsp40) homolog, subfamily C, member 13	KLF6	Kruppel-like factor 6
CLASP1	cytoplasmic linker associated protein 1	EN1	engrailed homeobox 1
OSBPL3	oxysterol binding protein-like 3	EN2	engrailed homeobox 2
GAPVD1	GTPase activating protein and VPS9 domains 1	NR6A1	nuclear receptor subfamily 6, group A, member 1
HECA	headcase homolog (Drosophila)	B4GALT1	UDP-Gal:betaGlcNAc beta 1,4-galactosyltransferase, polypeptide 1
LRRN1	leucine rich repeat neuronal 1	ZIC3	Zic family member 3 heterotaxy 1 (odd-paired homolog, Drosophila)
PKNOX2	PBX/knotted 1 homeobox 2	CUL3	cullin 3
MPP5	membrane protein, palmitoylated 5 (MAGUK p55 subfamily member 5)	CDC42BPA	CDC42 binding protein kinase alpha (DMPK-like)
RNF145	ring finger protein 145	MAT2A	methionine adenosyltransferase II, alpha
RNF182	ring finger protein 182	DYNC1LI2	dynein, cytoplasmic 1, light intermediate chain 2
C7orf41	chromosome 7 open reading frame 41	PBX3	pre-B-cell leukemia homeobox 3
EED	embryonic ectoderm development	PDGFRA	platelet-derived growth factor receptor, alpha polypeptide
FLJ38973	hypothetical protein FLJ38973	ARFGEF2	ADP-ribosylation factor guanine nucleotide-exchange factor 2 (brefeldin A-inhibited)
POM121	POM121 membrane glycoprotein (rat)	NFAT5	nuclear factor of activated T-cells 5, tonicity-responsive
CNTN4	contactin 4	LRBA	LPS-responsive vesicle trafficking, beach and anchor containing
ANKRD43	ankyrin repeat domain 43	SOX5	SRY (sex determining region Y)-box 5
ZNF800	zinc finger protein 800	NR4A3	nuclear receptor subfamily 4, group A, member 3
C3orf59	chromosome 3 open reading frame 59	TARDBP	TAR DNA binding protein
RSPO2	R-spondin 2 homolog (Xenopus laevis)	SIRT1	sirtuin (silent mating type information regulation 2 homolog) 1 (S. cerevisiae)
ADAMTS6	ADAM metallopeptidase with thrombospondin type 1 motif, 6	G3BP2	GTPase activating protein (SH3 domain) binding protein 2
SS18L1	synovial sarcoma translocation gene on chromosome 18-like 1	YWHAG	tyrosine 3-monooxygenase/tryptophan 5-monooxygenase activation protein, gamma polypeptide
OTUD4	OTU domain containing 4	SSX2IP	synovial sarcoma, X breakpoint 2 interacting protein
ADAMTS18	ADAM metallopeptidase with thrombospondin type 1 motif, 18	KLF15	Kruppel-like factor 15
FBXO33	F-box protein 33	NPTXR	neuronal pentraxin receptor

Symbol	Description	Symbol	Description
MBOAT2	membrane bound O-acyltransferase domain containing 2	MAP1B	microtubule-associated protein 1B
SLITRK1	SLIT and NTRK-like family, member 1	ST8SIA4	ST8 alpha-N-acetyl-neuraminide alpha-2,8-sialyltransferase 4
CNTNAP3	contactin associated protein-like 3	LPP	LIM domain containing preferred translocation partner in lipoma
HOXC8	homeobox C8	PIK3R3	phosphoinositide-3-kinase, regulatory subunit 3 (gamma)
GPBP1	GC-rich promoter binding protein 1	BHLHB2	basic helix-loop-helix domain containing, class B, 2
C17orf39	chromosome 17 open reading frame 39	IRS2	insulin receptor substrate 2
DERL1	Der1-like domain family, member 1	PCAF	p300/CBP-associated factor
LIN28	lin-28 homolog (C. elegans)	AKAP6	A kinase (PRKA) anchor protein 6
RNF34	ring finger protein 34	DUSP5	dual specificity phosphatase 5
CPEB4	cytoplasmic polyadenylation element binding protein 4	RAB11A	RAB11A, member RAS oncogene family
ANKRD13C	ankyrin repeat domain 13C	NMT2	N-myristoyltransferase 2
C6orf62	chromosome 6 open reading frame 62	CDYL	chromodomain protein, Y-like
SPRY4	sprouty homolog 4 (Drosophila)	ATG5	ATG5 autophagy related 5 homolog (S. cerevisiae)
PPP1R12B	protein phosphatase 1, regulatory (inhibitor) subunit 12B	TBPL1	TBP-like 1
FOXP1	forkhead box P1	ZFP36L1	zinc finger protein 36, C3H type-like 1
ADO	2-aminoethanethiol (cysteamine) dioxygenase	SEL1L	sel-1 suppressor of lin-12-like (C. elegans)
SYNE1	spectrin repeat containing, nuclear envelope 1	ETS1	v-ets erythroblastosis virus E26 oncogene homolog 1 (avian)
PURB	purine-rich element binding protein B	PRKCE	protein kinase C, epsilon
DOCK7	dedicator of cytokinesis 7	LRRC32	leucine rich repeat containing 32
E2F7	E2F transcription factor 7	LEMD3	LEM domain containing 3
RABGEF1	RAB guanine nucleotide exchange factor (GEF) 1		

H2: A list of 222 *miR-181d* targets predicted by miRanda, MirTarget2, PITA, RNAhybrid and TargetScan

Symbol	Description	Symbol	Description
PCDHA6	protocadherin alpha 6	CD69	CD69 molecule
GAPVD1	GTPase activating protein and VPS9 domains 1	QSER1	glutamine and serine rich 1
OSBPL3	oxysterol binding protein-like 3	C14orf43	chromosome 14 open reading frame 43
CLASP1	cytoplasmic linker associated protein 1	SLC9A6	solute carrier family 9 (sodium/hydrogen exchanger), member 6
TRIM2	tripartite motif-containing 2	MTMR12	myotubularin related protein 12
DNAJC13	DnaJ (Hsp40) homolog, subfamily C, member 13	PAPD5	PAP associated domain containing 5
DMXL2	Dmx-like 2	NKAIN2	Na+/K+ transporting ATPase interacting 2
HISPPD1	histidine acid phosphatase domain containing 1	FAM3C	family with sequence similarity 3, member C
TBC1D1	TBC1 (tre-2/USP6, BUB2, cdc16) domain family, member 1	TCERG1	transcription elongation regulator 1
PHF3	PHD finger protein 3	CREBZF	CREB/ATF bZIP transcription factor
GPD1L	glycerol-3-phosphate dehydrogenase 1-like	PALM2	paralemmin 2
HIC2	hypermethylated in cancer 2	ARL5A	ADP-ribosylation factor-like 5A
PHF20L1	PHD finger protein 20-like 1	KIAA1553	KIAA1553
CDON	Cdon homolog (mouse)	ACVR2B	activin A receptor, type IIB
SEMA4G	sema domain, immunoglobulin domain (Ig), transmembrane domain (TM) and short cytoplasmic domain, (semaphorin) 4G	ADM	adrenomedullin
PCDHA5	protocadherin alpha 5	ATP2B1	ATPase, Ca++ transporting, plasma membrane 1
PCDHA3	protocadherin alpha 3	ATP1B1	ATPase, Na+/K+ transporting, beta 1 polypeptide
PCDHA2	protocadherin alpha 2	ADRBK1	adrenergic, beta, receptor kinase 1
PCDHA13	protocadherin alpha 13	ACVR2A	activin A receptor, type IIA
PCDHA10	protocadherin alpha 10	CYR61	cysteine-rich, angiogenic inducer, 61
PCDHA1	protocadherin alpha 1	EN2	engrailed homeobox 2
PCDHAC1	protocadherin alpha subfamily C, 1	S1PR1	sphingosine-1-phosphate receptor 1
CTTNBP2 NL	CTTNBP2 N-terminal like	DPYSL2	dihydropyrimidinase-like 2
C10orf6	chromosome 10 open reading frame 6	DDX3X	DEAD (Asp-Glu-Ala-Asp) box polypeptide 3, X-linked
FIGN	fidgetin	CPD	carboxypeptidase D
TMEM16 A	transmembrane protein 16A	KLF6	Kruppel-like factor 6
BTBD3	BTB (POZ) domain containing 3	FOXK1	forkhead box K1
TBC1D4	TBC1 domain family, member 4	YTHDC1	YTH domain containing 1

Symbol	Description	Symbol	Description
TSC22D2	TSC22 domain family, member 2	AP1G1	adaptor-related protein complex 1, gamma 1 subunit
GREM1	gremlin 1, cysteine knot superfamily, homolog (Xenopus laevis)	ATP2B2	ATPase, Ca++ transporting, plasma membrane 2
G3BP2	GTPase activating protein (SH3 domain) binding protein 2	ITSN1	intersectin 1 (SH3 domain protein)
SIRT1	sirtuin (silent mating type information regulation 2 homolog) 1 (S. cerevisiae)	PAM	peptidylglycine alpha-amidating monooxygenase
ILF3	interleukin enhancer binding factor 3, 90kDa	GRM5	glutamate receptor, metabotropic 5
MIP	major intrinsic protein of lens fiber	GABRA1	gamma-aminobutyric acid (GABA) A receptor, alpha 1
TARDBP	TAR DNA binding protein	FKBP1A	FK506 binding protein 1A, 12kDa
KLHL2	kelch-like 2, Mayven (Drosophila)	CD4	CD4 molecule
UBL3	ubiquitin-like 3	GPD2	glycerol-3-phosphate dehydrogenase 2 (mitochondrial)
ADAMTS 5	ADAM metallopeptidase with thrombospondin type 1 motif, 5 (aggrecanase-2)	TIMP3	TIMP metallopeptidase inhibitor 3 (Sorsby fundus dystrophy, pseudoinflammatory)
SOX5	SRY (sex determining region Y)-box 5	TGFBI	transforming growth factor, beta-induced, 68kDa
CALM1	calmodulin 1 (phosphorylase kinase, delta)	NR3C1	nuclear receptor subfamily 3, group C, member 1 (glucocorticoid receptor)
LRP12	low density lipoprotein-related protein 12	LMO3	LIM domain only 3 (rhombotin-like 2)
BAZ2B	bromodomain adjacent to zinc finger domain, 2B	GRB10	growth factor receptor-bound protein 10
SSX2IP	synovial sarcoma, X breakpoint 2 interacting protein	PPARA	peroxisome proliferator-activated receptor alpha
DAZAP2	DAZ associated protein 2	TNRC6B	trinucleotide repeat containing 6B
TOX	thymocyte selection-associated high mobility group box	ABI1	abl-interactor 1
DOCK4	dedicator of cytokinesis 4	GOLGA8 E	golgi autoantigen, golgin subfamily a, 8E
DOCK10	dedicator of cytokinesis 10	ATP11C	ATPase, class VI, type 11C
UBE3C	ubiquitin protein ligase E3C	KIAA202 2	KIAA2022
BRD1	bromodomain containing 1	ENAH	enabled homolog (Drosophila)
UBP1	upstream binding protein 1 (LBP-1a)	CTDSPL	CTD (carboxy-terminal domain, RNA polymerase II, polypeptide A) small phosphatase-like
RABGEF1	RAB guanine nucleotide exchange factor (GEF) 1	LMBRD2	LMBR1 domain containing 2
GHITM	growth hormone inducible transmembrane protein	SLC25A2 5	solute carrier family 25 (mitochondrial carrier; phosphate carrier), member 25
LEMD3	LEM domain containing 3	LIN28B	lin-28 homolog B (C. elegans)
KLF15	Kruppel-like factor 15	LYCAT	lysocardiolipin acyltransferase
LRBA	LPS-responsive vesicle trafficking, beach and anchor containing	ESR1	estrogen receptor 1

Symbol	Description	Symbol	Description
SLC38A2	solute carrier family 38, member 2	EIF4A2	eukaryotic translation initiation factor 4A, isoform 2
E2F7	E2F transcription factor 7	NFAT5	nuclear factor of activated T-cells 5, tonicity-responsive
MAMDC2	MAM domain containing 2	SEL1L	sel-1 suppressor of lin-12-like (C. elegans)
EED	embryonic ectoderm development	ZFP36L1	zinc finger protein 36, C3H type-like 1
CPNE2	copine II	ONECUT 2	one cut homeobox 2
MIER3	mesoderm induction early response 1, family member 3	ATG5	ATG5 autophagy related 5 homolog (S. cerevisiae)
LONRF1	LON peptidase N-terminal domain and ring finger 1	NMT2	N-myristoyltransferase 2
ARHGEF7	Rho guanine nucleotide exchange factor (GEF) 7	KIF3B	kinesin family member 3B
SYNPR	synaptoporin	RAB11A	RAB11A, member RAS oncogene family
MBOAT2	membrane bound O-acyltransferase domain containing 2	TGFBR1	transforming growth factor, beta receptor I (activin A receptor type II-like kinase, 53kDa)
DCBLD2	discoidin, CUB and LCCL domain containing 2	RPS6KA 3	ribosomal protein S6 kinase, 90kDa, polypeptide 3
SLITRK1	SLIT and NTRK-like family, member 1	DUSP5	dual specificity phosphatase 5
BRWD1	bromodomain and WD repeat domain containing 1	AKAP6	A kinase (PRKA) anchor protein 6
ATP2A2	ATPase, Ca++ transporting, cardiac muscle, slow twitch 2	GATA6	GATA binding protein 6
POM121	POM121 membrane glycoprotein (rat)	PRKCE	protein kinase C, epsilon
DIP2B	DIP2 disco-interacting protein 2 homolog B (Drosophila)	TOM1L1	target of myb1 (chicken)-like 1
ADAMTS 18	ADAM metallopeptidase with thrombospondin type 1 motif, 18	ARFGEF 2	ADP-ribosylation factor guanine nucleotide-exchange factor 2 (brefeldin A-inhibited)
OTUD4	OTU domain containing 4	PRKCD	protein kinase C, delta
SS18L1	synovial sarcoma translocation gene on chromosome 18-like 1	DYNC1LI2	dynein, cytoplasmic 1, light intermediate chain 2
ZC3H6	zinc finger CCCH-type containing 6	RNF6	ring finger protein (C3H2C3 type) 6
SRPK2	SFRS protein kinase 2	MAT2A	methionine adenosyltransferase II, alpha
RSPO2	R-spondin 2 homolog (Xenopus laevis)	ST8SIA4	ST8 alpha-N-acetyl-neuraminide alpha-2,8-sialyltransferase 4
C3orf59	chromosome 3 open reading frame 59	NFIB	nuclear factor I/B
WDR40B	WD repeat domain 40B	LPP	LIM domain containing preferred translocation partner in lipoma
PPM1B	protein phosphatase 1B (formerly 2C), magnesium-dependent, beta isoform	INPP5A	inositol polyphosphate-5-phosphatase, 40kDa
ANKRD43	ankyrin repeat domain 43	HOXA1	homeobox A1
CNTN4	contactin 4	LRRC32	leucine rich repeat containing 32
CNTNAP3	contactin associated protein-like 3	PCAF	p300/CBP-associated factor

Symbol	Description	Symbol	Description
DOCK7	dedicator of cytokinesis 7	CCNK	cyclin K
FOXP1	forkhead box P1	RNMT	RNA (guanine-7-) methyltransferase
PKNOX2	PBX/knotted 1 homeobox 2	PAWR	PRKC, apoptosis, WT1, regulator
SEC24A	SEC24 related gene family, member A (S. cerevisiae)	TNFRSF11B	tumor necrosis factor receptor superfamily, member 11b (osteoprotegerin)
RBM25	RNA binding motif protein 25	NOVA1	neuro-oncological ventral antigen 1
ZBTB4	zinc finger and BTB domain containing 4	MAP3K3	mitogen-activated protein kinase kinase kinase 3
LRRN1	leucine rich repeat neuronal 1	ADAM11	ADAM metallopeptidase domain 11
SIPA1L2	signal-induced proliferation-associated 1 like 2	LBR	lamin B receptor
KIAA1219	KIAA1219	IPO5	importin 5
SPIRE1	spire homolog 1 (Drosophila)	KPNA1	karyopherin alpha 1 (importin alpha 5)
PLEKHA3	pleckstrin homology domain containing, family A (phosphoinositide binding specific) member 3	ITGB8	integrin, beta 8
CCNJ	cyclin J	HMGB2	high-mobility group box 2
ZFAND6	zinc finger, AN1-type domain 6	ACSL1	acyl-CoA synthetase long-chain family member 1
MPP5	membrane protein, palmitoylated 5 (MAGUK p55 subfamily member 5)	PLAG1	pleiomorphic adenoma gene 1
HOXC8	homeobox C8	MAPK1	mitogen-activated protein kinase 1
BCL11A	B-cell CLL/lymphoma 11A (zinc finger protein)	MAP2K1	mitogen-activated protein kinase kinase 1
SCOC	short coiled-coil protein	IRS2	insulin receptor substrate 2
FAM160A2	family with sequence similarity 160, member A2	BHLHB2	basic helix-loop-helix domain containing, class B, 2
PPP1R12B	protein phosphatase 1, regulatory (inhibitor) subunit 12B	PIK3R3	phosphoinositide-3-kinase, regulatory subunit 3 (gamma)
SPRY4	sprouty homolog 4 (Drosophila)	PPFIA1	protein tyrosine phosphatase, receptor type, f polypeptide (PTPRF), interacting protein (liprin), alpha 1
C6orf62	chromosome 6 open reading frame 62	CDC42BPA	CDC42 binding protein kinase alpha (DMPK-like)
ANKRD13C	ankyrin repeat domain 13C	CUL3	cullin 3
CPEB4	cytoplasmic polyadenylation element binding protein 4	ZIC3	Zic family member 3 heterotaxy 1 (odd-paired homolog, Drosophila)
LPCAT1	lysophosphatidylcholine acyltransferase 1	UBE2B	ubiquitin-conjugating enzyme E2B (RAD6 homolog)
LIN28	lin-28 homolog (C. elegans)	STC1	stanniocalcin 1
DERL1	Der1-like domain family, member 1	CLIP1	CAP-GLY domain containing linker protein 1
C17orf39	chromosome 17 open reading frame 39	PTPN9	protein tyrosine phosphatase, non-receptor type 9
RIN2	Ras and Rab interactor 2	ETV6	ets variant gene 6 (TEL oncogene)